Modelling and Control of Lightweight Underwater Vehicle-Manipulator Systems

Corina BARBALATA

Ocean Systems Laboratory

School of Engineering and Physical Sciences

Heriot-Watt University

A thesis submitted for the degree of

Doctor of Philosophy

March 2017

Abstract

This thesis studies the mathematical description and the low-level control structures for underwater robotic systems performing motion and interaction tasks. The main focus is on the study of lightweight underwater-vehicle manipulator systems. A description of the dynamic and hydrodynamic modelling of the underwater vehicle-manipulator system (UVMS) is presented and a study of the coupling effects between the vehicle and manipulator is given. Through simulation results it is shown that the vehicle's capabilities are degraded by the motion of the manipulator, when it has a considerable mass with respect to the vehicle. Understanding the interaction effects between the two subsystems is beneficial in developing new control architectures that can improve the performance of the system. A control strategy is proposed for reducing the coupling effects between the two subsystems when motion tasks are required. The method is developed based on the mathematical model of the UVMS and the estimated interaction effects. Simulation results show the validity of the proposed control structure even in the presence of uncertainties in the dynamic model. The problem of autonomous interaction with the underwater environment is further addressed. The thesis proposes a parallel position/force control structure for lightweight underwater vehicle-manipulator systems. Two different strategies for integrating this control law on the vehicle-manipulator structure are proposed. The first strategy uses the parallel control law for the manipulator while a different control law, the Proportional Integral Limited control structure, is used for the vehicle. The second strategy treats the underwater vehicle-manipulator system as a single system and the parallel position/force law is used for the overall system. The low level parallel position/force control law is validated through practical experiments using the HDT-MK3-M electric manipulator. The Proportional Integral Limited control structure is tested using a 5 degrees-of-freedom underwater vehicle in a wave-tank facility. Furthermore, an adaptive tuning method based on interaction theory is proposed for adjusting the gains of the controller. The experimental results show that the method is advantageous as it decreases the complexity of the manual tuning otherwise required and reduces the energy consumption. The main objectives of this thesis are to understand and accurately represent the behaviour of an underwater vehicle-manipulator system, to evaluate this system when in contact with the environment and to design informed low-level control structures based on the observations made through the mathematical study of the system. The concepts presented in this thesis are not restricted to only vehicle-manipulator systems but can be applied to different other multibody robotic systems.

I would like to dedicate this thesis to my mother and grandmother.

In the loving memory of my father.

Acknowledgements

First and foremost I would like to express my sincere gratitude to Dr. Matthew W. Dunnigan for his guidance, advices, support and kindness during the past years of my PhD studies. I am deeply grateful and extremely lucky for the opportunity of working under his supervision. I am thankful to Prof. Yvan Petillot for his advices, support and for giving me the chance to work with amazing robots. A special thank you is for Leonard McLean, the technician of the Ocean Systems Laboratory without whom any practical experiment would not be possible. I am grateful to my amazing colleagues in the Ocean Systems Laboratory for their constructive suggestions, encouragements and for all the fun time spent together. I would like to thank SeeByte Ltd. for the financial support offered for my studies and for the valuable time spent in the company. Special thanks to my family for their endless patience, constant support and encouragements. I am forever indebted to my mother for the sacrifices she made to give me the chance to pursue a PhD, to my grandmother for her unconditional love and to my brother for teaching me to never give up.

ACADEMIC REGISTRY

Research Thesis Submission

Name*:*	CORINA BARBALATA		
School:	Engineering and Physical Sciences (EPS)		
Version: *(i.e. First, Resubmission, Final)*	Final	Degree Sought:	Doctor of Philosophy (PhD) Electrical Engineering

Declaration

In accordance with the appropriate regulations I hereby submit my thesis and I declare that:

1) the thesis embodies the results of my own work and has been composed by myself
2) where appropriate, I have made acknowledgement of the work of others and have made reference to work carried out in collaboration with other persons
3) the thesis is the correct version of the thesis for submission and is the same version as any electronic versions submitted*.
4) my thesis for the award referred to, deposited in the Heriot-Watt University Library, should be made available for loan or photocopying and be available via the Institutional Repository, subject to such conditions as the Librarian may require
5) I understand that as a student of the University I am required to abide by the Regulations of the University and to conform to its discipline.
6) I confirm that the thesis has been verified against plagiarism via an approved plagiarism detection application e.g. Turnitin.

* *Please note that it is the responsibility of the candidate to ensure that the correct version of the thesis is submitted.*

Signature of Candidate*:*		Date:	

Submission

Submitted By *(name in capitals):*	
Signature of Individual Submitting:	
Date Submitted:	

For Completion in the Student Service Centre (SSC)

Received in the SSC by *(name in capitals):*			
Method of Submission *(Handed in to SSC; posted through internal/external mail):*			
*E-thesis Submitted (**mandatory for final theses)***			
Signature:		Date:	

Please note this form should be bound into the submitted thesis.

Contents

List of Figures

List of Tables

Nomenclature

Abbreviations

AUV	Autonomous Underwater Vehicle
COMEX	Compagnie maritime d'expertises
D-H	Denavit-Hartenberg parameters
DOF	Degree-of-freedom
DVL	Doppler Velocity Log
FBL	Feedback Linearisation
FC-MC	Force Coupling Model Control
GPS	Global Positioning System
GRMS	Generalized root mean square error
HOCU	Operator Control Unit
I-AUV	Intervention Autonomous Underwater Vehicle
ID	Inverse Dynamics
IK	Integration Kit
ISMC	Integral Sliding Mode Control
PD	Proportional Derivative Controller
PI	Proportional Integral Controller
PID	Proportional Integral Derivative Control
PILIM	Proportional Integral Limited Control
ROV	Remotely Operated Vehicle

SAUVIM	Semi Autonomous Underwater Vehicle for Intervention Mission
SMC	Sliding Mode Control
UVMS	Underwater Vehicle-Manipulator System
VSC	Variable Structure Control
VSMD	Variable Structure Model Dynamic Control

Notations

$\circ$	composition operation
$\times$	cross product operation
$\mathbb{N}$	natural numbers
$\mathbb{R}$	real numbers
$\mathbb{R}^+$	positive real numbers
t	time (sec)
x_{des}	desired value of variable x
$\| x \|$	Euclidean norm of vector x
$f : X \to Y$	function that maps the set X on the set Y
$x \in \mathbb{R}^n$	real vector of dimension n
$\dot{x}$	derivative of x with respect to time
$A \in \mathbb{R}^{n \times n}$	real square matrix of dimension $n \times n$
$A \in \mathbb{R}^{n \times m}$	real matrix of dimension $n \times m$
A^T	the transpose of matrix A
A^{-1}	the inverse of matrix A
$A^\dagger$	the pseudo-inverse of matrix A
$\tilde{A}$	estimate of matrix A
γA	boundary error for matrix A
I_n	the identity matrix of dimension n
$O_{n \times n}$	the zero matrix of dimension $n \times n$

τ	generalized force vector applied to the system (Nm)
ρ	UVMS position vector (m; rad)
ξ	UVMS velocity vector (m/sec; rad/sec)
q	manipulator joint position vector (rad)
η	vehicle position vector (m; rad)
ν	vehicle velocity vector (m/sec; rad/sec)
J_m	manipulator Jacobian
J_e	vehicle Jacobian
J	UVMS Jacobian
M	inertia matrix
C	Coriolis and centripetal matrix
D	hydrodynamic damping matrix
g	restoring forces vector
f_f	friction forces vector (N)
F	interaction with environment vector (N)
K_e	stiffness coefficient (N/m)
K_P	proportional gain matrix
K_D	derivative gain matrix
K_P	integral gain matrix
F_c	vector of coupling effects between subsystems (N)
e	generalized error vector
e_p	position error vector (m; rad)
e_f	force error vector (N)
u_f	force control effort vector (N; Nm)
u_p	position control effort vector (N; Nm)
V	Lyapunov function
k_τ	vector of torque constants

i_a	vector of motor currents (A)
E	Young's modulus
α_c	connection weight

Chapter 1

Introduction

Over two-thirds of the Earth's surface is covered by oceans, yet only 5% of the oceans have been explored. Shallow oceans provide most of the available information regarding this environment while exploration of the deep oceans represents a significant challenge. Currently, the scientific world has taken an interest in investigating the use of deep waters for generating energy, food and other resources. The deep layer is the lowest layer of the ocean and is encountered at depths greater than 1000 meters. Ocean exploration is fundamental to understanding the deep oceans and provides environmental information for reliably managing the available resources. One of the first methods used to explore the deep oceans was the use of manned submarines. Starting in 1964, Alvin, a manned deep ocean submersible owned by the United States Navy has performed more than 4400 dives. The system can reach 4500 meters depth and can carry three people at a time. The submersible was used to find hydrogen bombs in the Mediterranean, inspect the wreck of the Titanic and the obtained data helped to produce more than 2000 scientific papers. Nonetheless, certain tasks in the underwater environment can be performed only with the help of professional divers. Offshore divers perform different tasks for the oil and gas industry. HAZMAT and nuclear diving are the most dangerous types of diving as the divers have to handle dangerous chemicals, go into raw sewage or be exposed to radiation. Moreover as the shallow-ocean resources become more scarce the need to reach deeper waters is constantly increasing. The recommended technical diving limit for commercial divers is 100 meters while the maximum depth reached officially is 704 meters and was achieved by the divers of the French company COMEX who specialized in engineering and deep diving operations. To reach this depth the divers were breathing specially formulated gas mixtures and used a special pressurization regime known as saturation diving.

Deep ocean exploration is full of challenges and it is dangerous. New technologies emerged in the quest to provide solutions for these challenges. The technologies available today provide a means of exploring the oceans systematically and in a cost effective manner. Satellite and acoustic communication, sampling devices and live video feeds allow data and information transmission and real time validation by experts. The transition from manned submersibles to remotely operated vehicles (ROVs) came as a result of the need to ensure the safety, efficiency and cost of the missions. A remotely operated vehicle (ROV)

is a tethered underwater robotic system, highly manoeuvrable and operated by humans on a vessel. The system consists of a neutrally buoyant cable that provides the connection between the vehicle and the host ship. This cable is termed the umbilical and consists of a group of cables that provide electrical power, video and data signals between the two ends. Dependent on the task they have to perform the ROVs can have different shapes, sizes and capabilities. An ROV performs tasks based on the commands sent by a human operator. This type of master-slave communication can be subject to delays due to the slow data transmission and for certain tasks experienced operators are required.

To remove the human out of the loop, an artificial intelligence component is added to the system that led to the development of the autonomous underwater vehicle (AUV). These types of robots do not rely on information from an operator and are able to perform the tasks in an independent manner. This makes them an appropriate choice for investigating extreme environments. Autonomous underwater vehicles are slow systems with a navigation speed up to 2 m/s. Due to their geometrical configuration, water currents can decrease the maximum vehicle speed and can lead to navigational drifts. In this case, it is possible for an AUV to change the profile of the mission, making decisions during execution that are based on the data received from the sensors. One of the main applications for the AUV is to sample water columns at depths where humans cannot reach. This represents a cost effective method to study the inshore coastal marine habitats. Detailed maps of the seafloor are obtained using AUVs that can be used in the oil and gas industry to investigate the terrain before building subsea infrastructure or for military applications for reconnaissance and surveillance. The scientific community is interested in improving the AUVs capabilities to obtain systems that have longer autonomy, better sensors and that are capable of reaching greater depths.

Nonetheless, as the AUVs reached the stage of being commercially available the need to adapt them for intervention tasks with the environment emerged. For the oil and gas industry the development and maintenance of the in-situ sites would gain from the use of autonomous systems. Moreover, it is desired to reduce the dangers human divers are subject to and autonomous intervention systems would offer this. An autonomous system able to perform intervention tasks consists of a robotic manipulator added to an autonomous underwater vehicle and is referred to as an underwater vehicle-manipulator system (UVMS) or an intervention autonomous vehicle (I-AUV). These complex systems are characterised by large numbers of degrees-of-freedom and highly coupled dynamics. One of the first systems developed for autonomous intervention is SAUVIM (Semi Autonomous Underwater Vehicle for Intervention Mission) [1], a system developed by the University of Hawaii. The system consists of an autonomous vehicle with three degrees-of-freedom and a seven degrees-of-freedom hydraulic manipulator, having a total dry mass of 6500 kilograms, capable of reaching depths up to 6000 meters. The system was tested in open waters and demonstrated capabilities of underwater surveillance and autonomous manipulation in underwater environments. Nevertheless, due to the large size, the system is difficult to operate and is not able to explore difficult and narrow terrains.

As a solution to these problems lightweight underwater vehicle-manipulator systems have started to be studied. The system consists of a lightweight vehicle and electrical manipulator. For these systems, the weight of the manipulator is comparable with the weight of the vehicle, this leads to a highly complex system. The main challenges of these systems are the station keeping issues encountered due to the coupling effects between the manipulator and the vehicle. Moreover, interaction with the environment using lightweight vehicle-manipulator systems can be highly challenging due to the hydrodynamic effects, uncertainties in the dynamic model, redundancy of the system and difficulties in maintaining vehicle position keeping when interacting with the environment. In these cases, the simple control strategies are not sufficient to perform the desired task and to reduce the coupling effects between the subsystems. The TRIDENT EU FP-7 project proposed a solution for the underwater intervention tasks for different applications using a lightweight system with a total dry mass of 170 kilograms. The scenario starts with a path following survey until an object is detected. The I-AUV starts to move towards a waypoint defined in the vicinity of the object. When this location is reached, the vehicle is set in station keeping and the manipulation task takes place.

The need to perform intervention tasks in the underwater environment is constantly increasing and that led to the development of lightweight underwater vehicle-manipulator systems. Proper understanding of the systems and characteristics is needed before starting to commercially develop these type of systems. Information regarding the dynamic behaviour of the system is important to have a reliable behaviour for the tasks to be executed.

1.1 Thesis Objectives

As previously described there are still limitations to explore the deep oceans. Humans cannot reach the deep oceans as these are life threatening. The use of manned submarines is time consuming, costly and has limited applications. The ROVs can reach the deep oceans but experienced human operators are needed and the tethered cable represents a disturbance as it limits the manoeuvrability of the system. The AUVs solve all these issues and are currently used in industry, research and for military applications. Nevertheless commercial AUVs do not have the capability to interact with the environment. The need to perform intervention tasks in the underwater environment is constantly increasing. Having a system that is easy to manoeuvre, cost effective and has the autonomy capabilities of the AUVs lead to the development of lightweight underwater vehicle-manipulator systems. Before becoming commercially available, proper understanding of the system and its characteristics is needed. Moreover, the control of these systems is challenging as it is subject to disturbances. In this context, the work presented in this thesis aims to offer an analysis of this kind of system and to propose robust low-level controllers that could be beneficial for obtaining reliable lightweight vehicle-manipulator systems. The main objectives are to analyse the behaviour and interactions between the lightweight vehicle and the manipulator, to analyse the system when interaction with the underwater world is taking place and

to provide reliable low-level control architectures for motion and interaction tasks.

This thesis aims to develop control structures for a lightweight vehicle-manipulator system operating in the underwater environment. The focus is to address the problem of the coupling effects between the vehicle and manipulator through the implementation of robust control structures for both motion and intervention tasks. The main challenges in the development of these control strategies are the large number of degrees-of-freedom, the coupling effects between the subsystems and the effect of the hydrodynamic forces on the robotic system. The thesis aims to propose a detailed mathematical model of the lightweight underwater vehicle-manipulator system. It is demonstrated that using the mathematical model in the control architecture of the UVMS achieves robust behaviour of the system. The proposed laws are part of the model based control strategies and are evaluated through a simulation environment developed using the Python programming language and ROS (Robotic Operating Systems) [2]. For visualisation purposes the UWSim (UnderWater Simulator) [3] is used. Several of the control strategies proposed in this thesis have been tested separately with a 5 degrees-of-freedom (DOF) vehicle and a 6-joint electric manipulator in a water tank available in the Ocean Systems Laboratory.

1.2 Thesis Structure

The thesis presents in Chapter 2 an overview of the research available in the area of modelling and control of underwater robotic systems. A survey on the development of the dynamic modelling approach is given. This is followed by a detailed presentation of the studies dealing with the approximation of the hydrodynamic forces that affect underwater robotic systems. An overview of the low-level control architectures developed and used in the robotic community is subsequently reported. Unconstrained and constrained motion control strategies are investigated and comparative evaluations are given.

In Chapter 3 a detailed representation of the dynamic and hydrodynamic modelling is given for an underwater vehicle-manipulator system. The proposed structure to describe the robot is based on a detailed study of the characteristics of the system. This chapter proposes a system where the coupling effects between the vehicle and manipulator can be represented through a mathematical relationship. It is intended to show how the dry mass ratio between the vehicle and the manipulator is directly dependent on the degree of interaction between the two subsystems. Furthermore, through the simulation results it is shown how the effects of the hydrodynamic forces influence the behaviour of the system.

The mathematical computed interaction forces between the vehicle and manipulator are incorporated into a control law for motion tracking in Chapter 4. The control law presented is part of the model based control laws and aims to provide accurate motion tracking for the manipulator and vehicle. Moreover, robust station keeping capabilities for the vehicle are obtained under the effects of the manipulator movement. Through the simulation results it is shown that the control law proposed is able to handle the coupling effects between the subsystems.

Chapter 5 proposes a solution for constrained motion tasks using a lightweight underwater vehicle-manipulator system. A parallel position/force control scheme is proposed together with two different strategies to implement the control law on an UVMS. The control law is developed in the operational space and can be implemented for the overall system (the coupled strategy) or only for the underwater manipulator while the vehicle has a different control law (the decoupled strategy). The chapter aims to evaluate the differences in the behaviour of the system when the two strategies are used and to evaluate the advantages of one strategy over the other.

Chapter 6 shows experimental results using a 6 degrees-of-freedom manipulator for the position/force tasks. The chapter aims to validate the control law described in Chapter 5 for a fixed based manipulator. A comparative evaluation with the impedance control law is presented. The control structure is tested using different environment stiffnesses and a wide range of different goals in the workspace.

The vehicle control strategy used in the decoupled structure presented in Chapter 5 is experimentally tested in Chapter 7. Moreover, an adaptive tuning scheme is proposed to be used with this control structure to reduce the complexity and costs of manual tuning for an autonomous underwater vehicle. The overall control structure is tested in a controlled environment and for the case when the system is subject to wave disturbances. It is shown that the proposed strategy represents a valid option and comparable results are obtained with the manual tuning approach. The final chapter is an overview of the work presented in this thesis, presents the conclusions of this work and suggestions for further work are given.

1.3 Author's Contributions

The main novel contributions of this thesis are in Chapter 3, Chapter 4, Chapter 5 and Chapter 7. The thesis starts with a detailed study of the dynamics and hydrodynamic effects of the underwater vehicle-manipulator system. One of the contributions is to present an investigation into the relationship between the dry mass ratio of the vehicle-manipulator system and the coupling effects between these two subsystems in Chapter 3. A novel control law is proposed in Chapter 4 taking into account the coupling effects between the vehicle and manipulator. The method is validated through simulations. This is followed by a novel control structure for position/force tasks based on the parallel position/force and sliding mode theory. The method is experimentally evaluated using a fixed based manipulator. Furthermore, to the best knowledge of the author in Chapter 5, it is the first time where a comparative evaluation is made for the coupled strategy and the decoupled strategy of implementing the low-level control for an UVMS. In Chapter 7 the novelty is represented by the implementation of an adaptive tuning strategy for the Proportional Integral Limited control structure on an autonomous underwater vehicle and compared to manual tuning.

Chapter 2

Literature review

The study of underwater vehicle-manipulator systems includes the study of the system characteristics, simulating the environment where the system operates and the analysis of real experimental results. A number of factors have to be taken into account such as kinematics, dynamics, hydrodynamic forces, external forces, thruster allocation as well as control methods applied to obtain robust performance.

Having a simulator is beneficial as it can be used to analyse the behaviour of the system, determine the appropriate challenges and help prepare the real experimental set-up. Using a simulation approach to analyse the system is a tool that can be generally valid for different types of system configurations. The simulation environment is described by the kinematic and dynamic models of the system. The kinematic model represents the geometry of the system and the dynamics represent the behaviour of the system, the changes in acceleration, velocity and position with time. In the case of an underwater vehicle-manipulator system the kinematic model can be described in different coordinate systems:

- vehicle base coordinates
- manipulator joint coordinates
- end-effector coordinates

The dynamic model is based on the study of forces, torques and inertias of the system. It provides the behaviour in time, the acceleration the system undergoes when an external force is applied to the system. In other words the dynamic model presents the equations of motion of the system. The dynamic modelling approach involves two different calculations:

- forward dynamics: the acceleration is computed when the input is a force;
- inverse dynamics: the force that needs to be applied to a system is computed so that a certain acceleration is achieved.

The forward dynamics modelling approach is the main structure used in simulating robotic system. The inverse dynamic models are mostly used in control strategies and planning applications.

The control strategies can be defined at different levels:

- low-level control: describing specific individual components of an operation such as navigating to a destination or interacting with the environment.
- high-level control: describes operations where the overall goals are defined based on the specific characteristics of the environment or restrictions applied to the system, e.g. the plan for a robot to pick and move an object out of a room.

This chapter presents an overview of the dynamic and hydrodynamic models used mainly for the underwater vehicle-manipulator systems in Section 2.1 and Section 2.2. In Section 2.3 the focus is on the low-level control architectures available for an UVMS for both free and restricted motions. The interest is on methods and architectures that are directly relevant to the system and the problem under study.

2.1 Dynamic modelling

The study of dynamic models for underwater vehicle-manipulator systems is mostly based on two well known classic techniques:

- the Newton-Euler equations.
- the Euler-Lagrange equations.

A wide number of different approaches were designed based on these two algorithms in order to improve the computational efficiency of the dynamic models or to highlight the interaction forces between subsystems.

The main focus in this section is on the available literature that describes the dynamic modelling of underwater vehicle-manipulator systems. A brief description of the Newton-Euler and Euler-Lagrange equations is presented, followed by a detailed presentation of the available literature where these methods and variations of these methods are used.

2.1.1 The Newton-Euler approach

The Newton-Euler representation of the system is based on the principle of action and reaction, computing linear and angular momentum. The method is regarded as an open form method, due to the fact that interactions between system components are computed. For a system with multiple links/bodies, the Newton-Euler method presents the dynamic equations separately for each of the parts. A closed form dynamic equation can be achieved by eliminating the reaction forces and performing back-substitution.

The Newton dynamic equations states that the sum of forces is equal to the variation of the linear momentum. For a rigid body with multiple links, the Newton equation for link i is given by Equation (2.1), [4].

$$f_i - f_{i+1} = m_i a_{ci} - m_i g \tag{2.1}$$

where f_i is the force applied from link $(i-1)$ on link i, f_{i+1} is the force applied from link i on link $(i+1)$, m_i is the mass of link i, $m_i g$ is the gravity force and a_{ci} is the linear acceleration of the center of mass of link i.

The Euler dynamic equation, Equation (2.2) says that the sum of torques is equal to the variation of angular momentum.

$$\tau_i - \tau_{i+1} + f_i \times r_{i-1,ci} - f_{i+1} \times r_{i,ci} = I_i \dot{\omega}_i + \omega_i \times (I_i \omega_i) \tag{2.2}$$

where τ_i is the torque applied from link $(i-1)$ on link i, τ_{i+1} is the torque applied from link i on link $(i+1)$, $f_i \times r_{i-1,ci}$ is the torque due to force f_i with respect to center of mass of link i and $-f_{i+1} \times r_{i,ci}$ is the torque due to the force $-f_{i+1}$ with respect to the center of mass of link i, I_i is the inertia of link i, ω_i is the velocity of body i and the symbol $\dot{\omega}_i$ is the angular acceleration of body i.

A detailed overview of the iterative Newton-Euler method is given in [5]. The authors start by describing the vehicle dynamic equations in a closed matrix form. The dynamic equations of the manipulator are computed based on the iterative Newton-Euler equations in the base coordinates. The two models are joined together, the manipulator having an initial velocity equal to the velocity of the vehicle. The interactions of the manipulator due to the weight and movement of the links are taken into account in the model as external disturbances. The model properties are presented and a feedback linearisation control technique is briefly introduced. The paper does not present any simulation or experimental results. A similar approach is used in [6] to describe the underwater vehicle-manipulator system. The focus of this paper is on the control method rather than on the dynamic modelling. Dunnigan *et al.* [7] present a detailed description of the system dynamics and the focus of the paper is on the study of the interaction forces between subsystems. The authors show that for their particular system, a vehicle with 6 degrees-of-freedom and a 3 link manipulator, the coupling effects mostly affect the yaw DOF. Having a reliable control technique for this DOF means that the end-effector accuracy can be improved.

2.1.2 The Euler-Lagrange approach

The Euler-Lagrange representation is an energy-based, closed form method, providing the acceleration of the system based on the generalized forces acting on the system. This approach is based on the computation of kinetic and potential energy, the robotic system being considered as a single system. The Euler-Lagrange approach does not provide an explicit formulation of the internal reaction forces, closed-form equations being obtained.

The Lagrangian equation is presented in Equation (2.3). Based on the least action principle of Hamilton and the virtual work principle, the Euler-Lagrange equation is presented in Equation (2.4).

$$L(q, \dot{q}) = K(q, \dot{q}) - P(q) \tag{2.3}$$

$$\frac{d}{dt}\frac{\partial L}{\partial \dot{q}} - \frac{\partial L}{\partial q} = \tau \tag{2.4}$$

where K is the kinetic energy of the system, P is the potential energy, q and $\dot{q}$ are the position and velocity of the system, τ is the generalized force performing the work on the joint q.

As presented in [8], the Euler-Lagrange method is advantageous to be used for underwater vehicle-manipulator systems as it is easily accessible to researchers, being extensively used in field robotics. Furthermore, it is an energy based method and can be extended to include new subsystems. Nevertheless, the authors argue that expressing the Lagrangian in terms of velocities in inertial frames for an underwater vehicle-manipulator system is not convenient. This is because the manipulator is placed on a moving base and not fixed on an inertial frame. A quasi-Lagrange approach is proposed, having a similar formulation as the classical Lagrange-Euler method. The equations of motion are generated in this case in a body-fixed, noninertial frame. The same method is used in [9] for an UVMS system in order to determine the constraint dynamics and apply passivity-based position/force control methods. The authors argue that for obtaining simultaneous tracking of contact force, posture and operational position of the manipulator, the Lagrangian form provides good results, due to its characteristic in preserving passivity when the arm end-effector interacts with other planes. The unified dynamics of an UVMS are modelled through a quasi-Lagrange approach further in [10], [11]. The aim of the papers is to present a coupled dynamic model and control strategy to achieve the desired end-effector configuration.

2.1.3 Alternative approaches

Variations of the two methods presented previously are available in the literature. These are developed either to improve the computational complexity or to fit the requirements of a specific application.

In [12] the author aims to incorporate the advantages of both the Newton-Euler algorithm and the Euler-Lagrange method in a new method named Kane's model. The interaction forces from the Newton-Euler algorithm are eliminated as well as the energy function used in the Euler-Lagrange method. An advantage of this method is represented by the possibility of direct integration of the environmental forces into the model. The authors present the dynamic model for a 6 DOF vehicle and a 3 DOF arm. The authors argue that the dynamical model presents useful information to study the behaviour of the system. Further developments of this approach are presented in [13]. An example of a vehicle with two manipulators is used in the paper and the dynamics of the system are represented based on Kane's method. The goal of this work is to use coordinated control for the manipulators based on the dynamic model. The mathematical representation of the system provides the necessary means to understand and evaluate the behaviour of the system. The control strategy is based on a nonlinear feedback model, the main goal is to achieve coordinated control between all subsystems. The authors present results that validate their method for representing the system and for controlling the coupled vehicle-manipulator system.

The vehicle-manipulator dynamics classically described by a Lagrange-Euler approach

is re-written based on Lie group theory and the generalized Lagrangian method in [14]. The goal of the paper is to present a framework that reduces the gap between representation of the dynamic model of the manipulator and the model of the vehicle. The manipulator dynamics are presented based on the Lagrange approach. The dynamic equations are represented based on a set of configuration states, a vector of velocity states and different mapping configurations between the two sets. In the paper the vehicle dynamics are represented based on the Lie group topology. The method proposed in this paper has as its main feature the avoidance of singularities. The authors argue that the system proposed has the same complexity as classical methods used to design the model of an UVMS and it is easier and more appropriate for simulations.

In [15], the author presents the rigid-body dynamic algorithms, Composite Rigid Body Algorithm and Articulated Body Algorithm, based on a spatial vector notation. The Composite Rigid Body Dynamics algorithm is an inertia matrix method where first the elements of the inertia matrix are computed and then the obtained matrix is factorized to solve a set of linear equations for obtaining the accelerations. The Articulated Body Algorithm is a propagation method where the coefficients of the equations are computed and then propagated to the neighbouring bodies. In [16] Hosseini *et al.* use the Composite Rigid Body Algorithm (CRB) for simulating an underwater vehicle equipped with multiple arms. The authors have taken into account the hydrodynamic modelling as well as the thruster dynamics and have considered the vehicle as the reference link, having a six degrees-of-freedom joint. The system is represented as a tree-structure. The method presented in the paper to compute the dynamics starts by defining the inertia matrix and the inverse dynamics are computed based on the recursive Newton-Euler equations. In the last step of the algorithm, the acceleration of the system is computed. The simulation results presented in this paper show that the simulation platform provides a clear description of the coupling effects between the two subsystems. It has to be mentioned that this method is straightforward and represents the simplest method to compute the inertia matrix [15]. The Articulated Body Algorithm (AB) is used in the paper of McMillan [17] to simulate an underwater vehicle with a robotic manipulator. Similar representation and hydrodynamic parameters as in Hosseini [16] were made. The algorithm has three parts: in the first part the velocity of each link is computed, in the second part the inertia matrix is computed and in the last step the acceleration is computed. The paper contains the framework presentation, no simulation results are presented. The advantage of this method is the low computational complexity. The authors argue that it is the fastest method to compute the forward dynamics based on a kinematic tree representation but it is also a more complex method than the CRB method.

The principle of dynamic balance is used for underwater vehicle-manipulator systems in [18]. The principle of dynamic balance, as defined in [19], is useful to describe interacting multi-body subsystems based on the notion of composition of subsystem dynamics. The assumption that individual dynamics are known is made and the challenge is to express accurately the interaction between subsystems. The kinematic and dynamic representation is made through the notions of twists and wrenches. The body twist is the equivalent of the

velocity and the wrench is the equivalent of force when analysing the kinematics and dynamics. The authors argue that using twist/wrench definition of the system is advantageous as it provides a compact formulation of dynamics and expresses the behaviour of the system directly at a twist level. The composite dynamics is based on the d'Alembertian concept which suggests to consider the dynamic balance between the wrenches and torques of the subsystems. The expression is based on the kinematic constrains, restricting the subsystem interactions.

A Bond graph model is used for an AUV and manipulator system in [20]. The authors argue that the Bond graph is a suitable method to design the dynamics of the system as it highlights the interactions between the AUV and manipulator. The Bond graph represents a graphical description of the dynamic system. The arcs in a bond graph are bi-directional and represent exchange of energy. The arc links are either single-ports, double-ports or multi-ports. The paper starts by designing independent bond graphs for the vehicle and for the manipulator. In the second step, the integration of the two models considering the interactions between the subsystems is performed. The advantage of this method rests in the fact that the physical interactions are modelled based on the power, effort and flow of the junctions (velocities) of the system.

In Table 2.1 a comparison of the methods used for dynamic simulation of underwater vehicle-manipulator systems is presented. Dependent on the characteristics of the system and the applications the robot has to solve, any of the methods can be used to mathematically represent it. For the cases when a single body robot is considered or when the coupling effects do not need to be known, the methods that provide closed form representation are indicated. Furthermore, if the model is intended to be used in the control structure or the computational capabilities of the system are low then one has to consider the implementation complexity. Based on this and taking into account that one of the goals of this research is to analyse the behaviour of the vehicle subject to disturbances provided by the manipulator, the dynamic model used in this research should provide the interaction forces between the two subsystems and should be able to provide the recursive and closed form of the system.

2.2 Hydrodynamic modelling

Hydrodynamic forces are highly important in the development of an underwater vehicle-manipulator system model. Proper knowledge of the hydrodynamic effects creates a reliable dynamic model that can be used as a realistic simulation of the system. Inaccuracies in the hydrodynamic parameters create discrepancies between the real system and the simulation. This can lead to an unreliable model that is not optimal for developing control architectures for the underwater vehicle-manipulator system. The impact of the hydrodynamic effects represents a challenge that has to be taken into consideration when designing the control system. The hydrodynamic effects considered for the underwater vehicle-manipulator system are:

Properties	Methods							
	EL	QEL	NE	KM	DB	BG	CRB	AB
Closed form	•	•		•			•	•
Recursive form			•		•	•	•	•
Single body representation	•	•		•				
Multiple body representation			•		•	•	•	•
Subsystems interaction forces			•		•	•	•	•
External forces	•	•	•	•	•	•	•	•
Implementation complexity	$O(n^4)$	$O(n^4)$	$O(n)$	$O(n)$	$-$	$-$	$O(n)$	$O(n)$

Table 2.1. Dynamic model algorithms, where EL is Euler-Lagrange, QEL is Quasi Euler-Lagrange, NE is Newton-Euler, KM is Kane's Method, DB is Dynamic Balance, BG is Bond Graph, CRB is the Composite Rigid Body and AB is Articulated Body

- added mass - due to inertia of the surrounding fluid
- damping effects: drag, lift, side forces - due to vortex shedding
- restoring forces: weight and buoyancy

When a rigid body is accelerating or decelerating in a fluid, the body must move some of the volume of the fluid with its motion. The weight added to the system based on this represents the added mass. The added mass force opposes the motion of the system and can be observed in more than one direction. The added mass force in one direction can be caused by the motion of the system in the other direction. For a body in motion, the added mass force acting on the body can be expressed by Equation 2.5 and the added mass moment is defined by Equation 2.6, [21].

$$F_j = -\dot{U}_i m_{i,j} - \varepsilon_{j,k,l} U_i \Omega_k m_{j,i}, \quad i \in \{1,\cdots,6\} \quad j,k,l \in \{1,2,3\} \tag{2.5}$$

$$M_j = -\dot{U}_i m_{j+3,i} - \varepsilon_{j,k,l} U_i \Omega_k m_{i+3,j} - \varepsilon_{j,k,l} U_k U_i \Omega_k m_{l,i}, \quad i \in \{1,\cdots,6\} \quad j,k,l \in \{1,2,3\} \tag{2.6}$$

where F_j is the force in the j direction, M_j is the moment in the j direction m_{ij} is the added mass in the i direction due to a unit acceleration in the j direction, U_i is the translational velocity in the i direction, Ω_k is the rotational velocity in the k direction. $\varepsilon_{j,k,l}$ is the alternative tensor defined as:

$$\varepsilon_{j,k,l} = \begin{cases} 0, & \text{if any } j,k,l \text{ are equal} \\ 1, & \text{if } j,k,l \text{ are in cyclic order} \\ -1, & \text{if } j,k,l \text{ are in anti-cyclic order} \end{cases} \tag{2.7}$$

When the rigid body moves in the water the object is affected by the drag force which acts in parallel to the direction of fluid flow and the lift force that has a perpendicular orientation to the direction of movement of the flow. The lift and drag forces are defined

based on the lift and drag coefficients using the following relations, [22].

$$F_L = \left(\frac{1}{2}\rho_w v^2\right) C_L A_L \tag{2.8}$$

$$F_D = \left(\frac{1}{2}\rho_w v^2\right) C_D A_D \tag{2.9}$$

where ρ_w is the fluid density, v is the speed of the fluid, A_L and A_D represent the area of the object and C_L and C_D are the lift and drag coefficients. A detailed study of methods to compute these coefficients is given in the next chapter.

When an object is introduced into a fluid, its surface is subject to pressure. Based on Archimedes' principle the resultant force that acts on an object due to pressure can be computed with Equation 2.10.

$$B = \rho_w g V_l \tag{2.10}$$

where ρ_w is the density of the fluid, V_l is the volume of the object. The force is applied at the center of buoyancy of the submerged object. The centre of buoyancy is computed based on the centre of mass of the displaced fluid.

Even though the physics that describe the hydrodynamic forces are straightforward, the computation of the hydrodynamic parameters is much more challenging. The coefficients can be extracted either from experimental studies or through mathematical modelling.

System identification techniques are the main type of experimental validation of hydrodynamic parameters used for underwater vehicles. In the work of Ross *et al.* [23] a free decay test is used to obtain the drag and added mass coefficients for an underwater vehicle. The parameters are identified for all degrees-of-freedom and the system is studied based on decomposition of the system into two different subsystems: lateral and longitudinal. A camera system is used to obtain the state measurements. The vehicle is actuated using a spring system and then system identification techniques are applied to the measured data to extract the added mass and linear damping of the two subsystems. The obtained data is validated in a simulation environment. Even though in the simulation the system converges to the obtained parameters, the system has to be tested with a real experimental system. In [24] the authors use the free decay test to estimate the parameters and the spring oscillation is replaced by a pendulum movement. To reduce experimental studies and simplify the set-up, the authors propose the use of a scaled down model. This model is assumed to have a pendulum movement: it is set to oscillate, but due to the hydrodynamic forces the amplitude of the oscillations will decrease over time. Based on the on-board sensors, the parameters are measured. Having these parameters for the reduced model, laws of similitude are used to scale the parameters to the normal manipulator size.

The hydrodynamic effects between a vehicle and a manipulator are studied in the work of McLain [22]. The study is based on an experimental setup, where a cylindrical single link manipulator is attached to a small vehicle. The main finding in this study is the fact that the added-mass coefficients and drag coefficients for the manipulator link are not only

dependent on the shape and physical properties of the link but also on the distance travelled by the link. This work represents a step forward in modelling the hydrodynamic effects due to the fact that the coefficients are no longer considered as constant. Further developments are presented in the work of Leabourne [25] where a two-link manipulator hydrodynamic model is based on the analysis of three-dimensional flow effects. The author argues that the existing dynamic model of manipulators are in error by 25% when applied to a practical underwater manipulator. Small accelerations of the manipulator are considered in this paper. This assumption is used for using constant added-mass coefficients. The work is focused on drag coefficients, considering that they are the dominant hydrodynamic effect and the most challenging to model. After experiments it is concluded that the drag coefficient is dependent on the angle between the first and second link, as well as the distance travelled by each link and the geometry of the body.

Mathematical models are also used to extract the coefficients of the hydrodynamic parameters. In [26] the hydrodynamic forces for an underwater manipulator are derived using the Navier-Stokes equations. To compute the hydrodynamic coefficients, the following assumptions are made: the velocity of the manipulator is slow, each link has 3 axes of symmetry and the geometry of the links is approximated through cylinders. For the drag coefficients the ratio between the viscous force and internal forces is used. The effects of the underwater currents are analysed based on simulations in [27]. Using the continuum mechanics approach and numerical simulations the authors propose a model for the underwater currents that is rotational and turbulent. The paper studies two behaviours: the effects of the change in the underwater currents direction and the effects of changes in the speed of the underwater currents. These effects are studied from the point of view of the changes in joint torques. The authors argue that changes in the current velocity determine changes in the load of the joints that can affect the control of the system. Furthermore, small changes in the direction of currents can influence the joint torque required to maintain the position of the arm.

Fossen [21] assumes that the hydrodynamic forces and moments that affect a remotely operated vehicle (ROV) can be linearly estimated. Assuming that the vehicle is fully submerged and has a decoupled structure, the added mass is represented as a diagonal matrix. In the case when the system is highly coupled, the added mass becomes a full rank matrix. The elements of the matrix are computed based on the shape and physical characteristics of the vehicle. Morrison's equation [28] is used to compute the viscous damping force. The damping coefficients are computed based on the Reynolds number and vehicle shape. A similar approach is used in [17] where the authors present the computation of the hydrodynamic forces applied to an underwater vehicle-manipulator system. The force due to added mass is presented and the drag and force moments are computed based on the surface integral. The added mass coefficients and drag coefficients are considered constant. The authors state that the coefficients are coupled and difficult to compute. This represents the main reason why they assume that constant coefficients are an adequate choice. Levesque *et al.* [29] studied the computation of hydrodynamic drag and local buoyancy. The goal

of this research is to efficiently develop a simulation platform for a manipulator system. The authors used the geometry of the system and based on numerical integrations the drag coefficients are computed. The buoyancy of the system is computed based on Archimedes rule.

In [30] the authors present the hydrodynamic modelling of an underwater vehicle-manipulator system based on a simulated environment. The system is an underactuated system, having a 6 DOF manipulator attached to a spherical vehicle. The main contribution of this paper rests in the study of the shadowing effects and their influence in the development of the hydrodynamic model. At the moment when one link moves towards the next link, a shadow is created over the current link. The term shadow is described as a region of the link, computed based on the angle between the current link and its neighbour. The authors argue that the shaded part should not be considered in the computation of the hydrodynamic effects.

Simplifications are made when modelling the hydrodynamic effects based on mathematical models. Both the vehicle and manipulator are approximated with simple geometrical shapes such as cylindrical or spherical shapes. This reduces the complexity of the hydrodynamic parameter estimation but might be seen as a disadvantage when creating an accurate simulation of a real system. Most of the commercially available manipulators are not represented by cylinders, but through more complicated geometric representations.

2.3 Low-level control structures

The principal actions a robotic system has to perform are focused on variations of the following tasks: the robot moves freely in the environment, the robot is in contact with the environment performing a specified operation and return to home position. The approach that is normally followed is to design a high-level controller that generates position or velocity set-points and a low-level controller that fulfils these conditions. In this thesis the focus is on the design of the low-level type of controllers and a study of the literature is made for these types of controllers.

The evaluation of the system can be made based on the quality of the task execution (e.g: velocity and position errors or energy requirements) and based on the robustness of the system (e.g. changes to environmental disturbances). The limitations that the low-level controllers have to take into account are:

- low execution speed (limited bandwith)
- uncertainties in the dynamic model
- compliance of the robot

The control methods can be differentiated based on the different characteristics as presented in [31]:

1. Dependent on the desired application:
    - position control - a desired position is requested
    - force control - a desired force is requested
2. Dependent on the coordinate system:
    - joint space control
    - task/operational space control
3. Dependent of the approach used:
    - hard-control - model/stability based
    - soft-control - heuristic methods

Based on these possible actions the low-level control strategies can be divided into two main categories:

- control for unconstrained motions - position control
- control for constrained motions - position and force control

2.3.1 Unconstrained motion

When the robot moves freely and no constraints are imposed by interaction forces, position/tracking controllers are used to fulfil the task.

Joint space control

The control methods are designed in the joint frame and the goal is to obtain the configuration of each joint as close as possible to the desired configuration. In most cases the desired configuration is given in operational space coordinates and inverse kinematics computation is needed to correlate both spaces.

Task space control

The coordinate frame attached to the end-effector of a manipulator is called task space. In most cases the desired trajectory/task is given in task space and the control law is designed in this space, computing the necessary force to perform the desired application. The joint torques/vehicle forces for an underwater vehicle-manipulator system are computed based on the pseudo-kinematics transformation using the transpose of the Jacobian. A task space approach is used in [32] for position keeping of an underwater vehicle-manipulator system in the presence of ocean currents. Singularities in the vehicle configuration are avoided using a quaternion based representation [1]. An attitude control scheme is designed using quaternions in [33], [34].

Hard control

The most simple and used type of controller in industry are the PID type (Proportional-Integral-Derivative) and derivatives of it such as the PI controller or the PD controller. These can be implemented independently in the joint space or in the task space. The controller is based on computing the error between the measured value and the desired set-point. The PID controller has proved to be efficient for set-point control of land manipulators [35]. These type of controllers have been widely analysed. The tuning of the system is possible based on the system parameters or on the analysis of the tracking error. It is shown that by choosing appropriate gains the position tracking error can be bounded [36]. The main advantages are the simplicity and the feasibility of the method. For complex nonlinear systems the PID controller without appropriate tuning based on the environment and system information does not present robust behaviour to changes in the environment [37]. In underwater applications the classic PID controllers are mostly applied in point-to-point motions. In [38] a PID controller with anti wind-up integration is presented. A cascade position-velocity controller is used and separate controllers are defined for each degree-of-freedom. The simulation set-up uses a 5 DOF vehicle and a 3 DOF arm. The paper shows good results for body position control of the AUV with small oscillations in the orientation of the vehicle when changes in the payload of the system takes place. To track a reference trajectory a nonlinear PID controller is proposed in [39]. The overall structure of the control loop consists of a PID controller, a feed-forward controller and an uncertainty estimator. Simulation tests have been performed where a 3-link underwater manipulator has to follow a certain trajectory in the presence of uncertainties. The validity of the method is demonstrated by comparison with a classical PID controller where the proposed strategy improves the error accumulation. Classic PID controllers are used by McLain in [22] for a dynamical coordinated controller of a vehicle with a one link manipulator. Separate PID feedback controllers are applied to the vehicle and manipulator acting based on the prediction of the interaction forces between subsystems. Real experiments are performed and the results show that predicting the interaction force between the two subsystems can improve the behaviour of the controller with small increase in the control effort.

Torque-based control techniques are used for trajectory tracking tasks. The computed-torque technique is based on the dynamic model used as the compensator of the system [40]. In practice, disturbances can perturb the behaviour of this type of controller: the initial state differs from the desired trajectory, inaccuracies and unmodelled dynamic parameters or uncertainties in the system payload. Due to all these uncertainties in the system, a feedback component has to be added to the controller architecture to obtain a stable behaviour. Inverse dynamics control and a PD controller is presented in [41], where simulations are performed with a 3-link manipulator. Inverse dynamic models are used in [12], [13] to obtain a linearisation of the underwater system. A system consisting of a 6 DOF vehicle and a 3-link manipulator is simulated and the results of the feedback controller with linearisation of the system is presented. The authors argue that the performance of the system degrades

if the dynamics are not taken into account in the control architecture. In [30] an inverse dynamics control algorithm is presented for the trajectory-tracking of the end-effector of an underactuated underwater UVMS. The authors claim that using the proposed method eliminates the uncertainties and disturbances in the underwater environment. The steady-state errors in the simulation results are small and it is argued that they can be reduced at the expense of an increase of the control effort.

In robust control the robot is treated as an unknown system, the only information that can be obtained being the order of the system based on the analysis of the system response. This type of control is designed to achieve stability when the modelling errors are bounded. In uncertain conditions, inverse dynamics control represents an approximation of the robot and the system remains nonlinear. In this case an external robust control term should be added to the control architecture. Robust control is based on the theory of guaranteed stability for linear uncertain systems [42]. These methods are based on Lyapunov stability analysis as presented in [43] and [44]. The main disadvantage is that the control law is discontinuous and can be difficult to implement due to the chattering effect. For underwater vehicle-manipulator systems the most used type of robust controller is sliding mode control based on a discontinuous function. Implementing this function in discrete-time the control signal switches between different values, the chattering effect characterises this type of architecture. In [45] a sliding mode controller is proposed for an underwater vehicle-manipulator systems to avoid kinematic singularities. To ensure that no singularity is present in the orientation of the vehicle, the attitude controller is designed based on a quaternion representation. The simulated scenario consists of a vehicle in station keeping mode and a two-link manipulator commanded to reach a desired position. The results show that the interactions between the two subsystems mostly affects the roll DOF of the vehicle due to the UVMS configuration. Nevertheless, the task is completed successfully with smooth control effort. A sliding mode controller is used in [46] for an underwater gripper. In this case only mono-directional control actions are considered. The challenge is the approximate relationship between the electrical input signals and the mechanical outputs which is considered as an uncertainty. Due to this the authors argue that the sliding mode controller is an appropriate choice for this system. A model based sliding mode controller is used in [47]. The system is analysed using an underwater manipulator performing a trajectory tracking task in a test tank. A comparative study of the proposed methodology with a PD controller shows the validity of the control architecture. In the results presented in the paper, the steady-state error using the sliding mode controller is smaller than the case when the PD controller is used. It has to be noted that the gains used for the PD controller are considerably smaller than the ones used for the sliding mode controller. The authors motivate their choice by the fact that high PD gains will cause oscillations, reducing the performance of the system. A similar dynamic sliding mode controller is used in [48]. The system is composed of a 3 degrees-of-freedom vehicle and a 3 degrees-of-freedom manipulator described in a planar plane. The authors present a redundancy resolution approach to minimize the restoring forces that affect the vehicle. The results presented in simulation

show that the end-effector tracks the desired trajectory represented by a straight line with a small error. It has to be noted that at the beginning of the simulation a large pitch angle is observed but is rapidly compensated for.

Adaptive control is an area of control theory covering automatic adjustment of controllers in real time in order to maintain constant performance of the system when uncertainties are present in the dynamic model. The principle methodology applied in this case includes a linear parametrisation of the dynamic model and a nonlinear control law based on the dynamic parameters. Uncertainties in the kinematic and dynamic model of a manipulator have been studied in [49]. A separate kinematic adaptive law and dynamic adaptive law are used in the control architecture together with a sliding vector component. The adaptive control law proposed ensures asymptotically trajectory tracking in task space. In an underwater scenario the adaptive control can be advantageous as there are a wide range of parameters that are difficult to estimate. In [50] uncertainties in the model are caused by partially known characteristics of the thrusters of a 6 DOF vehicle. A combination of sliding mode control and an on-line estimation algorithm is used to compensate for the uncertainties in the system. The results show that all tracking errors converge to zero in the presence of uncertainties in the system. In [51] an adaptive non-regression controller together with a disturbance observer is presented. The disturbance observer aims to linearize the nonlinear dynamic system. The adaptive controller compensates for the disturbances that the underwater environment can have on the vehicle. The authors compare a PID and disturbance observer controller with the adaptive-disturbance observer controller. The adaptive method presents better results, the steady-state error being smaller and smoother than in the case when the PID-observer controller is used. An adaptive compensation of the dynamic model is presented in [52] together with a PD compensator. The authors argue that the proposed method guarantees null steady-state error in the presence of constant external disturbances and partial knowledge of the dynamic model. Experimental results are presented using the ODIN vehicle in a swimming pool where disturbances to the system are created by a pump that circulates water. The currents are strong and affect the vehicle dynamics, nevertheless the proposed controller can compensate for these disturbances. An adaptive non-regression method is presented in [53] for an underwater vehicle-manipulator system. The authors design separate controllers for the vehicle and manipulator and propose combined path-planing. An adaptive method where the gains are tuned adaptively based on the components of the controller is proposed. Computer simulations are performed with the ODIN vehicle and a 3-link manipulator. The system has to follow a desired trajectory for two cases: (i) when joint limits are included as a restriction of the system and (ii) when the joint limits are not included. In both cases the end-effector adapts to the trajectory and the steady-state error decreases in time.

Soft control

Neural network control is based on the network ability to learn the characteristics of the system by weight adjustment. Neural network theory allows the computation of the nonlinear model of the system that can lead to successful control. In [54] the neural network approximates the dynamics of the UVMS for each degree-of-freedom and this approximation is integrated into the control law. The neural network is trained based on sinusoidal trajectories for the system. The simulation results present a comparison between a PD controller and a PD plus neural network compensator, the latter one outperforming the first controller. Further simulations consider the case when the payload of the system is increased by two kilograms. The neural network controller achieves a steady stable behaviour being robust to payload variations. In [55] the authors present a neural network compensator with a sliding mode controller for an underwater manipulator. The authors argue that using a neural network compensator has the advantage of reducing the difference between the sliding surface and current state necessary for obtaining a good system behaviour when the sliding mode controller is implemented. The simulation shows the behaviour of a two-link manipulator in an underwater environment. The accuracy in estimating the system dynamic parameters is up to 70% of the real system parameters. The uncertainty is reduced by using the neural network compensator. An adaptive controller based on the neural network has been developed in [56]. The controller has a learning part where the dynamic model of the system is simulated and integrated in the final controller. The controller is applied for heading control of an underwater vehicle and the experimental results show that the proposed architecture keeps the vehicle on the target direction. The authors argue that the system is robust to changes in the dynamic parameters.

Fuzzy logic controllers are based on heuristic rules. The main idea behind these types of controllers is to incorporate expert-knowledge in controlling a process whose input-output relationship is described by a collection of IF-THEN rules. In [57] a fuzzy model-based controller for an underwater vehicle is designed. The system takes into account the thruster dynamics. The Tagaki-Sugeno-Kang fuzzy model for the dynamic system is used and the control law is developed based on the corresponding rules. Simulation results are presented for an underwater vehicle, the steady-state error being small over a wide range of thruster operations. Cases when the thrusters do not function at full capacity are studied. The fuzzy-model based controller presents good performances being robust to external disturbances. The control of an underwater manipulator is studied in [58]. A fuzzy model based controller is implemented and tested through simulations. The proposed control architecture learns how to control the nonlinear system and produces good tracking results in the presence of external disturbances such as the wave disturbances and underwater currents. A feedforward controller designed as a self-adaptive recurrent neuro-fuzzy controller is used in [59] together with a PD feedback controller for an autonomous underwater vehicle. The controller is designed based on two phases: (i) inverse dynamic modelling and (ii) feedback error learning. A recurrent neuro-fuzzy architecture that includes the dynamic elements of

the system is used so that each state corresponds to a fuzzy rule that linearly combines the firing history and those of the other rules. Computer simulations have been performed with the ODIN vehicle showing the proposed algorithm outperforms an adaptive controller with feedforward neuro-fuzzy control.

Briefly discussed in this section but closely related to the high-level control strategies are the methods in the reinforcement learning group. In the learning control methods the system has generic optimization goals and it is allowed to fail during the learning process. For a robotic system that has to execute a required task the robot has to find an appropriate control policy and provide commands that represent changes in the task requirements. Learning control is characterised by direct and indirect methods, by the learning method used and by the type of task the system has to achieve. In [60] a reinforcement learning approach based on Q-Learning is used to coordinate and control the thrusters of an underwater vehicle. In [61] Reinforcement Learning Direct Policy Search is used to learn the action mapping of the behaviour of the underwater vehicle based on the direct-gradient algorithm. The algorithm was tested through simulations with a 5 DOF vehicle, the results presenting a low convergence speed towards the desired solution. Underwater manipulation is performed through iterative learning control and time-scale transformation in [62]. This represents a time optimal control strategy for a trajectory tracking task. The algorithm is tested with a 3 DOF manipulator through underwater experiments. Based on the obtained results the authors argue that the proposed method provides robust behaviour and is more accurate than classical methods.

2.3.2 Constrained motion

Constrained motion control describes the control of a robotic system where trajectory tracking of a system is restricted by the contact of the robot with the environment. In most cases a position controller is implemented to satisfy the trajectory requirements and a force controller is needed to maintain appropriate interaction.

For these types of applications either a switching capability is available to pass from trajectory control to interaction control or one of the tasks is controlled indirectly through the other. Controlling interaction with the environment requires a good knowledge of the robot dynamic model as well as an accurate model of the characteristics of the environment [63]. This is rarely the case and using similar methods for both position and force control may be inefficient as free movement control assumes that the uncertainties present in the model are external disturbances and have to be eliminated. Several approaches to control both position and force in robotic systems are available in the literature. Most of the applications are based on using either fixed robotic manipulators or mobile manipulators. The main groups of position/force control are:

- impedance/admittance control
- hybrid control

- parallel control

Based on these control methods, new strategies have been used as position/force controllers. Robust or adaptive components have been added to solve uncertainties in the systems. In the following part a detailed description of all these methods is presented.

Research in the area of position/force control of underwater vehicle-manipulator systems is at an early stage. Most of the available literature is based on the classic types of force control: impedance or hybrid control. The difficulties encountered in the interaction between the UVMS and the environment include uncertainties in the model knowledge, the hydrodynamic effects, redundancy of the system, the coupling effects between the manipulator and the vehicle and the effects on the vehicle station keeping when interacting with the environment.

Impedance and Admittance control

Impedance/Admittance control is based on the dynamic relationship between the position and force variable, controlling one of them through the other. If a desired force is required and the motion of the manipulator is controlled based on the force-motion assignment, admittance control is used. This is either used as classic admittance control in [64], [65] or presented together with adaptive strategies to solve the uncertainties in the dynamic model [66], [67]. The admittance controller is shown to have a good performance for contact control tasks.

In the case when the force required to interact with the environment is set based on the desired motion trajectory, the system is under impedance control. In this type of control the desired behaviour of the system is specified through a generalized dynamic impedance. The impedance controller is used especially when the contact forces are not mandatory to be accurately regulated, while for admittance control they have to be very well specified. The behaviour of the system is presented in the task space, but the impedance control implementation is in most cases done at robot joint level. The main advantage of impedance control is that when tuned appropriately, it can imitate the behaviour of the human hand. It can give fast and stiff response in free motion but avoids large impact forces with the environment. Starting with Hogan *et al.* [68], the impedance controller is one of the most used controllers as it presents a robust behaviour to uncertainties [63]. Developments of this type of controller include a robust impedance controller [69], [70] or an adaptive impedance controller [71], [72].

In [73] a modified impedance controller is presented as an alternative to the parallel position/force controller. The controller is modified to be able to control both position and force based on the reference values. A variable impedance is added to the system that takes into account the force squared error. The parameters of the controller are generated based on a minimization function for creating a robust controller. The simulation results show that the method can be used as an alternative for parallel control. A fuzzy approach is used to switch between an admittance controller and a force controller when the task is to reach an

object and apply a constant force to it [74]. The simulation results present the advantages of fuzzy logic for switching between controllers.

In [75], the authors present an impedance controller considering the UVMS as a single dynamic system. The authors argue that this type of control is appropriate as the motion of the end-effector is slow. Simulation results were shown with a 6 DOF vehicle and a 3 DOF manipulator in contact with the environment while sliding down a surface. Good results are obtained using appropriate tuning for the impedance control. The contact force did not have a significant effect on the vehicle as the contact forces are small and the mass of the vehicle is large (1073 kg in air). Multiple impedance controllers are used in [76]. The goal is to move a heavy cylinder and put it in an underwater structure using two manipulators mounted on a moving base. The multiple impedance controller approach is based on enforcing the same impedance behaviour on all the parts that contribute to the manipulation. The authors consider uncertainties in the dynamic model of the UVMS that are treated as disturbing forces/moments. In the simulation results, the authors present good trajectory tracking and robust contact with the environment. The controller is able to compensate for the uncertainties in the model.

Hybrid position/force control

Hybrid control is based on the assumption that the environment imposes either a position constraint or a force constraint to the manipulator [63]. The hybrid control approach considers the task that has to be performed by the robot can be defined in two separate orthogonal and complementary directions covering the 6D space. As initially presented in [77], the assumption that characterises the hybrid approach is that if contact with the environment is happening in n directions, where $n \leq 6$, then the free motion of the end-effector is available in the rest of the $6-n$ directions. The control of the system is based on the separation between the two type of constrains: the contact force at the end-effector is controlled in n axes and the position of the end-effector is controlled in $6-n$ axes. After the task to be solved is set, a selection matrix is defined for each degree-of-freedom that sets for each of the end-effector axes if the position or the interaction force is under control. The selection matrix is defined taking into account the model of the manipulator, the action that has to be performed and the characteristics of the environment where contact takes place. One disadvantage of the basic hybrid control is that the behaviour of the system is pre-planned and cannot be changed during execution of the mission [77]. This is due to the fact that the selection matrix is defined before the start of the execution of the task. By adding a higher level artificial intelligence component this limitation can be removed and it would be possible to modify online the selection matrix during the execution of the task. Another disadvantage is in the case when the initial interpretation of the system is not correct and the system can require force control in the free environment or position control even if contact occurs. Task space is the most natural type of control for this approach, [78], [79], taking into account the information from the force and position sensors [77]. Hybrid con-

trol has developed during the years by adding an adaptive part to the system or considering unknown environments [80].

The paper of Bechlioulis *et al.* [81] presents hybrid control, taking into account a transformed error. The new errors are based on the predefined performance indices. The results show that while classic hybrid control loses contact with the environment during transient behaviour the proposed method is able to maintain contact. Moreover, the overshoot for this new controller is maintained between the requested boundaries. Adaptive fuzzy hybrid position/force control is used for manipulators mounted on oscillatory bases in [66]. An oscillatory base creates an unknown dynamic model and the system can perform poorly. With the control method proposed, the authors present good results for both path following and for damping the oscillations to zero. The authors state that the fuzzy controller is responsible for reducing the coupling motion of the overall system.

In [82] a hybrid position/force control strategy is presented for a hydraulic manipulator. Simulation and practical results are presented and good results are obtained. Hybrid control was used in [83]. The goal of the paper is to present a method to improve the behaviour of the ROV when the manipulator is in contact with the environment. The authors state that the main challenge in controlling the effects of the arm on the vehicle is to estimate the torque produced by the manipulator on the platform. The authors propose the use of a sensor placed between the two subsystems which produces the information used to design an internal force controller. This force control is beneficial to correct the command for the thrusters of the vehicle. The simulation results presented in the paper display a good stable response for the vehicle. A free-floating base with a manipulator is presented in [84]. Restoring forces produced by the thrusters are used to compensate for the interaction forces between the manipulator and the environment as well as the interaction forces between subsystems. The goal is to use these reaction forces so that contact is not lost with the environment. A 2 DOF manipulator on a floating base is presented in the simulation section. Good performance plots are shown in the paper, however no interpretation of the results are provided. An adaptive impedance controller is used together with a hybrid controller in [85]. The system is switched between the two controllers by using fuzzy logic approaches. The authors argue that using both types of controllers is beneficial for systems where uncertainties are present in the system. Moreover, for certain underwater tasks it is difficult to have environment information and the proposed controller is able to track the force trajectory. The simulation system consists of a heavy vehicle and a light manipulator, no discussion for the interaction between the two subsystems is presented.

Parallel position/force control

Parallel control combines a motion controller and a force controller. It appeared as a method to increase the robustness of position/force control as it has the advantages of both impedance and hybrid control. It is simple and gives the possibility to control the position and force separately [86]. This type of control takes into account the errors in position,

velocity and force and gives priority to force constraints while keeping the geometric constrains. In this type of control method the force controller has priority over the position control. This is to ensure that if the interaction with the environment is lost, the controller will enforce contact and then will follow the desired trajectory [63]. In [87], the authors study the parallel position/force controller for the case where the end-effector is in contact with a moving object, the reference velocity being estimated online.

A gravity compensation term is added for a parallel controller to regulate position and force for a soft robotic finger in contact with a flat unknown surface [88]. The simulation results show that the force and position response have the expected behavior. Osypiuk *et al.* [89] present a two-loop control system for position/force control. The authors describe the system represented through the plant model and by the real process. Two controllers are used, one is the main controller and another is the corrective controller implemented as a hybrid controller. The authors present experimental results that show improvements for force control compared with one single control loop approach. For a SCARA robot a neural network is used for position/force control in [90]. The neural network controller is used together with feedback controller. A different control loop is used for trajectory tracking and another for contact with environment. The neural network controller is used to compensate the disturbances present due to contact with the environment.

A parallel position/force controller is presented in [91]. The force is controlled with a PI controller and the motion controller is implemented with a Nonlinear Model Predictive Control law. Simulation experiments are based on Girona 500 AUV and a 4 DOF manipulator. The main objective is to drive the end-effector of the system to interact with a planar space and maintain a desired force. The authors argue that the proposed structure of the controller ensures good steady-state performance, low overshoot in force error and smooth interaction with the environment. An external force controller is presented by Antoneli *et al.* in [92]. The control structure contains an internal loop for position control and an external PID controller for force. One of the challenges of this type of system that has to be taken into account is the difference between the control bandwidth of the vehicle and the manipulator. The simulation results show that the control is advantageous in the case of loss of contact. In [93] the authors use the notion of closed-loop passive mapping to simultaneously track the pose, control the contact force and maintain a redundant pose. The authors assume no knowledge of the system dynamics and use a model-free nominal continuous control law. Simulations propose an example for welding on the nose of a submarine, with a free floating body with a 7 DOF manipulator. The results show how the UVMS preserves passivity during the contact task when the end-effector is moving on a rigid surface.

Table 2.2 presents a review of characteristics of the main methods used in position/force control. In the case when accurate tracking of both position and force have to be obtained the hybrid and parallel controllers are appropriate. The parallel control law is advantageous over the hybrid method as it controls side-by-side the position and force in all axes. Moreover, the method can be used to rapidly react to unwanted collisions between the manipulator and the environment.

Properties	Methods			
	Admittance	Impedance	Hybrid	Parallel
Direct position control		•	•	•
Direct force control	•		•	•
System disturbances	•	•	•	•
Environment uncertainties	•	•		•

Table 2.2. Position/force control architectures

2.4 Summary

This chapter presents an overview of the methodologies available to simulate an underwater vehicle-manipulator system. The dynamic and hydrodynamic effects contribute to the development of the mathematical model of the system. It is important to have a detailed survey of the work done in this area as it gives an insight of the advantages and disadvantages of the different strategies. Furthermore, a detailed analysis of the low-level control methods used for unconstrained and constrained motions is presented. The analysis is based on the research available for different type of manipulators, underwater vehicles and underwater vehicle-manipulator systems. In the following chapters, the methodology used in developing the simulation environment and the control structures for the lightweight underwater vehicle-manipulator systems are designed taking into account the characteristics of the methods reviewed in this chapter.

Chapter 3

Mathematical model of the underwater vehicle-manipulator system

In this chapter the complete mathematical model of a lightweight underwater vehicle-manipulator system is presented. The model is based on the recursive Newton-Euler representation of the dynamic system as introduced in [16]. The mathematical model presented in this research includes the hydrodynamic forces (added mass, damping forces and restoring forces), forces due to interaction with the environment and friction forces.

The model represents a general description that can be implemented for any type of underwater vehicle-manipulator and is not restricted to the system presented in this thesis. The mathematical model of an underwater vehicle-manipulator depends on the design of the system. The characteristics that have to be considered are:

- number of degrees-of-freedom;
- types of joints: prismatic or revolute;
- position of manipulator with respect to the vehicle;
- ratio between dry mass of vehicle and dry mass of manipulator.

The aim in developing a complete mathematical model for a lightweight underwater vehicle-manipulator system is to have a clear understanding of the behaviour of the system when a real robot is not available. This can be valuable to design appropriate control architectures. This chapter is focused on understanding the dynamic coupling between the manipulator and the vehicle and how the movement of the manipulator affects the vehicle. The answer to this question rests in the computation of the linear and angular acceleration of the vehicle, determined by the forces that act on the vehicle.

In Section 3.1 the kinematic model is presented. The dynamic model is described in Section 3.2 and in Section 3.3 the hydrodynamic model is presented and added to the overall system. The implementation details are given in Section 3.4 followed by the analysis of the coupling effects in Section 3.5.

3.1 Kinematic representation

The kinematic model of a robot represents the relationship between the motion of the constituent parts and the overall motion of the system. Kinematic mechanisms are built by connecting pair joints together using rigid links [94]. The coordinate frames attached to the kinematic model are assigned based on the Cartesian coordinate frame relative to each part of the robot. The position and orientation of the coordinate frames on each part is not generally set, being dependent on the type of robot.

3.1.1 Vehicle kinematic model

Underwater vehicles can be described by defining two coordinate systems: the inertial frame and the body fixed coordinate frame. The inertial or earth-fixed frame is a coordinate system with the origin fixed to a point on the surface of the Earth. The x-axis points towards the North, the y-axis points towards East and the z-axis points towards the centre of Earth. The body-fixed frame has the origin and axes fixed with respect to the geometry of the vehicle. The origin of the body normally coincides with the centre of gravity of the vehicle having the same axes orientation for both frames.

The vehicle is described by its position and orientation with respect to the inertial frame. The linear and angular positions of the vehicle are represented in the reference frame and the linear and angular velocities are expressed in body coordinates. Based on [21] in Table 3.1 the representation of the vehicle coordinates is given.

Name	Description	Position		Velocity		Force	
		Notation	Unit	Notation	Unit	Notation	Unit
Surge	motion along x	x	[m]	u	[m/s]	X	[N]
Sway	motion along y	y	[m]	v	[m/s]	Y	[N]
Heave	motion along z	z	[m]	w	[m/s]	Z	[N]
Roll	rotation along x	ϕ	[rad]	p	[rad/s]	K	[Nm]
Pitch	rotation along y	θ	[rad]	q	[rad/s]	M	[Nm]
Yaw	rotation along z	ψ	[rad]	r	[rad/s]	N	[Nm]

Table 3.1. Vehicle kinematic notations as presented in [21]

The relation between the velocity in body coordinates and the velocity in the inertial frame is given by Equation (3.1) using Euler angles.

$$\upsilon = J_e^{-1}(R_B^I)\dot{\eta} \tag{3.1}$$

where $\eta \in \mathbb{R}^6$ is the position vector, defined by Equation (3.2) and $\upsilon \in \mathbb{R}^6$ is the velocity vector defined by Equation (3.3). Equation (3.4) is the vehicle Jacobian where R_B^I represents the rotation matrix between the inertial frame and body-fixed frame, Equation (3.5). The transformation between the body fixed velocity vector ν_2 and the Euler rate vector $\dot{\eta}_2$ is

given by Equation (3.6).

$$\eta = [\eta_1,\ \eta_2]^T = [x,\ y,\ z,\ \phi,\ \theta,\ \psi]^T \tag{3.2}$$

$$\upsilon = [\upsilon_1,\ \upsilon_2]^T = [u,\ v,\ w,\ p,\ q,\ r]^T \tag{3.3}$$

$$J_e(R_B^I) = \begin{bmatrix} R_B^I & O_{3\times3} \\ O_{3\times3} & J_{\nu_2}(R_B^I) \end{bmatrix} \tag{3.4}$$

where

$$R_B^I(\eta_2) = \begin{bmatrix} \cos(\theta)\cos(\psi) & -\sin(\psi)cos(\phi)+\cos(\psi)\sin(\theta)\sin(\phi) & \sin(\psi)\sin(\phi)+\cos(\psi)\sin(\theta)\cos(\phi) \\ \cos(\theta)\sin(\psi) & \cos(\psi)cos(\phi)+\sin(\psi)\sin(\theta)\sin(\phi) & -\cos(\psi)\sin(\phi)+\cos(\phi)\sin(\theta)\sin(\psi) \\ -sin(\theta) & \cos(\theta)\sin(\phi) & \cos(\theta)\cos(\phi) \end{bmatrix} \tag{3.5}$$

$$J_{\nu_2}(R_B^I) = \begin{bmatrix} 1 & \sin(\phi)\tan(\theta) & \cos(\phi)\tan(\theta) \\ 0 & \cos(\phi) & -\sin(\phi) \\ 0 & \sin(\phi)/\cos(\theta) & \cos(\phi)/\cos(\theta) \end{bmatrix} \tag{3.6}$$

3.1.2 Manipulator kinematic model

A robotic manipulator can be described as an articulated chain that has one end attached to a fixed or mobile base while the other end of the chain is free and can consist of an end-effector [95]. From the kinematic point of view two problems are discussed in the literature when addressing robotic manipulators:

1. What is the position of the end-effector with respect to a reference coordinate system?
2. Can the manipulator reach the desired end-effector position and orientation?

These questions are referred to as the forward kinematic problem and the inverse kinematic problem. A short overview of these two problems is presented here.

Forward kinematics

The forward kinematics of a robotic manipulator represents the configuration of the end-effector based on the joint positions. The forward kinematic configuration for open-chain robots is developed based on the rigid motion of individual joints and can be computed based on the Denavit-Hartenberg method.

Denavit and Hartenberg [96] introduced the notion of a homogeneous matrix to represent the spatial transformation between two frames. The method represents explicitly the physical interpretation of the system and it is easy to implement, being the most common approach used in kinematic representation [97]. The transformation is dependent on the type and position of the joints with respect to the adjacent links. To properly construct the

D-H parameter	Description
θ_i	joint angle (angle about z_{i-1} from x_{i-1} to x_i)
α_i	link twist (angle about x_i, from z_{i-1} to z_i)
a_i	length of common normal
d_i	link offset (offset along z_{i-1})

Table 3.2. Denavit-Hartenberg parameters

Denavit-Hartenberg representation of a robotic system the coordinate frames attached to the corresponding joints should respect the following rules:

- The axis z_{i-1} is specified along the i-th joint rotation axis.
- The axis x_i is designed perpendicular to the axis z_{i-1} and pointing away from it.
- The axis y_i is defined such that the resulting frame respects the right hand rule.

By using this frame representation the D-H parameters are presented in Table 3.2 and Figure 3.1.

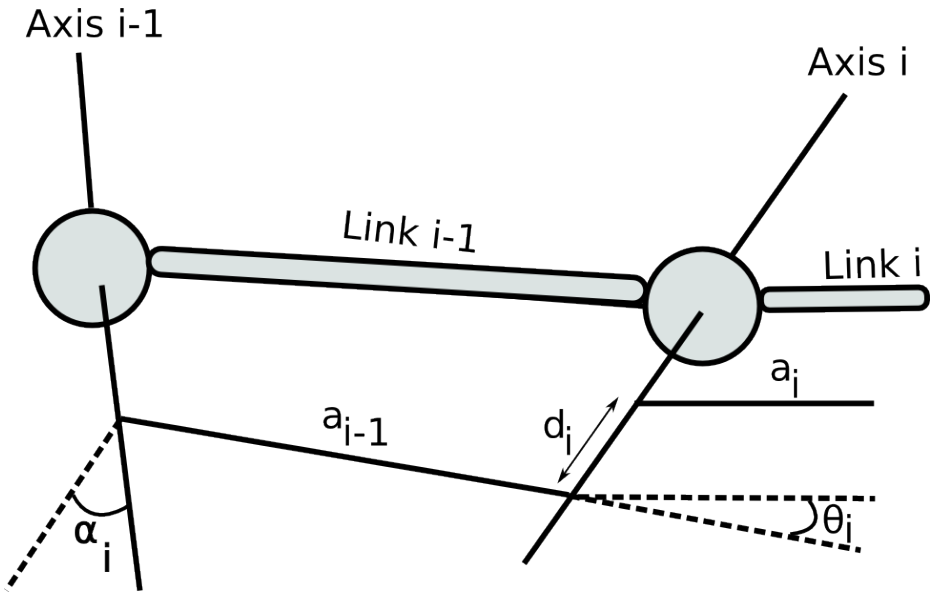

Figure 3.1. Schematic of Denavit-Hartenberg parameters

The Denavit-Hartenberg (D-H) transformation matrix for the robotic arm is described by Equation (3.7).

$$T = A_1 \cdot A_2 \cdots A_n = \begin{bmatrix} R_n^0 & \eta_n \\ 0 & 1 \end{bmatrix} \tag{3.7}$$

where $T \in \mathbb{R}^{4\times4}$ is the transformation of the link n coordinate frame into the base coordinate frame of the robotic arm and $A_i \in \mathbb{R}^{4\times4}$ represents the D-H transformation between i and $(i-1)$ coordinate frame. $R_n^0 \in \mathbb{R}^{3\times3}$ is the rotation matrix of the n-th coordinate system with respect to the base and $\eta_n \in \mathbb{R}^3$ is the position pointing from the base to the n-th coordinate system.

The transformation between two consecutive frames is dependent on the type of the joint that connects the two consecutive links. The transformation matrix that connects frame $(i-1)$ to frame i is expressed based on D-H parameters as presented in Equation (3.8), Equation (3.9) and Equation (3.10), where q_i is the i-th joint position.

$$A_i = A_i(q_i) = Trans(z,d_i) \cdot Rot(z,\theta_i) \cdot Trans(x,a_i) \cdot Rot(x,\alpha_i) \tag{3.8}$$

$$A_i = \begin{bmatrix} 1 & 0 & 0 & 0 \\ 0 & 1 & 0 & 0 \\ 0 & 0 & 1 & d_i \\ 0 & 0 & 0 & 1 \end{bmatrix} \begin{bmatrix} \cos(\theta_i) & -\sin(\theta_i) & 0 & 0 \\ \sin(\theta_i) & \cos(\theta_i) & 0 & 0 \\ 0 & 0 & 1 & 0 \\ 0 & 0 & 0 & 1 \end{bmatrix} \begin{bmatrix} 1 & 0 & 0 & a_i \\ 0 & 1 & 0 & 0 \\ 0 & 0 & 1 & 0 \\ 0 & 0 & 0 & 1 \end{bmatrix} \begin{bmatrix} 1 & 0 & 0 & 0 \\ 0 & \cos(\alpha_i) & -\sin(\alpha_i) & 0 \\ 0 & \sin(\alpha_i) & \cos(\alpha_i) & 0 \\ 0 & 0 & 0 & 1 \end{bmatrix} \tag{3.9}$$

$$A_i = \begin{bmatrix} \cos(\theta_i) & -\sin(\theta_i)\cos(\alpha_i) & \sin(\theta_i)\sin(\alpha_i) & a_i\cos(\theta_i) \\ \sin(\theta_i) & \cos(\theta_i)\cos(\alpha_i) & -\cos(\theta_i)\sin(\alpha_i) & a_i\sin(\theta_i) \\ 0 & \sin(\alpha_i) & \cos(\alpha_i) & d_i \\ 0 & 0 & 0 & 1 \end{bmatrix} \tag{3.10}$$

Inverse kinematics

The inverse kinematics problem is defined as computing the joints position of the robotic arm when a certain configuration of the end-effector is given. The inverse kinematics is of particular importance when the required task is defined in the end-effector coordinates and the robot is commanded in joint coordinates. The inverse kinematics problem is challenging as it can have several possible solutions or no solution at all and it can require complex computations. Two methods to compute the position of the joints based on the end-effector motion are: the geometric approach and the analytic method.

The geometric method is based on analysing the geometrical representation of the robot, dependent on the kinematic structure of the manipulator. There are types of robotic systems that can be decomposed into a kinematically decoupled structure. The method is suitable for simple robotic manipulators as the geometric computation is tedious for systems with large numbers of joints or for parallel systems [95].

The analytical approach is based on obtaining the instantaneous joint velocities derived from the Cartesian velocities. The Jacobian matrix of the manipulator is used to define the relationship between the joint velocities and the end-effector velocities, Equation (3.11).

$$\dot{q} = J_m^{-1}(q)v \tag{3.11}$$

where $\dot{q} \in \mathbb{R}^n$ is the joint velocity vector, $v \in \mathbb{R}^n$ is the velocity of the end-effector and $J_m^{-1}(q) \in \mathbb{R}^{6\times n}$ is the inverse Jacobian matrix that defines how joint positions change relative to the change in the end-effector. The Jacobian represents a matrix of partial derivatives of the overall system. This represents the most popular solution to obtain the inverse kine-

matics representation [31].

Robust inverse kinematics methods

Singular configurations can affect the performance of robotic systems when using inverse kinematics. To avoid deterioration of the system performances the singularities can be bypassed by using robust inverse kinematics models. A few alternative methods to compute the inverse kinematics are briefly presented.

Jacobian transpose The Jacobian transpose method is used in [98] for the inverse kinematics. In this approach the inverse of the Jacobian is replaced by the transpose of the Jacobian, Equation (3.12).

$$\dot{q} = \alpha J_m^T(q) v \tag{3.12}$$

where $\alpha \in \mathbb{R}$ is an appropriate scalar. The challenge in this method is to properly estimate the scalar parameter. In [99] a minimization approach is proposed. This method reduces the computational load of computing the inverse kinematics and removes the numerical instability.

Pseudoinverse The pseudoinverse method computes the position of the joints based on the Moore-Penrose inverse of the Jacobian, Equation (3.13).

$$\dot{q} = J_m^{\dagger}(q) v \tag{3.13}$$

where $J_m^{\dagger}(q) \in \mathbb{R}^{n \times 6}$ is the pseudoinverse matrix. In [99] the pseudoinverse is estimated through Equation (3.14). The authors argue that the method performs poorly in the vicinity of singularities, leading to large changes in joint position.

$$\dot{q} = J_m^T(q)(J_m(q)J_m^T(q))^{-1} v \tag{3.14}$$

The method is characterized by the $(I - J_m^{\dagger}(q)J_m(q))$ term that performs a projection on the nullspace of $J_m(q)$. The method is advantageous when secondary tasks are requested to be fulfilled by the system. This method is used in the thesis to compute the inverse kinematics.

Damped least square The damped least square method is defined by Equation (3.15).

$$\dot{q} = J_m^T(q)(J_m(q)J_m^T(q) + \lambda^2 I)^{-1} v \tag{3.15}$$

where $\lambda \in \mathbb{R}$ is a non-zero damping constant that has to be defined dependent on the characteristics of the system and the target position. A study into determining appropriate values for the damping constant has been made in [100]. By choosing a proper parameter the damped least square method handles the singularity problems, but the parameter should be small enough so that the convergence rate is not too slow. Other methods that can be used to

compute the inverse kinematics are: the singular value decomposition, the pseudo-inverse method with optimization criterion or the selectively damped least squares.

3.1.3 Vehicle-manipulator kinematic model

In the case of the underwater vehicle-manipulator system the robotic arm is attached to a floating base represented by the vehicle. The manipulator's end-effector motion with respect to the inertial frame has to take into account the motion of the vehicle.

Defining $\rho = [\eta,\ q]^T$ as the generalized coordinates of the vehicle and manipulator the end-effector position and orientation with respect to the inertial frame is defined by Equation (3.16).

$$x_E^I = f(\rho) \tag{3.16}$$

where $x_E^I \in \mathbb{R}^6$ is the end-effector pose in the inertial frame and $f(\rho)$ represents the general transformation dependent on the pose of the vehicle and joint positions, represented by Equation (3.17).

$$f(\rho) = \begin{bmatrix} R_E^I & p_E^I \\ 0 & 1 \end{bmatrix} \tag{3.17}$$

where $p_E^I \in \mathbb{R}^3$ is the position of the end-effector in the inertial frame, defined by Equation (3.18) and $R_E^I \in \mathbb{R}^{3\times3}$ is the rotation matrix of the end-effector, expressed by Equation (3.19).

$$p_E^I = \eta_1 + R_B^I(\eta_2)\eta_E \tag{3.18}$$

$$R_E^I = R_B^I(\eta_2)R_E^0 \tag{3.19}$$

where $\eta_1 \in \mathbb{R}^3$ is the position of the vehicle, $R_B^I(\eta_2) \in \mathbb{R}^{3\times3}$ defines the rotation matrix of the vehicle, η_E is the end-effector position in fixed coordinates and R_E^0 is the rotation matrix of the end-effector expressed in the fixed base coordinates.

3.2 Dynamic representation

The robot dynamic model represents the mathematical formulation of the equation of motion of the system. The behaviour of the robot is described and for a lightweight underwater vehicle-manipulator system the coupling effects between the two subsystems can be investigated.

To study thoroughly the interaction effects between the vehicle and the onboard manipulator a chain representation of the UVMS is advantageous. The underwater vehicle-manipulator can be represented through a chain of connected bodies. The vehicle and the links of the manipulator are separated rigid bodies with constant mass. To describe the behaviour of the robotic system the recursive Newton-Euler method and the Composite-Rigid Body Algorithm [15] are described in detail in this part of the thesis.

3.2.1 System representation

To understand the interactions between the vehicle and the manipulator a recursive approach to represent the underwater vehicle-manipulator system is valuable. To ease the implementation of this type of method a chain (tree) representation of the UVMS is proposed in this work.

To describe the vehicle-manipulator system as a kinematic tree the vehicle is described as part of the manipulator. The vehicle can be considered as an external link to the manipulator attached by a 6 degrees-of-freedom joint. Furthermore, the vehicle can be decomposed as having 6 independent joints connected by 5 zero-mass bodies or virtual links. The link that connects the last degree-of-freedom (the last virtual joint) to the first real joint of the manipulator has the geometric characteristics (mass, radius, diameter, inertial coefficients) of the vehicle. Using this representation the vehicle-manipulator system is viewed as a serial manipulator attached to a fixed virtual base. This allows a conventional algorithm used in serial link manipulators to describe the behaviour of the UVMS. A sketch of the system can be seen in Figure 3.2.

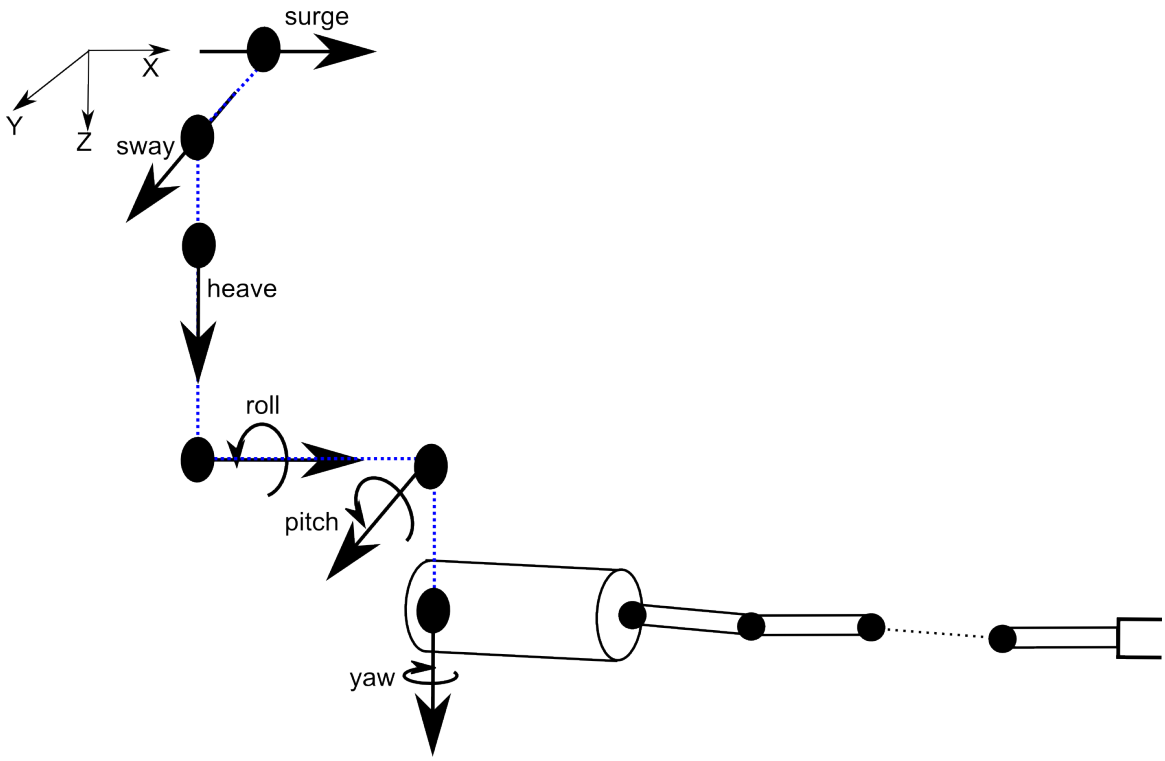

Figure 3.2. Underwater vehicle-manipulator representation

A tree representation is described as consisting of nodes and arcs. The node is a data structure having certain information, while the arc connects the nodes based on some constrains. In the tree representation the child represents the node directly connected to another top node, while the parent represents the converse notion of the child. Using this notion for the underwater vehicle-manipulator system the nodes are described by the bodies (links) of the UVMS and the arcs are represented by the joints of the UVMS.

A joint represents a kinematic constraint between two bodies. According to Feather-

stone [15] in the case of a chain representation of a robotic system attached to a fixed base, the rigid body that precedes the joint is defined as the predecessor $p(i)$ of the joint and the rigid body following the joint represents its successor, $s(i)$. Using these notions the parent vector of each body is defined as:

$$\lambda(i) = \mathtt{min}(p(i), s(i)), \quad 1 \leq i \leq n \tag{3.20}$$

where n is the number of joints. Furthermore, similar to the notion of a parent, the notion of children of the body, marked with $\mu(i)$, is the set of all joints connected by links to the the current joint i. $\kappa(i)$ is the set of all joints from i to the base of the system. These concepts are further used in the computation of interactions between the consecutive bodies.

3.2.2 Mathematical modelling

The aim in developing a dynamic model of a lightweight underwater vehicle-manipulator system is to understand the behaviour of the system. Based on this an appropriate control architecture can be developed for the UVMS. Understanding the dynamic coupling between the manipulator and the vehicle and how the movement of the manipulator affects the position keeping of the lightweight vehicle represents the starting point of this research. The answer to these questions rests in the computation of the linear and angular accelerations of the system described by the forces that act on the vehicle. In the quest to develop the dynamics of the UVMS the advantages and disadvantages of various methods presented in the literature were mentioned in Chapter 2. The main methods used for dynamic modelling are the Lagrange-Euler method and the Newton-Euler method. While the Lagrange-Euler method develops the equations of motion in closed form, the Newton-Euler method highlights the interactions between the different rigid bodies of the system.

The dynamic model can be divided into two categories, depending on the requirements of the system: (i) forward dynamics and (ii) inverse dynamics. The forward dynamics computes the joint accelerations, velocities and positions based on the forces and torques applied to the system. The inverse dynamics computes the forces and torques based on the behaviour of the system. The forward dynamics is used for simulation purposes, while the inverse model is mostly used for feedforward control [15]. The forward dynamic model assumes that the forces acting on the system are known and the interest is in obtaining the motion behaviour of the system.

For a kinematic tree, as described in the previous section, a simple dynamic model of a robotic system can be expressed by Equation (3.21).

$$M(\rho)\ddot{\rho} + C(\dot{\rho}, \rho)\dot{\rho} = \tau \tag{3.21}$$

where ρ, $\dot{\rho}$, $\ddot{\rho} \in \mathbb{R}^n$ are the generalized position, velocity and acceleration of the system, $C(\dot{\rho}, \rho)\dot{\rho} \in \mathbb{R}^n$ represents the Coriolis and Centripetal forces, $M(\rho) \in \mathbb{R}^{n \times n}$ represents the inertia matrix and $\tau \in \mathbb{R}^n$ describes the applied forces on the system, n is the number of

degrees-of-freedom of the system. In this representation, M and C represent the coefficients of the equation, while $\ddot{\rho}$ and τ represent the variables.

Using the tree representation for a lightweight underwater vehicle-manipulator system, a method that computes the acceleration of each degree-of-freedom and interaction forces between subsystems is preferred. A method based on the recursive Newton-Euler approach is the most appropriate technique to present the dynamic model for studying the coupling effects between the vehicle and manipulator. Based on Equation (3.21) the dynamic modelling of the system can be divided into solving the following steps:

1. Compute the the Coriolis and Centripetal forces, $C(\dot{\rho},\rho)\dot{\rho}$.
2. Compute the rigid body inertia matrix, $M(\rho) \in \mathbb{R}^{n\times n}$.
3. Solve the equation of motion based on the input forces, τ, applied to the system:

$$\ddot{\rho} = M^{-1}(\rho)(\tau - C(\dot{\rho},\rho)\dot{\rho}) \tag{3.22}$$

A detailed description of these steps is presented in the following part.

Coriolis and centripetal forces

Applying Newton's laws in a rotating frame of reference, the Coriolis force and centrifugal force are defined. The Coriolis force is computed in the direction perpendicular to the rotation axis, proportional to the angular rigid body velocity and the centrifugal force acts outwards in the radial direction being computed based on the distance of the rigid body from the rotating frame [101]. To compute the Coriolis and centripetal forces $C(\dot{\rho},\rho)\dot{\rho}$ the inverse dynamics methodology is used. According to [15] in this case the acceleration is considered to be $\ddot{q} = 0$ and the desired information is the force that acts on the system. The recursive Newton-Euler algorithm represents one of the most popular and simple solutions to solve this problem.

Having a tree representation of the UVMS allows one to compute the information for each rigid body in the system. In the first step the velocity and acceleration of the i-th rigid body is computed by Equation (3.23) and Equation (3.24). Applying recursively these equations from the first to the last degree-of-freedom computes the velocity and acceleration for every rigid body in the system.

$$v_i = v_{\lambda(i)} + s_i\dot{\rho}_i, \quad v_0 = 0 \tag{3.23}$$

$$a_i = a_{\lambda(i)} + s_i\ddot{\rho}_i + \dot{s}_i\dot{\rho}_i, \quad a_0 = 0 \tag{3.24}$$

where v_i represents the velocity of the body i, a_i is the acceleration of body i, $v_{\lambda(i)}$ and $a_{\lambda(i)}$ the velocity and acceleration of the parent of the body i, s_i represents the allowed movement of the joint, $\ddot{\rho}_i$, $\dot{\rho}_i$ are the acceleration and velocity of the generalized degree-of-freedom i. The net force f_i^b applied on the i-th rigid body, dependent on the joint acceleration and

Algorithm 1 Recursive Newton - Euler

procedure RNE(ρ)
  $v_0 = 0$
  $a_0 = -a_g$
  for $i = 1$ to n **do**
    $v_i = v_{\lambda(i)} + s_i\dot{\rho}_i$
    $a_i = a_{\lambda(i)} + s_i\ddot{\rho}_i + \dot{s}_i\dot{\rho}_i$
    $f_i = I_i a_i + v_i \times I_i v_i - f_i^x$
  end for
  for $i = n$ to 1 **do**
    $C_i = s_i^T f_i$
    if $\lambda(i) \neq 0$ **then**
      $f_{\lambda(i)} = f_{\lambda(i)} + f_i$
    end if
  end for
end procedure

velocity, is represented by Equation (3.25) and it is computed based on the inertial value of the current component I_i.

$$f_i^b = I_i a_i + v_i \times I_i v_i \tag{3.25}$$

The force transmitted from the parent body $\lambda(i)$ across joint i is marked as f_i and it is described by Equation (3.26) and depends on the force applied on the current link f_i^b, the force f_j in the set of children of the body i, $\mu(i)$ and external forces f_i^x. The external forces can be caused by the environmental conditions. In this thesis the interest is on the forces caused by the hydrodynamic effects and friction forces. This will be discussed in details in the following section.

$$\begin{aligned} f_i^b &= f_i + f_i^x - \sum_{j \in \mu(i)} f_j \\ f_i &= f_i^b - f_i^x + \sum_{j \in \mu(i)} f_j \end{aligned} \tag{3.26}$$

The $C(\dot{\rho},\rho)\dot{\rho}$ vector is the vector of all the generalized forces at the joints, as given by Equation (3.27).

$$C(\dot{\rho},\rho)\dot{\rho} = \left[s_1^T f_1,\ s_2^T f_2, \cdots, s_n^T f_n\right]^T \tag{3.27}$$

The method is summarized in Algorithm 1.

Rigid body inertia matrix

Bearing in mind that the dynamic model described in this chapter can be used for designing a robust control architecture, implementing a computationally efficient model is highly desirable. Due to these considerations, the Composite Rigid Body Algorithm [15] is used in this work. The algorithm is mentioned for the first time in [102]. The authors argue that the new method is faster than previous methods to compute the joint space inertia matrix of a kinematic tree. Setting $C(\dot{\rho},\rho)\dot{\rho}$ to zero, $M(\rho)$ is interpreted as the matrix of forces

Algorithm 2 Composite Rigid Body

procedure CRB(ρ)
  $I^c = I$
  for $i = n$ to 1 **do**
    if $\lambda(i) \neq 0$ **then**
      $I^c_{\lambda(i)} = I^c_{\lambda(i)} + I^c_i$
    end if
  end for
  $M = 0$
  for $i = 1$ to n **do**
    $M_{ii} = s_i^T I_i^c s_i$
    $j = i$
    while $\lambda(j) \neq 0$ **do**
      $j = \lambda(j)$
      $M_{ij} = s_i^T I_i^c s_j$
      $M_{ji} = M_{ij}$
    end while
  end for
end procedure

that distributes an acceleration on a stationary system. Each column of the $M(\rho)$ matrix is interpreted as the vector of forces to produce a unit acceleration onto the corresponding link. To compute the values of the column i, it is considered that the links from i to the last link are moving, while the previous links are static. Based on this assumption every joint transmits a force, defined based on the inertial components, onto the subsequent link. The matrix $M(\rho)$ is computed according to Equation (3.28).

$$M_{ij} = \begin{cases} s_i^T I_i^c s_j & \text{if } i \in \lambda(j) \\ s_i^T I_j^c s_j & \text{if } j \in \lambda(i) \\ 0 & \text{otherwise} \end{cases} \tag{3.28}$$

where $\lambda(j)$ represents the set of parents for joint j and I_i^c is the inertia of the subtree that starts at the rigid body i. The inertia is computed based on the sum of inertias of all links that are part of the subtree, Equation (3.29).

$$I_i^c = I_i + \sum_{j \in \mu(i)} I_j^c \tag{3.29}$$

where $\mu(i)$ is the set of the children of joint i. The method is summarized in Algorithm 2.

3.3 Hydrodynamic representation

The hydrodynamic forces can have significant effects on the behaviour of the underwater system. Modelling the hydrodynamic effects for complicated systems is an open topic. They are caused by the pressure distribution induced by the rigid bodies and can be dif-

ferentiated into two different categories: the in-line forces and the transverse forces. The in-line forces are applied in the direction of the motion of the rigid body and the transverse forces are applied to a direction normal to the motion of the body. The in-line forces represent the prime interest in the study of the hydrodynamic forces. The transverse forces do not have significant effects due to the short duration of motion in robotic systems [103]. For underwater vehicle-manipulator systems the work of McLain [103] represents the basis of the analysis of these effects. Nevertheless the system studied has one single link manipulator. A further study is developed by Leabourne [25] where a two-link manipulator is investigated. To study the hydrodynamic effects for a manipulator attached to a vehicle appropriate facilities are needed such as a large tank, a wave simulator and specific sensors attached to the system. This can be time consuming and expensive. The alternative method is to design mathematical models based on appropriate numerical theories. In this thesis the aim is to combine the relevant methods available in the literature to represent the hydrodynamic forces as accurately as possible for the considered UVMS. It has to be noted that an experimental fitting of data is the most reliable method to compute the hydrodynamic parameters. Nevertheless, a detailed mathematical model based on all the available information of the system can be advantageous for having an accurate representation of the system and designing on-line dynamic controllers. The hydrodynamic forces considered in this work are the added mass, hydrodynamic drag and the restoring forces.

3.3.1 Added mass inertia

The added mass is the additional weight caused by the volume of the fluid displaced during the movement of the system. The force is opposite in direction to the motion of the rigid body. The added mass forces can affect the rigid body not only in the direction of the movement of the rigid body but in adjacent directions, creating a 6×6 matrix of added coefficients. In this work the added mass forces and moments consist of inertia force and moments and the Coriolis and centripetal force and moments.

Considering unbounded fluid with irrational flow and low values of viscosity, Newman [104] presents in his work a set of equations that compute the added mass force acting on an accelerating rigid body. The equations connect the acceleration of the body with the added mass inertia matrix (also named added mass coefficients), as presented in Equation (3.30).

$$f_b^A = -I_b^A \begin{bmatrix} \dot{v}_b \\ \dot{\omega}_b \end{bmatrix} - \begin{bmatrix} \tilde{\omega}_b & 0 \\ \tilde{v}_b & \tilde{\omega}_b \end{bmatrix} I_b^A \begin{bmatrix} \dot{v}_b \\ \dot{\omega}_b \end{bmatrix} \tag{3.30}$$

where $v_b \in \mathbb{R}^3$ and $\omega_b \in \mathbb{R}^3$ are the body translational and angular velocities, $\dot{v}_b \in \mathbb{R}^3$ and $\dot{\omega}_b \in \mathbb{R}^3$ are the time derivatives of v_b and ω_b with respect to the body reference frame, $\tilde{v}_b \in \mathbb{R}^{3\times3}$ and $\tilde{\omega}_b \in \mathbb{R}^{3\times3}$ are the skew symmetric representation of v_b and ω_b. $I_b^A \in \mathbb{R}^{6\times6}$ is the added mass inertia matrix. For a fully submerged, three plane symmetric body the added mass inertia matrix is considered as a positive and diagonal matrix. For a cylinder with radius $r \in \mathbb{N}$ and length $l \in \mathbb{N}$, Figure 3.3, the added mass force in the x-direction is computed

by integrating the pressure P over the area projected in that direction A_x, Equation (3.31).

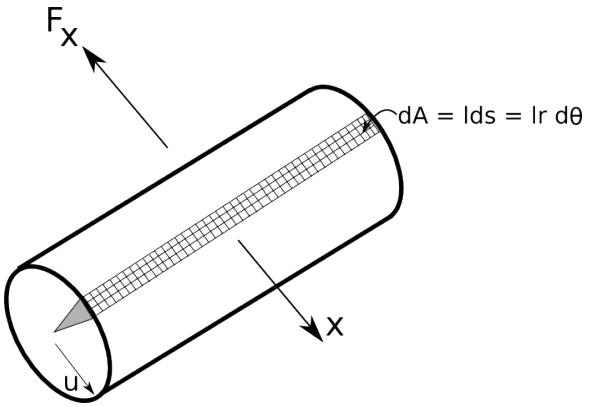

Figure 3.3. Added mass force computation in x direction

$$F_x = \int P \cdot dA_x \tag{3.31}$$

where

$$dA_x = \cos(\theta) dA = \cos(\theta) l ds = l r \cos(\theta) \mathrm{d}\theta \tag{3.32}$$

and according to the Bernoulli equation [105] the equation for pressure is defined by:

$$P = -\rho_w \left[\frac{\partial \Phi}{dt} + \frac{1}{2} \mid \nabla \Phi \mid^2 \right] \tag{3.33}$$

After substituting Equation (3.32) and Equation (3.33) into Equation (3.31) and performing all the simplifications the added mass force exerted in the x-direction is given by Equation (3.34), [105]:

$$F_x = \int_0^{2\pi} \left[-\rho_w \left[\frac{\partial \Phi}{dt} + \frac{1}{2} \mid \nabla \Phi \mid^2 \right] \right] l r \cos(\theta) \mathrm{d}\theta = -\rho_w \pi r^2 l \dot{u} \tag{3.34}$$

where $\dot{u} \in \mathbb{R}$ is the acceleration of the rigid-body in the x-direction. The negative sign shows that the force is opposing the acceleration of the rigid body. From this it can be observed that the added mass of the rigid body is strictly related to the shape of the body. This method is based on constant parameters such as the radius and length of the rigid method and it represents the most common approach to model the added mass coefficients [106]. The strip theory is used to compute the three-dimensional hydrodynamic parameters [21].

McLain suggested that the added mass coefficients are not constant [22] but also dependent on the motion of the rigid bodies. Based on repeated experiments it is observed that the added mass coefficients can be related to the distance travelled by the rigid body, as presented in Figure 3.4. Based on the distance the rigid body travels, the vortexes formed around the body vary in shape and affect the system differently. The added mass coefficient can be represented as cubic-spline polynomials dependent on the travelled distance. The results of the measurements are fitted to the cubic-spline polynomial based on optimization theory. As can be seen, initially the added mass coefficient is considered as having value 1

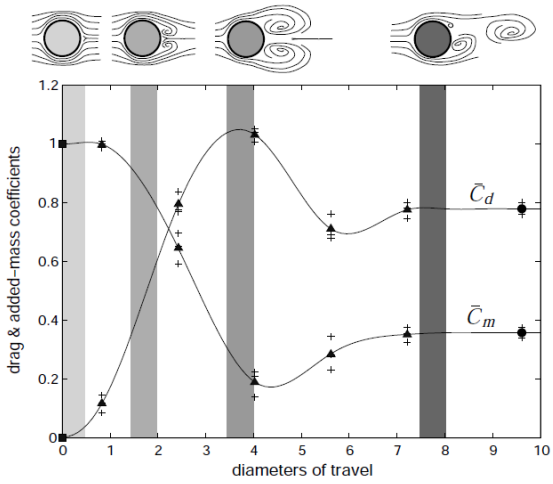

Figure 3.4. Drag and added mass spline model, [22]

but once the vortices start to grow the coefficients start to decrease. At the moment when the vortices stabilise, the coefficients reach steady-state as well.

This approach has the advantage of creating a more realistic approximation of the added mass compared to the case when only constant values are considered. The disadvantage of computing the added mass coefficients based on the distance travelled by the rigid bodies represents the high computational time. Calculating the distance of the end-tip of each link at every time step can be computationally expensive, slowing the process. Moreover, the time to compute them increases as the added mass coefficients have to be computed for all linear and angular components.

3.3.2 Hydrodynamic drag

Drag in fluid dynamics is the force dependent on the velocity of the rigid body, opposing the motion of the body with respect to the surrounding fluid. Due to the fact that it is dependent on fluid density, drag represents the most important hydrodynamic effect that alters the system for any kind of velocity. Similar to the added mass component the drag effect is studied based on flow theory. The challenge of studying this effect is high when the system has a complicated geometric representation. Most of the literature is focused on approximating each rigid body of the system by simple geometric shapes such as spheres or cylinders. McMillan [17] uses strip theory in his work to compute translational and angular drag effects based on line integrals, dividing each link into circular disk elements. To obtain the drag force the moment integral along the length of the cylinder has to be performed as presented in Equation (3.35).

$$f_d = -\rho_w C_D r \int_0^l \| v \| v dx \tag{3.35}$$

where $C_D \in \mathbb{R}$ is the drag coefficient, $l \in \mathbb{N}$ is the length of the link, $r \in \mathbb{N}$ is the radius of the link and $v \in \mathbb{R}$ is the velocity relative to the fluid and normal to the edge of each disk. The drag component in the direction of the cylinder axis can be computed based on

Equation (3.36), [16].

$$f_d = -0.5\rho_w C_D \pi r^2 \parallel v \parallel v \tag{3.36}$$

Another factor that influences the drag forces is the effect of the angle between adjacent links on the computation of the hydrodynamic in-line forces, as presented by [25]. The author proposes the computation of the drag coefficients based on distance travelled as well as the angle between rigid bodies. Experiments show that there is a strong connection between the behaviour of the hydrodynamic drag and the manipulator configuration.

The method to compute the drag effect is straightforward but the challenge remains in the computation of the drag coefficients. One of the methods for computing the drag coefficient is based on the shape of the rigid body and Reynolds Number. The relation between drag coefficient and Reynolds Number is presented in Figure 3.5.

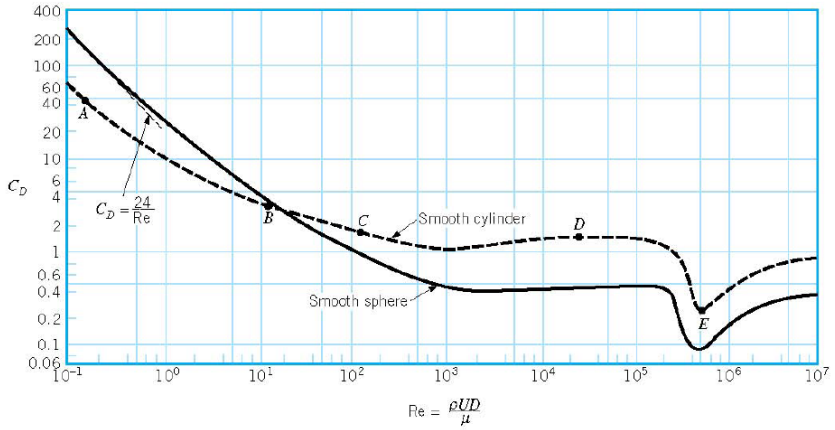

Figure 3.5. Drag coefficient versus Reynolds Number, [22]

Based on Figure 3.4, the drag coefficient can be also described based on the distance travelled by the rigid body. The drag coefficients can be extracted from the spline model, being directly proportional to the distance travelled by the body for small distances, reaching a steady-state at larger distances.

3.3.3 Restoring forces

Gravitational and buoyancy forces acting on the underwater rigid bodies are grouped together forming the restoring forces. The vehicle weight, buoyancy and relative positions of the centres of gravity and buoyancy are the information needed to compute the restoring forces. To obtain a system that requires minimum effort and to maintain a desired depth, the underwater systems are designed to be neutral with the center of buoyancy and center of gravity being located at the same place. Although this would be ideal, most of the vehicles are positively buoyant, the center of buoyancy being located vertically above the center of gravity. This represents a safety measure. In the case the motors of the vehicle stop functioning due to unforeseen events the robot will not sink and it will surface.

The buoyancy force is proportional to the mass of the fluid displaced by the moving body. It is exerted opposite to the gravitational force, as presented by Archimedes principle,

Equation (3.37).

$$f_b = -m_d a_g = -\rho_w V a_g \tag{3.37}$$

where $m_d \in \mathbb{N}$ is the mass of the fluid displaced, $V \in \mathbb{N}$ is the volume displaced and $a_g = 9.8\ \mathrm{m/s^2}$ is the gravitational acceleration. The restoring force can be described by Equation (3.38), where $m \in \mathbb{N}$ represents the mass of the rigid body.

$$f_r = m a_g + f_b \tag{3.38}$$

3.3.4 External disturbances

In this part other effects are discussed which are included in the mathematical model of the underwater system: the friction between the links of the manipulator, the underwater currents and the forces generated by the contact of the end-effector with the environment.

Friction

The effect of friction in robotics is presented in detail in [107]. The authors argue that having a good friction model can help to develop reliable control methods. The friction models are developed based on observations and experimental data, representing a simplification of the real friction model. A few of the most popular types of friction models are the following:

1. Static friction models:

   - viscous friction - presents the friction force as a linear function of the velocity of the rigid body. It is the most simple and robust friction model but according to Wronka [31] the model is not valid for small velocities:

     $$f_v = c\xi \tag{3.39}$$

     where $c \in \mathbb{R}^+$ represents the viscous coefficient and $\xi \in \mathbb{R}$ is the velocity of the rigid body;

   - Coulomb friction model [108] - given by Equation (3.40);

     $$f_c = \mu f_n \mathrm{sign}(\xi) \tag{3.40}$$

     where $\mu \in \mathbb{R}^+$ is the friction coefficient, $f_n \in \mathbb{R}$ is the normal force and $\xi \in \mathbb{R}$ is the velocity of the rigid body;

   - Stribeck friction model - represents a friction model that can be used at low velocities. The force is modelled as having a general form as the one presented in Equation (3.41) but is dependent on velocity.

     $$f_s = f_k + (f_s - f_k)\mathrm{e}^{-\left(\frac{\xi}{\xi_s}\right)^\gamma} + f_v \tag{3.41}$$

where $f_s \in \mathbb{R}$ is the level of static friction, $f_k \in \mathbb{R}$ is the minimum level of kinetic friction, $\xi \in \mathbb{R}$ is the velocity of the rigid body, $\xi_s \in \mathbb{R}^+$ is the scaling parameter, $\gamma \in \mathbb{N}$ is an empirical parameter and $f_v \in \mathbb{R}$ is the viscous friction.

2. Dynamic friction models:

   - LuGre friction model [109] - behaves as a spring for small displacements and is represented by Equation (3.42). The LuGre model is an extension of the Dahl friction model [110]. It captures the Stribeck effect and can describe the stick-slip motion.

$$\begin{aligned} \dot{z} &= v - \sigma_0 \frac{\xi}{f_c} z \\ f_l &= \sigma_0 z + \sigma_1 \dot{z} + f_v \end{aligned} \tag{3.42}$$

     where v is the velocity between the two surfaces in contact, the parameter $\sigma_0 \in \mathbb{N}$ is the stiffness, $\sigma_1 \in \mathbb{R}^+$ is the damping, $f_v \in \mathbb{R}$ is the viscous friction, $z \in \mathbb{N}$ is the internal friction state and $f_c \in \mathbb{R}$ is the Coulomb friction, $f_l \in \mathbb{R}$ is the predicted friction force.

Interaction with environment

For tasks where contact with the environment is required, modelling the effects and incorporating these into the dynamic behaviour of the system is needed to obtain an accurate simulation of the underwater vehicle-manipulator system. The first simulations of systems in contact with the environment have made no assumptions about the environmental characteristics. In this case it is assumed that the interaction with the environment is producing measurable forces [111]. A mechanical ground representation of the interaction with the environment is presented in [112]. In this case the environment is compliant and a sensor is present in wrist of the robot. A second-order system is used to describe the contact with the environment in [113]. The authors argue that this type of model is more accurate and more restrictive than the previous methods. Nevertheless, an accurate model of the interaction between a manipulator and the environment is usually difficult to obtain due to the complexity of the end-effector of the robot and it is dependent on the environmental conditions. The environment in contact with the end-effector usually represents a surface. Regardless of this, most of the simulation environments treat it as a single point contact to reduce the complexity of the model.

The interaction force vector $F = \left[\tilde{f}_n,\ \tilde{f}_t\right]$ can be modelled as having a normal force component and a tangential contact component, caused by friction contact between the end-effector and the environment. Analysing only the single point contact with the environment, the tangential component is set to zero as the friction between the end-effector and the environment is minimal. The interaction force by the environment is modelled with Equation (3.43).

$$F = K_e(x - x_e) \tag{3.43}$$

where $x \in \mathbb{R}$ is the end-effector position, $x_e \in \mathbb{R}$ is the end-effector position at the contact point and $K_e \in \mathbb{R}^+$ is the stiffness of the environment.

Water currents

The underwater ocean currents represent one of the most common environmental disturbances. The currents are caused by phenomena such as the tidal movement, local wind characteristics or by nonlinear waves. The effects of these forces can be incorporated in the mathematical model of the rigid body moving through water.

The study of the current induced forces and moments are considered starting with the assumption that the equation of motion can be represented based on the relative velocity [21]. The velocity of the underwater currents, $v_c = \begin{bmatrix} v_{c_x}, & v_{c_y}, & v_{c_z}, & 0, & 0, & 0 \end{bmatrix}^T$ can be described by a constant and unidirectional model. The relative velocity of the system is represented by Equation (3.44) and the dynamic model can be defined based on these relative velocities.

$$\xi_r = \xi - J^{-1}(R_E^I)v_c \tag{3.44}$$

where $J^{-1}(R_E^I) \in \mathbb{R}^{n\times 6}$ is the inverse of the Jacobian of the system and $\xi_r \in \mathbb{R}^n$ is the relative velocity, $n \in \mathbb{N}$ is the number of degrees-of-freedom of the system.

3.4 Problem statement

This chapter presents the mathematical model for a lightweight UVMS. Special interest is devoted to the coupling effects between the underwater vehicle and the manipulator attached to the vehicle. Having an accurate model of the UVMS and understanding how the effects of the manipulator motion affect the movement of the vehicle can be beneficial to design proper control laws for the system. Furthermore, designing control architectures that incorporate these disturbances can improve the performance of the underwater vehicle-manipulator system. Nevertheless, having an accurate model of the real robotic system is beneficial as this can reduce the time and costs of software development and testing. The challenge is to have a correct representation of the system, especially in the design of the vehicle as an additional link of the manipulator and the modelling of the hydrodynamic effects.

In a closed method form, the mathematical model of an underwater vehicle-manipulator system is described by Equation (3.45).

$$M(\rho)\dot{\xi} + C(\rho,\xi)\xi + D(\rho,\xi)\xi + g(\rho) + f_f(\rho) = \tau - J^{-1}F \tag{3.45}$$

where the position of the UVMS is $\rho = [\eta,\ q]^T$, $\eta \in \mathbb{R}^6$ is the position vector of the vehicle, $q \in \mathbb{R}^n$ is the manipulator joint velocity, $\xi \in \mathbb{R}^{6+n}$ vector is the system velocity vector, $M(\rho) \in \mathbb{R}^{(6+n)\times(6+n)}$ is the inertia matrix, $C(\rho,\xi)\xi \in \mathbb{R}^{6+n}$ is the Coriolis and Centripetal matrix, $D(\rho,\xi)\xi \in \mathbb{R}^{6+n}$ is the hydrodynamic damping, $g(\rho) \in \mathbb{R}^{6+n}$ is the restoring forces

vector, $f_f \in \mathbb{R}^{6+n}$ is the friction of the system, $F \in \mathbb{R}^6$ is the vector of interaction with the environment and $\tau \in \mathbb{R}^{6+n}$ is the vector of generalized forces applied to the vehicle and manipulator. The dynamic model is characterized by the following properties, the proofs being found in [21].

Property 3.4.1 The inertia matrix $M(\rho)$ is symmetric and positive: $M(\rho) = M^T(\rho) > 0$

Property 3.4.2 $\dot{M}(\rho) - 2C(\rho, \xi)$ is a skew symmetric matrix.

Property 3.4.3 The hydrodynamic damping $D(\rho, \zeta)$ is positive $D(\rho, \zeta) = D^T(\rho, \zeta) > 0$

3.4.1 Mathematical model

To obtain the complete mathematical model representation in closed form and having access to the interaction forces between subsystems, a recursive modelling of the system is implemented in this thesis.

Underwater vehicle-manipulator representation

The UVMS is represented as a kinematic tree where the vehicle is considered as part of the manipulator. The 6 DOFs of the vehicle are considered as 6 additional joints to the manipulator, included at the base of the manipulator: 3 prismatic joints corresponding to the translational degrees-of-freedom of the vehicle and 3 revolute joints corresponding to the roll, pitch and yaw. This is also known as the floating base system. The new joints corresponding to the vehicle are connected by zero mass links. An extra link having the geometric characteristics of the vehicle connects the last additional joint of the manipulator (last degree-of-freedom of the vehicle) and the first joint of the real manipulator. All the links of the overall manipulator are considered as having a cylindrical representation with mass m, length l and radius r. The kinematic representation of the system is performed as presented in Section 3.1 based on the Denavit-Hartenberg parameters. A schematic of the overall vehicle-manipulator system is presented in Figure (3.6).

Dynamic modelling

In this part the mathematical description of the system is computed based on Equation (3.21). The Coriolis and centripetal matrix is computed based on the recursive Newton-Euler equations (Algorithm 1). The interaction between subsystems are computed in this part. The rigid body inertia matrix is computed based on the Composite Rigid Body method (Algorithm 2). The hydrodynamic forces are grouped together, resulting in the external force that is included in Equation (3.26) and defined as:

$$f_i^x = f_{a_i} + f_{d_i} + f_{r_i} + f_{l_i} \tag{3.46}$$

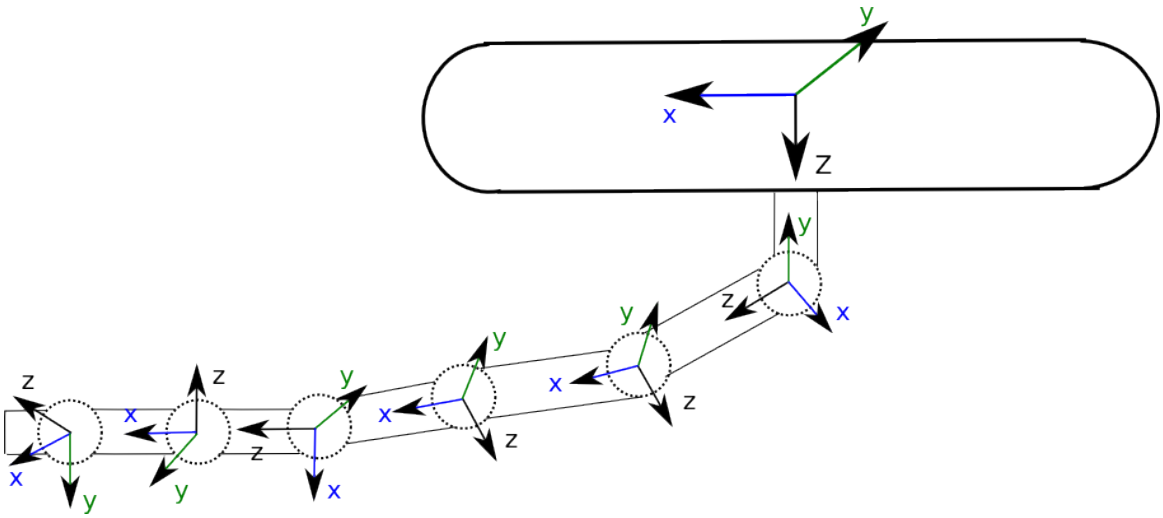

Figure 3.6. Kinematic tree of the vehicle-manipulator

The implementation details of each of the external forces is further discussed.

Hydrodynamic and external forces

Added mass, f_{a_i}: The added mass inertia matrix coefficients are computed based on the characteristics of the rigid body and the distance travelled by the end-effector tip of each link. As presented in [21] the added mass coefficients for each rigid body in the system represented through a cylinder can be computed as a diagonal matrix using Equation (3.47).

$$I_i^A = \begin{bmatrix} -\rho_w \pi r^2 l & 0 & 0 & 0 & 0 & 0 \\ 0 & -\rho_w \pi r^2 l & 0 & 0 & 0 & 0 \\ 0 & 0 & C_m(d) & 0 & 0 & 0 \\ 0 & 0 & 0 & -\rho_w \pi r^2 l^3/12 & 0 & 0 \\ 0 & 0 & 0 & 0 & -\rho_w \pi r^2 l^3/12 & 0 \\ 0 & 0 & 0 & 0 & 0 & 0 \end{bmatrix} \tag{3.47}$$

where $C_m(d) \in \mathbb{R}$ are the coefficients dependent on the distance travelled by the link, defined based on Figure 3.4. The rotational motion around the z-axis (the axis through the center of the cylinder) does not produce any flow and the coefficient of the added mass inertia is zero. The force exerted by the added mass component is defined by Equation (3.30).

Hydrodynamic damping, f_{d_i}: The drag coefficients tend to be modelled based on the shape of the rigid body, inclination and flow conditions. The Reynolds number is defined based on the fluid velocity relative to the rigid body, the diameter of the equivalent sphere and the kinematic viscosity of the fluid. Based on the Reynold number in Figure 3.5 and the distance travelled by the links, the drag coefficients are defined. The angle between adjacent manipulator links is considered into the computation of the drag effects. The drag force taking into account the configuration of the system is presented by Equation (3.48).

$$f_{d_i} = \begin{cases} -0.5\rho_w C_{Di}(d_i)\pi r_i^2 \parallel v_i \parallel v_i - 0.5\rho_w C_{Di}(d_i)\pi(r_i^2 + l_i\cos(\rho_{i+1})) \parallel v_i \parallel v_i & \text{if } i \leq n \\ -0.5\rho_w C_{Di}(d_i)\pi r_i^2 & \text{if } i = n \end{cases} \tag{3.48}$$

where $C_{Di}(d_i) \in \mathbb{R}$ are the coefficients dependent on the distance travelled by the link, ρ_{i+1} is the angle between the link i and link $i+1$ and v_i is the velocity corresponding to link i of the rigid body.

Restoring forces, f_{r_i}: The restoring forces include the buoyancy and the gravity forces and are defined by:

$$f_{r_i} = m_i a_g - \rho_w V a_g \tag{3.49}$$

where $m_i \in \mathbb{N}$ is the mass of the rigid body, a_g is the gravitational acceleration, $V \in \mathbb{N}$ is the volume displaced and ρ_w is the density of the water.

Friction forces, f_{l_i}: In [114] the authors argue that the LuGre model contains a small number of parameters and can be approximated and matched to experimental data. Based on this and due to the fact that the model incorporates most of the classical friction characteristics, the LuGre friction model is used in this research, modelled by Equation (3.42).

The water currents and the interaction with the environment are not incorporated in the simulation environment. The study is focused on understanding the coupling effects between the two subsystems and how the hydrodynamic effects contribute to these effects. Incorporating the water currents adds a higher level of complexity that makes it harder to understand what the effects caused by the hydrodynamic characteristics are and what effects are due to the water current. Furthermore, the interaction with the environment will be incorporated in Chapter 5 when a rigorous study of these effects are needed to design force/position control strategies.

3.5 Simulation results

In this section the simulation results focus on presenting the coupling effects between a lightweight underwater vehicle and the attached manipulator. The system has 11 degrees-of-freedom. The work in the thesis is developed based on two real robotic systems available in the Ocean Systems Laboratory: Nessie VII, an autonomous underwater vehicle developed as a research platform in the laboratory and a commercially available underwater manipulator, HDT-MK3-M developed by HDT Global [115]. The Nessie VII AUV is a torpedo shaped 5 degrees-of-freedom (DOFs) vehicle with a mass of 60 kg, a length of 1.1 m and is 0.3 m in diameter. The thrusters are arranged in such a way that the vehicle roll degree-of-freedom is not controlled. Although this DOF is not controlled, in this chapter the effects of the manipulator movement is analysed on roll DOF as well. The manipulator has 6 revolute joints and a mass of 9 kg. The manipulator is attached at a distance

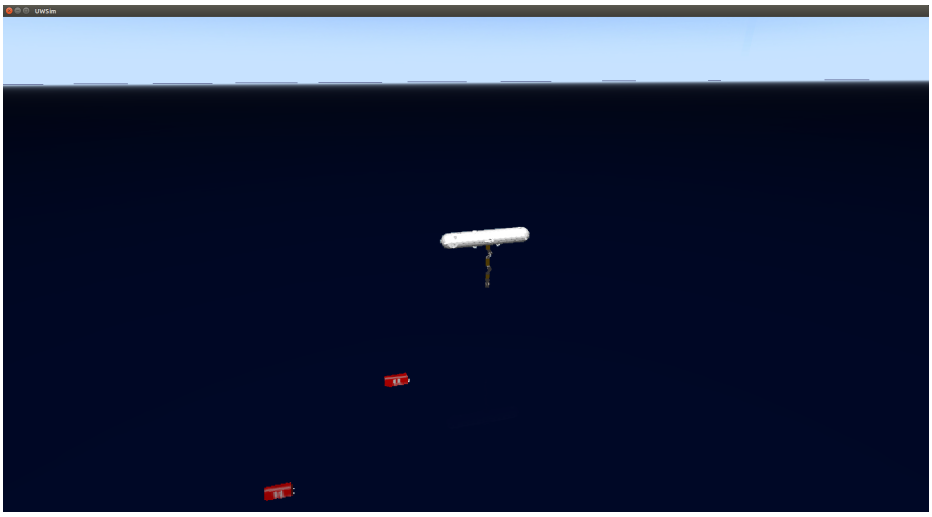

Figure 3.7. Nessie VII - HDT-MK3-M lightweight system in UWSim environment

$r = 0.15$ from the centre of mass of the vehicle, where r represents the radius of the vehicle. This configuration is chosen to match the only possible configuration of attaching the HDT-MK3-M manipulator to the actual Nessie VII AUV. The manipulator is attached by a revolute joint along the z-axis of the first link. The simulation environment (the mathematical model) is built in Python according to a real underwater environment consisting of hydrodynamic effects. The simulator's input is the force expressed in vehicle and joint coordinates and the output of the simulator is the acceleration, velocity and position of the system. The mathematical model is incorporated in UWSim for visualisation purposes. The overall simulation environment is shown in Figure 3.7. The following assumptions are made for analysing the coupling effects between the vehicle and manipulator:

- The vehicle has three planes of symmetry.
- Actual joint acceleration is well approximated by desired arm-joint acceleration.

3.5.1 No hydrodynamic effects

The first set of results presents the behaviour of the vehicle and manipulator when no hydrodynamics are considered in the mathematical model of the UVMS. The simulations aim to present the coupling effects between the vehicle and manipulator. Of particular interest is to study the effects of the variation of the dry mass ratio between the vehicle and manipulator and the influence this has on the coupling effects between the two subsystems. A detailed description of the tested configurations is presented in Table 3.3. Different weights for the manipulator are considered while the weight of the vehicle remains constant. The changes in the weight of the manipulator are proportional to changes in the mass of each link of the manipulator. For the cases considered, the mass of the manipulator is distributed across the links as presented in Table 3.4.

In this scenario no external force is applied to the thrusters of the underwater vehicle. Two different cases for the manipulator movement are investigated. One movement towards

Ratio	Manipulator weight [kg]	Vehicle weight [kg]
1 : 30	2	60
1 : 10	6	60
1 : 7	9	60
1 : 5	12	60

Table 3.3. Vehicle-manipulator dry mass ratio

Manipulator weight [kg]	Links weights [kg]					
	L1	L2	L3	L4	L5	L6
2	0.33	0.39	0.45	0.35	0.28	0.20
6	0.99	1.06	1.11	1.04	0.94	0.86
9	1.49	1.56	1.61	1.54	1.44	1.36
12	1.99	2.06	2.11	2.04	1.94	1.86

Table 3.4. Manipulator mass distribution across the links

the front of the vehicle and another movement towards the side of the vehicle.

Manipulator movement towards the front of the vehicle

The velocity of the vehicle caused by the movement of the arm towards the front of the vehicle is presented in Figure 3.8. From the simulation results it can be observed that the heavier the manipulator is, the more significant are the effects on the vehicle. The influence that the manipulator has on the station keeping of the underwater vehicle is directly dependent on the dry mass ratio between the vehicle and manipulator. When the dry mass of the manipulator is 2 kg the vehicle velocity changes slightly at the beginning of the simulation. By increasing the weight of the manipulator the vehicle starts slowly to change its location. For most DOFs the change in the weight is directly proportional to the change in velocity. The velocities of the translational degrees-of-freedom are small. The simulation results show that the pitch DOF is the most affected component of the vehicle when a pure dynamic model is considered, regardless of the ratio between the vehicle and manipulator. In the case of vehicle : manipulator ratio of 1 : 5 the roll rate is up to 0.01 rad/sec (equivalent of 0.57 deg/sec), the pitch rate has a peak of 0.07 rad/sec (4.01 deg/sec) and the yaw rate has a peak of 0.04 rad/sec (2.43 deg/sec). Moving the manipulator in this way creates a pitch movement. To create this movement towards the nose of the vehicle a constant torque is applied to the second joint of the manipulator, while the rest of the joints are commanded to have zero torque.

In Figure 3.9 the velocities of the manipulator joints are shown when a constant torque of 20 N is applied to the second joint. The same torque for joint 2 is applied for each simulation, regardless of the weight of the manipulator. The torque applied is large enough to move the joints for all the considered cases. It can be seen that the velocity of the actuated joint reaches a steady-state when constant torque is applied. When the friction forces are

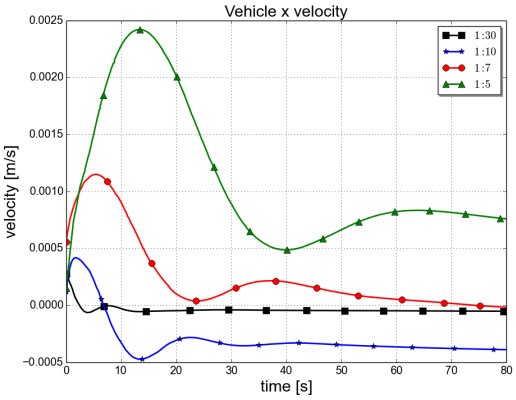

(a) x velocity

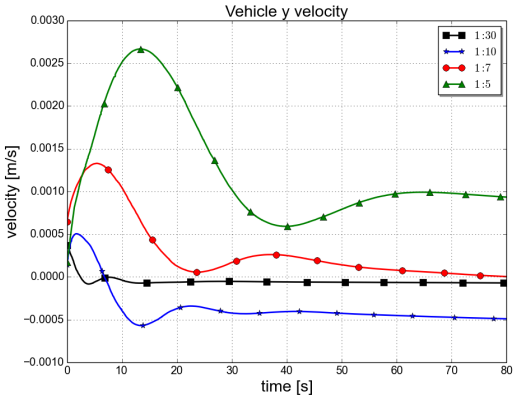

(b) y velocity

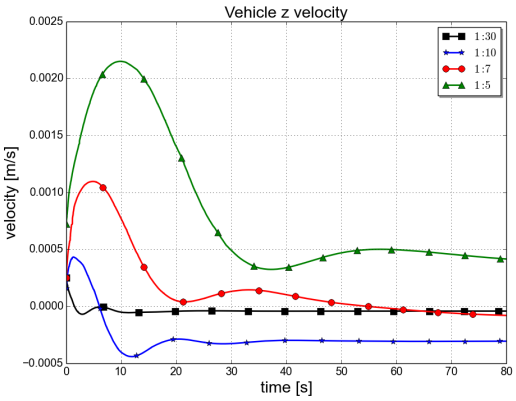

(c) Vehicle z velocity

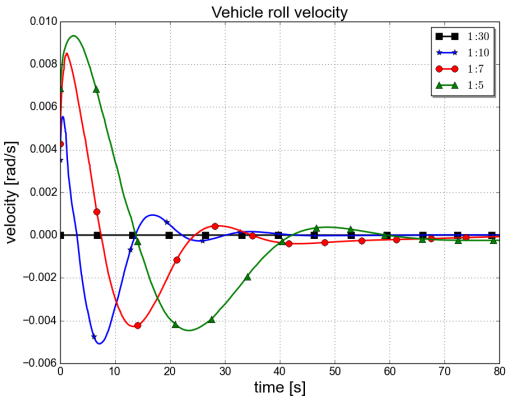

(d) roll velocity

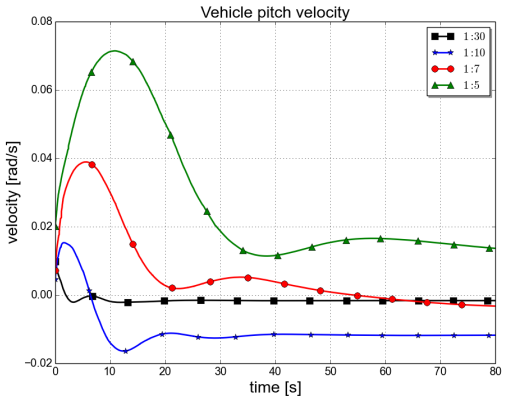

(e) pitch velocity

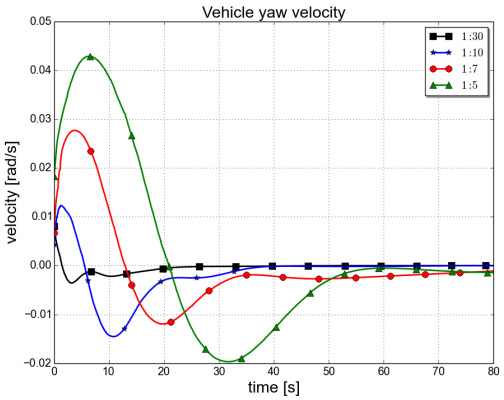

(f) yaw velocity

Figure 3.8. Vehicle velocities when joint 2 torque is 20 Nm (no vehicle control and no manipulator control)

incorporated into the system the velocity reaches a constant value after a certain moment in time. It is natural to assume that by increasing the weight of the links, when the same torque is applied, the velocities of the joints decrease. This can be observed for the actuated joint Figure 3.9b, where the steady-state value of the velocity is reached at a lower rate when the mass of the manipulator is increased. It can be seen that the rest of the joints (that are not actuated) still present a profile velocity. This is caused due to the coupling effect between adjacent links. Furthermore, the effects due to the interactions between links are

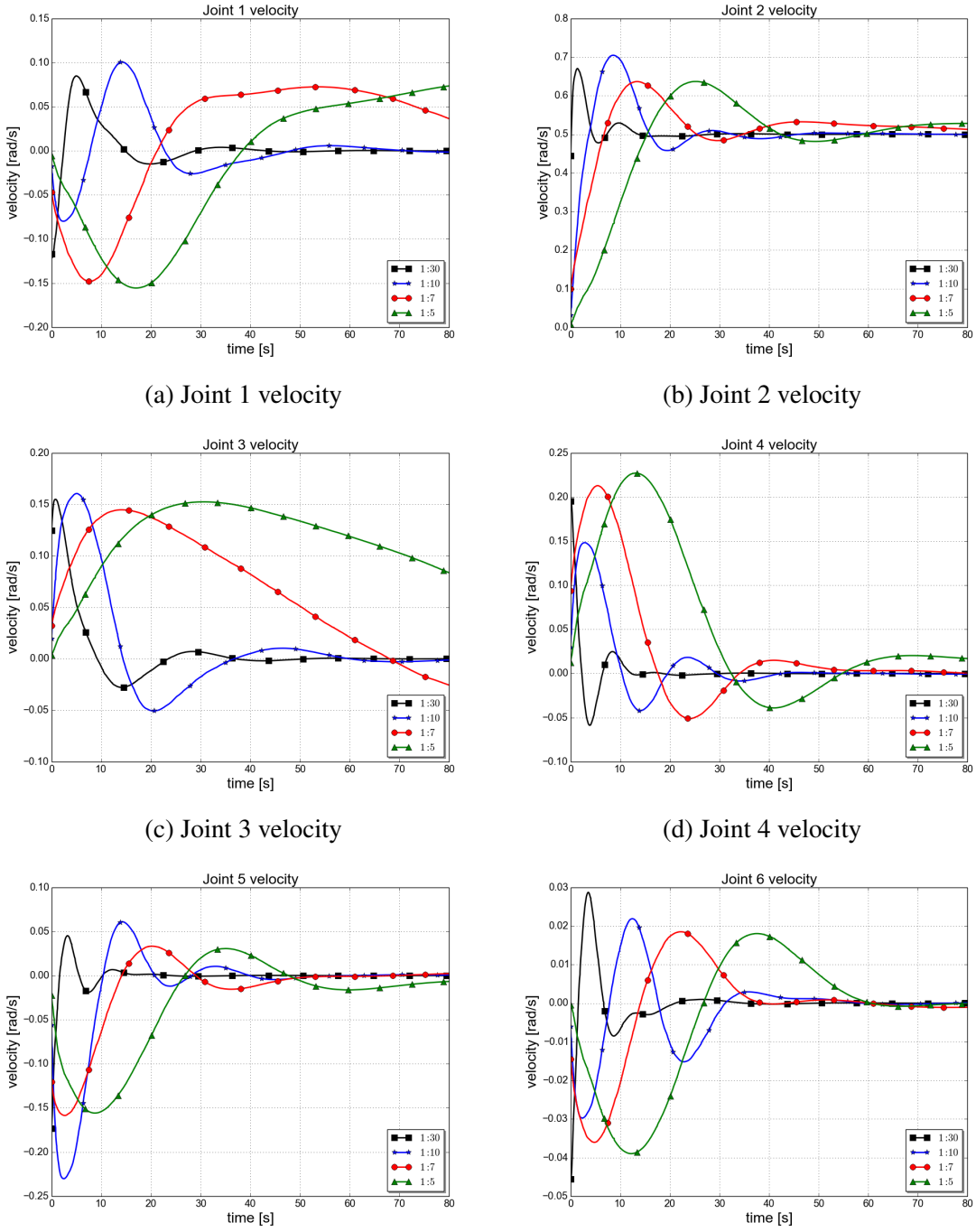

(a) Joint 1 velocity

(b) Joint 2 velocity

(c) Joint 3 velocity

(d) Joint 4 velocity

(e) Joint 5 velocity

(f) Joint 6 velocity

Figure 3.9. Manipulator velocities when the second joint torque is 20 Nm (no vehicle control and no manipulator control)

dependent on the distance from the actuated joint (joint 2 in this case). For example for joint 6, Figure 3.9f, the velocity rate for the vehicle : manipulator ratio of 1 : 7 has a peak of 0.02 rad/sec (1.14 deg/sec) while for joint 3, in the same case, the velocity peak is of 0.15 rad/sec (8.59 deg/sec), Figure 3.9c. As soon as the steady-state velocity of the actuated joint is reached, the velocity of the rest of the joints reach a zero velocity.

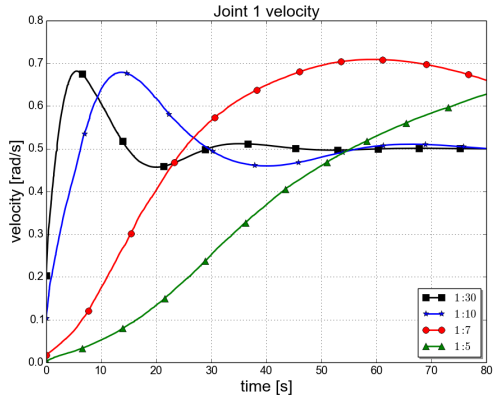

(a) Joint 1 velocity

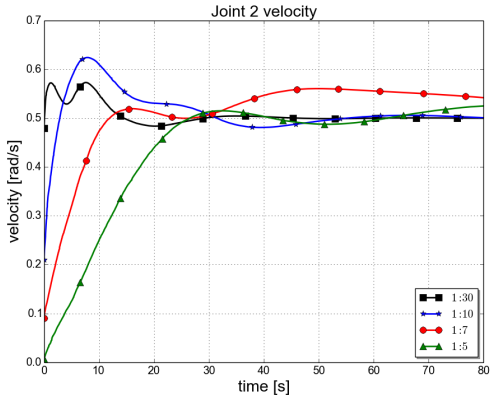

(b) Joint 2 velocity

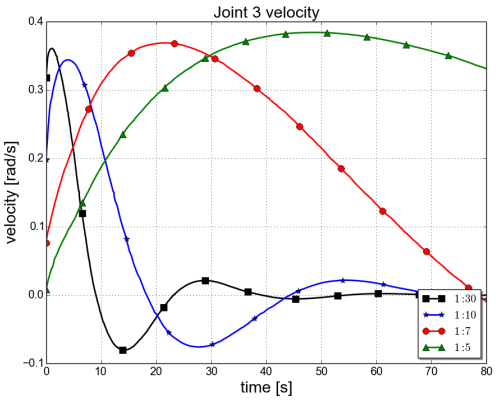

(c) Joint 3 velocity

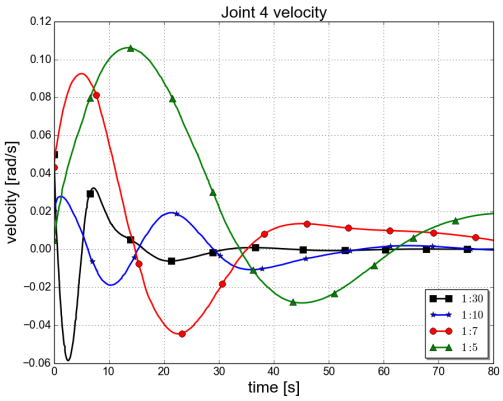

(d) Joint 4 velocity

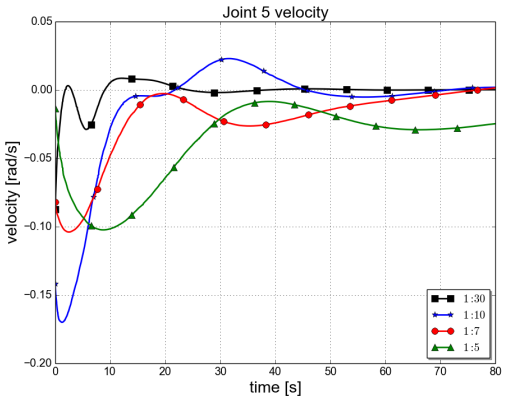

(e) Joint 5 velocity

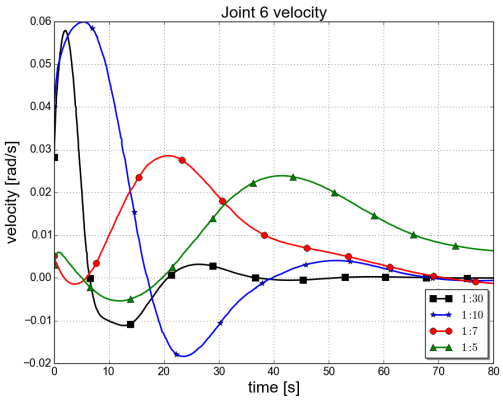

(f) Joint 6 velocity

Figure 3.10. Manipulator velocities when the joint 1 and joint 2 torques are 20 Nm (no vehicle control and no manipulator control)

Manipulator movement towards the side of the vehicle

The second test case when no hydrodynamic effects are considered shows the behaviour of the vehicle when the manipulator moves towards the side of the vehicle. To obtain this movement two of the joints of the manipulator are actuated, joint 1 and joint 2. On each of these two joints a torque of 20 Nm is applied. The joint velocity profiles are presented in Figure 3.10. As expected the velocities of the actuated links reach constant values in time due to the effects of the resistive forces. Similar comments as for the previous test

case can be made here. The heavier the links of the manipulator are the slower is the time to reach the velocity steady-state. For joint 1 for the case when manipulator ratio is 1 : 30 the velocity reaches a steady-state after 30 seconds, while for 1 : 10 case the velocity reaches a steady-state after 60 seconds. For the other two cases when the manipulator has a considerable mass, the steady-state velocity is reached at a later time. The coupling effects between the links of the manipulator also have a contribution to the time needed to reach the velocity steady-state. The joints that are not actuated present a slight movement due to these coupling effects.

The effects of this type of movement on the vehicle are shown in Figure 3.11. The translational axes of the vehicle are not influenced greatly by this movement. The effects of the side movement of the manipulator on the vehicle rotational axes presents differences compared with the longitudinal movement. In this case the velocities on roll and pitch axes are higher compared with the case when the movement is along the length of the manipulator. The roll's velocity rate is up to 0.04 rad/sec (4.5 deg/sec) and the yaw's velocity peak is 0.08 rad/sec (4.5 deg/sec), for the case when the vehicle : manipulator ratio is 1 : 5. Similar to the previous case, an increase in manipulator weight causes larger effects on the vehicle. In the case when a very light manipulator is attached on the vehicle, even for a complicated movement, the effects are not significant: the velocity for all degrees-of-freedom is very small. Increasing the weight causes a rise in the vehicle velocity. Based on the simulation results of the two different movements of the manipulator it can be stated that the ratio between the vehicle's dry mass and the manipulator's dry mass has a clear influence in the behaviour of the system. Furthermore, it is shown that different types of movement of the manipulator affect differently the degrees-of-freedom of the vehicle. Without knowing exactly the type of movement it is hard to predict what degree-of-freedom is going to be the most affected.

3.5.2 Hydrodynamic effects

In this part the effects of the hydrodynamic forces on the system are presented. The coupling effects between the two subsystems are under investigation. Furthermore the interest is in understanding on how the hydrodynamic forces affect the behaviour of the overall system. For these simulations it is considered that the vehicle : manipulator ratio is 1 : 7. This corresponds to the real robotic system used in this research. The Nessie VII AUV has a weight of 60 kg and the HDT-MK3-M manipulator has a weight of 9 kg. Including the hydrodynamic effects for the UVMS, the effects of the two different movements of the manipulator on the vehicle are analysed here.

Manipulator movement towards the front of the vehicle

The behaviour of the manipulator when the hydrodynamic effects are included in the mathematical model can be seen in Figure 3.12. In this case the movement towards the front of the manipulator is achieved by applying a constant torque of 20 Nm to the second joint of

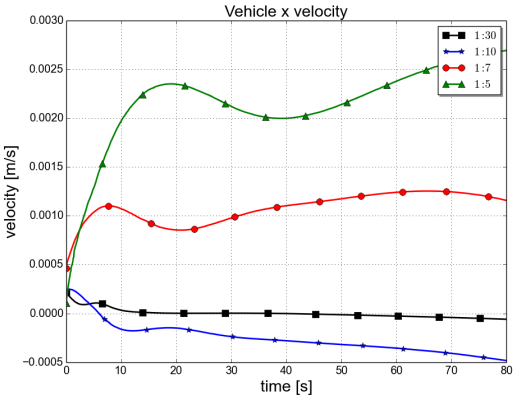

(a) x velocity

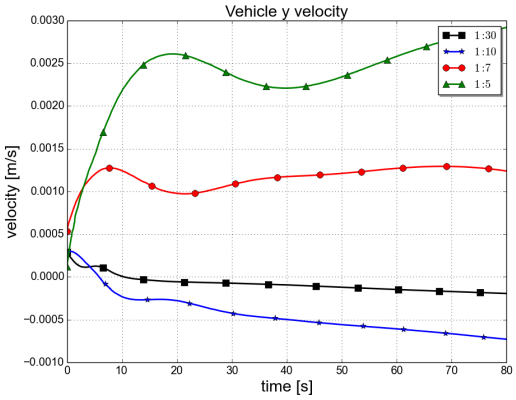

(b) y velocity

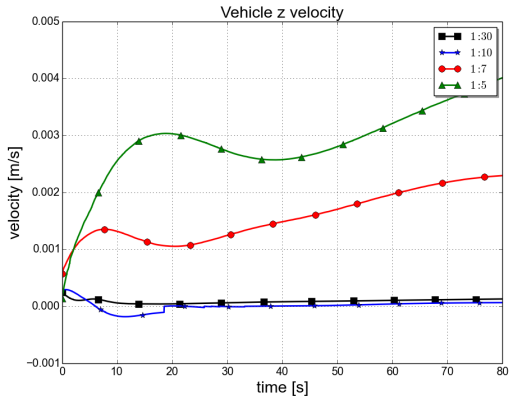

(c) Vehicle z velocity

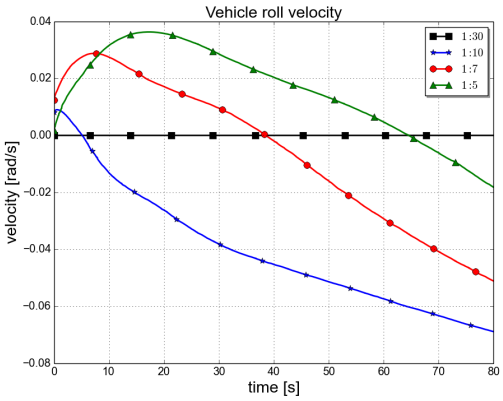

(d) roll velocity

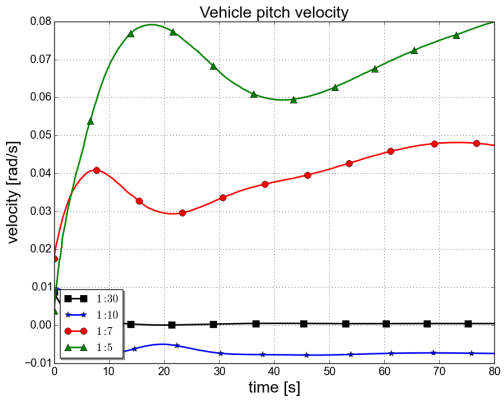

(e) pitch velocity

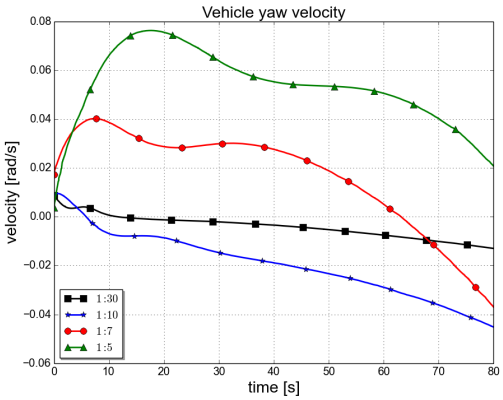

(f) yaw velocity

Figure 3.11. Vehicle velocities when joint 1 torque is 20 Nm and joint 2 torque is 20 Nm (no vehicle control and no manipulator control)

the manipulator. When the hydrodynamic effects are incorporated the velocity of the actuated joint is lower than when the hydrodynamic effects are not included. This is expected as the force opposed by the water reduces the speed of movement of a rigid body. Furthermore, the velocities caused by the coupling effects between the links of the manipulator are lower in the case when the hydrodynamics are incorporated.

In Figure 3.13 the effects of the movement of the manipulator on the vehicle are presented. The figures show the cases when the hydrodynamics are not included and when they

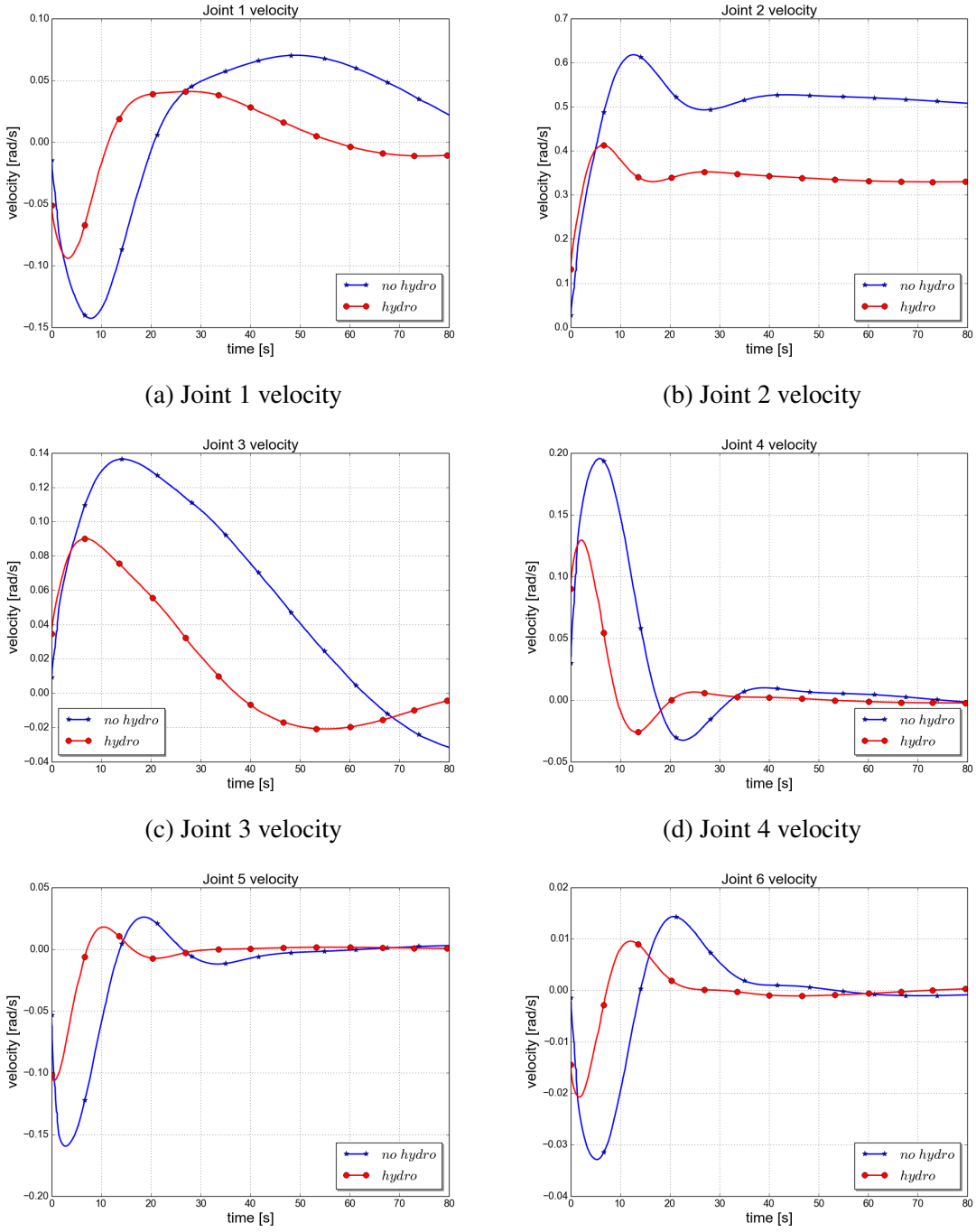

(a) Joint 1 velocity

(b) Joint 2 velocity

(c) Joint 3 velocity

(d) Joint 4 velocity

(e) Joint 5 velocity

(f) Joint 6 velocity

Figure 3.12. Hydrodynamic effects on manipulator velocities when joint 2 torque is 20 Nm (no vehicle control and no manipulator control)

are considered into the mathematical representation of the system. In the case when the hydrodynamics are incorporated the velocities of the manipulator joints are lower than in the case when they are not considered, as seen in Figure 3.12. This, in principle, causes a reduction of the vehicle velocity caused by the coupling effects. This is confirmed for the roll DOF, which has an absolute peak in the velocity rate of 0.002 rad/sec (1.14 deg/sec) when the coupling effects are considered, compared with 0.004 rad/sec (2.29 deg/sec) when the hydrodynamic effects are not incorporated. In the pitch and yaw degrees-of-freedom, at

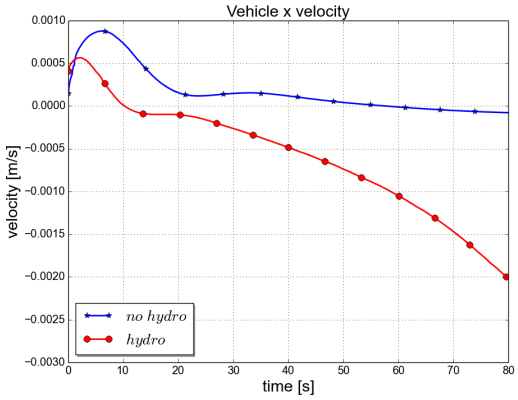

(a) x velocity

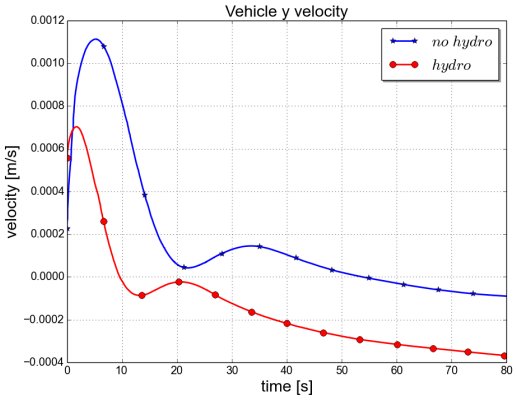

(b) y velocity

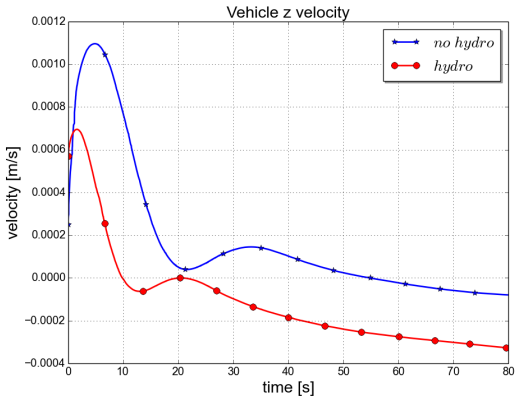

(c) Vehicle z velocity

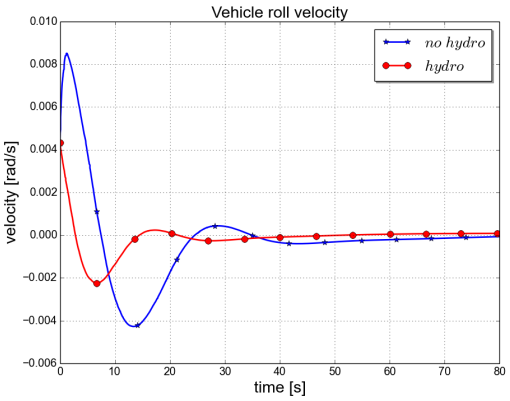

(d) roll velocity

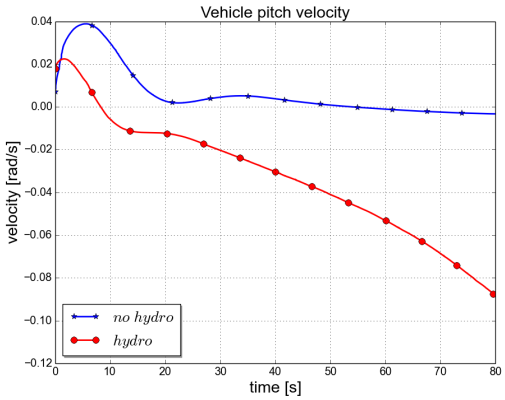

(e) pitch velocity

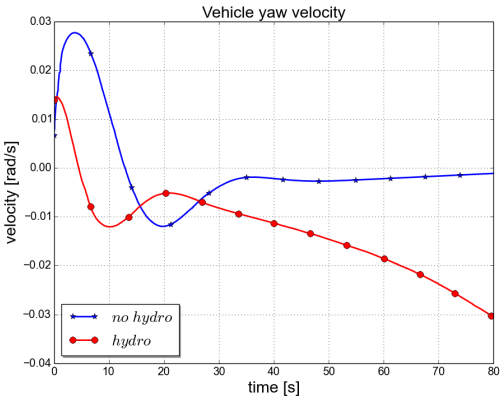

(f) yaw velocity

Figure 3.13. Hydrodynamic effects on vehicle velocities when joint 2 torque is 20 Nm (no vehicle control and no manipulator control)

the beginning of the simulation the velocity is lower in the case when the hydrodynamic is included. After a certain moment in time, the velocity increases. The velocity caused by the manipulator movement is amplified for these two degrees-of-freedom due to the velocity generated as a result of the hydrodynamic effects. The added mass is responsible in decreasing the velocity of the vehicle. When the manipulator moves, vortexes are created producing a change in the added mass and damping coefficients. After a certain moment in time, these effects are going to affect the behaviour of the vehicle by increasing the velocity

of the DOFs that are most affected initially by the coupling effects between the vehicle and manipulator. It can be seen that when including the hydrodynamic effects the velocity of the vehicle, caused by the movement of the manipulator, does not stabilise in the simulation results. That is caused by the vortexes created by the manipulator. These effects reach the vehicle at a later moment in time and cause an increase in the vehicle velocities towards the end of the simulation.

Manipulator movement towards the side of the vehicle

The second test case when the hydrodynamic effects are incorporated in the model describes the behaviour of the system when a side movement of the arm is requested. To obtain this behaviour, joint 1 and joint 2 are actuated by applying a torque of 20 Nm on each of them. The comparison between the manipulator velocity profiles when the hydrodynamic forces are included in the model and the pure dynamic case are presented in Figure 3.14. Similar to the case when the manipulator moves towards the front of the vehicle, the velocities of the manipulator joints when the hydrodynamic forces are included in the model are lower compared to the case when are not considered. This is caused due to the added mass incorporated in the system. The behaviour of the vehicle is presented in Figure 3.15. In this case, due to the lower manipulator velocity, the vehicle velocities are at the beginning of the simulation lower than the case when no hydrodynamics are incorporated. However, due to the hydrodynamic effects that affect the vehicle these velocities tend to increase in time. The difference between this case and the case when the manipulator moves towards the front of the manipulator can be seen in the roll behaviour Figure 3.15d. In this case the roll with and without hydrodynamic effects has a much higher velocity than for the case when the manipulator moves towards the front. With the addition of the hydrodynamic effects this velocity is increased while the same hydrodynamic affects maintain a constant behaviour for the case of the movement towards the front. It can be concluded that incorporating the hydrodynamic effects the observations made regarding what DOF of the vehicle is the most affected by the manipulator movement do not change. Nevertheless, the velocity of the manipulator decreases. This lowers the significance of the coupling effects on the vehicle. Incorporating complicated hydrodynamic forces adds complexity to the system and creates a more realistic environment.

3.6 Summary

In this chapter the equations of motion for a lightweight underwater vehicle-manipulator have been presented based on a tree representation of the system. A recursive description of the Newton-Euler approach was used together with the Composite Rigid-Body Algorithm to describe the behaviour of the system. The hydrodynamic effects have been represented and incorporated into the UVMS equations based on mathematical models. This chapter introduced a complete model of the underwater vehicle-manipulator system. The

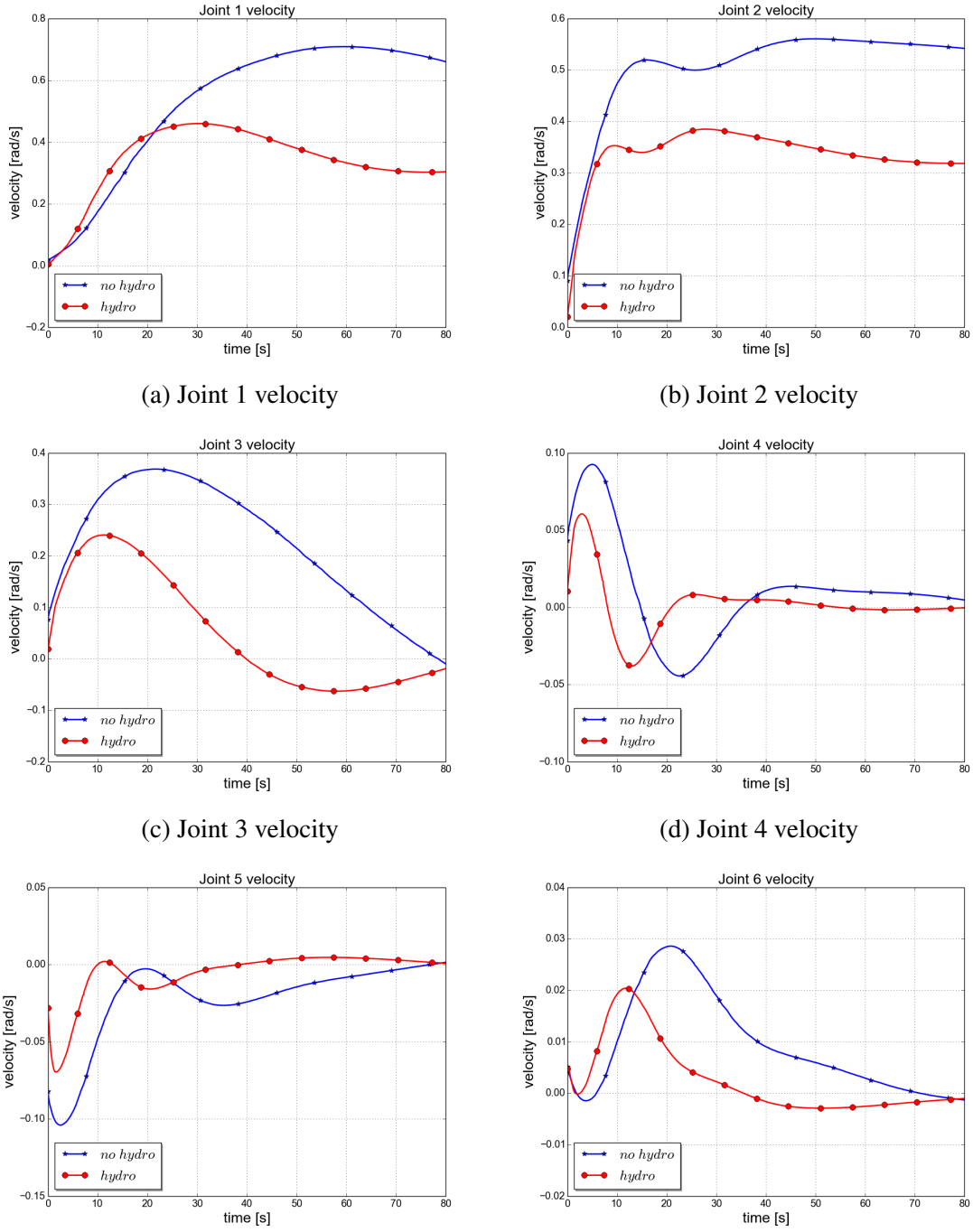

(a) Joint 1 velocity

(b) Joint 2 velocity

(c) Joint 3 velocity

(d) Joint 4 velocity

(e) Joint 5 velocity

(f) Joint 6 velocity

Figure 3.14. Hydrodynamic effects on manipulator velocities when joint 1 torque is 20 Nm and joint 2 torque is 20 Nm (no vehicle control and no manipulator control)

coupling effects between the vehicle and manipulator have been studied. The effects of the movement of the manipulator on the vehicle location were analysed when the hydrodynamic effects are included in the model and when they are not considered. The effect of the manipulator weight was also considered in the simulations. It can be concluded that without knowing precisely the movement of the arm it was hard to predict the behaviour of the system. Nevertheless, the mathematical model used to represent the UVMS was able to compute at any moment in time the coupling effects between the manipulator and ve-

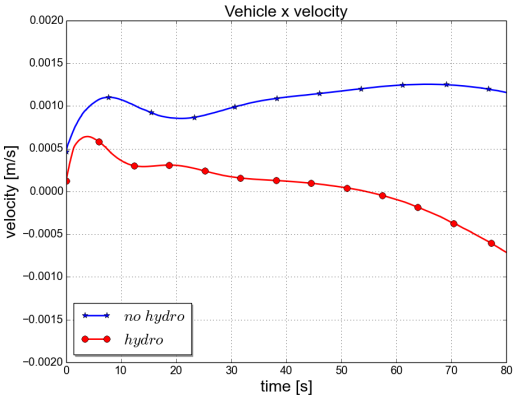

(a) x velocity

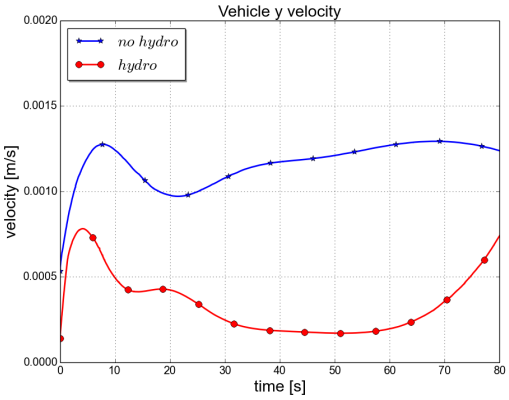

(b) y velocity

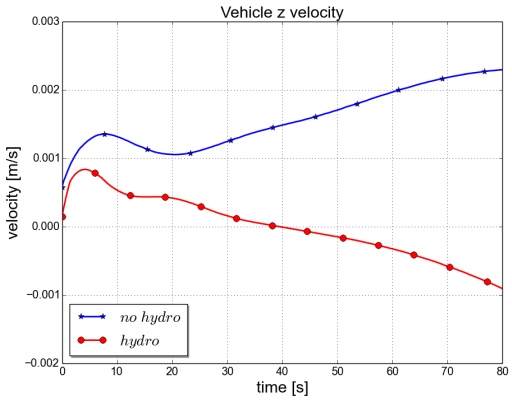

(c) Vehicle z velocity

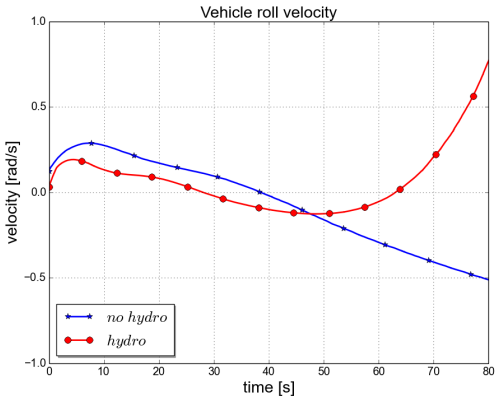

(d) roll velocity

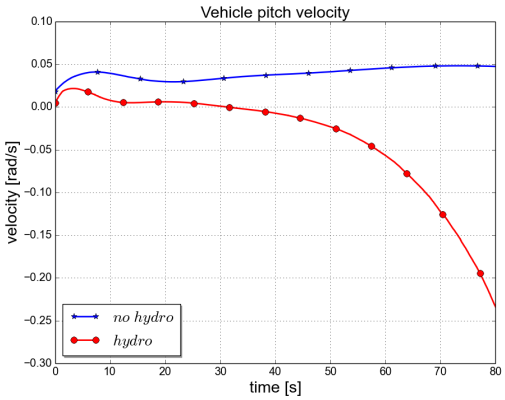

(e) pitch velocity

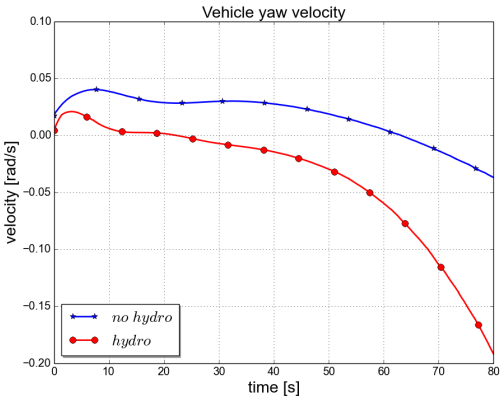

(f) yaw velocity

Figure 3.15. Hydrodynamic effects on vehicle velocities when joint joint 1 is 20 Nm and joint 2 torque is 20 Nm (no vehicle control and no manipulator control)

hicle. The main contribution in this chapter was the investigation into different dry mass ratios between vehicle-manipulator systems. The information about these coupling effects is further incorporated into the control structures presented in Chapter 4.

Chapter 4

Model based position control of an UVMS

In Chapter 3 the mathematical model of a lightweight vehicle-manipulator system was presented. Through simulations it was demonstrated that for this type of system the coupling effects between the manipulator and vehicle are significant, the vehicle being affected by the manipulator movement. Based on this observation, a control structure using the dynamic model is proposed for the control of a lightweight underwater vehicle-manipulator system. It is shown that having an accurate system model and properly understanding the interactions between the subsystems is beneficial for obtaining robust behaviour of the UVMS. This chapter starts by presenting an overview of different model based controllers for robotic systems. These types of controllers are generally valid when the uncertainty in the robot parameters is small. Control architectures that take into account the dynamic model of the system can be incorporated in robust control, adaptive control or learning control techniques [116]. The most common types of model based control architectures are feedback linearisation of nonlinear systems and feedforward control methods [117]. These controllers have a straightforward implementation of the dynamic model of the system into the control law. In Section 4.1 the computed torque controller and the feedforward control architecture are presented. In Section 4.2 a model based controller for a lightweight underwater vehicle-manipulator system is proposed. The evaluation of the controller is made through simulations and the results are presented in Section 4.3.

4.1 Model based controllers

The model based controllers represent control strategies that incorporate the mathematical model of the system to improve the behaviour of the robots. The first step in designing these types of control strategies rests in accurately identifying the kinematic and dynamic parameters of the robots. These models can be further incorporated into the position control, trajectory tracking and force control to obtain high performance strategies. In [118] the authors argue that using the dynamic model of the robot in the control strategy improves

the tracking performances by compensating for the inertia, friction and gravity forces. A list of different model based controllers is presented in Table 4.1. All the control laws take into account the dynamic model information such as inertia matrix, Coriolis and centripetal vectors and gravity forces.

PD Computed Torque Control [119]: $\tau = M(\rho)\left(\dot{\xi}_{des} + K_P e + K_D \dot{e}\right) + N(\rho, \xi)$
PD+ Control [120]: $\tau = K_P e + K_D \dot{e} + M(\rho)\dot{\xi}_{des} + N(\rho, \xi_{des})$
PD Feedforward Control [120]: $\tau = K_P e + K_D \dot{e} + M(\rho_{des})\dot{\xi}_{des} + N(\rho_{des}, \xi_{des})$
Model-reference adaptive control [116]: $\tau = \tilde{M}\dot{\xi}_{des} + \tilde{N}(\rho_{des}, \xi_{des}) - K_D s$, where $\dot{\hat{a}} = -\Gamma Y^T s$
T-S Model-Based Fuzzy Control [121]: IF z_1 is F_1^k AND $\cdots$ z_{2n} is F_{2n}^k, THEN $\tau = -K_k e + g\,[r(t) + D]$

Table 4.1. Model based control laws

In Table 4.1 the following notations are made: $\tau \in \mathbb{R}^n$ is the output of the controller, $\rho \in \mathbb{R}^n$ is the position of the system, $\xi \in \mathbb{R}^n$ is the velocity of the system, $\rho_{des} \in \mathbb{R}^n$ is the desired position, $\xi_{des} \in \mathbb{R}^n$ is the desired velocity, $e \in \mathbb{R}^n$ is the error of the system, K_P, K_D, K_k, $g \in \mathbb{R}^{n\times n}$ are gain matrices, M, $D \in \mathbb{R}^{n\times n}$, $N \in \mathbb{R}^n$ are dynamic model parameters, $\tilde{M} \in \mathbb{R}^{n\times n}$, $\tilde{N} \in \mathbb{R}^n$ and $r(t) \in \mathbb{R}^n$ are estimates of the dynamic parameters, F_i^k is a fuzzy set and z_i is a measurable variable.

The two most straightforward methods to incorporate the dynamic model into the control strategy are the computed torque control law (feedback linearisation) and the feedforward control strategy. An overview of these methods is given in the following section.

4.1.1 Computed torque controller

The computed torque controllers are part of the nonlinear controllers' class and are used extensively in robotic systems including robotic arms [116] and underwater vehicles [21]. They represent an application of feedback linearisation of nonlinear systems computing the torques/forces of the system based on a nonlinear feedback control law. The control structure is designed using the dynamic model of the robot. An accurate knowledge of the model and the physical parameters of the robot leads to a robust performance of the controller. The controller does not perform properly, reducing the behaviour of the system, when uncertainty and large variations in the physical parameters and the mathematical model occur [122]. One of the objectives of the computed torque controllers is to decouple and linearise the systems so that each degree-of-freedom is considered to be independent. This reduces the complexity of the control strategy. In [123] it is regarded as a controller

that is precise, energy efficient and has the benefit of reducing the control gains of the classical control laws.

The computed torque controllers can be described based on two control loops, an inner control loop that handles the non-linearities and an external control loop that is the feedback control loop. A general scheme of the controller is given in Figure 4.1. The computed torque controllers can differ based on the design of the strategy's feedback component.

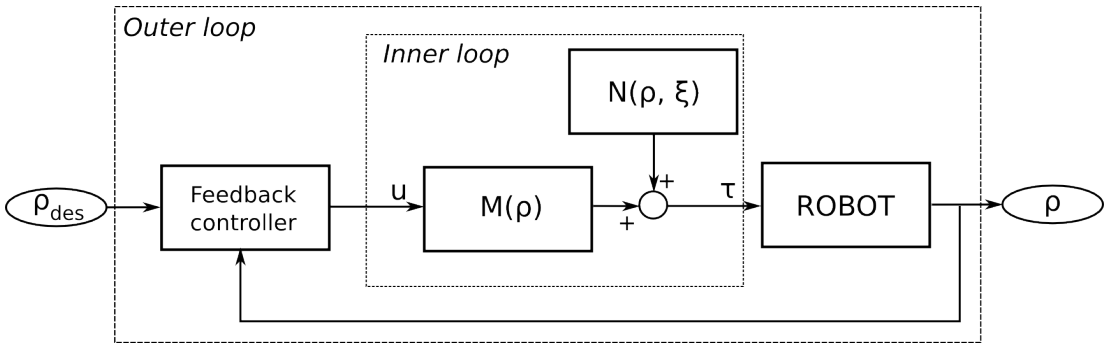

Figure 4.1. Computed torque controller

As a reminder from the previous chapter, the dynamic model of the underwater vehicle-manipulator system without the interaction with the environment can be described by Equation (4.1).

$$M(\rho)\dot{\xi} + C(\rho,\xi)\xi + D(\rho,\xi)\xi + g(\rho) + f_f(\rho) = \tau \tag{4.1}$$

or in a restricted form by Equation (4.2).

$$M(\rho)\dot{\xi} + N(\rho,\xi) = \tau \tag{4.2}$$

where

$$N(\rho,\xi) = C(\rho,\xi)\xi + D(\rho,\xi)\xi + g(\rho) + f_f(\rho) \tag{4.3}$$

The desired trajectory for each degree-of-freedom of the system is defined by $\rho_{des} \in \mathbb{R}^n$. The tracking error, $e \in \mathbb{R}^n$ defined by Equation (4.4) is used to analyse the trajectory tracking behaviour of the system.

$$e = \rho_{des} - \rho \tag{4.4}$$

Differentiating the tracking error twice and introducing it into the dynamic equation, the following relations are obtained:

$$\begin{aligned} \dot{e} &= \xi_{des} - \xi \\ \ddot{e} &= \dot{\xi}_{des} - \dot{\xi} \\ \dot{\xi} &= \dot{\xi}_{des} - \ddot{e} \end{aligned} \tag{4.5}$$

$$\begin{aligned} M\left(\dot{\xi}_{des} - \ddot{e}\right) + N &= \tau \\ M\dot{\xi}_{des} - M\ddot{e} + N &= \tau \\ M\ddot{e} &= M\dot{\xi}_{des} + N - \tau \\ \ddot{e} &= \dot{\xi}_{des} + M^{-1}(N - \tau) \end{aligned} \tag{4.6}$$

The input control law defined by Equation (4.7) is called the feedback linearising transformation. The feedback linearisation has the role to decouple the system so that an independent feedback controller for each degree-of-freedom can be implemented.

$$u = \dot{\xi}_{des} + M^{-1}(N - \tau) \tag{4.7}$$

By inverting Equation (4.7) the computed control law expression is given by:

$$\tau = M\left(\dot{\xi}_{des} - u\right) + N \tag{4.8}$$

By choosing u so that the trajectory tracking error converges to zero, for example u can be a PD controller, the nonlinear control input given by Equation (4.8) ensures trajectory following for the system. Using the presented equations, the nonlinear control design problem is reduced to a linear control problem consisting of a series of decoupled systems. The method is dependent on the dynamic model of the system. In Equation (4.8) the control law is computed based on the desired acceleration of the system.

As mentioned in [116] a variety of methods can be used to design the outer loop control signal u, from classical control methods to robust and adaptive control laws.

Different strategies for the outer loop together with the model based linearisation technique are presented in Table 4.2, where $\tilde{M} \in \mathbb{R}^{n \times n}$ and $\tilde{N} \in \mathbb{R}^n$ are estimations of the dynamic model parameters of the system.

PD Computed Torque:
$\tau = M(\rho)\left(\dot{\xi}_{des} + K_P e + K_D \dot{e}\right) + N(\rho, \xi)$
PID Computed Torque:
$\tau = M(\rho)\left(\dot{\xi}_{des} + K_P e + K_D \dot{e} + K_I \int_0^t e d\tau\right) + N(\rho, \xi)$
PD Gravity Control:
$\tau = K_P e + K_D \dot{e} + g(\rho), \quad \text{where} \quad M = I \quad \text{and} \quad N = g(\rho) - \dot{\xi}_{des}$
Approximate Computed Torque Control [116]:
$\tau = \tilde{M}(\dot{\xi}_{des} - u) + \tilde{N},$ where $\ddot{e} = (I - \Delta)u + d, \quad \Delta = I - M^{-1}\tilde{M}, \quad \delta = M^{-1}\left(N - \tilde{N}\right)$ and $d(t) = M^{-1}\tau_d + \Delta\dot{\xi}_{des}(t) + \delta(t)$

Table 4.2. Computed torque control laws

4.1.2 Feedforward controller

The open-loop control strategies based on the inverse dynamics approach use the desired trajectory and velocity of the system to compute the torques/forces required to complete specified tasks. In [124] these methods are considered to be part of conceptually simple architectures. In the case when the dynamic model replicates exactly the robotic system the forces/torques computed with these methods ensure trajectory tracking. However, in practice the dynamic model is not perfectly known and a feedback controller is needed to compensate for the errors in the trajectory tracking.

The system to control is defined by Equation (4.1). The desired trajectory ρ_{des} and the desired velocity ξ_{des} are assumed to be bounded. The goal is to obtain $\rho(t) \to \rho_{des}$ when $t \to \infty$. By defining the error vector by Equation (4.4), the input $\tau \in \mathbb{R}^n$ has to be defined such that:

$$\lim_{t\to\infty} e = 0 \tag{4.9}$$

Using the inverse dynamic model defined based on the desired response of the system, the feedforward control law is designed according to Equation (4.10).

$$\tau = M(\rho_{des})\dot{\xi}_{des} + C(\rho_{des},\xi_{des})\xi_{des} + D(\rho_{des},\xi_{des})\xi_{des} + g(\rho_{des}) + f_f(\rho_{des}) \tag{4.10}$$

Substituting Equation (4.10) into Equation (4.1) gives:

$$\begin{aligned} M(\rho_{des})\dot{\xi}_{des} + C(\rho_{des},\xi_{des})\xi_{des} + D(\rho_{des},\xi_{des})\xi_{des} + g(\rho_{des}) + f_f(\rho_{des}) = \\ M(\rho)\dot{\xi} + C(\rho,\xi)\xi + D(\rho,\xi)\xi + g(\rho) + f_f(\rho) \end{aligned} \tag{4.11}$$

Equation (4.11) can be rewritten based on the system error:

$$\begin{aligned} M\dot{\xi} - M\dot{\xi}_{des} &= M_{des}\dot{\xi}_{des} - M\dot{\xi}_{des} + C_{des}\xi_{des} - C\xi + D_{des}\xi_{des} - D\xi + g_{des} - g + f_{f_{des}} - f_f \Leftrightarrow \\ \Leftrightarrow -M\ddot{e} &= M_{des}\dot{\xi}_{des} - M\dot{\xi}_{des} + C_{des}\xi_{des} - C\xi + D_{des}\xi_{des} - D\xi + g_{des} - g + f_{f_{des}} - f_f \Leftrightarrow \\ \Leftrightarrow \ddot{e} &= -M^{-1}\left[\dot{\xi}_{des}(M_{des} - M) + C_{des}\xi_{des} - C\xi + D_{des}\xi_{des} - D\xi + g_{des} - g + f_{f_{des}} - f_f\right] \end{aligned} \tag{4.12}$$

Equation (4.12) is simplified to:

$$\ddot{e} = -M^{-1}\left[\dot{\xi}_{des}(M_{des} - M) + H(\rho)\right] \tag{4.13}$$

where

$$H(\rho) = C_{des}\xi_{des} - C\xi + D_{des}\xi_{des} - D\xi + g_{des} - g + f_{f_{des}} - f_f \tag{4.14}$$

Equation (4.13) represents the error tracking dynamics. It can be seen that the error depends only on the dynamic characteristics of the system making it difficult to change the equilibrium points or their stability properties.

The method is an open-loop strategy as it doesn't depend on the position or the velocity of the system. Moreover, in this strategy there is no parameter that has to be tuned, a fact

that makes it an attractive control strategy. As it uses the mathematical model of the system, the method is known as a model based feedforward control strategy. The advantage of this type of control structure is in the implementation characteristics. Knowing the parameters and the desired position, velocity and acceleration of the system, the ideal dynamic components $M(\rho_{des})$, $C(\rho_{des}, \xi_{des})$, $D(\rho_{des}, \xi_{des})$ can be computed. The method is advantageous especially for repetitive tasks when this information can be computed off-line and reused during all experiments. The method is mostly used to compensate for known or measurable disturbances that might affect the system. Nevertheless, for making this strategy reliable for real robotic systems a precise knowledge of the parameters is needed. The disadvantage of the method is the lack of robustness when external perturbation is present or when there are uncertainties in the model parameters.

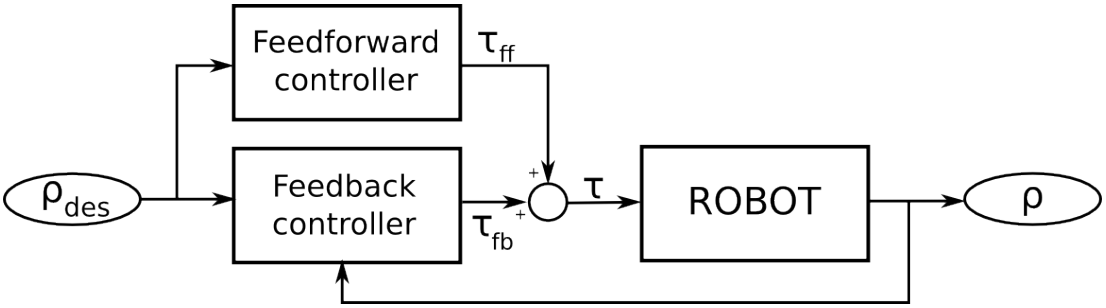

Figure 4.2. Feedforward plus feedback controller

In practical applications for underwater environments the feedforward control on its own does not represent a viable option due to the uncertainty in the model of the robotic system. Nonetheless, due to the small number of computations required for this control law and for improving the tracking accuracy of the system, the feedforward control law can be used reliably with feedback controllers. The feedforward component is the principle part of the control scheme, while the feedback is used to ensure that there is no significant deviation from the normal behaviour. This approach results in high precision control structures that are mostly used when high acceleration and small settling time is needed [125]. A feedforward control law together with a feedback control law can be represented in Figure 4.2.

4.2 Problem statement

The aim of this chapter is to demonstrate that for lightweight vehicle-manipulator systems having an accurate model and understanding the interactions between the components can be useful to reduce the coupling effects between subsystems. Section 4.1.1 and Section 4.1.2 presented a theoretical background of the two most used types of model based control. This section is focused on introducing a controller based on these approaches. The proposed strategy aims to reduce the coupling effects between the vehicle and manipulator. Furthermore, the control law aims to provide a reliable position control strategy for

the UVMS. The control structure proposed is based on three components: a feedforward controller, a linearised feedback controller and the subsystem coupling effects. The control architecture developed aims to incorporate the mathematical knowledge of the robotic systems and the prediction of the interactions between subsystems. Using the mathematical knowledge of the system can be beneficial for the case when the parameters and relationships between the components of the system are known, reducing the computation time and the complexity of the system by handling the non-linearities.

A comparison of this strategy with two other control strategies is presented in the results section: a PID/PILIM feedback controller and a feedback linearisation controller.

The robotic platform used to develop the control strategy is the same as the one presented in Chapter 3. The underwater vehicle-manipulator system consists of a 5 DOF vehicle and a 6-link manipulator. The equations of motion are based on a tree representation of the UVMS and are described with the Newton-Euler algorithm. Hydrodynamic effects and friction considerations are taken into account in the forward dynamic model. The mathematical structure and the implementation characteristics of the overall control architecture are presented in the following section.

4.2.1 Force Coupling - Model Control structure

The overall control architecture is presented in Figure 4.3. The main components of the controller are the feedforward open-loop controller, the model feedback controller and the mathematical computed interaction forces between subsystems. The overall control law is indicated as the Force Coupling - Model Control (FC-MC). In the next part a detailed presentation of each component of the FC-MC Control is given.

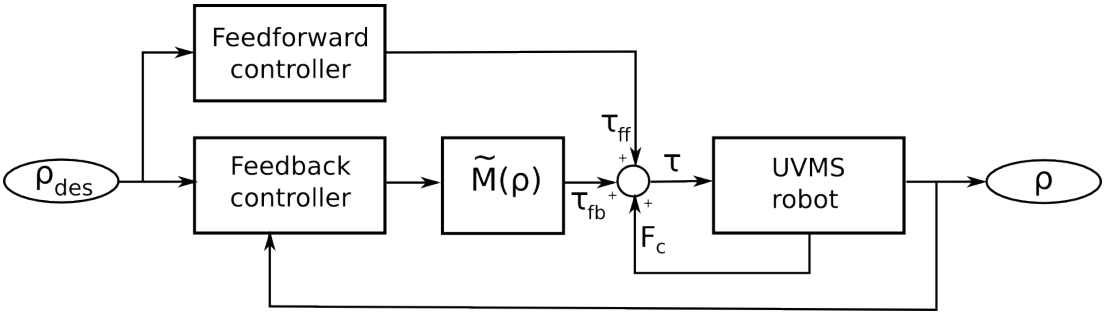

Figure 4.3. Force Coupling - Model Control structure

Feedforward controller component

The feedforward controller used is based on the inverse dynamic model developed in Chapter 3. The inverse dynamic (ID) model computes the forces acting on the system when the acceleration of the system is already known. To properly implement this controller, the desired trajectory of the system has to be formulated for each degree-of-freedom as a trajectory. The Composite Rigid Body Dynamics represents one of the easiest, efficient

and most used methods to compute the forces that act on a robotic system. The feedforward torque/force $\tau_{ff} \in \mathbb{R}^n$ can be computed based on the Composite Rigid Body Dynamic equations and rewritten in a closed-loop matrix form as shown in Equation (4.15).

$$\tau_{ff} = \tilde{M}(\rho_{des})\dot{\xi}_{des} + \tilde{N}(\rho_{des}, \xi_{des}) \tag{4.15}$$

where

$$\tilde{N}(\rho_{des}, \xi_{des}) = \tilde{C}(\rho_{des}, \xi_{des})\xi_{des} + \tilde{D}(\rho_{des}, \xi_{des})\xi_{des} + \tilde{g}(\rho_{des}) + \tilde{f}_f(\rho_{des}) \tag{4.16}$$

$\tilde{M}(\rho_{des})$ is an estimate of the inertia term, $\tilde{C}(\rho_{des}, \xi_{des})$, $\tilde{D}(\rho_{des}, \xi_{des})$, $\tilde{g}(\rho_{des})$, $\tilde{f}_f(\rho_{des})$ are estimates of the real values of the system according to the boundary errors, $\delta M(\rho_{des})$, $\delta C(\rho_{des}, \xi_{des})$, $\delta D(\rho_{des}, \xi_{des})$, $\delta g(\rho_{des})$, $\delta f_f(\rho_{des})$ are defined by Equation (4.17):

$$\begin{aligned}
|\, \Delta M(\rho_{des}) \,| &\leq \delta M(\rho_{des}) \quad & \Delta M(\rho_{des}) &= M(\rho_{des}) - \tilde{M}(\rho_{des}) \\
|\, \Delta C(\rho_{des}, \xi_{des}) \,| &\leq \delta C(\rho_{des}, \xi_{des}) \quad & \Delta C(\rho_{des}, \xi_{des}) &= C(\rho_{des}, \xi_{des}) - \tilde{C}(\rho_{des}, \xi_{des}) \\
|\, \Delta D(\rho_{des}, \xi_{des}) \,| &\leq \delta D(\rho_{des}, \xi_{des}) \quad & \Delta D(\rho_{des}, \xi_{des}) &= D(\rho_{des}, \xi_{des}) - \tilde{D}(\rho_{des}, \xi_{des}) \\
|\, \Delta g(\rho_{des}) \,| &\leq \delta g(\rho_{des}) \quad & \Delta g(\rho_{des}) &= g(\rho_{des}) - \tilde{g}(\rho_{des}) \\
|\, \Delta f_f(\rho_{des}) \,| &\leq \delta f_f(\rho_{des}) \quad & \Delta f_f(\rho_{des}) &= f_f(\rho_{des}) - \tilde{f}_f(\rho_{des})
\end{aligned} \tag{4.17}$$

Using these estimations in the feedforward control law implies that the parameters of the system are not perfectly known and there are discrepancies between the real system and the model used in the control law.

Coupling effects controller component

Using the inverse dynamic model as the feedforward controller can be sufficient to obtain a reliable control law when the system is perfectly known. Nonetheless, uncertainties in the system might lead to inappropriate behaviour, especially for lightweight systems where the effects of the movement of the manipulator affects the vehicle behaviour. To this extent having the knowledge of the interaction between subsystems can be taken into account in the control strategy. In this case the coupling effects between the vehicle and manipulator are computed based on the real position and velocity of the system. The recursive Newton-Euler algorithm [15] as described in Chapter 3 is used to obtain the coupling effects, $F_c \in \mathbb{R}^n$, Equation (4.18). In concise form, the components of $F_c = \left[f_1^0,\, f_2^1, \cdots, f_n^{n-1}\right]$ can be expressed based on the spatial force propagation as presented in Equation (4.19):

$$F_c = \mathrm{NE}(\rho, \xi)\dot{\xi} \tag{4.18}$$

$$f_{i+1}^i = R_{i+1}^i(f_i + m_i\dot{\xi}_{c_i} + b_i) \tag{4.19}$$

where $R^i_{i+1} \in \mathbb{R}^{n\times n}$ is the geometric transformation between subsystems $(i+1)$ and i, $f_i \in \mathbb{R}^n$ is the force applied on the current component i, $m_i \in \mathbb{R}^n$ is it's mass, $\dot{\xi}_{c_i} \in \mathbb{R}^n$ is the acceleration of the centre of mass of subsystem i and $b_i \in \mathbb{R}^n$ are the external forces applied to the component i.

The coupling force approximation is essential for obtaining accurate trajectory tracking even in the presence of uncertainties in the model. Being able to predict the coupling effects between subsystems and how these affect the overall capabilities of the UVMS is valuable information to incorporate in the controller.

Model feedback controller component

As presented in [126], to obtain a reliable behaviour of the system the feedforward controller has to be used with a feedback controller to compensate for the uncertainties in the system. The model feedback (MF) control law consists of a feedback control law and the mathematical approximation of the inertia matrix of the system. For each degree-of-freedom of the UVMS a feedback control law is designed. Different feedback control strategies are implemented for the manipulator and the vehicle.

Proportional Integral Derivative Controller In the case of the feedback control law of the manipulator, the Proportional Integral Derivative (PID) Control is used. The mathematical representation of a PID controller is presented in Equation (4.20).

$$\tau_q = K_{P_q} e_q + K_{D_q} \dot{e}_q + K_{I_q} \int_0^t e_q d\tau \tag{4.20}$$

where $e_q = q_{des} - q$ is the error in position for the manipulator joints, $K_{P_q} \in \mathbb{R}^{m\times m}$ is the proportional gain matrix, $K_{D_q} \in \mathbb{R}^{m\times m}$ is the derivative gain matrix and $K_{I_q} \in \mathbb{R}^{m\times m}$ is the integral gain matrix where m are the number of degrees-of-freedom of the manipulator. The gain matrices can be defined as diagonal positive matrices so that:

$$K_P = diag\{k_{p_i}\} \quad K_D = diag\{k_{d_i}\} \quad K_I = diag\{k_{i_i}\} \tag{4.21}$$

Proportional Integral Limited Controller The feedback control strategy for each of the degrees-of-freedom of the vehicle is designed starting with the assumption that the maximum speed of the vehicle is 2 m/sec for x, y, z and 0.75 rad/sec for the *pitch* and *yaw*. The feedback control strategy proposed is called Proportional Integral Limited (PILIM) and represents a simple and efficient method. The main characteristics of the control law are fast transient response and no overshoot in the behaviour of the system. The controller was proposed for the first time by Bellec in [127] and can be represented as shown in Figure 4.4. The controller consists of two control loops: an outer control loop for the position and an inner control loop for the velocity control. Both control loops are subclasses of the PID control strategy. The position control loop has a proportional component. The velocity control loop has a proportional and an integral component. An essential component

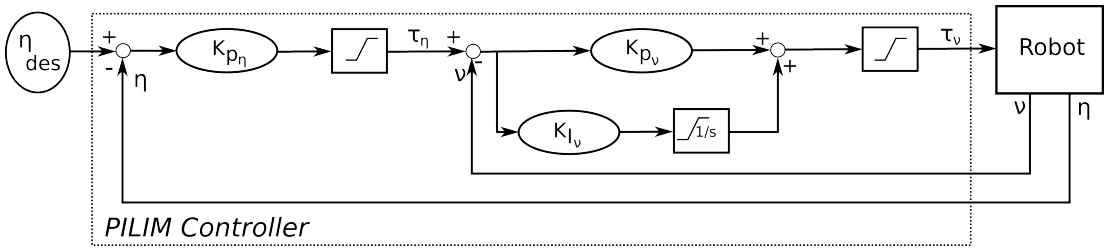

Figure 4.4. Proportional Integral Limited compensator, [127]

included in this feedback control architecture is the integrator anti wind-up component responsible for handling the overshoot in the case of control saturation.

One important characteristic in the behaviour of the system includes the distance between the current position of the vehicle and the goal. If the vehicle is close to the goal, the system is under position control, while if the distance between the vehicle and the goal is large the vehicle is under velocity control. The equations characterizing the system are presented in Equation (4.22).

$$\begin{aligned} e_\eta &= \eta_{des} - \eta \\ e_\nu &= \tau_\eta - \nu \\ \tau_\eta &= K_{P_\eta} e_\eta \\ \tau_\nu &= K_{P_\nu} e_\nu + K_{I_\nu} \int_0^t e_\nu d\tau \\ F_{min_\eta} &\leq \tau_\eta \leq F_{max_\eta} \\ F_{min_\nu} &\leq \tau_\nu \leq F_{max_\nu} \end{aligned} \tag{4.22}$$

where $\eta \in \mathbb{R}^6$ represents the position of the vehicle, $\nu \in \mathbb{R}^6$ is the velocity of the vehicle, $\eta_{des} \in \mathbb{R}^6$ is the desired position, $e_\eta \in \mathbb{R}^6$ is the error in position, e_ν is the error in velocity, $\tau_\eta \in \mathbb{R}^6$ is the force generated by the position controller, $\tau_\nu \in \mathbb{R}^6$ is the force acting on the system, $K_{P_\eta} \in \mathbb{R}^{6\times6}$ is the position proportional gain, $K_{P_\nu} \in \mathbb{R}^{6\times6}$ is the velocity proportional gain and $K_{I_\nu} \in \mathbb{R}^{6\times6}$ is the velocity integral gain. F_{min_η}, F_{min_ν}, F_{max_η}, $F_{max_\nu} \in \mathbb{R}^6$ represent the control limits.

The model feedback control incorporates an approximation of the inertia matrix, $\tilde{M}(\rho)$ into the control strategy. The aim in using this component in the control law is to linearise the system without overloading the computational complexity of the control strategy. This can be regarded as an imperfect compensation of the system inverse dynamics. In this case only the most powerful component of the mathematical model is taken into account, the feedback controller being responsible for the trajectory tracking and for obtaining a stable system. The overall MF control strategy is presented by Equation (4.23).

$$\begin{aligned} \tau_{\nu,q} &= \left[\tau_\nu,\ \tau_q\right]^T \\ \tau_{fb} &= \tilde{M}(\rho) \cdot \tau_{\nu,q} \end{aligned} \tag{4.23}$$

where $\tilde{M}(\rho) \in \mathbb{R}^{n\times n}$ is an approximation of the inertia matrix of the system and $\tau_{fb} \in \mathbb{R}^n$ is

the torque/force component of the controller based on the model feedback control law and n is the total number of degrees-of-freedom of the underwater vehicle-manipulator system. Using the approximation of the inertia matrix implies that the model is not perfectly known and there is not a perfect match between the real system and the model used to linearise the system.

Final Control Law: FC-MC Controller

In the proposed control law uncertainty in the dynamic model used for the feedforward component and in the linearisation component are present. It is shown through simulation results that using an uncertain model can be beneficial for obtaining a robust behaviour from the system. The total control law is defined by Equation (4.24), incorporating all the components previously described.

$$\tau = \tau_{ff} + \tau_{fb} + F_c \tag{4.24}$$

where

$$\begin{aligned} \tau_{ff} &= \tilde{M}(\rho_{des})\dot{\xi}_{des} + \tilde{N}(\rho_{des}, \xi_{des}) \\ \tau_{fb} &= \tilde{M}(\rho)\tau_{v,q} \\ F_c &= \mathrm{NE}(\rho, \xi)\dot{\xi} \end{aligned} \tag{4.25}$$

The role of each of the controller components is summarised here:

- τ_{ff} is the feedforward controller component, representing the principle component responsible for the trajectory tracking.
- τ_{fb} is the feedback component that ensures that there is no significant deviation from the trajectory tracking. The component consists of a linearisation component that decouples the system and allows the creation of independent feedback laws for each degree-of-freedom of the UVMS.
- F_C is the estimation of coupling effects and has the role of reducing the effects of the manipulator movement on the vehicle.

In Appendix B the Lyapunov stability study is presented for the proposed controller.

4.3 Simulation results

In this section the results obtained using the proposed controller (marked as FC-MC controller) are compared with the feedback PID/PILIM controller and the feedback linearisation technique (marked as FBL controller). The feedback PID/PILIM controller has the same structure as the one described in detail in Section 4.2.1. The same feedback controller is used in the feedback linearisation method, where the full dynamic model is used to obtain a decoupled system.

The system to be controlled is represented by the 5 DOFs vehicle and the 6-link manipulator described in Chapter 3. The roll DOF of the vehicle is not controlled due to the placement of the thrusters. The ratio between the vehicle and the manipulator dry mass is $1:7$, the effects of the movement of the manipulator on the vehicle being considerable in the pitch and yaw DOFs as presented by the simulation results in Chapter 3. The goal of the control structure is to obtain accurate trajectory tracking for both the vehicle and manipulator. Moreover, the control law proposed aims to reduce the effects of the manipulator movement on the vehicle station keeping. Two different trajectories for the manipulator movement are used in this chapter: the cycloid function and a sinusoidal path.

4.3.1 Cycloid movement of manipulator joints

The first set of simulations aims to display the station keeping capabilities of the vehicle when the manipulator has to reach a certain goal. The controllers are evaluated based on the performance of manipulator trajectory tracking and on the vehicle capability to maintain its position.

These tests are performed considering the desired trajectories for the manipulator links are cycloidal functions. These functions are responsible in defining the waypoints for each degree-of-freedom until the final goal is reached. The trajectory generated is an alternative for the step function. In Equation (4.26) the cycloid function [128] is defined:

$$\begin{aligned} \rho_{des}(t) &= \rho_{init}(0) + [\omega t - \sin(\omega t)]\frac{\Delta}{2\pi} \\ \xi_{des}(t) &= (1-\cos(\omega)t)\,\frac{\Delta}{t_f} \\ \dot{\xi}_{des}(t) &= 2\pi\sin(\omega t)\frac{\Delta}{t_f^2} \end{aligned} \tag{4.26}$$

where

$$\omega = 2\pi/t_f, \quad \Delta = \rho_{des}(t_f) - \rho_{init}(0), \quad 0 \le t \le t_f$$

The sampling frequency ω is responsible for the type of trajectory obtained. If ω has very small values a continuous trajectory is obtained, while if a larger value is used, small steps are visible in the generated trajectory. The requirements of the cycloid function for the links of the manipulator, for the simulations presented in this chapter, are:

- $t_f = 12$ sec;
- $\rho_{init_m} = [0,\ 0,\ 0,0,\ 0,\ 0]$ rad;
- $\rho_{des_m} = [-0.7,\ 1.1,\ -1.1,\ 1.35,\ 0.95,\ 0.95]$ rad.

The behaviour of the manipulator is shown in Figure 4.5 where the FC-MC controller is represented along with the PID controller and the feedback linearisation. The curves represented in green are the reference trajectories as described by the cycloid function. The PID

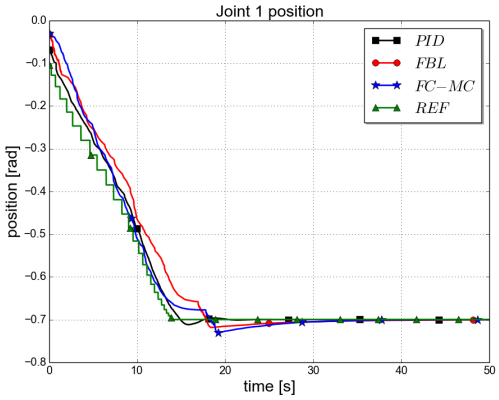

(a) Joint 1 position

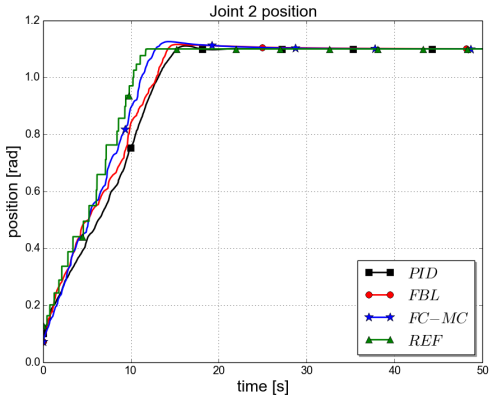

(b) Joint 2 position

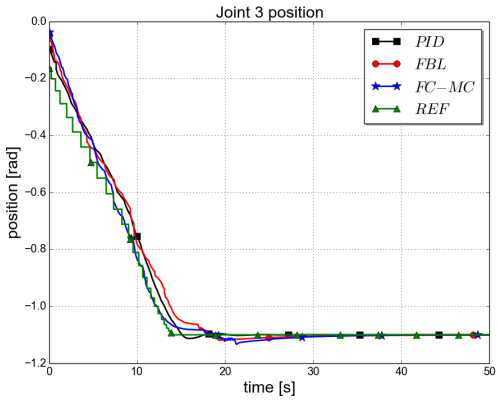

(c) Joint 3 position

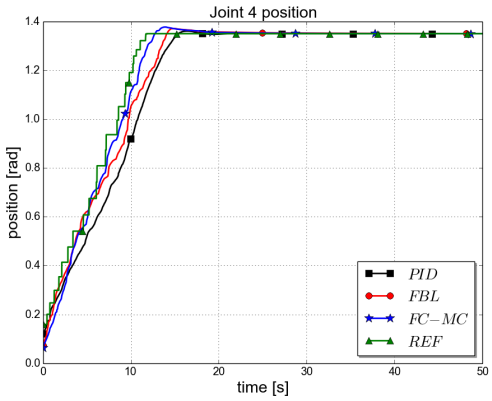

(d) Joint 4 position

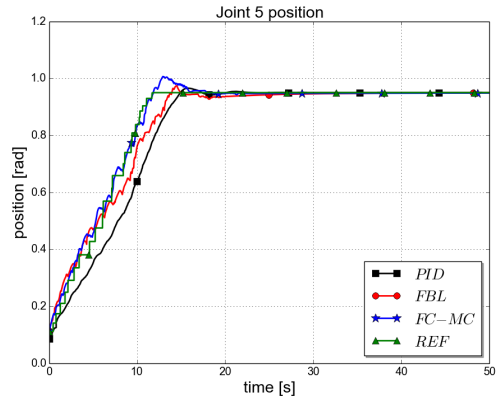

(e) Joint 5 position

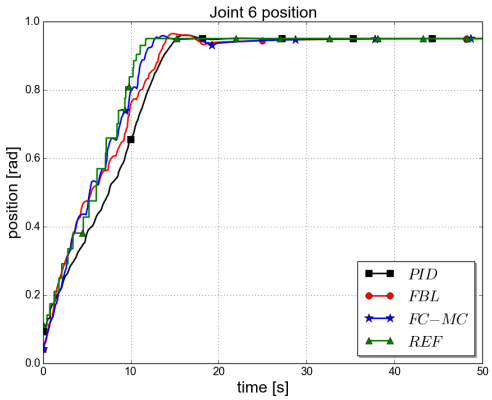

(f) Joint 6 position

Figure 4.5. Cycloidal joint positions tracking

controllers are represented by a black colour and the red lines represent the behaviour of the manipulator when the feedback linearisation is used. The FC-MC controller is represented by the blue lines. Using any of the proposed controllers, the joint trajectories are followed in a similar way. The desired trajectory consists of small step functions and an accurate following of this leads to the oscillatory behaviour in the response of the joints' position. The model based controllers present a more oscillatory behaviour than the PID control strategy as can be seen in the behaviour of joint 5, Figure 4.5e. In this case although the FC-MC response has considerably more overshoot than the FBL response, it more accurately follows

the joint trajectory. For all joints, the FC-MC controller presents a small improvement in the trajectory tracking as opposed to the PID and FBL controllers.

For this test case, the task to be executed by the vehicle is to maintain its current position. From this it can be evaluated how the proposed control strategies resolves the coupling effects between the vehicle and manipulator. More precisely how these effects are reduced to not affect the overall behaviour of the system. The same colour code is maintained for the three control strategies. As observed previously in Figure 4.5, the joints have a consid-

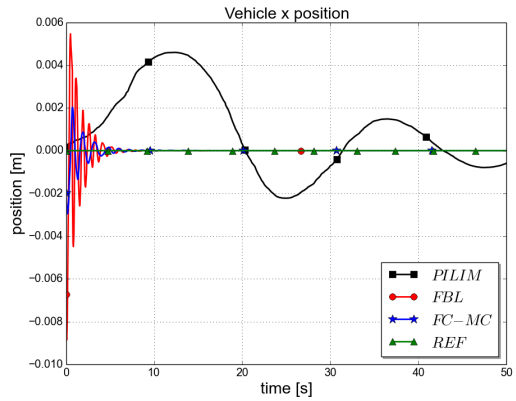

(a) Vehicle x position

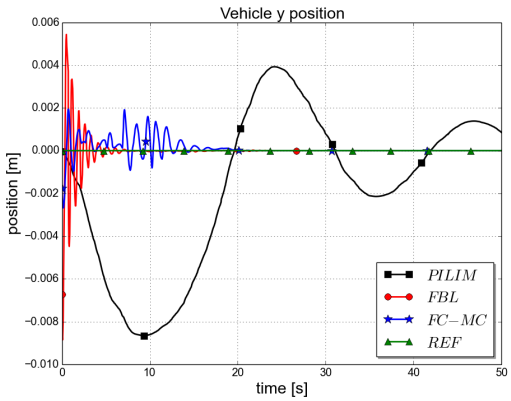

(b) Vehicle y position

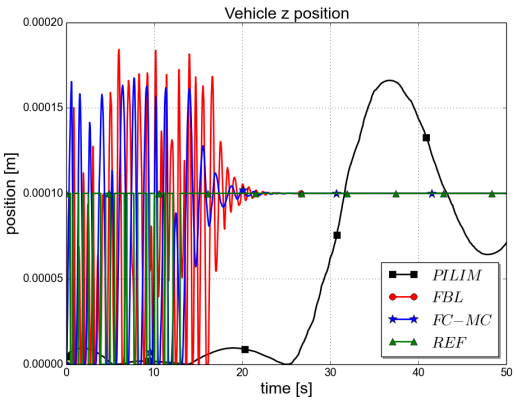

(c) Vehicle z position

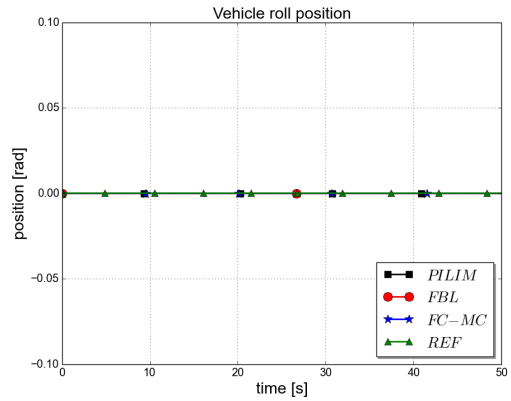

(d) Vehicle *roll* position

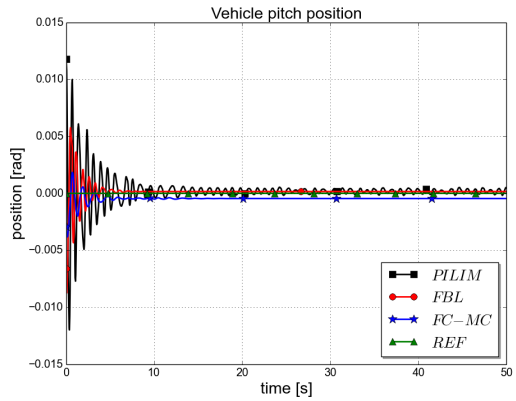

(e) Vehicle *pitch* position

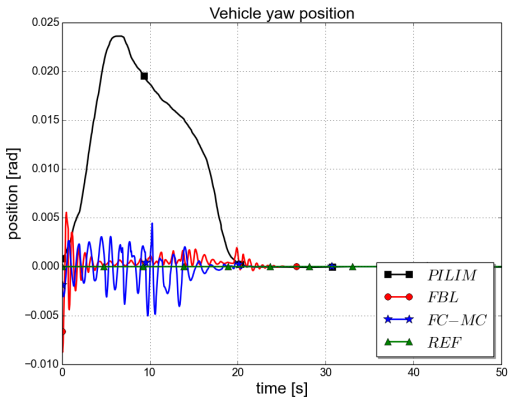

(f) Vehicle *yaw* position

Figure 4.6. Vehicle station keeping for cycloid joint movements

erable velocity over a short period of time. Figure 4.6 shows the station keeping capability

of the vehicle when the manipulator moves as presented in Figure 4.5. Differences in the response of the vehicle can be seen dependent on the type of controller used. The two model based controllers present a more oscillatory behaviour for the case when the manipulator is actively moving, while the PILIM controller makes the system oscillate at a slower rate, but with larger amplitude. For the translation degrees-of-freedom x, y and z the effects of the manipulator movement are very small, all the three control strategies reduce the coupling effects. For the surge of the vehicle, Figure 4.6a the FC-MC controller presents the best behaviour, having the lowest oscillation amplitude and for the shortest duration. The feedback linearisation technique presents at the beginning of the simulation the largest movement but the time needed to reach a steady-state position is similar with the one obtained using the FC-MC controller. The PILIM controller produces oscillations in the system at a slower rate than the other two controllers and the settling time for this DOF is considerably higher. A similar case can be observed for the sway axis. In this case the amplitude of the oscillations produced by the FC-MC controller is the smallest compared with the other two controllers but the settling time is higher than the case when the feedback linearisation is used. A maximum displacement of 0.09 m from the current location is observed in the y-axes, Figure 4.6b when the feedback PILIM controller is used. For the z-axes, Figure 4.6c, all the three controllers perform reliably well, the amplitude of the oscillations being very small.

The *roll* degree-of-freedom represents a particular case as it is not actuated and no control strategy is implemented for this degree-of-freedom. As mentioned in Chapter 3 using the lightweight vehicle-manipulator system and the mathematical model proposed in this thesis, the most affected degrees-of-freedom of the vehicle when the manipulator is moving are the *pitch* and *yaw* DOFs. One of the goals of the current chapter is to obtain a good control method that reduces these effects. In Figure 4.6e the *pitch* angle behaviour is presented. In this case all controllers perform similarly, the oscillations of the PILIM controller have the same frequency as the model based controllers. The peak position using the PILIM controller is of 0.013 rad (0.07 deg) at the beginning of the simulation. The oscillatory behaviour of the system is present for a longer period when using this controller but the value is negligible. Slightly smaller oscillations are obtained with the other two controllers. Using the PILIM controller for the *yaw* of the vehicle, Figure 4.6f, causes the largest displacement of the system from the desired configuration. By the time the manipulator reaches the final configuration a displacement of the *yaw* of 0.025 rad (1.43 deg) is achieved. The controller recovers from this displacement and the settling time for this system is reached in 20 sec similar to the case when the FC-MC controller or FBL controller is used. The two model based controllers perform similarly.

The influence of the movement of the manipulator on the behaviour of the vehicle when using the model based controllers can be seen in the simulation results. Using the model based controllers, in the first 10 sec of the simulation the manipulator moves at a considerable velocity and oscillations occur on the vehicle station keeping. After the manipulator reaches the steady-state position these oscillations are damped. These effects are introduced

by the estimated dynamic model used in the control strategy that would add a small force in the control effort linked to the behaviour of the other subsystems. The mean of the amplitude of the oscillations is smaller when using the proposed FC-MC controller. The coupling effects incorporated in this control law help to reduce these oscillations. Nonetheless, these oscillations do not affect the behaviour of the system and the model based methods present improved results compared to the PILIM controller.

4.3.2 Sinusoidal movement of manipulator joints

To observe how the controllers handle the coupling effects over a longer period of time a sinusoidal path is used to define the trajectory for the manipulator as presented by Equation (4.27):

$$\rho_{des} = Asin(\omega t + \phi) \tag{4.27}$$

where A is the amplitude, ω is the angular frequency and ϕ is the phase.

In Figure 4.7 the trajectory tracking of the manipulator joints is presented. In this case the first four joints are commanded to move and the last two have to keep the initial configuration. Different amplitudes of the sinusoidal trajectories are required for the joints. This generates a considerable manipulator movement but the time to change the configuration of the manipulator is slow. In the previous case, using the cycloidal function for trajectory generation, the interest is in having a relatively high velocity of the manipulator and analysing how this is handled by the controllers. In this case, the velocity requirement is low but the amplitude of the movement is larger and the time of manipulator movement is longer. The controller behaviour is studied in this case. The joints accurately follow the requested trajectory, no substantial difference being encountered between the tested controllers. A particular behaviour is observed when the desired movement of the arm has a small amplitude, Figure 4.7c, or when it is requested to keep the initial location, Figure 4.7e and Figure 4.7f. Small deviations in the joint position output from the desired value is obtained using the model based controllers. These effects are caused by the extra torque introduced by the dynamic model component and interaction forces between joints. Furthermore, the incomplete estimate model for the linearisation of the system contributes to these effects. Using the PID controllers, this behaviour is reduced compared with the cases when the model based controllers are implemented. Nevertheless, the amplitude of these displacements is not significant. The maximum amplitude reached is less than 0.01 rad (0.57 deg) in 130 sec and does not affect the performance of the manipulator movement.

The vehicle station keeping behaviour when the manipulator has sinusoidal movement is presented in Figure 4.8. In this case a few differences between the three controllers can be observed. For the x-axis, Figure 4.8a, and the y-axis, Figure 4.8b, the PILIM controller allows the vehicle to have small displacements, up to 0.2 m from the initial location during the movement of the arm. These oscillations over the settling point develop at a slow rate relative to the rate of the movement of the joints. The model based controllers have a stronger influence on the station keeping of these two degrees-of-freedom. In this case the

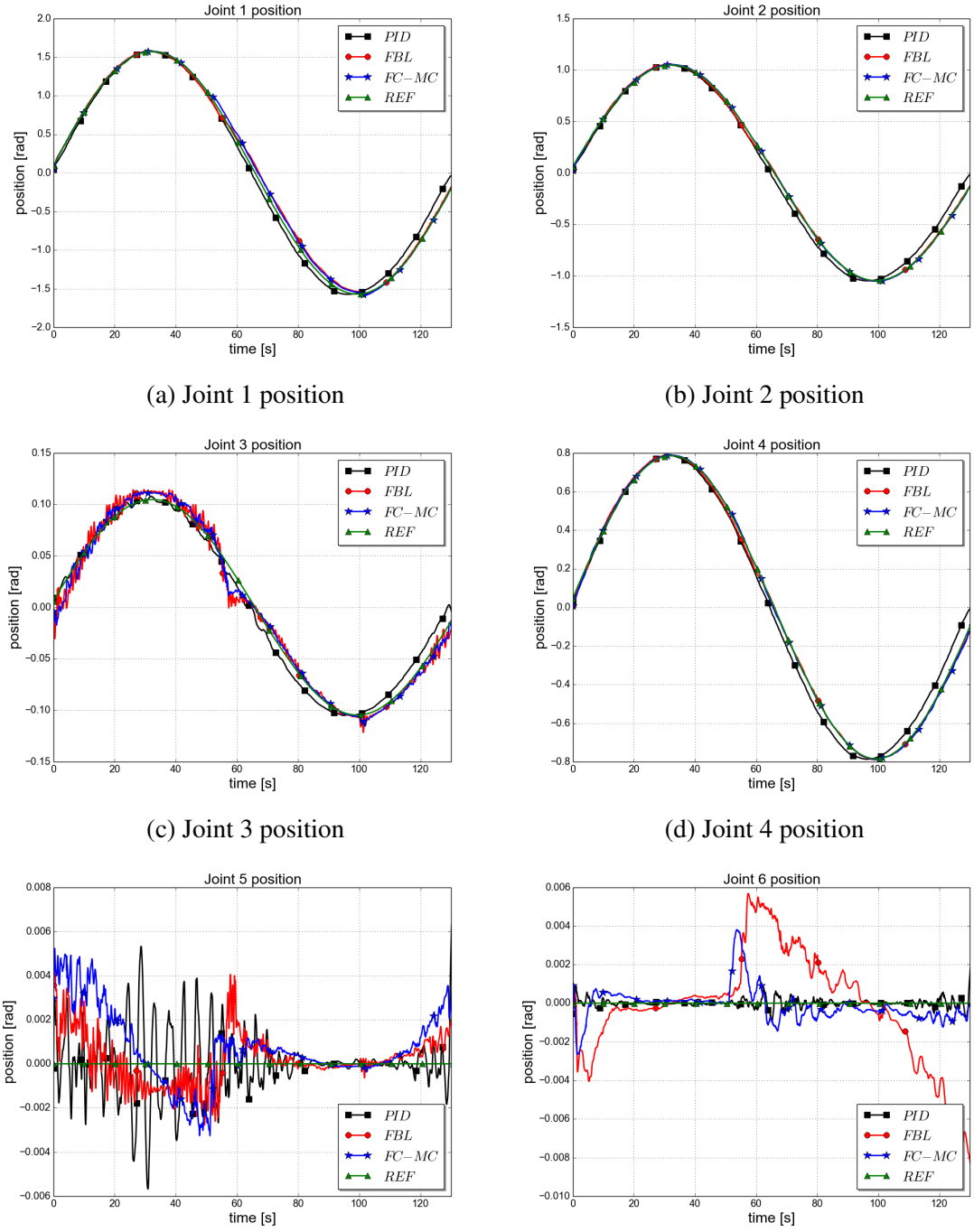

(a) Joint 1 position

(b) Joint 2 position

(c) Joint 3 position

(d) Joint 4 position

(e) Joint 5 position

(f) Joint 6 position

Figure 4.7. Sinusoidal joint positions movement

displacement from the initial vehicle position is significantly smaller and present only at the beginning of the simulation. Furthermore, the FC-MC controller presents the best results for these cases. The FC-MC controller performs better as at low velocities of the system the dynamic model incorporated in the control law and the interaction forces predicted match the UVMS and are efficient in reducing the coupling effects. Similar comments can be made for the *yaw* DOF. For the z-axis and the *pitch* degree-of-freedom all the three controllers are effective in achieving an accurate position keeping. These two degrees-of-freedom are highly coupled due to the configuration of the vehicle. For the *pitch* DOF,

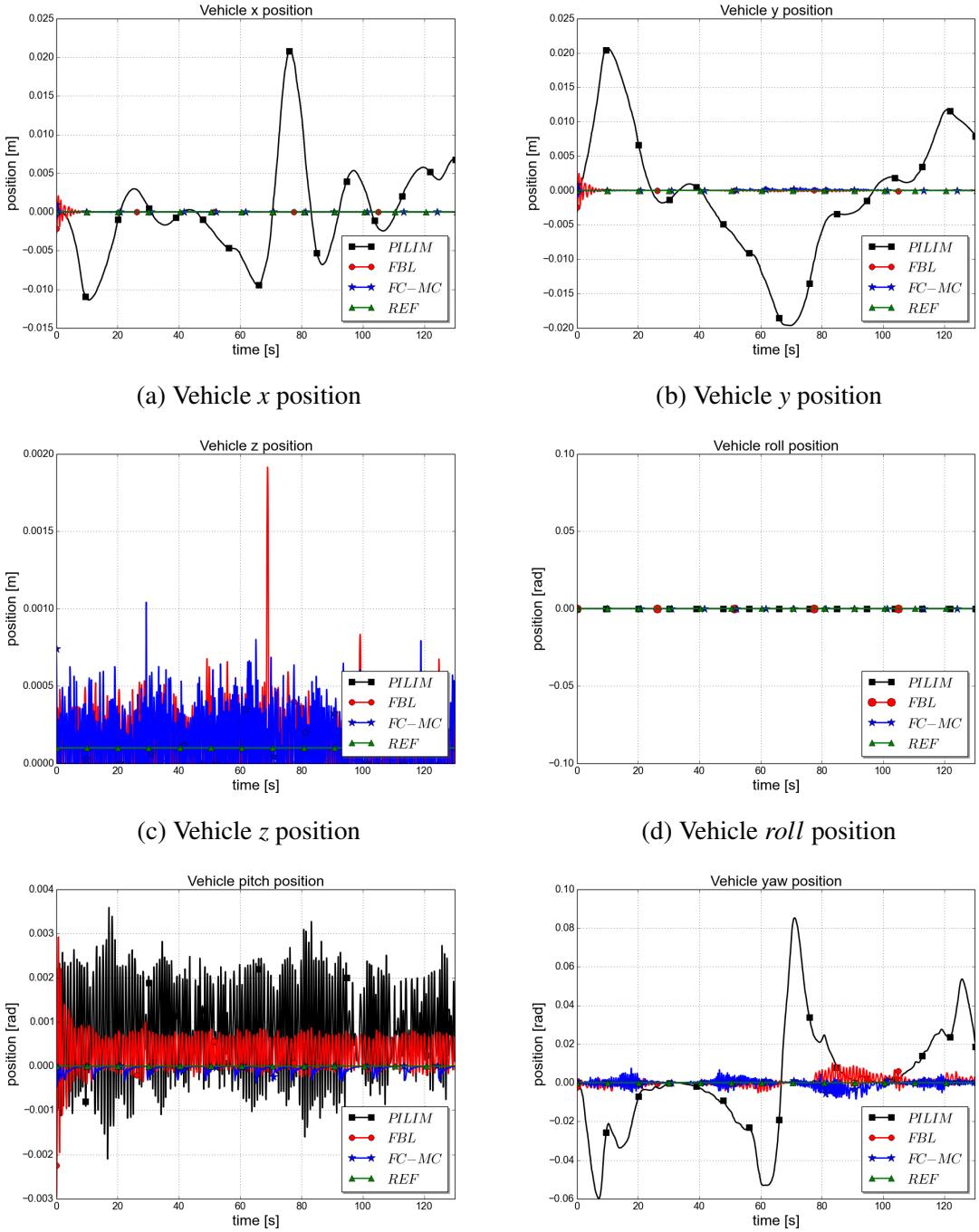

(a) Vehicle *x* position

(b) Vehicle *y* position

(c) Vehicle *z* position

(d) Vehicle *roll* position

(e) Vehicle *pitch* position

(f) Vehicle *yaw* position

Figure 4.8. Vehicle station keeping for sinusoidal joint movements

Figure 4.8e the deviation from the desired orientation has a mean of 0.002 rad (0.1 deg) when the PILIM controller is used. The FBL controller presents a mean value deviation of 0.001 rad (0.05 deg) that is further reduced by the FC-MC controller. It can be seen that using the model based controllers with a slow movement of the manipulator reduces the coupling effects.

4.3.3 Vehicle movement

In this part the aim is to show that the proposed FC-MC controller is beneficial not only for station keeping but also for path following by the vehicle. It is shown here that the performances of the model based controller are similar to the PILIM controller. The last

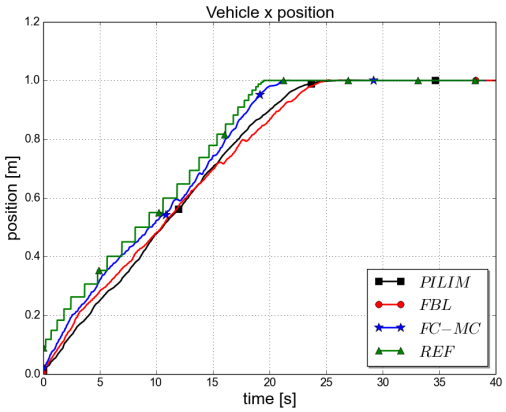

(a) Vehicle x position

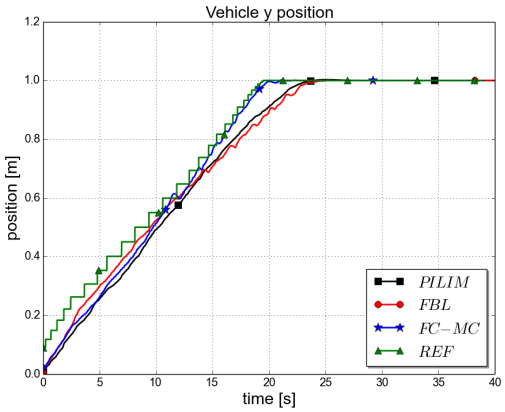

(b) Vehicle y position

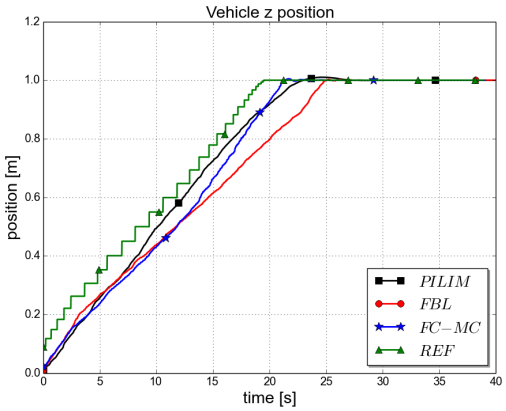

(c) Vehicle z position

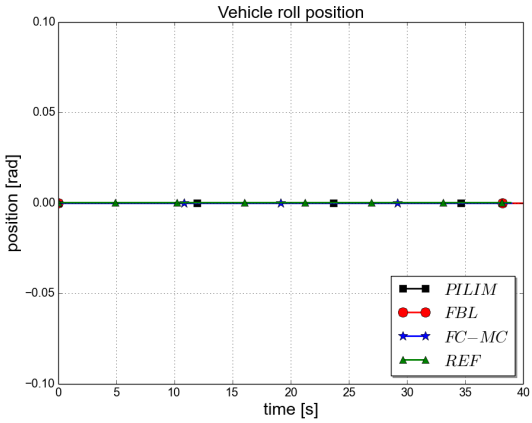

(d) Vehicle *roll* position

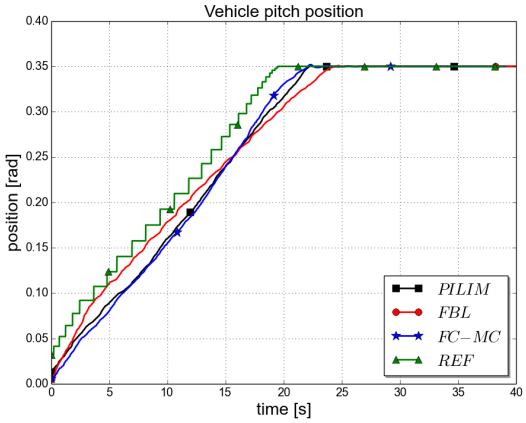

(e) Vehicle *pitch* position

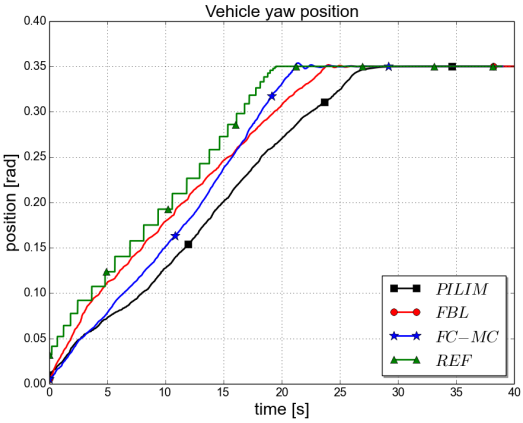

(f) Vehicle *yaw* position

Figure 4.9. Vehicle trajectory tracking

test case considers the movement of the vehicle. The desired position the vehicle has to reach is expressed in vehicle coordinates and it is defined as:

$$\eta_{des_v} = [1.0\text{ m},\ 1.0\text{ m},\ 1.0\text{ m},\ 0.0\text{ rad},\ 0.35\text{ rad},\ 0.35\text{ rad}]$$

The vehicle trajectory tracking is presented in Figure 4.9. Similar behaviour from all the three controllers can be observed. The vehicle moves at a slow velocity as commands are requested for the 5 DOFs simultaneously and underwater vehicles are designed to move at low speeds. After the desired end location is reached the vehicle is in station keeping. The proposed FC-MC controller produces similar transient responses to the PILIM controller. For the *yaw* degree-of-freedom, Figure 4.6f, the settling time is reduced by a few seconds.

4.3.4 Discussion

A generic evaluation of the control methods is presented based on the metric computation of the Generalized Root Mean Squared (GRMS) error, as defined by Equation (4.28), where N is the number of total measurements and e is the generalized error. The GRMS error is computed separately for the translational degrees-of-freedom of the vehicle: x, y and z axes, the rotational degrees-of-freedom: $pitch$, yaw of the vehicle and separately for the 6 revolute joints of the manipulator.

$$GRMS = \sqrt{\frac{1}{N}\sum_{k=1}^{N} e_k^2} \tag{4.28}$$

In Table 4.3 the results for the three controllers used in this chapter are presented. The mean error is computed over a set of 20 different experiments. For 10 experiments, cycloid movement of the manipulator is considered, each of the simulations having a different final value. The desired position of the manipulator joints is in the range 1 to 120 deg. Another 5 experiments are conducted when the sinusoidal functions is used with different amplitudes and frequencies. The last 5 sets of experiments assume that the vehicle moves while the manipulator keeps position.

	Vehicle		Manipulator
	Translation (m)	Rotation (rad)	Revolute (rad)
PID/PILIM	0.021	0.033	0.020
FBL	0.017	0.025	0.018
FC-MC	0.015	0.021	0.016

Table 4.3. Tracking errors for model based controllers

From the presented metric it can be stated that the two model based approaches have a similar behaviour. Not having the dynamic model incorporated in the control law leads to an increase in the tracking error. The simulation results presented showed that incorporating the dynamic model into the control strategy can reduce the effects of the manipulator movement and provides better station keeping capabilities for the vehicle. It can be seen from Table 4.3 that the proposed method FC-MC is advantageous to be used for the vehicle-manipulator system as overall it produces the smallest tracking errors.

One of the aims of this chapter is to show that incorporating the coupling forces approximated based on the mathematical model of the system into the control law is a valid strategy to obtain steady station keeping. The proposed method FC-MC performs well and succeeds in maintaining the initial location when the manipulator is moving. Furthermore, the same method produces comparable results with the PID controller for the manipulator path following. The feedback linearisation technique is another model based approach that improves the results of the simple feedback control by decoupling the system. For the model based approaches, a correlation between the movement of the manipulator and the behaviour of the vehicle can be seen.

The conclusion that can be drawn from these simulations is that the influence between subsystems can be reduced taking into account the coupling effects from the dynamic model. Based on the simulations presented in this chapter, it can be stated that a dynamic model with uncertainties can be beneficial, if the goal is to improve coupling effects. For trajectory tracking of the vehicle and manipulator the model based controllers perform slightly better than the feedback laws.

4.4 Summary

The main contribution of this chapter is the design of a control strategy for station keeping and trajectory tracking of a lightweight vehicle-manipulator systems. The control structure is based on classic control laws put together to obtain a reliable system for uncertain systems that are affected by underwater effects. An overview of the two most used common model based control laws is given in Section 4.1, followed by the description of a new control structure based on these two methods in Section 4.2.

In Chapter 3 it is shown that the movement of the manipulator affects the vehicle position, especially the pitch and yaw angles. Based on this observation in this chapter a model based control law is formulated. Without having an exact knowledge of the system the controller is beneficial for reducing the interaction between subsystems. Moreover, the knowledge of the forces acting on each subsystem is incorporated into the control strategy. A model based feedback controller is included in the final strategy for achieving accurate trajectory tracking and reduces further the coupling effects. The simulations have shown reliable behaviour and have demonstrated that any knowledge of the mathematical model of the system can be useful for control purposes.

Chapter 5

Position/force control of an UVMS

To increase the autonomy of underwater robotic systems, research on force control has increased over the past decades. For underwater vehicle-manipulator systems this represents a complex task due to the underwater effects and difficulties in maintaining a stable system during autonomous interaction with the environment.

To interact with the underwater environment the UVMS has to be first positioned at such a distance so that interaction is possible. There are two different possibilities to reach this desired position and to interact with an object when an underwater vehicle-manipulator system is used. The first method consists of separately commanding the vehicle to reach the vicinity of the object and then commands are sent separately to the manipulator to move it towards the object and interact with it. This method is referred to as the decoupled strategy. The second approach sends the commands to approach and interact with the object to the overall system based on the distance between the end-effector and the object. In this case the same type of commands are sent to the manipulator and the vehicle. The method is referred to as the coupled strategy. This chapter aims to highlight the differences between these two methods and discusses the benefits of each of these control strategies.

To perform this comparative analysis, a new control strategy is presented for position/force control of an UVMS that can be used either in a coupled or in a decoupled implementation. The control architecture proposed is used for the first time for a lightweight underwater vehicle-manipulator system in contact with the underwater environment. The control law is based on the sliding mode theory and the parallel position/force control strategy.

The chapter starts by describing the theoretical background used in designing the control structure. The parallel position/force control scheme is presented in Section 5.1 and the sliding mode control theory is presented in Section 5.2. The control architecture used for the UVMS is presented in Section 5.3.2 and the description of the coupled and decoupled strategies is presented in Section 5.3.3. The simulation results are discussed in Section 5.4.

5.1 Parallel position/force controller

The parallel position/force control approach was first introduced by Chiaverini *et. al* [129]. This control law is part of the group known as direct force control strategies. The authors argue that the method is superior over other force and position control laws as it does not separate the operational space into subspaces and both the position and force are directly controlled. The method is advantageous as it satisfies the task requirements by taking into account the force and position information and by replanning as the contact with the environment occurs. The position/force control law is designed using two control loops: one for position regulation and the other for force regulation. The main characteristic of this control structure is the dominant behaviour of the force loop over the position law. To obtain this behaviour a priority strategy is used in the design of the two control laws [63]. Moreover, a bounded deviation from the desired force requirement is achieved by giving priority to the force control loop. This offers the advantage of recovering from unplanned collisions between the manipulator and the surrounding environment. The method is advantageous in the case when errors are present in the task planning. When contact with the environment occurs in the direction where only position control is supposed to be obtained, the force controller receives this information. This leads to an increase in the force error and the controller structure tries to minimize this error by giving priority to the force component over the position tracking. The parallel position/force controller aims to present a control architecture that is robust to uncertainties in the environment. The overall control law is independent of the task that has to be solved. The two control loops are implemented in a parallel structure. Different types of control laws can be used for the position loop and the force loop. In [63] the authors propose to design these control strategies based on the dynamics of the interaction but independently of the geometry of the contact with the environment.

To describe the parallel strategy a robotic manipulator is represented in the operational space by Equation (5.1).

$$M(x)\ddot{x} + N(x,\dot{x}) = T - F \tag{5.1}$$

where $M(x) \in \mathbb{R}^{6\times 6}$ is a positive operational space inertia matrix, $N(x,\dot{x}) \in \mathbb{R}^6$ is the vector of Coriolis and centripetal forces, friction forces and gravitational force, $T \in \mathbb{R}^6$ is the vector of generalized forces at the end-effector and $F \in \mathbb{R}^6$ is the generalized forces/moments at the end-effector due to the contact with the environment. In the case where there is no interaction this vector is zero.

Equation (5.1) represents a nonlinear and coupled system. As mentioned in Chapter 4 feedback linearisation can be used to decouple the system. This leads to a control structure as proposed in [130] defined by Equation (5.2):

$$T = \tilde{M}(x)M_d^{-1}F_e + \tilde{N}(x,\dot{x}) + \tilde{F} \tag{5.2}$$

where $\tilde{M}(x) \in \mathbb{R}^{6\times 6}$, $\tilde{N}(x,\dot{x}) \in \mathbb{R}^6$, $\tilde{F} \in \mathbb{R}^6$ represent estimations of $M(x)$, $N(x,\dot{x})$, F and

$F_e \in \mathbb{R}^6$ is the decoupled command vector for the end-effector. $M_d \in \mathbb{R}^{6\times6}$ is the diagonal desired inertia matrix.

The control structure used to define F_e consists of two parallel controllers that are designed independently and described by Equation (5.3). The position and force control outputs are added together. This is valid as the manipulator admittance acts to sum the forces applied to it and computes the correspondent motion [68]. A generic overall scheme of the method is given in Figure 5.1. The scheme can be regarded as consisting of an impedance controller for the position regulator and a filtering component for the force.

$$F_e = u_p + u_f \tag{5.3}$$

where $u_p \in \mathbb{R}^6$ is the position control command and $u_f \in \mathbb{R}^6$ is the force control command.

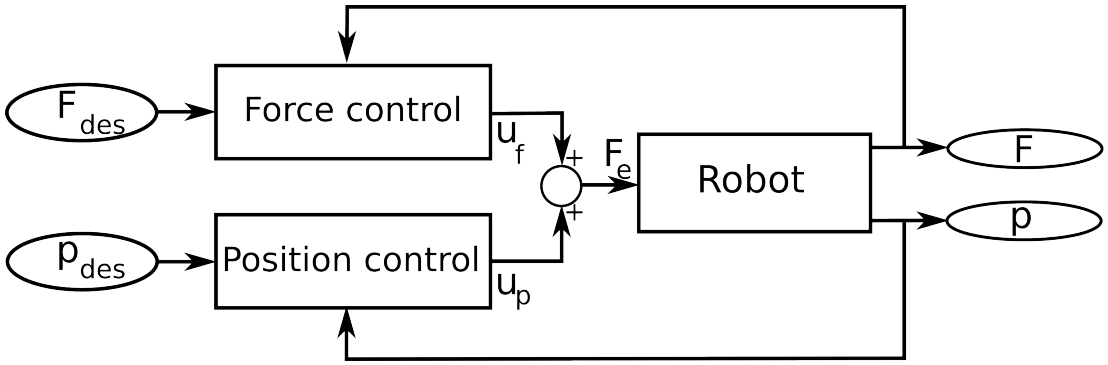

Figure 5.1. Parallel position/force control structure

In [63] the position controller consists of the resolved acceleration law as presented by Equation (5.4) and for the force control law a Proportional Integral (PI) control law is used, Equation (5.5).

$$u_p = M_d\ddot{x}_{des} + K_v(\dot{x}_{des} - \dot{x}) + K_p(x_{des} - x) \tag{5.4}$$

where $x_{des} \in \mathbb{R}^6$, $\dot{x}_{des} \in \mathbb{R}^6$ and $\ddot{x}_{des} \in \mathbb{R}^6$ are the desired position, velocity and acceleration of the end-effector. $K_v \in \mathbb{R}^{6\times6}$ is the diagonal velocity coefficients matrix and $K_p \in \mathbb{R}^{6\times6}$ is the diagonal position coefficients matrix.

$$u_f = K_f(F_{des} - F) + K_I \int_0^t (F_{des} - F)d\tau \tag{5.5}$$

where $F_{des} \in \mathbb{R}^6$ is the desired interaction force, $K_f \in \mathbb{R}^{6\times6}$ is the diagonal proportional coefficient matrix and $K_I \in \mathbb{R}^{6\times6}$ is the diagonal integral coefficient matrix. By using the notations $e_p = x_{des} - x$ and $e_f = F_{des} - F$ and by combining Equation (5.1), Equation (5.4) and Equation (5.5) yields:

$$M_d\ddot{e}_p + K_v\dot{e}_p + K_p e_p + K_f\dot{e}_f + K_I \int_0^t e_f d\tau = 0 \tag{5.6}$$

From Equation (5.6) it can be observed that by the current choice of the control laws, in steady-state, the position error might have a constant value while the force error is zero. This leads to a force control loop that has priority over the position control loop and compels the system to achieve the desired force in the case when the error in position is non-zero. The integral term ensures that the error in force is zero and no drifts occur in the behaviour of the end-effector. Nevertheless, the choice of the integral term has to be small enough to avoid system instability [131]. By giving priority to the force component unplanned collisions with the environment can be avoided.

The parallel position/force control law is efficient in terms of controlling the dynamics of the interaction and does not take into consideration the geometry of the environment. Different control laws can be used for each of the position and force control loops, the parallel notion referring to the fact that the position and the force regulation methods act alongside.

5.2 Sliding mode control

The sliding mode controller (SMC) technique is part of the group known as robust controllers that handles the discrepancies between the real robotic system and its mathematical model. The differences can be caused by the unknown disturbances, the parameters of the system or unmodelled dynamics [132]. The sliding mode controller is characterized by a discontinuity of the control action, often referred to as variable structure control (VSC). This facilitates the switch between different type of motions leading to insensitivity to disturbances and changes in the model parameters. The SMC facilitates the construction of a surface where the errors asymptotically approach zero. This makes it an attractive law to be used in the control of nonlinear processes exposed to disturbances and uncertainties. Among the advantages of the sliding mode control are reduced order dynamics, finite-time convergence and robustness. The notion of variable structure emerged in 1960's and it has been extensively used in automatic flight control, control of electric motors and robotic systems.

The sliding mode controller aims to design a surface that drives the states of the system towards that surface. The system states are then maintained in the vicinity of the surface. The SMC design can be divided into two steps:

1. The design of a sliding surface that ensures the design specification during the sliding motion. A stable hyperplane has to be chosen in the error space that restricts the motion of the system [133].

2. The design of a control law that makes the sliding surface to be a proper choice.

The properties that have to be considered when designing a sliding mode controller are:

- The design of the switching function has to ensure that the order of this function is less then the order of the system under control.

- The sliding mode is characterised only by the parameters of the switching function and not by the dynamics of the system.
- The control law is independently derived from the switching function.

The steps in designing the sliding mode controller are further presented. Considering the nonlinear dynamic system represented by Equation (5.7).

$$\ddot{x} = u + f(x, \dot{x}, t) \tag{5.7}$$

where $u \in \mathbb{R}^n$ is the control force and $f(x,t) \in \mathbb{R}^n$ is the disturbance vector consisting of viscous, friction forces and other resistance forces. The disturbance vector is assumed to be bounded $|f(x,t)| \leq L_1 > 0$.

The task that the sliding mode controller aims to solve is to design a feedback control law $u = u(x)$ that drives the state variables to the origin asymptotically, in the presence of disturbances.

In the first stage the desired compensated dynamics for the tracking error of Equation (5.7) is defined by Equation (5.8).

$$\dot{e} + ce = 0, \quad c > 0 \tag{5.8}$$

where $e = x_{des}(t) - x(t)$ is the output tracking error that enforces zero convergence as time increases. It can be observed that there is no effect of the disturbance on the compensated dynamics and that the order of the function is less than the order of the system. The equation is called the sliding surface and it corresponds to a straight line for a second order system.

The dynamics in Equation (5.8) are obtained by defining a state-space variable:

$$\sigma = \dot{e} + ce, \quad c > 0 \tag{5.9}$$

Using a SMC to design the control input u leads in driving $\sigma \to 0$ in finite time and maintaining it in the neighbourhood of zero. To drive the variable σ to zero in a finite time, the Lyapunov function technique applied to the σ dynamics can be used. To maintain σ close to zero, the tracking error is enforced to comply to the first order dynamics expressed by Equation (5.8).

The derivative of the sliding variable dynamics is expressed as:

$$\begin{aligned} \dot{\sigma} &= \ddot{x}_{des} + c\dot{x}_{des} - f(x, \dot{x}, t) - c\dot{x} - u \\ \dot{\sigma} &= \phi(x, \dot{x}, t) - u \end{aligned} \tag{5.10}$$

where $x_{des} \in \mathbb{R}^n$, $\dot{x}_{des} \in \mathbb{R}^n$ and $\ddot{x}_{des} \in \mathbb{R}^n$ are the desired position, velocity and acceleration requirements. $\phi(x, \dot{x}, t)$ is called the cumulative disturbance term and it is assumed to be bounded $|\phi(x, \dot{x}, t)| \leq L_2$.

For Equation (5.10) to be asymptotically stable about the equilibrium point ($\sigma = 0$) a

Lyapunov function is chosen such that the conditions are fulfilled:

$$\dot{V} < 0, \quad \text{for} \quad \sigma \neq 0 \tag{5.11}$$

$$\lim_{|\sigma| \to \infty} V = \infty \tag{5.12}$$

As presented in [132] a relaxation of Equation (5.11) can be made to achieve global finite-time stability, such that Equation (5.11) can be replaced with:

$$\dot{V} \leq -\alpha V^{1/2} \tag{5.13}$$

where α is a positive constant. By solving this inequality in the time interval $0 \leq \tau \leq t$, Equation (5.13) becomes:

$$V^{1/2}(t) \leq -\frac{1}{2}\alpha t + V^{\frac{1}{2}}(0) \tag{5.14}$$

This leads to obtain the zero convergence of $V(t)$ in a given time, t_{conv} bounded by:

$$t_{conv} \leq \frac{2V^{1/2}(0)}{\alpha} \tag{5.15}$$

Based on this assumption the control law has to fulfil the requirements expressed in Equation (5.13) to drive $\sigma \to 0$ in a finite time and maintain it in the vicinity of zero after that.

The Lyapunov function defined for the dynamics expressed in Equation (5.10) is given by Equation (5.16).

$$V = \frac{1}{2}\sigma^2 \tag{5.16}$$

The defined function satisfies the condition Equation (5.12). To validate Equation (5.11) the derivative $\dot{V}$ has to be computed.

$$\dot{V} = \sigma\dot{\sigma} = \sigma\left(\phi(x,\dot{x},t) - u\right) = \sigma\phi(x,\dot{x},t) - \sigma u \leq |\sigma|L_2 - \sigma u \tag{5.17}$$

$$u = \kappa \text{sign}(\sigma) \tag{5.18}$$

By selecting the control command as shown in Equation (5.18) and by substituting it in Equation (5.17), this can be re-written as:

$$\sigma\dot{\sigma} \leq |\sigma|(L_2 - \kappa) \tag{5.19}$$

In [132] it is demonstrated that:

$$\sigma\dot{\sigma} \leq -\overline{\alpha}|\sigma|, \quad \overline{\alpha} = \frac{\alpha}{\sqrt{2}} \tag{5.20}$$

From Equation (5.20) the control gain is selected according to:

$$\kappa = L_2 + \overline{\alpha} \tag{5.21}$$

In Equation (5.21) the first term accounts for the disturbances of the system and the second term $\overline{\alpha}$ ensures that the sliding surface is reached in the corresponding time t_{conv}. When designing the state space variable σ, it has to be enforced that $\dot{\sigma}$ is dependent on the control command u to ensure that the expected behaviour of the system is obtained. Based on the notions revised here the definition of the sliding mode controller can be expressed as:

Definition: The control law defined in Equation (5.18) that drives the state variables to the sliding surface in a finite time t_{conv} and keeps the state variables on the surface when disturbances on the system are present is called the sliding mode controller.

One of the characteristics of the sliding mode controller is the chattering effect. This effect is described by high frequency oscillations having a bounded amplitude. The chattering effect can be responsible for altering the behaviour of the system and it represents the main disadvantage of the sliding mode control outlined in Equation (5.18). This effect can be caused due to the practical limitation in the switching frequency or due to the neglected high bandwidth dynamics for the mathematical model [134].

5.3 Problem statement

Interacting with submerged objects using a lightweight underwater vehicle-manipulator system is a challenging task subject to disturbances in the environment and high coupling effects between subsystems. To solve this task different approaches for controlling the overall system are possible.

The aim of this chapter is to first propose a parallel position/force control law based on the sliding mode theory and secondly to describe two different strategies for applying this control law to the underwater vehicle-manipulator system. One of the proposed strategies separately controls the vehicle and the manipulator. In this case the control law proposed is based on the parallel position/force approach and used only for the manipulator, while an additional control law is needed for the vehicle. The second control strategy discussed in this chapter uses the parallel position/force for the entire UVMS without any separate control law for the vehicle. It is intended to show that both methods are able to handle the nonlinear system, the underwater disturbances and the coupling effects between the vehicle and the manipulator.

The proposed controller incorporates the theory of sliding mode control for position regulation and the integrative sliding mode control for force regulation in a parallel implementation. To ensure accurate trajectory and force tracking the control law incorporates a feedback linearisation component. The overall control law is designed in the operational space.

5.3.1 UVMS model in operational space

As presented in Chapter 3, the mathematical model of an underwater vehicle-manipulator system is described by Equation (5.22).

$$M(\rho)\dot{\xi} + C(\rho,\xi)\xi + D(\rho,\xi)\xi + g(\rho) + f_f(\rho) = \tau - J^{-1}F \tag{5.22}$$

For robotic systems, the problem to be solved is expressed in the task space coordinates. One approach is to use the operational space to design the control law as proposed by Kathib *et al.* [79]. The mathematical description of the system in operational space is dependent on the configuration of the system and it is given by:

$$M(x)\ddot{x} + C(x)\dot{x} + D(x)\dot{x} + G(x) + F_f(x) = T - F \tag{5.23}$$

where $x \in \mathbb{R}^6$ represents the independent parameters vector described in the operational space, $M(x) \in \mathbb{R}^{6\times6}$ is a positive operational space inertia matrix, $C(x)\dot{x} \in \mathbb{R}^6$ is the vector of Coriolis and Centripetal forces, $D(x)\dot{x} \in \mathbb{R}^6$ is the damping vector, $G(x) \in \mathbb{R}^6$ is the vector of restoring forces, $F_f(x) \in \mathbb{R}^6$ is the friction vector, all defined in operational space coordinates and $T \in \mathbb{R}^6$ is the vector of generalized forces at the end-effector.

The dynamic components in the operational space are defined with respect to the system coordinates by the following equations:

$$\begin{aligned} M(x) &= \left(JM^{-1}(q)J^T\right)^{-1} \\ C(x) &= \bar{J}^T C(\rho,\xi) - M(x)\dot{J}\dot{\rho} \\ D(x) &= \bar{J}^T D(\rho,\xi) - M(x)\dot{J}\dot{\rho} \\ G(x) &= \bar{J}^T g(\rho) \\ F_f(x) &= \bar{J}^T g(\rho) \\ T &= J^T\tau \\ \bar{J}^T &= M^{-1}(q)J^T M(x) \end{aligned} \tag{5.24}$$

where $\bar{J}^T$ is the dynamically consistent generalized inverse of the Jacobian. In the case o an invertible Jacobian, the following relation holds $\bar{J}^T = J^{-1}$.

The external disturbance vector, $F \in \mathbb{R}^6$, produced by the interaction with the environment is available based on sensor readings or mathematical approximation. In this thesis, to validate the controllers and analyse the behaviour of the system a simple model is used for the contact with the environment. A point contact is considered between the end-effector of the manipulator and a frictionless and elastically compliant environment. The approximation of the contact force is defined by Equation (5.25).

$$F = K_e(x - x_e) \tag{5.25}$$

where x_e is the end-effector position at the contact point, x is the end-effector position and $K_e \in \mathbb{R}^{6\times6}$ is the stiffness matrix of the environment [135].

5.3.2 Parallel Variable Sliding Mode Dynamic Controller

The goal of this section is to develop a position and force control law for an UVMS that has to reach a certain object and interact with it. The control law designed controls actively the position and force in parallel [69]. The underwater environment causes disturbances on the UVMS that are hard to be estimated and the coupling effects between the two components of the UVMS are significant. To solve these challenges the sliding mode theory is used. The proposed controller is designed in operational space. The manipulator joint commands and the vehicle forces and moments are mapped from the control law based on the Jacobian of the system. As mentioned in Section 5.1, the parallel position/force controller is composed of two separate control loops added together, as seen in Equation (5.26). One control loop for position control and another control loop for force control.

$$T = u_p + u_f \tag{5.26}$$

where $u_p \in \mathbb{R}^6$ is the position control law that makes the position asymptotically follow a reference profile and $u_f \in \mathbb{R}^6$ defines the force control law that keeps the contact force between the end-effector and environment to a desired known value. Both control laws are sliding mode controllers.

Position control law

For the position control loop, SMC theory is used to design the control law. In this case the goal is to obtain zero error in position tracking in finite time. That is:

$$\lim_{t\to\infty} e_p = 0 \tag{5.27}$$

where e_p is the force error defined as $e_p = x_{des} - x$. The goal is to define the control law u_p such that the sliding mode variable defined in Equation (5.28) fulfils $\delta \to 0$ in finite time.

$$\delta = \dot{e}_p + c_1 e_p, \quad c_1 > 0 \tag{5.28}$$

where $c_1 \in \mathbb{R}^{6\times 6}$ is a positive matrix. Asymptotic convergence of the position tracking is secured by:

$$\delta = \dot{e}_p + c_1 e_p = 0, \quad c_1 > 0 \tag{5.29}$$

The derivative of Equation (5.28) is used to describe the dynamics of the sliding variable in Equation (5.30)

$$\dot{\delta} = \ddot{e}_p + c_1 \dot{e}_p, \quad c_1 > 0 \tag{5.30}$$

Based on the dynamic model of the system, Equation (5.30) converts to:

$$\dot{\delta} = \ddot{x}_{des} - \ddot{x} + c_1 \dot{e}_p = \theta(x, \dot{x}, F) - M^{-1}(x) u_p \tag{5.31}$$

where $\mid \theta(x,\dot{x}) \mid \leq \Omega_p$ is the bounded cumulative disturbance.

$$\theta(x,\dot{x}) = \ddot{x}_{des} - M^{-1}(x)\left[-F - C(x,\dot{x})\dot{x} - D(x,\dot{x})\dot{x} - G(x) - F_f(x)\right] - M^{-1}(x)u_f \quad (5.32)$$

The control force u_p can be defined by the sliding mode existence condition [132]:

$$\delta\dot{\delta} \leq -\bar{\alpha} \mid \delta \mid, \quad \bar{\alpha} = \frac{\alpha}{\sqrt{2}}, \quad \alpha > 0 \quad (5.33)$$

$$\delta\dot{\delta} = \delta\left[\theta(x,\dot{x}) - u_p\right] \leq \mid \delta \mid \Omega_p - \delta u_p \quad (5.34)$$

By defining the control law as Equation (5.35) and incorporating it into the dynamics of the sliding variable Equation (5.34) the control gain of the force control is given by Equation (5.37)

$$u_p = \kappa_1 \mathtt{sign}(\delta) \quad (5.35)$$

$$\delta\dot{\delta} \leq \mid \delta \mid (\Omega_p - \kappa_1) = -\bar{\alpha} \mid \delta \mid \quad (5.36)$$

$$\kappa_1 = \Omega_p + \bar{\alpha} \quad (5.37)$$

Force control law

In Section 5.1 it was stated that in the parallel control structure the force component is given priority over the position controller to ensure that unwanted interaction with the environment is not taking place. To ensure this characteristic the force control law is designed using the Integral Sliding Mode Control (ISMC) theory [136]. The difference compared to the classical sliding mode control approach is that the ISMC maintains the order of the compensated system dynamics. This ensures the sliding mode behaviour and eliminates the uncertainties in the system from the start of the execution of the task. The ISMC is composed of a state feedback controller and a discontinuous controller. The feedback controller ensures the asymptotic stability of the system. The discontinuous controller secures the performance of the system and is not affected by disturbances. For the underwater vehicle-manipulator system the method is appealing as it handles the non-linearities, uncertainties and parameter variations. The ISMC control function can be expressed as:

$$u_f = u_1 + u_2 \quad (5.38)$$

where $u_1 \in \mathbb{R}^6$, compensates for the bounded disturbances and $u_2 \in \mathbb{R}^6$ drives the sliding variable to zero in a finite time, taking into account that the sliding variable dynamics are no longer perturbed.

The primary sliding variable is designed to be used in the u_2 control law and is expressed through:

$$\sigma = \dot{e}_f + c_2 e_f + c_3 \int_0^t e_f d\tau, \quad c_2, c_3 > 0 \quad (5.39)$$

where e_f is the error in the end-effector force, $e_f = F_{des} - F$, defined based on the difference

between the desired contact force $F_{des} \in \mathbb{R}^6$ and the current end-effector force $F \in \mathbb{R}^6$. Computing the sliding variable dynamics leads to:

$$\dot{\sigma} = \ddot{e}_f + c_2\dot{e}_f + c_3 e_f \tag{5.40}$$

where $c_2,\ c_3\ \in \mathbb{R}^{6\times 6}$ are positive constant diagonal matrices defined to model the sliding mode dynamics. The auxiliary sliding variable, used in the u_1 control law is designed by:

$$\begin{cases} s = \sigma - z \\ \dot{z} = -c_3 u_2 \end{cases} \tag{5.41}$$

The dynamic compensator for the auxiliary sliding variable is given by:

$$\begin{aligned} \dot{s} = \dot{\sigma} - \dot{z} = \ddot{e}_f + c_2\dot{e}_f + c_3 e_f - (-c_3 u_2) = \\ = \ddot{e}_f + c_2\dot{e}_f + c_3(F_{des} - F) + c_3 u_2 \end{aligned} \tag{5.42}$$

The next step is to express the dynamics of the auxiliary variable dependent of the operational space dynamics of the system, Equation (5.23) and the type of the control used, Equation (5.26) and Equation (5.38). This leads to the following expression:

$$\begin{aligned} \dot{s} = -c_3 u_1 - c_3 u_2 + \varphi(e_f, \dot{e}_f, u_p) + c_3 u_2 = \\ = -c_3 u_1 + \varphi(e_f, \dot{e}_f, u_p) \end{aligned} \tag{5.43}$$

where

$$\begin{aligned} \varphi(e_f, \dot{e}_f, u_p) = c_3\mu - c_3 u_p + c_3 F_{des} + c_2\dot{e}_f + \ddot{e}_f \\ \mu = M(x)\ddot{x} + C(x,\dot{x})\dot{x} + D(x,\dot{x})\dot{x} + G(x) + F_f(x) \end{aligned} \tag{5.44}$$

and $\mid \varphi(e_f, \dot{e}_f, u_p) \mid \leq \Omega_f$ is the bounded disturbance term.

As mentioned previously, the control command u_1 is designed to drive the sliding variable to zero in a finite time. The SMC function is used to obtain this and u_1 is expressed by Equation (5.45).

$$u_1 = \kappa_2 \mathtt{sign}(s) \tag{5.45}$$

Introducing this control law into the primary and auxiliary sliding mode variable dynamics, the following relations can be seen:

$$\begin{cases} \dot{\sigma} = -c_3 u_1 - c_3 u_2 + \varphi(e_f, \dot{e}_f, u_p) \\ \dot{s} = -c_3 u_1 + \varphi(e_f, \dot{e}_f, u_p), \quad u_1 = \kappa_2 \mathtt{sign}(s) \end{cases} \tag{5.46}$$

Describing the σ dynamics based on the auxiliary sliding mode (when $s = 0$) it can be seen that the primary sliding mode dynamics is not dependent of the bounded disturbances. The

equivalent control u_{1eq}, defined by Equation (5.47) satisfies $\dot{s} = 0$.

$$\begin{aligned} \dot{s} = 0 \Leftrightarrow -c_3 u_1 + \varphi(e_f, \dot{e}_f, u_p) = 0 \\ \Rightarrow u_{1eq} = c_3^{-1} \varphi(e_p, \dot{e}_p, F) \end{aligned} \tag{5.47}$$

From Equation (5.47) and Equation (5.46), the final expression for the primary sliding mode variable dynamics is given by Equation (5.48).

$$\dot{\sigma} = -c_3 u_2 \tag{5.48}$$

It can be concluded that the primary sliding mode dynamics does not depend on the disturbance term, $\varphi(e_p, \dot{e}_p, F)$ and the control law for this can be formulated as:

$$u_2 = K\sigma, \quad K > 0 \tag{5.49}$$

where $K \in \mathbb{R}^{6\times 6}$ is a positive matrix.

Using the ISMC theory, the overall force control law is given by the following relationship:

$$u_f = u_1 + u_2 = \kappa_2 \mathtt{sign}(s) + K\sigma, \quad \kappa_2,\ K > 0 \tag{5.50}$$

Total control law

The underwater vehicle-manipulator system is characterised by non-linearities and coupling effects. To reduce these non-linearities feedback linearisation is used in the final control law as seen in Equation (5.51).

$$T = \tilde{M}(x)\left[\ddot{x}_{eq} + u_p + u_f\right] + \beta = \tilde{M}(x)\left[\ddot{x}_{eq} + \kappa_1 \mathtt{sign}(\delta) + \kappa_2 \mathtt{sign}(s) + K\sigma\right] + \beta \tag{5.51}$$

where

$$\begin{aligned} \delta &= \dot{e}_p + c_1 e_p, \quad c_1 > 0 \\ \sigma &= \dot{e}_f + c_2 e_f + c_3 \int_0^t e_f d\tau, \quad c_2, c_3 > 0 \\ s &= \sigma - z \\ \dot{z} &= -c_3 u_2 \\ u_2 &= K\sigma, \quad K > 0 \\ \beta &= \tilde{C}(x,\dot{x})\dot{x}_{eq} + \tilde{D}(x,\dot{x})\dot{x}_{eq} + \tilde{G}(x) + \tilde{F}_f(x) + \tilde{F}_{eq} \\ \dot{x}_{eq} &= \dot{x}_{des} + c_1 e_p \\ F_{eq} &= F_{des} + c_2^{-1}\dot{e}_f + c_2^{-1} c_3 \int_0^t e_f d\tau \end{aligned} \tag{5.52}$$

$\tilde{M}(x)$ is an estimate of the inertia term, $\tilde{C}(x,\dot{x})$, $\tilde{D}(x,\dot{x})$, $\tilde{G}(x)$, $\tilde{F}_f(x)$ are estimates of the real values of the system defined in operational space coordinates according to the boundary

errors, $\delta M(x),\ \delta C(x,\dot{x}),\ \delta D(x,\dot{x}),\ \delta G(x)$ and $\delta F_f(x)$ by Equation (5.53).

$$\begin{aligned} |\,\Delta M(x)\,| &\leq \delta M(x) \quad \Delta M(x) = M(x) - \tilde{M}(x) \\ |\,\Delta C(x,\dot{x})\,| &\leq \delta C(x,\dot{x}) \quad \Delta C(x,\dot{x}) = C(x,\dot{x}) - \tilde{C}(x,\dot{x}) \\ |\,\delta D(x,\dot{x})\,| &\leq \delta D(x,\dot{x}) \quad \Delta D(x,\dot{x}) = D(x,\dot{x}) - \tilde{D}(x,\dot{x}) \\ |\,\Delta G(x)\,| &\leq \delta G(x) \quad \Delta G(x) = G(x) - \tilde{G}(x) \\ |\,\Delta F_f(x)\,| &\leq \delta F_f(x) \quad \Delta F_f(x) = F_f(x) - \tilde{F}_f(x) \end{aligned} \tag{5.53}$$

To summarise, the proposed control structure is characterised by the following components and their roles:

- Model linearisation: to decouple the system.
- Parallel force/position structure: control of the position and force behaviour of the system at the same time.
- Position control law, u_p: sliding mode control to ensure trajectory tracking in the presence of hydrodynamic disturbances, unknown model parameters and significant coupling effects between the manipulator and vehicle.
- Force control law, u_f: integral sliding mode control to ensure zero force error and gives priority to the force component over the position component. By giving priority to the force component unplanned collisions with the environment can be avoided.

The stability analysis of the proposed control law is presented in Appendix B.

Challenges

Chattering effects The most straightforward method to eliminate the chattering effect is to replace the discontinuous function $\iota(a) = \kappa\mathtt{sign}(a)$ in the control strategy by a smooth/continuous function. It can be seen that:

$$\lim_{\varepsilon \to 0} \frac{a}{|\,a\,| + \varepsilon} = \mathtt{sign}(a) \tag{5.54}$$

This leads to the use of the `sigmoid` function instead of the `sign` function to obtain the continuous/smooth behaviour:

$$\mathtt{sign}(a) \simeq \frac{a}{|\,a\,| + \varepsilon} \tag{5.55}$$

where ε is a small positive scalar that has to be chosen in such a way that a smooth control action is ensured and satisfactory behaviour of the system is obtained.

Singularity avoidance Designing the control architecture in the operational space can cause critical problems as singularities or joint limits. To ensure a successful performance of the task these challenges have to be analysed and handled. In the case when one of the joints is commanded to move beyond its maximum or minimum physical limit, the robot cannot move and the final task cannot be achieved. A singular configurations is

a certain end-effector pose for which the robots loses its rigidity [137]. The effects of the singular configuration can be seen in the high joint forces that would lead to sudden robot movements. This creates an unstable system that leads to an uncontrollable end-effector.To solve this latter problem an alternative is to use the information provided by the inertia matrix. The first step is to detect what dimension of the operational space is responsible in creating the singular configuration. This is due to the fact that in a singular configuration the robot loses the ability to move in one or more directions. In this case one of the linearly independent columns of the Jacobian matrix is lost and for a square Jacobian the determinant is zero. In the following step, the corresponding forces are set to zero based on the inertia matrix $M(x)$. If the robot is close to a singular configuration, the Singular Value Decomposition of the inertia matrix $M_x^{-1} = VSU^T$ is used to set the corresponding force to zero. By substituting the very small values of the singular diagonal matrix values with zeros the force in the degenerate direction is eliminated. The singularity avoidance is implemented as seen in Algorithm 3.

Algorithm 3 Singularity avoidance

$M^{-1}(x) = JM^{-1}(\rho)J^T$
if $\mid JJ^T \mid \geq th$ **then**
    $M(x) = \texttt{inv}(M^{-1}(x))$
else
    $U,\ S,\ V = \texttt{svd}(M^{-1}(x))$
    if $S < \varepsilon$ **then**
        $S = 0$
    else
        $S = 1/S$
    end if
    $M(x) = VSU^T$
end if

5.3.3 Decoupled versus coupled control strategies

This section describes the two different strategies of applying the controller proposed in Section 5.3.2 to an underwater vehicle-manipulator system. One approach (the decoupled strategy) is to use the proposed control law only for the manipulator while for the vehicle a position tracking control law is proposed. The decision for which component is used to perform the task is given by an interaction strategy. The second strategy (the coupled strategy) is to use only the parallel position/force control law for the overall system and there is no need for an interaction strategy.

Decoupled strategy

The decoupled strategy consists of three components: the vehicle control law, the manipulator control law and the interaction strategy. An overview of the components of the decoupled strategy is presented in the following part.

Vehicle controller The degrees-of-freedom of the vehicle are controlled separately as the operational speed of the AUV is relatively small when undertaking an interaction task. The vehicle controller, a PILIM (Proportional Integral Limited) scheme is designed using two control loops, one for position and one for velocity. The method is described in details in Chapter 4 and the output of the control law is marked with $\tau_v \in \mathbb{R}^6$.

Manipulator controller The manipulator has to perform the interaction task with the environment. The control law proposed in Section 5.3.2 is an appropriate choice to solve this task. The parallel controller is designed in the operational space. In Equation (5.56) the position of the end-effector is computed.

$$v_m = J_m(q)\dot{q} \tag{5.56}$$

where $v_m \in \mathbb{R}^6$ is the end-effector velocity, $J_m(q) \in \mathbb{R}^{6\times n}$ is the Jacobian matrix of the manipulator and $q \in \mathbb{R}^n$ is the manipulator joint positions. Equation (5.57) presents the control commands sent to the joints of the manipulator.

$$\tau_m = J_m^T(q)T \tag{5.57}$$

where T is defined as in Equation (5.51) with the dynamic components defined only for the manipulator system. The final control law for the underwater vehicle-manipulator system is computed according to Equation (5.58).

$$\tau = [\tau_v \ \tau_m]^T \tag{5.58}$$

Interaction strategy The underwater vehicle-manipulator system has to perform two tasks:

- to move close to an object placed in the underwater environment;
- to interact with the object using a desired end-effector force at a specified location and maintain the stability of the system during the interaction.

The object is defined based on its 3D position with respect to the fixed inertial frame. To interact with the object, the manipulator has to move towards the object until the object is in the workspace of the manipulator. To reach this configuration, the vehicle is commanded to move. The interaction strategy sets the goal for the vehicle. This goal represents the point in space until the vehicle moves. When this goal is reached by the vehicle, the manipulator starts moving towards the object and the vehicle maintains its location. A simple decision making policy is implemented in this chapter. The strategy relies on the Euclidean distance between the current location of the vehicle and the object. If the distance is greater than a predefined threshold, the vehicle is commanded to move and the manipulator keeps position. When the object is in the workspace of the manipulator, the vehicle is requested to

maintain the current location and the manipulator is commanded to move towards the object and interact with the required contact force. The strategy is presented in Algorithm 4, where p_{des} is the desired (object) position, p_v is the vehicle position, v_{des} is the vehicle desired position and m_{des} is the manipulator desired position.

Algorithm 4 Interaction strategy

1: $d(p_{des}, p_v) = \sqrt{\sum_{i=1}^{n} (p_{des_i} - p_{v_i})^2}$
2: **if** $d(p_{des}, p_v) \geq L$ **then**
3: $\quad v_{des} = p_{des}$
4: $\quad m_{des} = p_m$
5: **else**
6: $\quad v_{des} = p_v$
7: $\quad m_{des} = p_{des}$
8: **end if**

Coupled strategy

In the coupled strategy the parallel position/force control law presented previously is used to control the entire underwater vehicle-manipulator system. In this case the vehicle can be regarded as an extension of the manipulator, a set of 6 virtual joints. The same task as in the previous case has to be solved: reaching the goal and interaction with the object at a specified location. Using this strategy no control law has to be defined for the vehicle, this being controlled through the parallel/force law presented in Section 5.3.2. The control law in the joint/vehicle DOFs is given by Equation (5.59)

$$\tau = J^T T \tag{5.59}$$

where T is defined according to Equation (5.51) using the dynamic model of the overall vehicle-manipulator system. In this case the control structure is straightforward and no additional components being required.

5.4 Simulation results

Through the simulation results it is aimed to demonstrate that the proposed low-level controller can be implemented in either a coupled or decoupled strategy. A comparative evaluation of the two strategies is given highlighting the advantages and disadvantages of both methods. The focus in this section is on the characteristics of the two control strategies (coupled vs. decoupled) rather than the control architecture presented. A detailed evaluation of the low-level control method presented in Section 5.3.2 is given in Chapter 6, where experimental tests are made with the HDT-MK3-M manipulator.

The simulation platform, first presented in Chapter 3 is based on the two robotics systems available in the Ocean Systems Laboratory: Nessie VII an autonomous underwater

vehicle developed as a research platform and a commercially available underwater manipulator, HDT-MK3-M. As a reminder, Nessie VII AUV is a torpedo shaped 5 degrees-of-freedom vehicle with a mass of 60 kg. The vehicle *roll* degree-of-freedom is not controlled. The manipulator has 6 revolute joints and a total weight of 9 kg. The system represents a lightweight UVMS characterized by significant effects on the vehicle caused by the manipulator movement.

The two control strategies are implemented in Python using the dynamic model developed in Chapter 3. The final goal of the system is to reach a given object in the underwater environment and to interact with it at a required force. The contact force between the end-effector and the object is modelled as a frictionless, compliant point-contact along the x-axis of the end-effector. The interaction with the object takes place as soon as the desired final goal (the centre of the ball) is reached. Objects that have different stiffness coefficients are used to validate the results. The end-effector is controlled only on the translational degrees-of-freedom: x, y and z axes. The world coordinates coincide with the base of the manipulator represented by the point where the manipulator is attached to the vehicle. The end-effector initial position is at $p_{init} = (0.0,\ 0.0,\ 0.97)$ m.

To define the end-effector trajectory between the initial position and object location, a cycloid function as defined in Equation (5.60) is used. The function is an interpolation for the position $p_{des}(t)$ starting with an initial value $p_{init}(0)$ and a desired final value $p_{des}(t_f)$.

$$p_{des}(t) = p_{init}(0) + \Delta/2\pi[\omega t - \sin(\omega t)] \tag{5.60}$$

where

$$\omega = 2\pi/t_f, \quad \Delta = p_{des}(t_f) - p_{init}(0), \quad 0 \leq t \leq t_f$$

5.4.1 Environment stiffness coefficient $K_e = 10^3$ N/m

The first test case consists of interacting with an object that has a stiffness coefficient $K_e = 10^3$ N/m. The final goal where the contact has to take place is set at $(4.0,\ 2.0,\ -3.0)$ m and the desired interaction force is $F_{des} = 100$ N. The behaviour of the system in terms of motion of the end-effector is presented in Figure 5.2. The start point is considered $(0.0,\ 0.0,\ 0.0)$ m in world coordinates which corresponds to the point of attachment between the vehicle and manipulator. From this initial position the end-effector is commanded to move towards the goal. The decoupled and coupled strategy behaviour can be observed based on the 3D trajectory of the end-effector.

A better understanding of the behaviour of each of the controlled axes can be seen in Figure 5.3 and Figure 5.4. The results are presented in the world coordinate system. The manipulator is able to reach the goal that initially is placed outside of its working space. The results show the desired trajectory of the end-effector and the performance when the decoupled and the coupled methods are used. The decoupled approach at each time step validates if the current point is sent as a vehicle command or as a manipulator command. This leads to a slower trajectory generation in the end-effector coordinates and

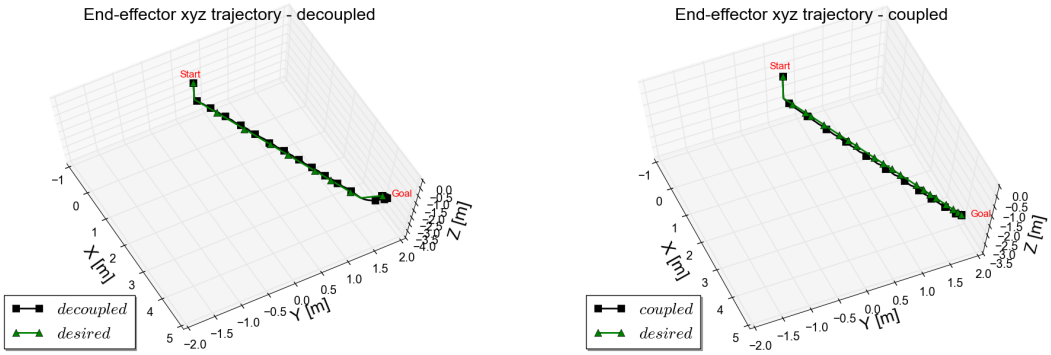

(a) Decoupled strategy (b) Coupled strategy

Figure 5.2. End-effector 3D position for goal at $(x, y, z) = (4.0, 2.0, -3.0)$ m

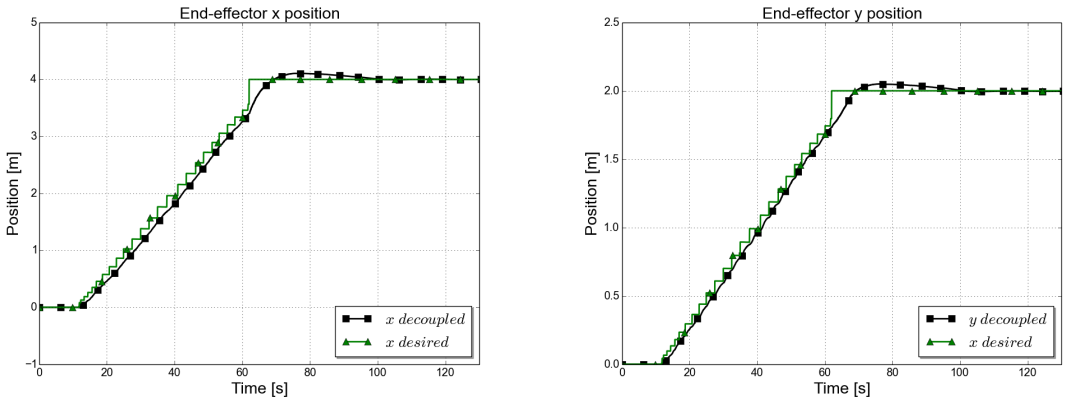

(a) x-position decoupled (b) y-position decoupled

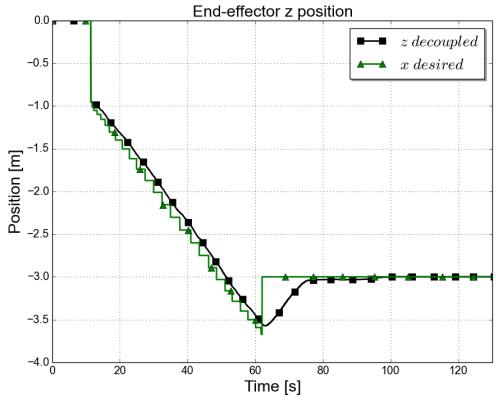

(c) z-position decoupled

Figure 5.3. Decoupled strategy UVMS end-effector position tracking, goal at $(x, y, z) = (4.0, 2.0, -3.0)$ m and $K_e = 10^3$ N/m

to a sudden change in the requested position. It can be seen that there is a small difference in the response of the end-effector between the two strategies. This difference is caused by the interaction component incorporated in the decoupled strategy that leads to a different behaviour of the system on the z-axis, Figure 5.3c. In this case the vehicle is under control while the manipulator is in station keeping until the system reaches in the vicinity of the

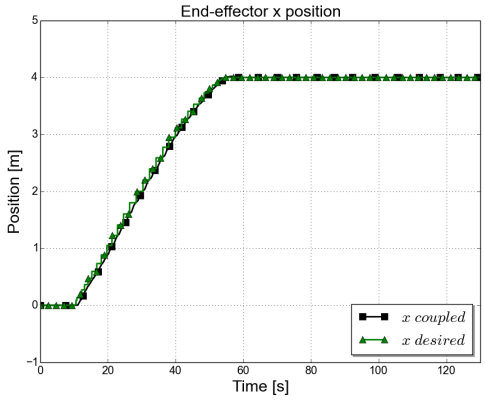

(a) x-position coupled

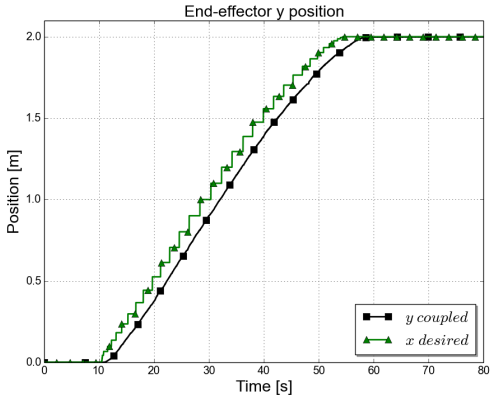

(b) y-position coupled

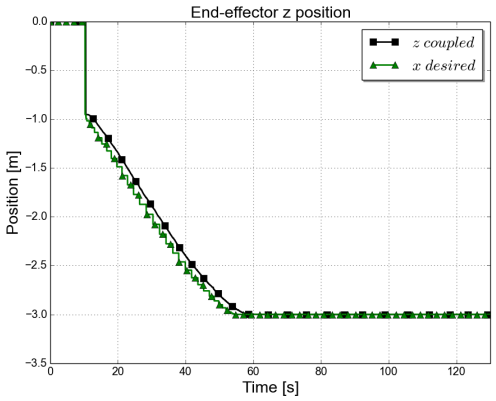

(c) z-position coupled

Figure 5.4. Coupled strategy UVMS end-effector position tracking, goal at $(x, y, z) = (4.0, 2.0, -3.0)$ m and $K_e = 10^3$ N/m

object with whom the system has to interact. This approach leads the end-effector to pass beyond the object before it is commanded to move and this causes a different behaviour on the z-axis in the decoupled strategy compared with the coupled approach. The interaction strategy represents a naive approach and a better path planning algorithm could lead to similar behaviour using a decoupled or a coupled strategy. It can be seen that in any of the two cases the position component of the controller performs well and the end-effector trajectory is accurately tracked. If only a single control law is used for the overall system the performances of the system are similar to the case when an appropriate controller is used for the vehicle in the decoupled strategy.

The proposed controller in Section 5.3.2 is evaluated not only through the trajectory performance but through the force contact. The performance of the system when interacting with the environment is seen in Figure 5.5. The contact with the environment takes place only at the moment when the desired location is reached with an accuracy of less than one centimetre. Due to this, in the decoupled strategy, the vicinity of the goal is reached in less than 60 seconds but due to the overshoot and large time to obtain zero steady-state error the contact with the environment starts only after 90 seconds. The settling time is large in this approach due to the fact that for a very short time both the vehicle and the manipulator

are moving towards the goal. This is caused by a small overshoot in the response when the vehicle controller is used, leading to an overshoot in the overall behaviour of the system. In both cases the desired contact force is achieved and maintained while the end-effector

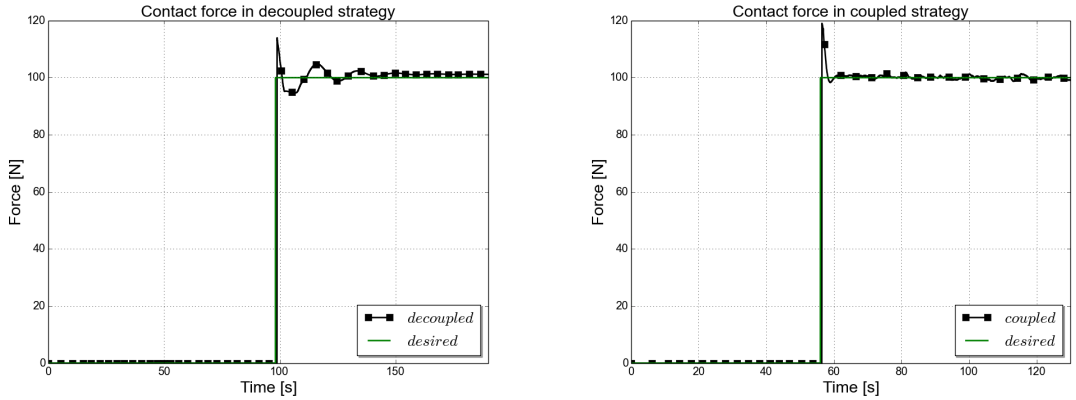

(a) Decoupled strategy

(b) Coupled strategy

Figure 5.5. Interaction with the environment when goal is at $(x, y, z) = (4.0, 2.0, -3.0)$ m and $K_e = 10^3$ N/m

location is kept. In the decoupled case oscillations are present while for the coupled case a larger first overshoot but smaller oscillations are seen in Figure 5.5b. At the moment when contact with the environment takes place, the manipulator compensates for the force and is trying not to lose position while maintaining contact. This will drive the manipulator to apply a larger force that results in an overshoot.

5.4.2 Environment stiffness coefficient $K_e = 10^5$ N/m

The proposed low-level controller is further evaluated by analysing the behaviour of the system when the contact is taking place with an object that has a higher stiffness coefficient, $K_e = 10^5$ N/m.

In Figure 5.6 it can be seen that the overshoot in the force response is larger when the environment is stiffer. The end-effector has to compensate for the force applied due to the interaction with the environment and does maintain the position of the system. As the end-effector achieves contact with the environment, in the decoupled behaviour, oscillations in the force response are present. Furthermore, the overshoot for this approach is higher than in the case when the coupled strategy is used. Based on the results seen in this simulation it can be said that the overshoot in the force contact is dependent of the stiffness of the environment. The manipulator applies larger contact forces and this results in a larger overshoot.

In this case the desired location of the contact with the object is set at $(2.0, 0.0, -2.0)$ m. As for the previous case, in the decoupled strategy the desired trajectory is set at a lower rate dependent on the decision component of the strategy. Analysing the behaviour of the end-effector, in the decoupled case Figure 5.7, an overshoot is seen in the x and y axes before the system reaches a steady-state. These overshoots are caused due to the tuning of

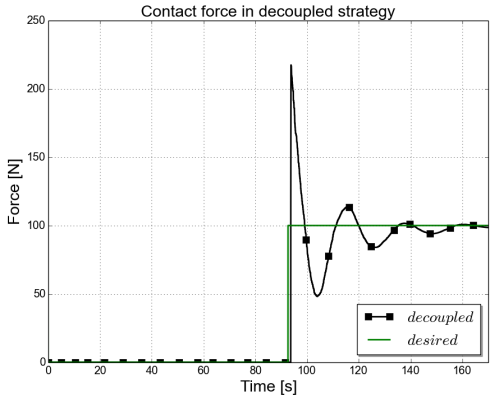

(a) Decoupled strategy

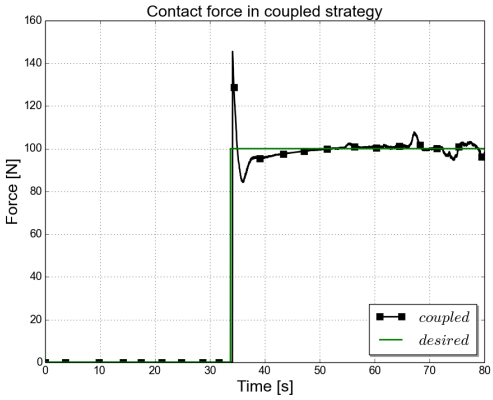

(b) Coupled strategy

Figure 5.6. Interaction with the environment when goal at $(x, y, z) = (2.0, 0.0, -2.0)$ m and $K_e = 10^5$ N/m

the controller that enforces zero steady-state error. The vehicle in the coupled approach, Figure 5.9b, compensates for the contact with the environment and the system reaches the steady-state faster with no overshoot.

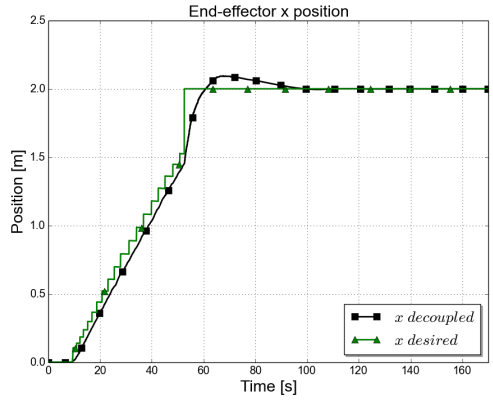

(a) x-position decoupled

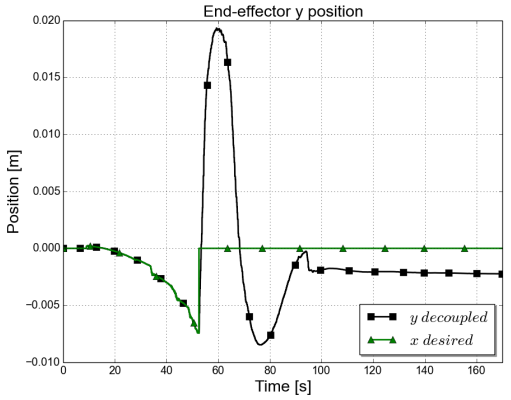

(b) y-position decoupled

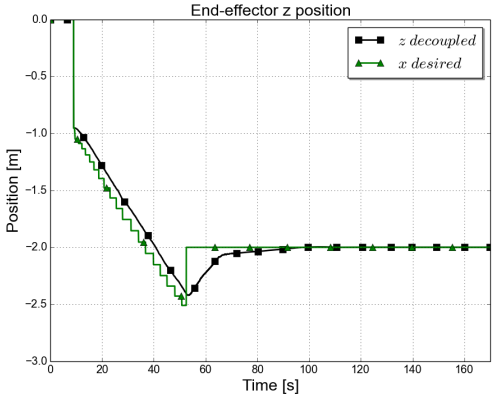

(c) z-position decoupled

Figure 5.7. Decoupled strategy UVMS end-effector position tracking for goal at $(x, y, z) = (2.0, 0.0, -2.0)$ m

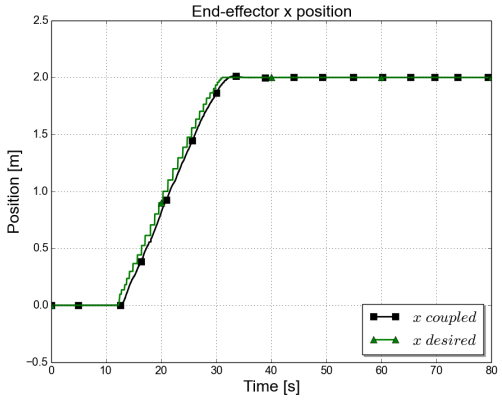

(a) x-position coupled

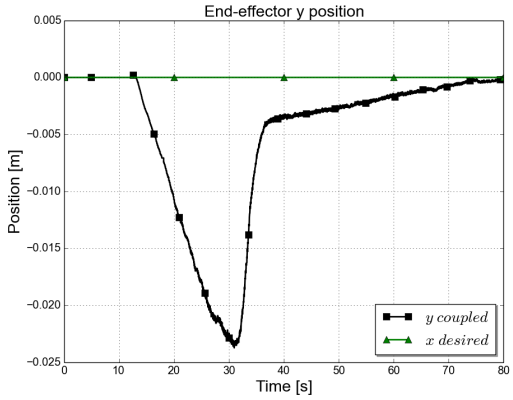

(b) y-position coupled

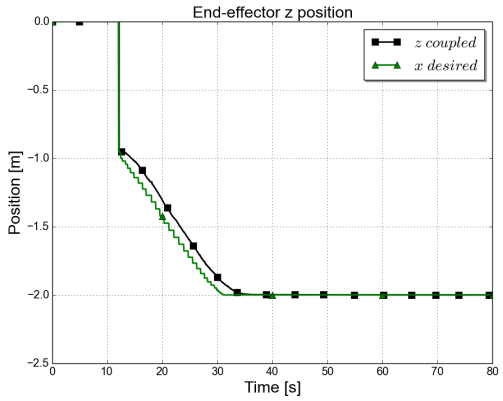

(c) z-position coupled

Figure 5.8. Coupled strategy UVMS end-effector position tracking for goal at $(x, y, z) = (2.0, 0.0, -2.0)$ m

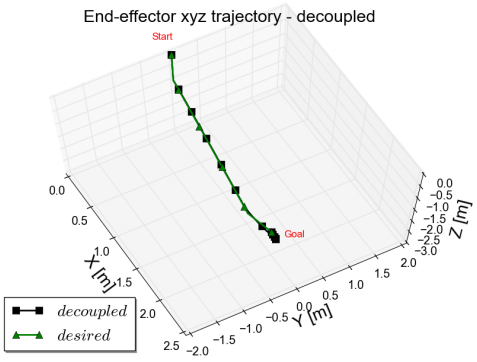

(a) Decoupled strategy

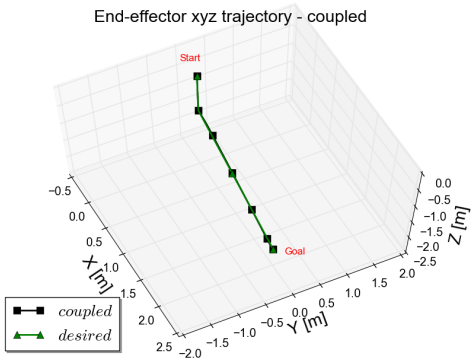

(b) Coupled strategy

Figure 5.9. End-effector 3D position, goal at $(x, y, z) = (2.0, 0.0, -2.0)$ m

The 3D behaviour of the end-effector when the goal is placed at $(2.0, 0.0, -2.0)$ m is seen in Figure 5.9. Using any of the strategies, the goal is reached and the desired trajectory is followed. The difference in the behaviour of the system is dependent on the strategy used. The coupled approach represents a straightforward method where the desired trajectory is generated based on the location of the end-effector. In the decoupled strategy the trajectory

is generated taking into account the position of the vehicle and the configuration of the manipulator.

5.4.3 Discussion

The operational space parallel position/force controller implemented in this thesis combines the theory of Sliding Mode Control with the dynamic model of the system. The advantages of this control structure rests in the elimination of the coupling effects between the vehicle and the manipulator and the robustness towards the uncertainties in the underwater environment. The control structure is used in a lightweight vehicle-manipulator system using two different strategies: a centralized method (the coupled approach) and a decentralised structure (the decoupled strategy). Some comments are next made regarding the two proposed strategies.

As presented in [22] the decoupled structure is a classical method to control the underwater vehicle-manipulator systems where a different control law is used for the vehicle and another control law is used for the manipulator. The main advantages of this type of strategy is the straightforward implementation. The method handles the coupling effects between the vehicle and manipulator by designing a robust vehicle control law that is able to handle the disturbances during the movement and the interaction of the manipulator with the environment. Furthermore, using the proposed manipulator control law defined in Section 5.3.2 the manipulator controller resolves the interaction with the environment and due to the PILIM control for the vehicle during the contact the vehicle maintains its position.

The decoupled method is characterised by the switch between the subsystems deciding what component is kept in station keeping. When the vehicle is keeping location it is common that the movement of the manipulator is large, being directly dependent on the threshold used in the switching component. If the threshold is small, the vehicle comes in very close proximity of the object whereas if the threshold is large it can happen that the object is out of reach for the end-effector. This can lead to extensive manipulator movements. Figure 5.10 shows the behaviour of the system when the threshold is not correctly set. In this case the manipulator joints reach their physical limits and there is a constant error in the steady-state response of the system, Figure 5.11. For the coupled case, the manipulator has a more restrictive displacement taking into account that the system to be controlled has more degrees-of-freedom. Treating the UVMS as a single system, the control law takes into account the error in the end-effector coordinates based on the location of the vehicle and manipulator.

In Figure 5.10 the behaviour of the joint positions using the two strategies and the physical limits of the joints are presented. The movement of the arm should allow the end-effector to reach the goal presented earlier $p_{des} = (2.0,\ 0.0,\ -2.0)$ m. In this case the threshold in the decoupled strategy is set to half of the manipulator length. The goal is to present how this threshold can affect the behaviour of the system. It can be seen based on Figure 5.10c, Figure 5.10e, Figure 5.10f that three of the six joints reach their limits

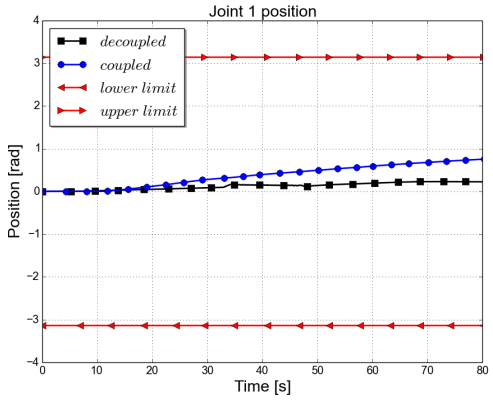

(a) Joint 1 position

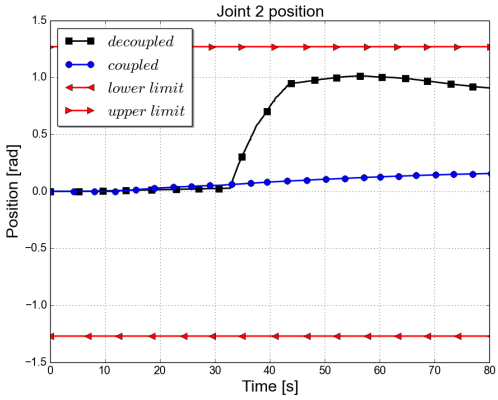

(b) Joint 2 position

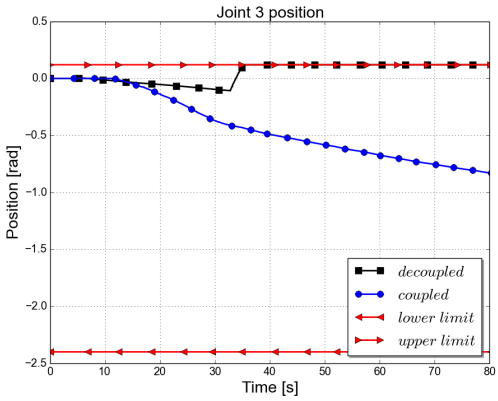

(c) Joint 3 position

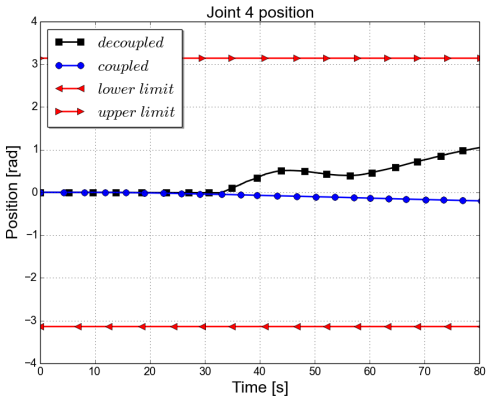

(d) Joint 4 position

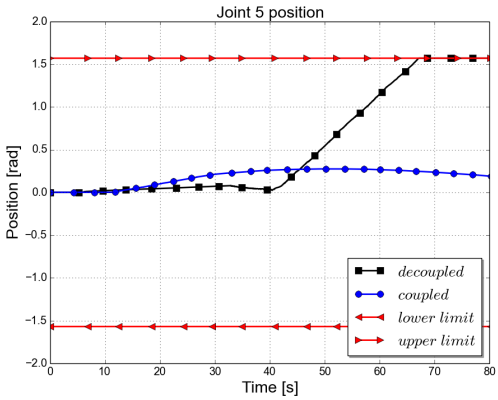

(e) Joint 5 position

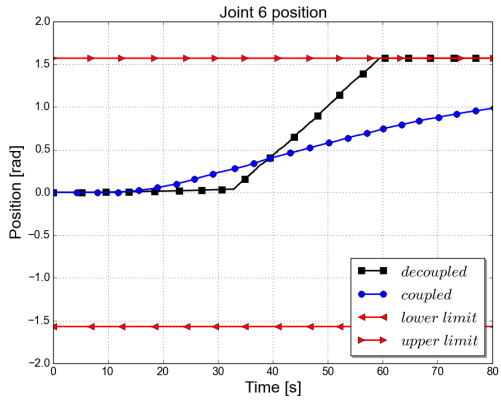

(f) Joint 6 position

Figure 5.10. Joint position for goal at $(x, y, z) = (2.0, 0.0, -2.0)$ m

and prevent the end-effector from reaching the desired goal. Using a poor choice for the threshold in the decoupled strategy reduces the performance of the system. The direct connection between the threshold and the success of the task represents a disadvantage of the decoupled approach. Nonetheless, this represents only a naive strategy to decide which subsystem is in station keeping. A path planning approach would eliminate this issue. Figure 5.10 shows also the behaviour of the joints when the coupled strategy is used. It can be observed that this shows a more restrictive movement of the arm.

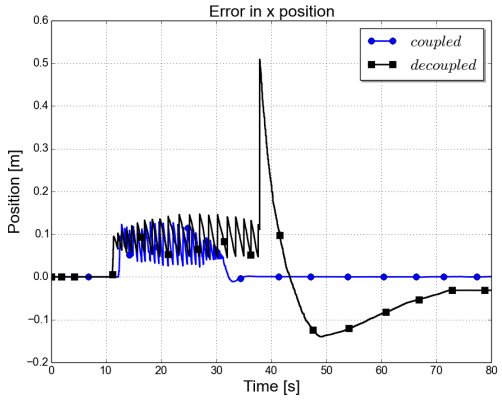

(a) x-axis error

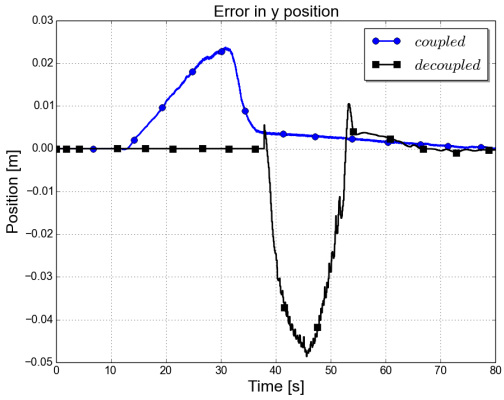

(b) y-axis error

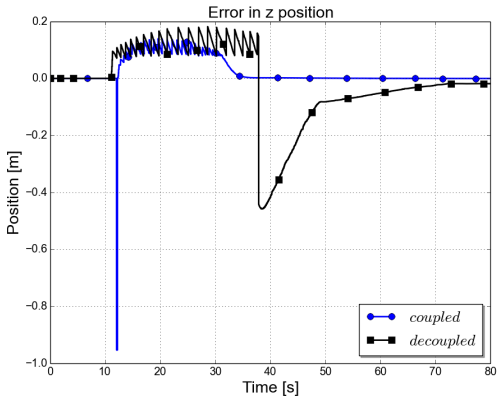

(c) z-axis error

Figure 5.11. End-effector position errors when goal is at $(x, y, z) = (2.0, 0.0, -2.0)$ m

The error in the end-effector, Figure 5.11, caused by the joint movement presented in Figure 5.10 shows how the end-effector is locked in a certain position and is not able to reach the desired goal due to a constant error in the x-axis. In this case, the exact location of the goal is not reached and the manipulator is not in contact with the object with no force being requested in the end-effector. This behaviour of the end-effector is due to the poor choice of the threshold. An appropriate threshold leads in obtaining the expected result.

To sum up, in the decoupled strategy the interaction strategy can play an important role that affects the behaviour of the system. A large threshold for the interaction strategy may prevent the contact between the manipulator and the environment while using a small threshold may lead to collisions between the UVMS and the surrounding environment. Furthermore improvements to the decoupled approach using a better tuning for the vehicle controller or by increasing the frequency used for the control loops. Nevertheless, in the results presented, due to the characteristics of the real systems and to obtain a reliable comparison between the two strategies, the same frequency is used for both controllers.

The inverse kinematics are responsible for generating the vehicle forces and manipulator torques for the coupled strategy. The control law is designed in operational space and the obtained forces are mapped to joint level torques and vehicle forces. By using a linearisation technique incorporating an estimate of the dynamic model the effects of the

manipulator movement on the vehicle are compensated. The full system, vehicle and manipulator, are compensating for the interaction with the object. The main advantage of this strategy rests in the reduction of the complexity of the strategy. In this case there is no need to design an interaction strategy and decide on an appropriate threshold for it. This makes the coupled strategy less sensitive to failure, guaranteeing the success of the task. Another important characteristic is that when using this method the execution time for the task is reduced as the system does not have to evaluate at each time step the distance to the goal and plan accordingly as happens in the decoupled strategy.

Different stiffnesses, from $K_e = 10^3$ N/m and $K_e = 5 \cdot 10^5$ N/m and ten different locations of the goal are used to test the two control strategies. To evaluate the results, the generalized root mean square error in end-effector coordinates, Equation (5.61), is used. The evaluation metric is computed separately for the position and force.

$$GRMS = \sqrt{\frac{1}{N}\sum_{k=1}^{N} e_k^2} \tag{5.61}$$

N is the number of total measurements and e is the generalized error. From Table 5.1 it can be observed that the performance of the trajectory tracking/position control is independent of the environment stiffness. The overall error in position is improved for the coupled approach, compared with the decoupled strategy. Nevertheless the difference is not significant and the decoupled approach provides accurate trajectory tracking results. For the force error, the coupled approach provides better results than the decoupled strategy. The oscillatory behaviour and the large overshot at high stiffness environments degrades the performance of the decoupled strategy. One specific case is represented by the most compliant environment where the decoupled strategy offers better results than the coupled approach. The object in this case does not oppose high contact forces and the desired force value is reached without any overshoot.

Characteristic	Strategy							
	Decoupled				Coupled			
K_e (N/m)	$1 \cdot 10^3$	$5 \cdot 10^3$	$1 \cdot 10^4$	$5 \cdot 10^4$	$1 \cdot 10^3$	$5 \cdot 10^3$	$1 \cdot 10^4$	$5 \cdot 10^4$
Position error (m)	0.13	0.13	0.13	0.13	0.10	0.10	0.10	0.10
Force error (N)	1.98	10.25	13.48	47.74	2.80	4.07	8.89	39.97

Table 5.1. Performance errors for decoupled and coupled strategies

Based on the generalized root mean square error it can be said that the coupled approach performs better in terms of position and force tracking. The error reduction is a result of the use of the overall UVMS dynamic model in the control law and not only for the manipulator. The coupling effects between the manipulator and the vehicle when the system is in contact with the object are handled in this case. The vehicle successfully reacts to these forces facilitating a better position keeping for the end-effector.

One common disadvantage for both strategies rests in the sensitive tuning of the controllers. Not setting the parameters accurately can lead to an oscillatory system or in having a large steady-state error. It can be concluded that both strategies can be used on the underwater vehicle-manipulator system. The decoupled strategy represents a controlled method where movement of the manipulator is restricted during the movement of the vehicle. This reduces the risk of collisions with the environment. Using appropriate vehicle and manipulator control structures and reliable interaction strategies, the decoupled method produces similar results to the coupled approach. The main advantage of the coupled approach is the use of a single controller for the overall system as this reduces the coupling effects between the vehicle and manipulator.

5.5 Summary

This chapter presented a new parallel position/force control based on sliding mode control theory together with two different strategies to control a lightweight underwater vehicle-manipulator system that interacts with an object in the underwater environment. A detailed description of the control law is given. The simulation results present how this method can be used on an UVMS either using a coupled or a decoupled strategy. The decoupled method incorporated the proposed control law for the manipulator while a different control law is used for the vehicle. An interaction strategy is used to decide which component is in station keeping and which one is requested to move. In the coupled strategy, the underwater vehicle-manipulator system is controlled by the parallel position/force law designed in the operational space. The joint and vehicle commands are computed from the control law output based on the full Jacobian of the system. The evaluation of the system is focused on the two control strategies and analysing the differences between them. Based on the simulation results, it can be concluded that both control strategies provide accurate position and force tracking. The desired interaction force is achieved both in compliant and stiff environments and the steady state is maintained. A detailed comparison between the coupled and decoupled strategies is presented for the first time for autonomous underwater systems, to the best knowledge of the author. The parallel position/force control law performances are further analysed in Chapter 6 based on real experiments.

Chapter 6

Experimental comparison of manipulator position/force controllers

In Chapter 5 the Parallel Variable Sliding Mode Dynamic Controller (VSMD) algorithm was developed for the underwater vehicle-manipulator system. This chapter aims to present the experimental validation of this method applied to the HDT-MK3-M manipulator. The strategy is evaluated by comparison with the Impedance Controller. The control methods used in this chapter are part of the operational space control methods. To properly design the desired trajectory of the end-effector, without putting the arm in a singular configuration, a path planner is used to reach the final goal.

The chapter starts by describing the Impedance control method and by making a short review of the VSMD algorithm in Section 6.1. In Section 6.2 the end-effector force is approximated, followed by the presentation of the experimental system in Section 6.3. The experimental results are presented and analysed in Section 6.4.

6.1 Manipulator position/force control strategies

This section is focused on the description of the Impedance Control Algorithm, followed by a short review of the VSMD method. The dynamic representation of the system in operational space can be described by Equation (6.1) [79], where $x \in \mathbb{R}^6$ represents the independent parameters vector described in the operational space.

$$M(x)\ddot{x} + C(x)\dot{x} + D(x)\dot{x} + G(x) + F_f(x) = T - F \tag{6.1}$$

where $M(x) \in \mathbb{R}^{6\times6}$ is a positive operational space inertia matrix, $C(x)\dot{x} \in \mathbb{R}^6$ is the vector of Coriolis and Centripetal forces, $D(x)\dot{x} \in \mathbb{R}^6$ is the damping vector, $G(x) \in \mathbb{R}^6$ is the vector of restoring forces, $F_f(x) \in \mathbb{R}^6$ is the friction vector, all defined in operational space coordinates, $T \in \mathbb{R}^6$ is the vector of generalized forces at the end-effector and $F \in \mathbb{R}^6$ is the vector of contact forces at the end-effector. This dynamic model is used to develop the control methods.

6.1.1 Impedance controller

The impedance control strategy aims to control the dynamic relationship between the position and force along all the directions of the operational space. One of the main advantages of the impedance controller is the robustness to the environmental modelling and to the uncertainty in the contact force [70]. One drawback of this method rests in the fact that by not imposing the contact forces, these can grow very large.

The impedance control method is based on imposing a dynamic behaviour to the contact between the environment and the robot end-effector. The contact forces are controlled indirectly through the position requirements. This dynamic behaviour is described by a mass-spring-damper system and the stiffness model used in the control law is responsible for the balance between controlling the position and force. The control law used starts with the linearisation of the system in the Cartesian space, Equation (6.2) and continues with the dynamic impedance model Equation (6.3) imposed by the external forces from the environment. The linearisation of the system in the Cartesian space is done using an approximate model of the dynamics of the system described in operational space and aims to decouple the axes of the end-effector in such a way that an independent impedance control law can be applied for each axes.

$$\tau = J_m^T(q)\left[\tilde{M}(x)\ddot{x} + \tilde{C}(x,\dot{x})\dot{x} + \tilde{D}(x,\dot{x})\dot{x} + \tilde{G}(x) + \tilde{F}_f(x) + F\right] \tag{6.2}$$

$$B_m(\ddot{x} - \ddot{x}_{des}) + D_m(\dot{x} - \dot{x}_{des}) + K_m(x - x_{des}) = F \tag{6.3}$$

where $\tilde{M}(x) \in \mathbb{R}^{6\times6}$, $\tilde{C}(x,\dot{x})\dot{x} \in \mathbb{R}^6$, $\tilde{D}(x,\dot{x})\dot{x} \in \mathbb{R}^6$, $\tilde{G}(x) \in \mathbb{R}^6$, $\tilde{F}(x) \in \mathbb{R}^6$ are the approximated dynamic parameters in Cartesian coordinates, described in detail in Chapter 5 and $B_m \in \mathbb{R}^6$ is the desired mass, $D_m \in \mathbb{R}^6$ is the desired damping and $K_m \in \mathbb{R}^6$ is the desired stiffness. $\ddot{x}_{des} \in \mathbb{R}^6$, $\dot{x}_{des} \in \mathbb{R}^6$, $x_{des} \in \mathbb{R}^6$ are the desired acceleration, velocity and position in operational space. The control law implemented at manipulator joint level is given by Equation (6.4).

$$\begin{aligned}\tau = M(q)J_m^{-1}(q)\{\ddot{x}_{des} - \dot{J}_m(q)\dot{q} + B_m^{-1}\left[D_m(\dot{x} - \dot{x}_{des}) + K_m(x - x_{des})\right]\} + \\ + C(q,\dot{q})\dot{q} + D(q,\dot{q})\dot{q} + g(q) + \left[M(q)J_m^{-1}(q)B_m^{-1} - I\right]F\end{aligned} \tag{6.4}$$

Lu *et al.* [138] state that the impedance control method represents a duality of the resolved acceleration method in the domain of the constrained motion control. Moreover, the authors argue that the method is disadvantageous when the Jacobian is non-singular. To solve these challenges in the paper an adaptive impedance controller is proposed.

In [139] the impedance control law is modified to ensure that the desired force is achieved regardless of the uncertainties in terms of the stiffness coefficients of the environment. The steps to achieve the desired position are presented further. To obtain a desired force interaction with the environment the desired position has to be specified taking into

account this desired force based on Equation (6.5).

$$x_{des} = x_e + \frac{F_{des}}{K_{eff}} \tag{6.5}$$

where $F_{des} \in \mathbb{R}^6$ is the desired force, $x_e \in \mathbb{R}^6$ is the position of the environment and $K_{eff} \in \mathbb{R}^6$ is the effective stiffness defined according to Equation (6.6).

$$K_{eff} = \frac{K_m K_e}{K_m + K_e} \tag{6.6}$$

where $K_e \in \mathbb{R}^6$ is the environment stiffness. The main challenge for this approach is the difficulty of knowing exactly the environment stiffness coefficient K_e. To overcome this, the impedance control law can be modified so that the system is not dependent on K_e. By incorporating the desired trajectory defined by Equation (6.5) into Equation (6.3) the force tracking is obtained in Equation (6.7).

$$\begin{aligned} B_m(\ddot{x} - \ddot{x}_{des}) + D_m(\dot{x} - \dot{x}_{des}) + K_m\left(x - x_e - \frac{F_{des}}{K_{eff}}\right) = F \Leftrightarrow \\ \Leftrightarrow F_e = B_m\ddot{\varepsilon} + D_m\dot{\varepsilon} + K_m\varepsilon\left(1 - \frac{F_{des}}{F_e}\right) + F_{des} \end{aligned} \tag{6.7}$$

where $\varepsilon = x_e - x$. A further modification is presented in Equation (6.7) ensuring that at steady-state $F_{des} = F_e$.

$$F_e - F_{des} = B_m\ddot{\varepsilon} + D_m\dot{\varepsilon} \tag{6.8}$$

In some cases, the environment location is uncertain and this would create difficulties in achieving proper force tracking. Including the uncertainty of the environment in Equation (6.8) this can be reformulated as:

$$B_m\ddot{\hat{\varepsilon}} + D_m\dot{\hat{\varepsilon}} = F_e - F_{des} \tag{6.9}$$

where $\hat{\varepsilon} = \varepsilon + \delta x_e$, $\delta x_e = \hat{x}_e - x_e$ and $\hat{x}_e$ is the uncertainty in the environment location. By specifying the uncertainty in the environment position in the impedance equation it is ensured that the contact with the environment is taking place. The drawback of this approach is the fact that when the end-effector moves along the environment, the force tracking is not guaranteed. To this extent in [139] the authors propose the addition of an adaptive term in the impedance controller.

Using any of the types of impedance controllers mentioned here, by correctly selecting the impedance controller parameters, the method regulates the force contact in the absence of force contact information [139]. According to Lawrence [140] high stiffness coefficients should be defined for the directions where a compliant environment is present and accurate position tracking is required. Low values of these parameters are appropriate for cases when small contact forces are required. The D_m parameter is related to the energy that must be dissipated while B_m has the role of smoothing the behaviour of the robot when

the end-effector is in contact with the environment. It must be said that perfect results for both position and force requirements are difficult to obtain. A compromise must be done in practice.

6.1.2 Parallel Variable Sliding Mode Dynamic Controller

The Parallel Variable Sliding Mode Dynamic Controller is described in detail in Chapter 5. In this part a short review of the method is presented and its implementation for a manipulator is described. The strategy can be considered as part of the parallel position/force controller class, where both the force and position tracking are under regulation. The method incorporates the dynamic model of the system and the class of sliding mode controllers in order to compensate for the disturbances and uncertainties in the system and environment. The control law for the manipulator is based on Equation (6.10).

$$T = \tilde{M}(x)\left[\ddot{x}_{eq} + u_p + u_f\right] + \beta = \tilde{M}(x)\left[\ddot{x}_{eq} + \kappa_1 \mathtt{sign}(\delta) + \kappa_2 \mathtt{sign}(s) + K\sigma\right] + \beta \quad (6.10)$$

where

$$\begin{aligned}
\delta &= \dot{e}_p + c_1 e_p, \quad c_1 > 0 \\
\sigma &= \dot{e}_f + c_2 e_f + c_3 \int_0^t e_f d\tau, \quad c_2, c_3 > 0 \\
s &= \sigma - z \\
\dot{z} &= -c_3 u_2 \\
u_2 &= K\sigma, \quad K > 0 \\
\beta &= \tilde{C}(x,\dot{x})\dot{x}_{eq} + \tilde{D}(x,\dot{x})\dot{x}_{eq} + \tilde{G}(x) + \tilde{F}_f(x) + \tilde{F}_{eq} \\
\dot{x}_{eq} &= \dot{x}_{des} + c_1 e_p \\
F_{eq} &= F_{des} + c_2^{-1}\dot{e}_f + c_2^{-1} c_3 \int_0^t e_f d\tau
\end{aligned} \quad (6.11)$$

κ_1 and κ_2 are positive constants, $\tilde{M}(x)$ is an estimate of the inertia term, $\tilde{C}(x,\dot{x})$, $\tilde{D}(x,\dot{x})$, $\tilde{G}(x)$ are estimates of the dynamic components defined for the manipulator system, in operational space coordinates.

The chattering effect is approximated by a smooth function, that is by replacing the `sign` function with the sigmoid function:

$$\mathtt{sign}(a) \simeq \frac{a}{\mid a \mid + \varepsilon} \quad (6.12)$$

where ε is a small positive scalar.

The controller is designed in the operational space. The position of the end-effector is computed using the following kinematic transformation of the manipulator.

$$v_m = J_m(q)\dot{q} \quad (6.13)$$

where $v_m \in \mathbb{R}^6$ is the manipulator end-effector velocity and $J_m(q) \in \mathbb{R}^{6\times n}$ is the manipulator task Jacobian matrix and n is the number of revolute joints of the manipulator. The control law at the joint level is described by Equation (6.14).

$$\tau = J_m^T(q)T \tag{6.14}$$

where T is defined as in Equation (6.10).

6.2 End-effector force approximation

The control strategies mentioned in Section 6.1 assume that the end-effector contact force is known. To have accurate end-effector force knowledge a sensor is required. Nevertheless, when this sensor is not available the force can be approximated based on joint information.

There are a few methods available in the literature to estimate the force contact. The most simple method is based on the torque on each joint. This method is straightforward and easy to use for the direct current type motors. In [141] the method is presented as disadvantageous due to the fact that the measured torques used in this technique have to be compensated previously for gravity and friction forces. In [142] the method is extended by using the dynamic model of the robot and a recursive least-squares algorithm for the force approximation. Using an Extended Kalman Filter (EKF) and a Lyapunov adaptive law the end-effector force is approximated in 3D for a three-link manipulator in [143]. A disturbance observer is used in [144] for the force contact estimation. At each joint an observer is applied that determines the dynamics of the system. The difference between the observed behaviour when no contact is present and the case when the robot is in contact with the environment enables the computation of the external forces applied to the system.

The model presented in this section is based on the torque-current relationship and uses the dynamic model of the robot. The force vector $F \in \mathbb{R}^6$ expressed in base frame, Equation (6.15), is connected to the corresponding joint effort, $\tau_f \in \mathbb{R}^n$, based on the Jacobian of the manipulator as presented in Equation (6.16).

$$F = [f_x,\ f_y,\ f_z,\ n_x,\ n_y,\ n_z]^T \tag{6.15}$$

$$\tau_f = J_m^T(q)F \tag{6.16}$$

where $J_m(q) \in \mathbb{R}^{6\times n}$ is the manipulator Jacobian and n is the number of degrees-of-freedom of the manipulator. Knowing the joint effort caused by the contact between the end-effector and environment it is possible to estimate the end-effector forces and torques:

$$F = (J_m^T(q))^{-1}\tau_f \tag{6.17}$$

The total torque, $\tau \in \mathbb{R}^n$, at joint level can be described based on Equation (6.18):

$$\tau = \tau_p - \tau_f \tag{6.18}$$

where $\tau_p \in \mathbb{R}^n$ is the torque needed to produce a certain motion or maintain a position. These torques can be computed based on the mathematical model of the robot as presented in Equation (6.19).

$$\tau_p = M(q)\ddot{q} + C(q,\dot{q})\dot{q} + D(q,\dot{q})\dot{q} + g(q) + f_f(q) \tag{6.19}$$

where $\ddot{q}$, $\dot{q}$ and q are provided by measurements. To estimate the total torque at joint level, the motor current-joints torque relationship can be used, in the case when joint torque sensors are not available for the manipulators. This relation is different for alternating current (AC) and direct current (DC) motors. For AC motors the current-torque relation is difficult to model due to non-linearities in the system. In this case, the relationship is dependent of the type of motor, its parameters and characteristics. If the motor at each joint is a permanent magnet DC motor that has current measurements available, the torque at each joint can be approximated based on Equation (6.20).

$$\tau = k_\tau^T i_a \tag{6.20}$$

where $k_\tau \in \mathbb{R}^n$ is the vector of torque constants and $i_a \in \mathbb{R}^n$ is the vector of motor armature currents. Substituting Equation (6.20) into Equation (6.18), the total torque can be re-written as:

$$k_\tau^T i_a = \tau_p - \tau_f \tag{6.21}$$

From Equation (6.21) the joint effort caused by the external interaction with the environment can be computed using Equation (6.22). This leads to an external force contact approximation defined in base coordinates according to Equation (6.23).

$$\tau_f = \tau_p - k_\tau^T i_a \tag{6.22}$$

$$F = (J_{man}^T(q))^{-1}(M(q)\ddot{q} + C(q,\dot{q})\dot{q} + D(q,\dot{q})\dot{q} + g(q) - k_\tau^T i_a) \tag{6.23}$$

6.3 Problem Statement

The goal of this chapter is to provide a quantitative and qualitative evaluation of the VSMD position/force control in comparison with the Impedance Control. The controllers are implemented on a real underwater manipulator placed on a fixed base. This section starts with the description of the HDT-MK3-M manipulator, followed by a few details regarding the implementation of the controllers on the real robotic system.

6.3.1 The HDT-MK3-M robotic manipulator

The Ocean Systems Laboratory at Heriot-Watt University owns a lightweight underwater manipulator developed by HDT Global [115]. The manipulator, named HDT-MK3-M, is a marinized version of the ground-base system produced by the same company. The overall system consists of a manipulator arm, an end-effector, an integration kit and an operator control unit. The components are presented in Figure 6.1. The system is modular and the end-effector can be detached from the manipulator arm. For the experiments performed in

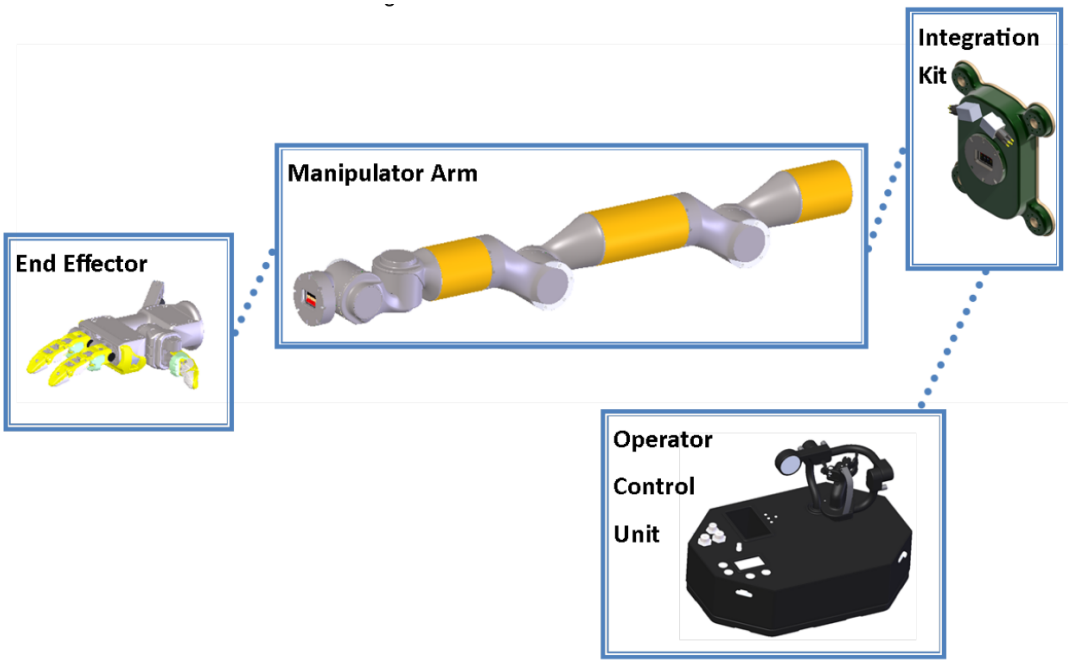

Figure 6.1. The HDT-MK3-M components

this chapter the interest was in the Manipulator Arm and in the Integration Kit. The end-effector was not used in this thesis. The Operator Control Unit represents the teleoperation capability of the robot and is out of the scope of this thesis.

Manipulator Arm

The manipulator arm has in total 6 degrees-of-freedom divided into the wrist assembly, elbow assembly and shoulder assembly, Figure 6.2. The shoulder assembly has two DOFs: the shoulder pitch and yaw joints, the elbow consists of one single DOF and the wrist assambly has roll, yaw and pitch DOFs. At each joint the manipulator has a position sensor, a current sensor, a torque sensor and a temperature sensor. The maximum joint speed is 0.7 rad/sec (equivalent of 40 deg/sec) and the maximum joint torque is 60 Nm. The weight in air of the arm is 9 kg while in water it has a weight of 3 kg. The manipulator joint position limits are presented in Table 6.1. The arm does not have an end-effector force sensor that can be used to measure the interaction force with the environment. To reduce the weight of the arm in the water, floats can be attached to each link. Nevertheless these

restrict the movement of the arm and this reduces the workspace of the arm. Due to this, they are not used in these experiments.

Figure 6.2. Manipulator arm components

Joint name	Minimum joint limit (rad)	Maximum joint limit (rad)
Shoulder roll	−3.14	3.14
Shoulder pitch	−1.57	3.14
Elbow pitch	−1.57	3.14
Wrist roll	−3.14	3.14
Wrist yaw	−1.57	1.57
Wrist pitch	−1.57	1.57

Table 6.1. Manipulator arm joint limits

Integration Kit

The Integration Kit (IK) is used as the mounting base for the arm and to produce the communication between the arm and the exterior world. The Integration Kit incorporates a micro-controller and consists of the manipulator mounting point and two electrical connectors. A detailed schematic of the Integration Kit is presented in Figure 6.3. The communication between the arm and external user is provided by the Integration Kit over a 100 Mbps Ethernet connection. A composite video connection is available to the camera placed at the end-effector. The IK has a MCBHRA4M connector for power and receives 48 VDC from an external source and can draw up to 600 W of power. A MCBHRA8M connector is used for communication with external sources. System information and control commands are sent across the network based on a TCP (socket) protocol to the IK. From here this information is transmitted forward to the manipulator drives based on a CAN communication bus. From an external source the manipulator drives can be commanded using the Robot Operating System (ROS) architecture. The commands that can be sent to the drives are joint position, joint velocity and joint currents.

6.3.2 Experimental set-up

The manipulator is mounted on the Integration Kit that is attached to a fixed base and placed in the indoor tank available in the Ocean Systems Laboratory. Two different set-ups

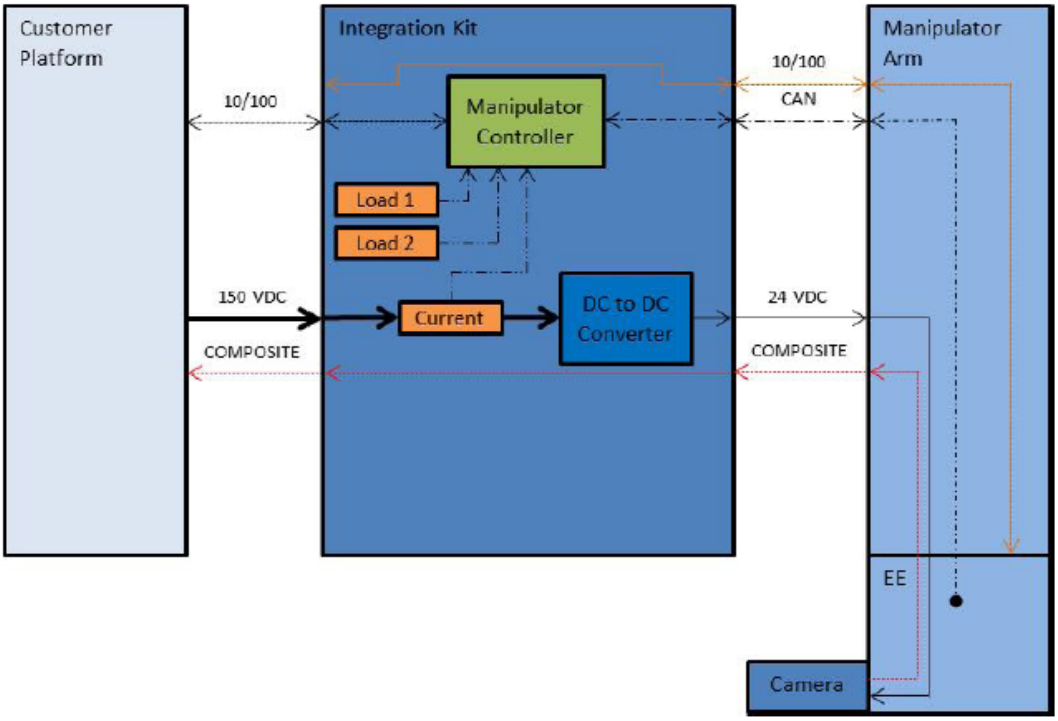

Figure 6.3. Integration Kit connection diagram

for interacting with the environment are used. One represented by a plastic ball submerged and the other scenario consisting of an aluminium plate submerged. The two cases can be seen in Figure 6.4.

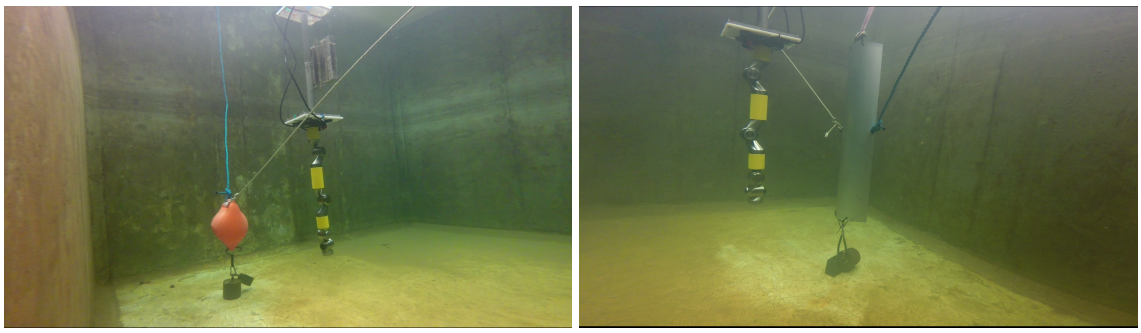

(a) Plastic ball (b) Aluminium plate

Figure 6.4. Experimental set-up

To evaluate the proposed strategies when the manipulator is in contact with the environment, an approximate stiffness coefficient has to be computed for the two objects used in these experiments. Computing accurately the stiffness coefficient is out of the scope of this thesis, the interest being on the order of the coefficient. To this extent, a simple point model is used for computing the axial stiffness based on Equation (6.24).

$$K_e = \frac{EA}{L} \tag{6.24}$$

where L is the length of the object, A is the cross-sectional area and E is the material

property or Young's modulus. The elasticity of the most used materials is presented in Figure 6.5. It can be seen that steel is 3 times stiffer than aluminium and 100 times stiffer than plastic. Based on the characteristics of the plastic ball, the stiffness coeffi-

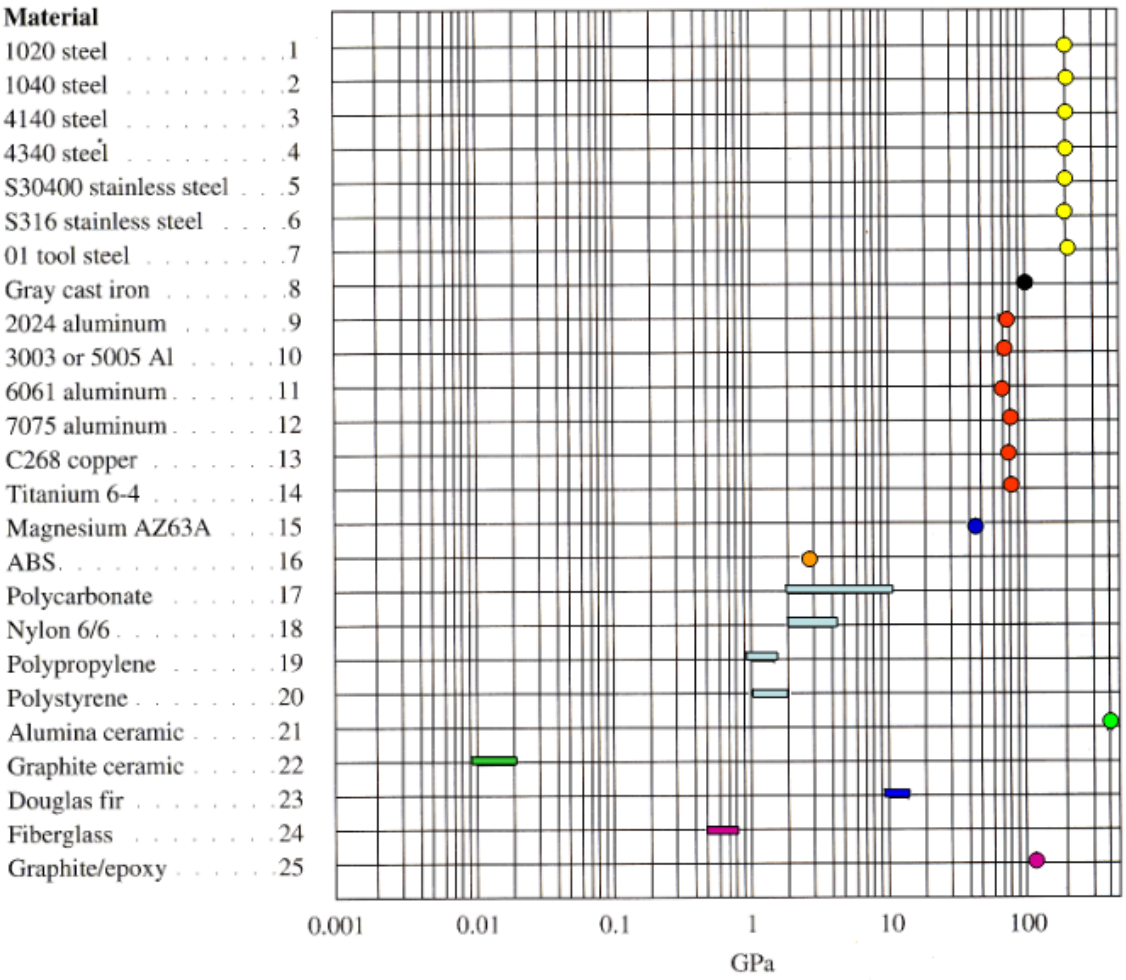

Figure 6.5. Modulus of elasticity of materials, [145]

cient is approximately $K_e = 1.75 \times 10^8$ Nm and for the aluminium plate the coefficient is $K_e = 3.3 \times 10^{11}$ Nm.

The two controllers described in Section 6.1 are implemented in Python on an external computer. The controllers compute the torque required for the end-effector to move and to obtain the desired contact force. This torque is sent directly to the drives of the manipulator arm, bypassing the existing joint controllers of the arm. The communication with the joint drives is facilitated through ROS at a rate of 10 Hz. This represents the maximum limit at which the arm can communicate. The drives provide in response the current joint position and velocity required in the control structures. The MoveIt [146] software is used to compute the forward and inverse kinematic models of the robot. The same software decides the optimal path the end-effector has to take to reach the desired goal. The path generated represents the optimal path and takes into consideration the joint limits and self-collision information. By using this method to generate the trajectory, it is ensured that the arm is not put into a singular configuration. As a safety feature the maximum current drawn by

each motor is limited to 3 Amperes.

6.4 Experimental results

The proposed controllers are evaluated through multiple experiments and the results are presented in this section. It has to be mentioned that in this case the end-effector control is implemented only for the x, y and z axes. The world coordinates are defined at the base of the manipulator coinciding with the base coordinates of the arm. An assumption is made that the end-effector contact with the environment is made principally on the x-axis. Based on this, the end-effector force contact is controlled only on a single axis.

6.4.1 Interaction with a plastic ball

The first group of experiments represents the interaction of the end-effector of the manipulator arm with a submerged plastic ball. In this case the ball is placed in a predefined location in the working-space of the manipulator. The desired position where the end-effector is requested to reach is represented by the position of the ball. The desired interaction force with the environment is requested in the neighbourhood of the desired position, based on a tolerance margin. As soon as the end-effector is outside of this tolerance boundary, the applied force to the object should be zero.

In a first experiment, the location of the centre of the ball (the desired position) is located at $(0.5,\ 0.3,\ -0.7)$ m in the world coordinates. To reach this location an optimal trajectory is computed for the end-effector and the arm is requested to follow this trajectory until it reaches the final goal. The plastic ball has a diameter of 0.3 m. This represents the tolerance area for applying the interaction force. In this case the desired contact force between the end-effector and environment is 100 N. In Figure 6.6 the behaviour of the $x,\ y$ and z axes is presented for the Impedance controller and for the VSMD controller. It can be seen that the two controllers produce a similar end-effector behaviour. The time needed to reach the steady-state is less than 15 sec. For the x and y axes, Figure 6.6a and Figure 6.6b, a small offset between the desired position and the real end-effector position is noticeable using any of the controllers. This can be explained based on the fact that the proposed controllers are designed in the operational space. To compute the joint torques needed to produce motion of the arm and to reach the desired end-effector location the output of the operational space controller is multiplied by the transpose of the Jacobaian. This enforces coupling effects between the end-effector axes and limits the capabilities of the designed controllers and in some cases an offset from the desired location is present. In the case of the z-axis, the VSMD controller ensures zero steady-state error, while using the Impedance controller a small offset is present.

Another difference in the two behaviours is represented by the overshoot present in all the three axes. While on the x-axis both the Impedance and the VSMD controllers have a small overshoot, on the other two controlled axes this overshoot is noticeable only using

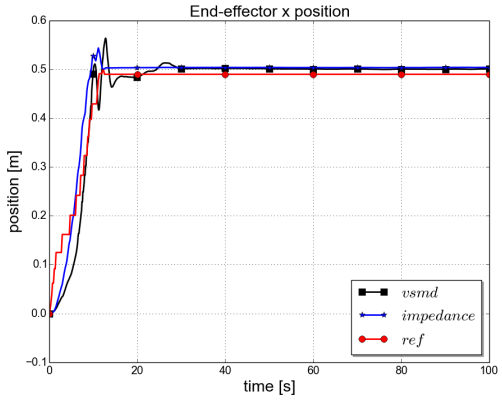

(a) x-axis trajectory

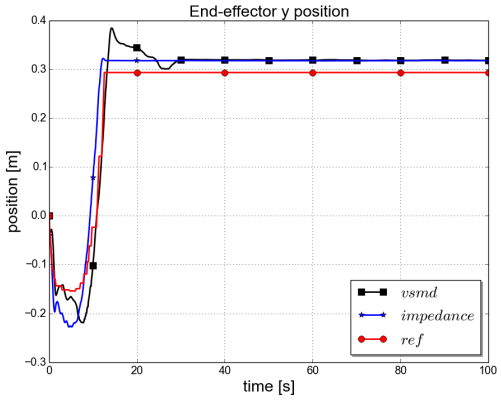

(b) y-axis trajectory

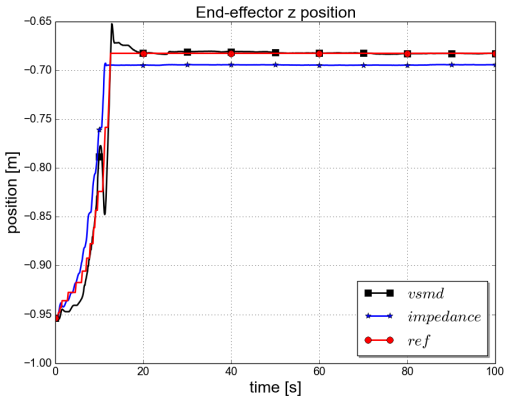

(c) z-axis trajectory

Figure 6.6. End-effector trajectory tracking, contact with a plastic ball

the VSMD controller. This overshoot can be explained based on the fact that the controller enforces at least one of the axes to have zero steady-state error and this causes the overshoot for all the axes as they represent a coupled system. The 3D behaviour of the end-effector is seen in Figure 6.7. The end-effector initial location is on $(0,\ 0,\ -0.97)$ m. As mentioned previously, the end-effector behaviour using the two controllers is similar, both having a small offset from the desired trajectory.

The joint movements are presented in Figure 6.8. These trajectory movements lead to the end-effector motion. The joints have a similar behaviour using both controllers. A small displacement of maximum 0.1 rad (5.7 deg) is present between the case when the Impedance controller and the VSMD controller is used. This displacement is the principle cause that leads to achieving the zero steady-state error on the z-axis when using the VSMD controller. Responsible for the overshoot in the VSMD controller are joint 1, joint 2 and joint 6. As can be seen from Figure 6.8a, Figure 6.8b and Figure 6.8f at joint level this overshoot is not significant but at the end-effector level the effects are more noticeable.

To obtain this joint movement and the end-effector trajectory tracking, the commanded currents sent after the output of the operational space controller is multiplied by the transpose of the Jacobian and is presented in Figure 6.9. As a safety measure, a maximum and minimum limit of ± 3 A is imposed on the current sent to the joints. This imposes a limit to

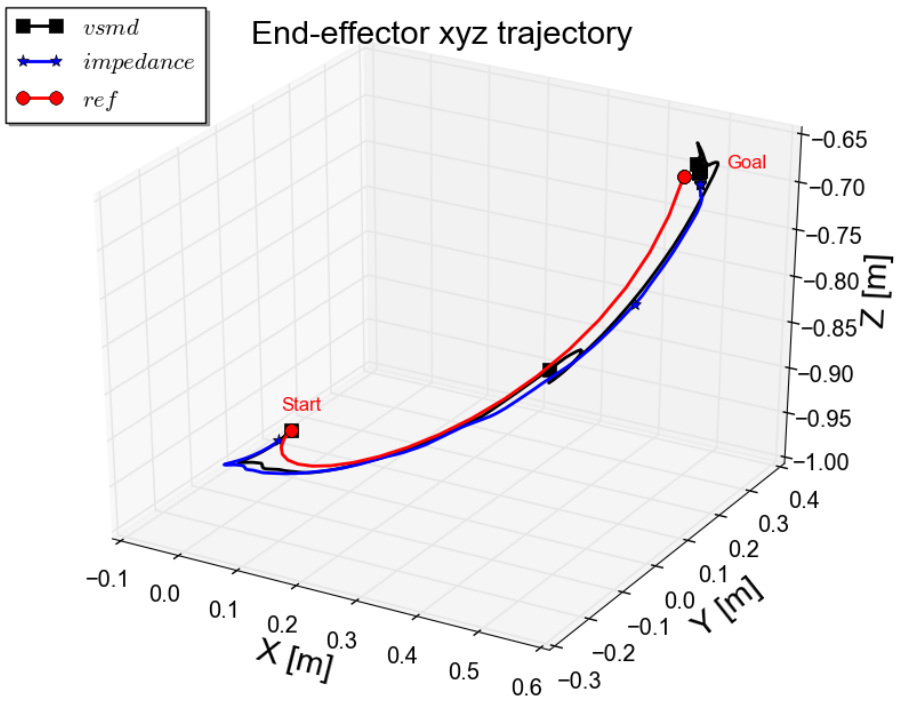

Figure 6.7. End-effector 3D trajectory, contact with a plastic ball

the velocity of the arm. For the VSMD controller, at the beginning of the execution time, the current sent is mainly dependent on the trajectory following of the end-effector, as the desired force to be applied by the manipulator is 0 N. When the end-effector reaches the ball the force component of the controller has more influence as now the desired force is 100 N. Due to this a spike in the currents sent to the manipulator can be seen in Figure 6.9 that enforces the manipulator to go from 0 N end-effector applied force to the environment to the 100 N applied force and also continue to move until it reaches the exact location. After the desired location is reached the controllers continue to send a constant current that ensures maintenance of the desired force. For the Impedance controller these spikes do not appear as the controller is based only on the position error. In this case also, a constant current is applied after the desired location is reached that ensures the end-effector contact is maintained. The plastic ball applies an opposite force on the end-effector and the manipulator is trying to maintain the location. In this way the force is controlled using the Impedance controller.

The end-effector contact force is presented in Figure 6.10. The two controllers present similar behaviour. The VSMD controller presents a more oscillatory response than the Impedance controller. At the moment of contact both the VSMD controller components are active at the same time. While the force controller tries to maintain the desired force the position controller tries to enforce the desired location. The Impedance and VSMD controllers maintain appropriate force contact with the ball.

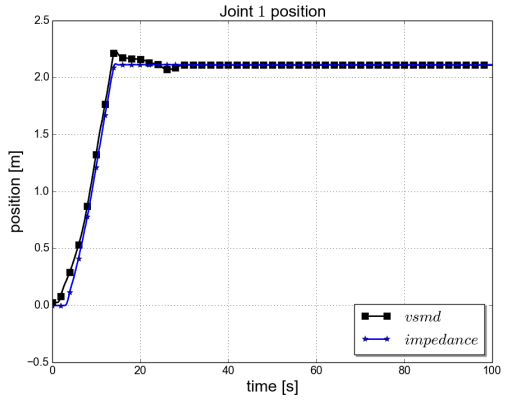

(a) Joint 1 position

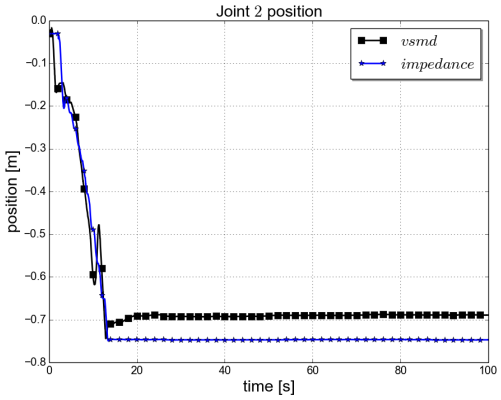

(b) Joint 2 effort

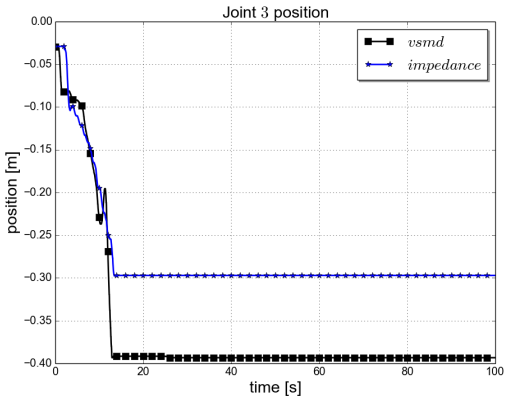

(c) Joint 3 effort

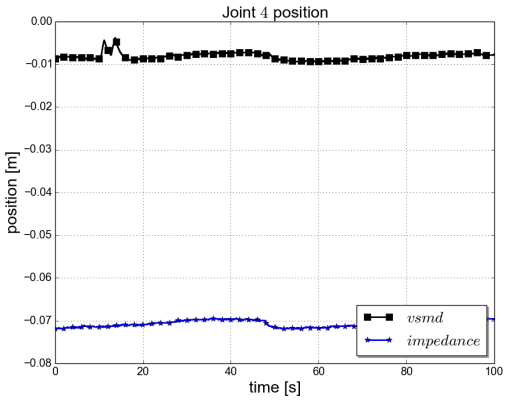

(d) Joint 4 position

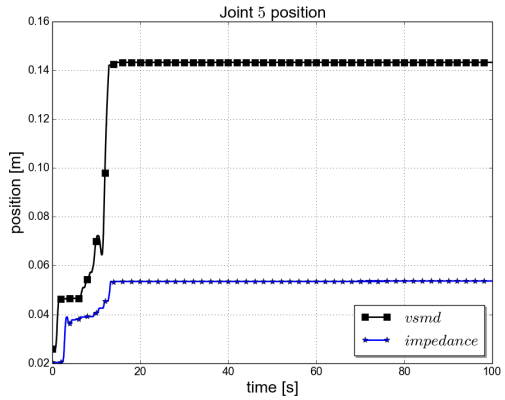

(e) Joint 5 position

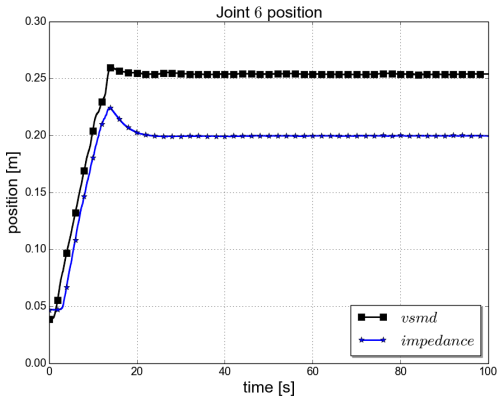

(f) Joint 6 position

Figure 6.8. Joint positions, contact with a plastic ball

6.4.2 Interaction with an aluminium plate

Another type of environment is considered to test the capabilities of the controller. In this case an aluminium plate with a width of 0.4 m and a hight of 1 m is placed at different locations in the workspace. In this case the desired end-effector location is specified as a point on the plate. In the following scenario the desired end-effector location is represented by the point placed at $(-0.22,\ -0.22,\ -0.8)$ m defined in the world coordinates. Around this point a circle with a radius of 0.3 m represents the tolerance area where the end-effector should apply a desired contact force of 10 N. The end-effector x, y and z axes behaviour

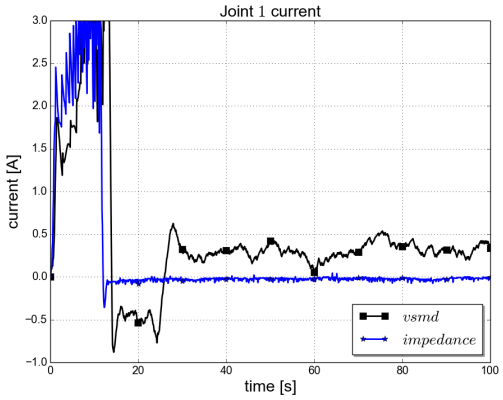

(a) Joint 1 current

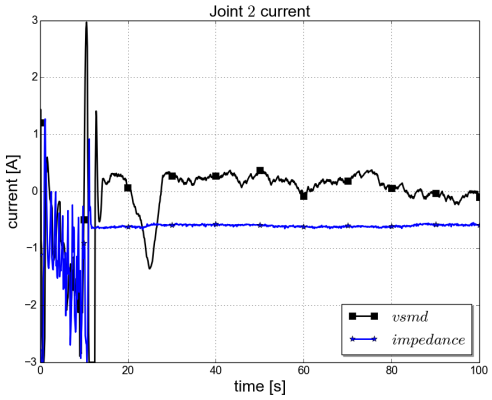

(b) Joint 2 current

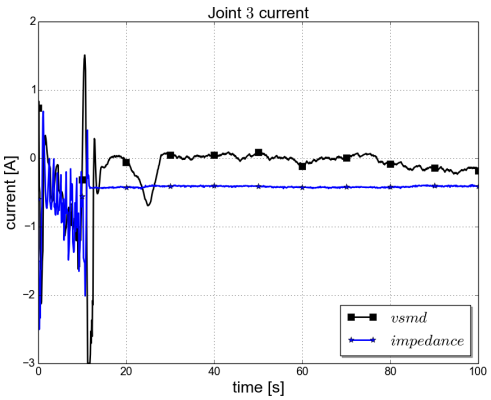

(c) Joint 3 current

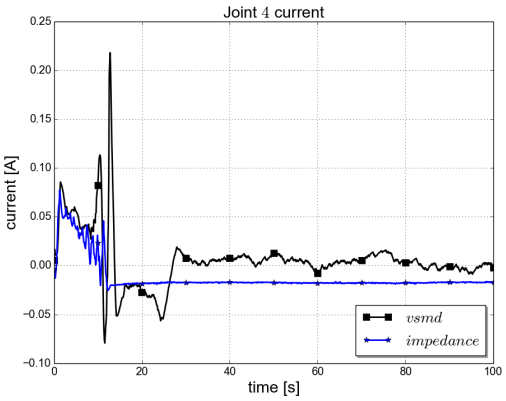

(d) Joint 4 current

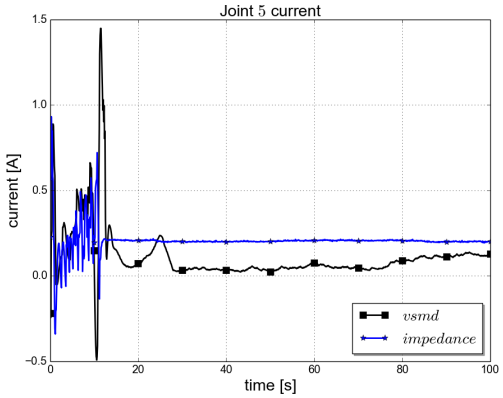

(e) Joint 5 current

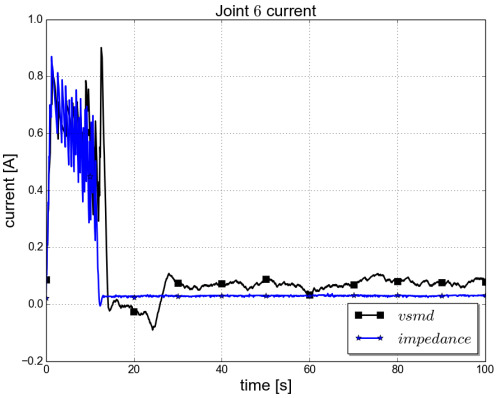

(f) Joint 6 current

Figure 6.9. Joint current commands, contact with a plastic ball

is presented in Figure 6.11. In this case the movement is more restrictive and the configuration of the arm required to reach this end-effector position is more challenging than in the previous case. In this case, the Impedance controller does not succeed in achieving the exact desired location. While for the x and y axes, the offset is small, 0.01 m, on the z axis the displacement is 0.1 m. The VSMD controller succeeds in achieving the desired location although at a very slow rate and presents overshoot for all axes, the most significant being on the x-axis. The settling time for this case is 60 seconds. The 3D behaviour of the end-effector is presented in Figure 6.12. Here it is more clear that both the Impedance

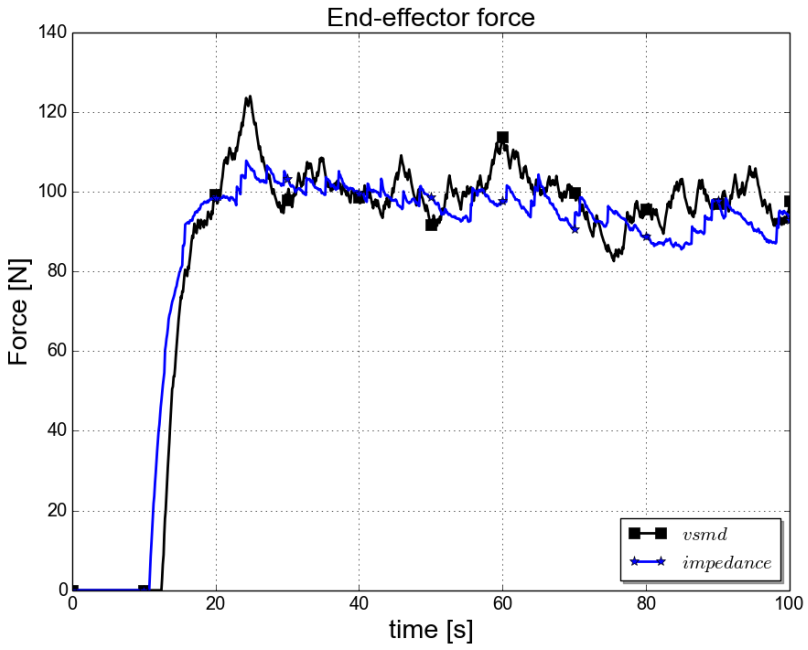

Figure 6.10. Interaction with a plastic ball

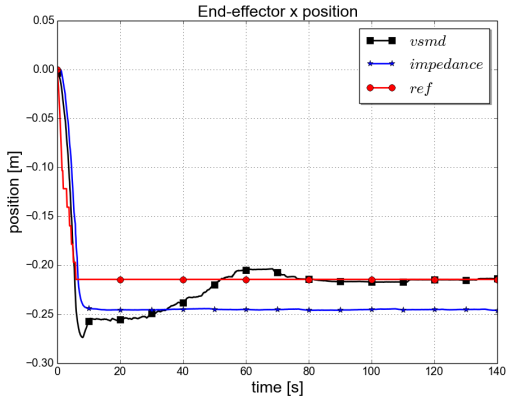

(a) x-axis trajectory

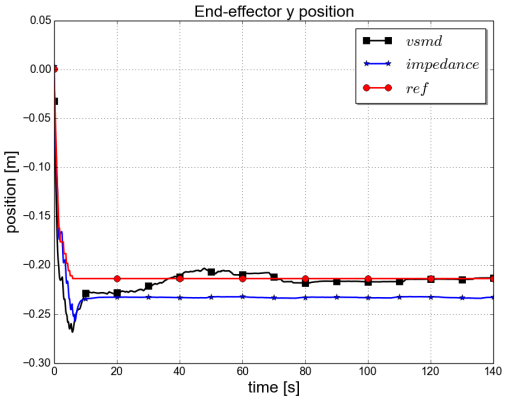

(b) y-axis trajectory

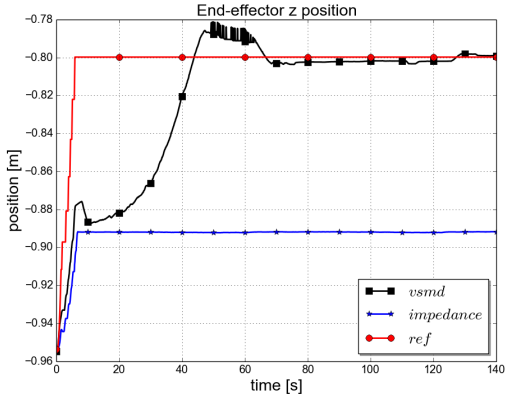

(c) z-axis trajectory

Figure 6.11. End-effector trajectory tracking, contact with an aluminium plate

and the VSMD controller have a consistent offset from the desired trajectory. The VSMD succeeds in eliminating this offset and reaches the desired position, but with an oscillatory

behaviour.

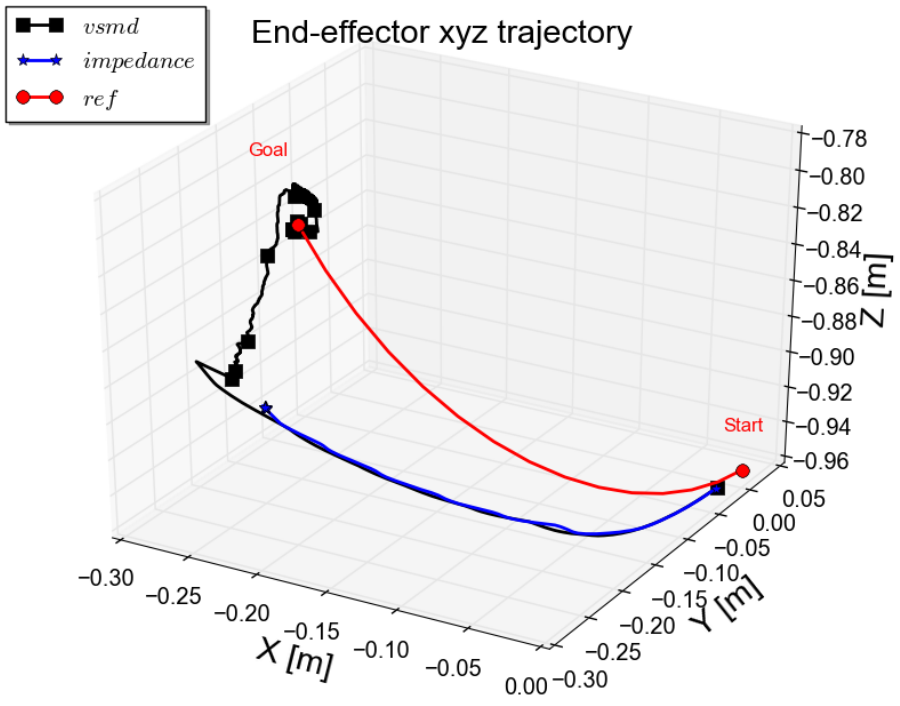

Figure 6.12. End-effector 3D trajectory, contact with an aluminium plate

In Figure 6.13 the end-effector interaction with the environment is presented. The contact force is very noisy in this case due to noisy sensor readings. The requested contact force with the environment is relatively small 10 N. A lower interaction force is requested to reduce the chances of damaging the arm, as the aluminium plate has a considerable stiffness coefficient. The force response presents an overshoot when the VSMD controller is used. This overshoot is correlated with the overshoot in the x-axis on the position response. This corresponds to the axis where the contact with the environment is under control. Moving towards the direction where the environment is placed leads to an increase in the force applied to the environment. As the desired x position is obtained, the desired end-effector force reaches the desired value. In the case of the Impedance controller a small offset in the contact force is observed. This is not eliminated as the force is controlled through the position errors, and as presented in Figure 6.11a, the error in the x-axis does not reach zero. Even without reaching the exact end-effector desired position, as the end-effector is in the tolerance area around the desired position, the interaction with the environment takes place. Similar comments as in the case of the interaction with the ball can be made for the joint position behaviour and the current commanded to the joints and is not repeated in this part.

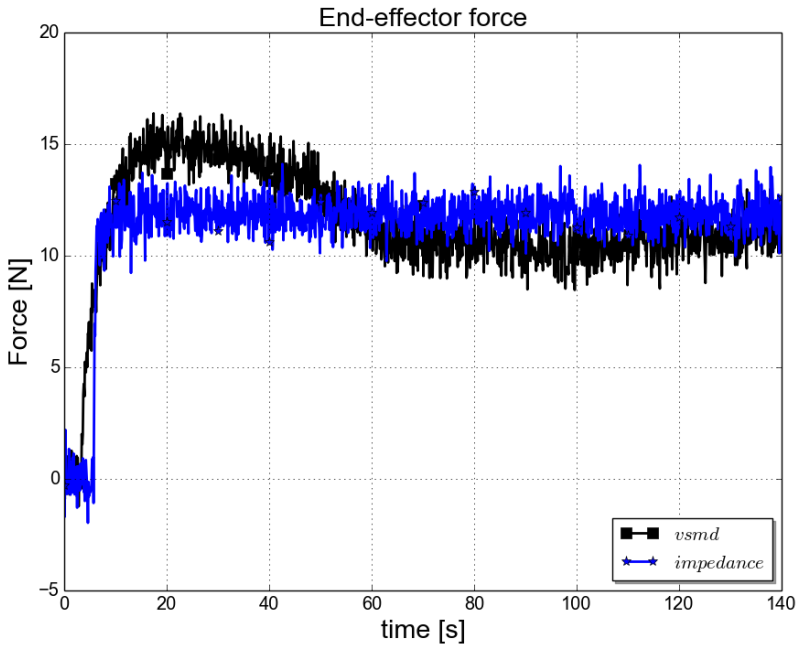

Figure 6.13. Interaction with an aluminium plate

6.4.3 Discussion

The tracking performance of the two controllers implemented on the HDT-MK3-M manipulator is analysed based on the generalized root mean-square error (GRMS), the peak tracking error and the lowest tracking error. A set of 20 different end-effector goals are used to compute the tracking performances of the controllers. For half of these goals the contact between the end-effector and the plastic ball is required. For the other half of the goals, the interaction takes place between the end-effector and the aluminium plate. Different desired interactions are requested for the goals, ranging from 1 N up to 100 N.

From Table 6.2, observing the experimental results it can be seen that the errors for the Impedance and the VSMD controller are similar. For the position errors, the peak tracking error is larger when using the Impedance controller but the lowest tracking error is similar using any of the two cases. The position error has a wider variation when using the Impedance controller while the position error when using the VSMD controller is always similar. It can be seen that the GRMS error is similar in both cases. Similar comments can be made regarding the force errors. The GRMS error is slightly higher for the case when the Impedance controller is used. The peak error is also higher for the Impedance controller, but the lowest error is obtained in this case. The variation between the peak and low errors is smaller for the VSMD controller.

From the tracking error analysis and based on the experimental results presented previously it can be concluded that both controllers perform similarly. Using an inaccurate dynamic model in the controller structure can introduce small torques to the system in order to compensate for false forces created by the model. Nevertheless, the VSMD controller is advantageous in this case as the inaccuracies in the model are handled by the sliding

Method	Position errors			Force errors		
	e_{GRMS} (m)	e_{peak} (m)	e_{low} (m)	e_{GRMS} (N)	e_{peak} (N)	e_{low} (N)
Impedance	0.06	0.1	0.04	2.58	4.02	0.76
VSMD	0.05	0.06	0.04	2.08	3.26	1.33

Table 6.2. Performance errors for position/force control of manipulator

mode component of the controller. The Impedance controller is advantageous as it doesn't require the force information and it is not included in the controller design. Not having an end-effector force sensor and using an approximation of the force can cause difficulties in obtaining the desired force tracking. The main source of disturbances in this case is represented by the noisy joint sensor readings and the use of the Jacobian to compute the end-effector force.

During the experimental testing, it was observed that tuning the operational-space controllers can be challenging. The controller output is mapped from operational space to joint space, making the current commands sent to the joints dependent on the arm configuration. In this case, although the tuning of the parameters at end-effector level is appropriate, when transformed to joint level this might lead to overshoot or not achieving zero steady-state error. Furthermore, in some specific cases the final goal is not possible to be reached due to the configuration of the manipulator.

In Figure 6.14 one of these goals is represented. The reference value is represented by the final goal to highlight the importance of using a trajectory tracking scheme for the operational space controllers. The final goal represents a valid position for the end-effector. Nonetheless, due to the nonlinearities in the manipulator Jacobian used to compute the joint torques that leads to the desired position, the end-effector remains stranded near a singular configuration. In this case any of the two tested controllers is not able to recover from this configuration and reach the desired goal. Both controllers cause the end-effector to be in a similar position. The difference in the x-axis between the desired location and current location of the end-effector is approximately 0.07 m, while the distance in the z-axis the difference is about 0.25 m. A better understanding of the robot behaviour is presented in Figure 6.15 where the 3D representation of the end-effector movement is shown. It can be concluded that for obtaining reliable results using operational space controllers the desired path of the end-effector has to be set and validated to not put the arm in a singular configuration or close to the joint limits.

6.5 Summary

In this chapter the experimental evaluation of the Variable Structure Model Dynamic Controller is presented in comparison to the Impedance Controller. The VSMD controller was tested for the first time on an underwater manipulator. The mathematical structure of the VSMD Controller is detailed in Chapter 5 and here a brief overview of the mathematical

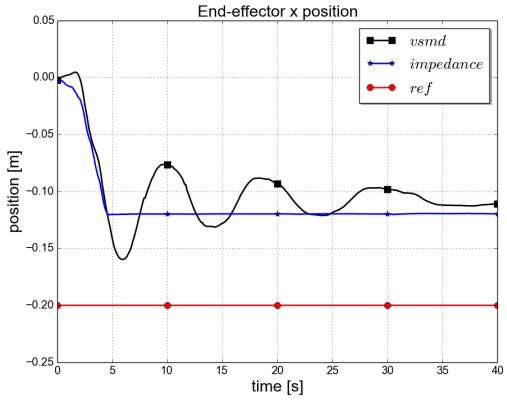

(a) x-axis trajectory

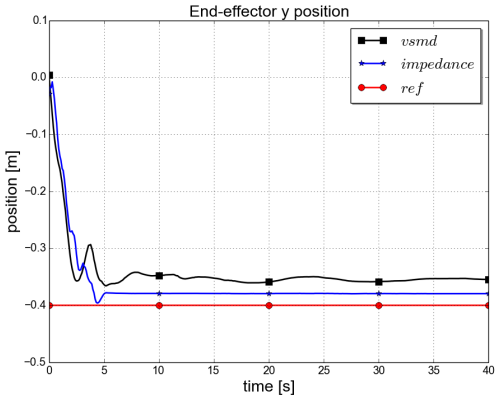

(b) y-axis trajectory

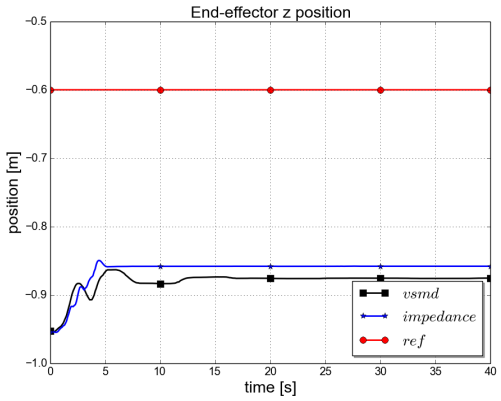

(c) z-axis trajectory

Figure 6.14. End-effector trajectory tracking, goal is out of reach

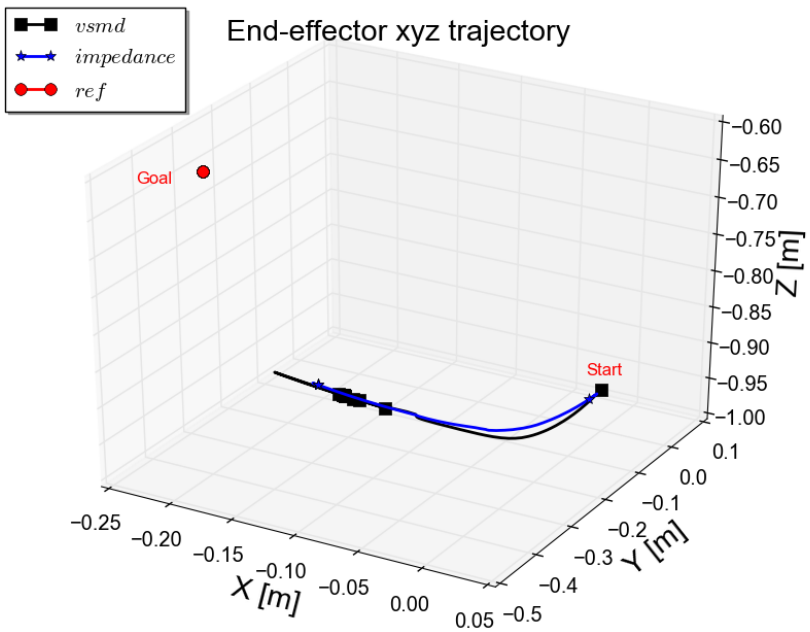

Figure 6.15. End-effector 3D trajectory, goal is out of reach

equations is performed. The interaction force between the end-effector and the environment is approximated based on the joint sensor information and the manipulator Jacobian. A detailed description of the robotic manipulator used is further presented. The experimental results show that the VSMD controller produces comparable results to the Impedance controller. Using appropriate trajectory generation for the end-effector, the desired goal is reached and the contact with the environment is maintained.

Chapter 7

Adaptive tuning for vehicle control

The lightweight underwater vehicle-manipulator system discussed in this thesis consists of an autonomous underwater vehicle (AUV) and an underwater manipulator. In Chapter 5 a decoupled strategy was presented for the position/force control of the underwater vehicle-manipulator system. The structure consisted of a separate control structure for the vehicle and a different control law for the manipulator. In this chapter the vehicle control law is experimentally evaluated. Furthermore, a new tuning algorithm is proposed for that specific control architecture. The algorithm is based on the adaptive interaction theory and the mathematical model of the vehicle.

For underwater vehicles, the design of the control structure is normally done for specific configurations without considering that different tasks may require changes in the payload of the vehicle. For example, the addition of an underwater arm is used for an intervention task or a pan and tilt unit with a state-of-the-art sonar is used for inspection purposes. To compensate for these changes, the control law has to be re-tuned every time the payload is modified. Furthermore, manually tuned control laws may produce large power consumption that leads to a decrease of the battery life span. In practice it is common to tune the control structure taking into account the worst case scenarios. This leads to sub-optimal control of the vehicle.

One other aspect that is disregarded in the design of the control structure for underwater vehicles is the coupling between the degrees-of-freedom of the system. When underwater vehicles are designed an aim is to reduce the number of thrusters used. This leads to a highly coupled system. Using classical controllers with standard tuning for these systems may lead to not obtain the appropriate behaviour from the vehicle.

To avoid sub-optimal control of the vehicle or failure of the mission and to maintain the simple structure of the classical control law, adaptive tuning may represent a valid solution. In this chapter this strategy is investigated and tested on a 5 degrees-of-freedom vehicle. In Section 7.1 the adaptive interaction theory is presented, followed by the description of the adaptive tuning algorithm for Proportional Integral Limited control in Section 7.2. The experimental results for this strategy and for the control law presented in Chapter 5 are analysed in Section 7.3.

7.1 Adaptive interaction theory

Adaptive interaction theory was first introduced in [147]. The method is equivalent to the gradient descendent algorithm and it is part of the class of optimization algorithms. The main characteristic of the adaptive interaction is the decomposition of complex systems into devices or subsystems and the representation of the interactions between these subsystems. The devices are modelled based on a general mapping between its inputs and outputs, allowing for this theory to be used in a similar way for both linear and nonlinear systems. The interaction between subsystems is described by a connection weight. This connection weight is computed based on the information from the neighbouring systems. The adaptive interaction theory results in an expression for the computation of the connection weights.

The theory of adaptive tuning has been used in [148] for system identification and control. This paper highlights the advantages of adaptive interaction theory for control purposes:

- simple structure,
- no information about the system is required,
- can be used for linear and nonlinear systems,
- no human interaction needed,
- after the system converges, stability is ensured.

In [149] it is demonstrated that the algorithm is equivalent to the backpropagation method that represents the standard strategy to train artificial neural networks. In [150] it is shown how adaptive interaction theory is used in a neural network controller. The method is advantageous as it reduces the complexity of the problem and the errors of the system.

A short overview of adaptive interaction theory [147] is presented in this section. A complex system can be decomposed into N subsystems, called devices. Each subsystem $n = \overline{1,N}$ is characterised by an input x_n and an output signal y_n. Both the input and output signals are defined to be integrable. Each device is described by a single input and single output. Each subsystem n is characterised by a causal function:

$$F_n : X_n \to Y_n, \quad n \in N \tag{7.1}$$

where X_n is the input space and Y_n is the output space. The functional F_n is called causal as the output depends only on the previous history of the input. The relation between the input and output of the device is described by Equation (7.2).

$$y_n(t) = (F_n \circ x_n)(t) = F_n[x_n(t)], \quad n \in N \tag{7.2}$$

where $\circ$ is the composition operator and $F_n[x]$ has a Fréchet derivative $F_n^{'}[x]$ [151] defined by Equation (7.3) and represents a generalization of the total derivative dependent of a

single real variable to the case multiple real variables are used to define the function.

$$\lim_{\|\Delta\|\to 0} \frac{\| F_n[x+\Delta]F_n[x] - F_n^{'}[x] \circ \Delta \|}{\| \Delta \|} = 0 \tag{7.3}$$

The interaction between subsystems is represented by an expression dependent on the output of one of the subsystems and the input of the other subsystem. This represents the information carrying connection $c \in C$. Each interaction is defined by a single connection information. For a device n, the set of input connections is defined as $I_n = \{c : prec_c = n\}$ and the set of output connections is $O_n = \{c : post_c = n\}$, where $prec_c$ is the device whose output is carried by c and $post_c$ is the device whose input is carried by c.

The theory of adaptive interaction considers the case when the input of a device is a linear combination of the set of outputs of the connected devices, defined by Equation (7.4).

$$x_n(t) = u_n(t) + \sum_{c \in I_n} \alpha_c y_{prec_c}(t), \quad n \in N \tag{7.4}$$

where $u_n(t)$ is an external input signal and α_c is the connection weight. Inserting this into Equation (7.2) the dynamics are expressed through Equation (7.5).

$$y_n = F_n \left[u_n(t) + \sum_{c \in I_n} \alpha_c y_{prec_c}(t) \right], \quad n \in N \tag{7.5}$$

The aim of the adaptive interaction theory is to minimize a performance index E by means of computing the best connection weights α_c. The performance index is a function dependent on the external inputs and outputs of the system. The performance index is defined dependent of the goal of the application and can be for example the error in position or the error in velocity.

In [147] the computation of the connection weights to achieve this goal is given according to the following theorem:

Theorem 1 *For the system with dynamics given by*

$$y_n = F_n[x_n] = F_n \left[u_n + \sum_{c \in I_n} \alpha_c y_{prec_c} \right], \quad n \in N$$

if connections weights α_c are adapted according to

$$\dot{\alpha_c} = \left(\sum_{s \in O_{post_c}} \frac{\frac{dE}{dy_{post_s}} \circ F^{'}_{post_s}[x_{post_s}]}{\frac{dE}{dy_{post_s}} \circ F^{'}_{post_s}[x_{post_s}] \circ y_{prec_c}} \alpha_s \dot{\alpha}_s - \gamma \frac{\partial E}{\partial y_{post_c}} \right) \circ F^{'}_{post_c}[x_{post_c}] \circ y_{prec_c}, \quad c \in C \tag{7.6}$$

and the above equation has a unique solution, then the performance index E will decrease monotonically with time. In fact, the following is always satisfied:

$$\dot{\alpha_c} = -\gamma \frac{\partial E}{\partial \alpha_c}, \quad c \in C \tag{7.7}$$

where $\gamma > 0$ is the adaption coefficient, F is the Fréchet derivative, x and y are the input and output of the subsystem and $\circ$ represents the mathematical composition function.

Proof To validate the theorem it has to be demonstrated that Equation (7.7) satisfies Equation (7.6). It can be seen that Equation (7.6) has a unique solution. Furthermore, E is a functional of y_n and the derivative of E with respect to α_c can be expressed as:

$$\begin{aligned} \frac{dE}{d\alpha_c} &= \frac{dE}{dy_{post_c}} \circ \frac{dy_{post_c}}{dx_{post_c}} \circ \frac{dx_{post_c}}{d\alpha_c} \Leftrightarrow \\ \Leftrightarrow \frac{dE}{d\alpha_c} &= \frac{dE}{dy_{post_c}} \circ \frac{dy_{post_c}}{dx_{post_c}} \circ y_{prec_c} \Leftrightarrow \\ \Leftrightarrow \frac{dE}{d\alpha_c} &= \frac{dE}{dy_{post_c}} \circ F'_{post_c}[x_{post_c}] \circ y_{prec_c} \end{aligned} \tag{7.8}$$

Considering that:

$$\begin{aligned} \frac{dE}{dy_n} &= \frac{\partial E}{\partial y_n} + \sum_{c \in O_n} \frac{dE}{dy_{post_c}} \circ \frac{dy_{post_c}}{dy_n} \Leftrightarrow \\ \Leftrightarrow \frac{dE}{dy_n} &= \frac{\partial E}{\partial y_n} + \sum_{c \in O_n} \alpha_c \frac{dE}{dy_{post_c}} \circ F'_{post_c}[x_{post_c}] \end{aligned} \tag{7.9}$$

Inserting Equation (7.8) in Equation (7.9):

$$\frac{dE}{dy_n} = \frac{\partial E}{\partial y_n} + \sum_{c \in O_n} \alpha_c \frac{dE}{d\alpha_c} \frac{\frac{dE}{dy_{post_c}} \circ F'_{post_c}[x_{post_c}]}{\frac{dE}{dy_{post_c}} \circ F'_{post_c}[x_{post_c}] \circ y_{prec_c}} \tag{7.10}$$

By using Equation (7.7) to substitute $\frac{dE}{dy_n}$, Equation (7.10) can be re-written as:

$$\begin{aligned} \frac{dE}{dy_n} &= \frac{\partial E}{\partial y_n} + \sum_{c \in O_n} \alpha_c \left(-\frac{\dot{\alpha_c}}{\gamma} \right) \frac{\frac{dE}{dy_{post_c}} \circ F'_{post_c}[x_{post_c}]}{\frac{dE}{dy_{post_c}} \circ F'_{post_c}[x_{post_c}] \circ y_{prec_c}} \Leftrightarrow \\ \frac{dE}{dy_n} &= \frac{\partial E}{\partial y_n} - \frac{1}{\gamma} \sum_{c \in O_n} \alpha_c \dot{\alpha_c} \frac{\frac{dE}{dy_{post_c}} \circ F'_{post_c}[x_{post_c}]}{\frac{dE}{dy_{post_c}} \circ F'_{post_c}[x_{post_c}] \circ y_{prec_c}} \end{aligned} \tag{7.11}$$

Inserting Equation (7.8) into Equation (7.7):

$$\dot{\alpha_c} = -\gamma \frac{dE}{dy_{post_c}} \circ F'_{post_c}[x_{post_c}] \circ y_{prec_c} \tag{7.12}$$

Now inserting Equation (7.11) into Equation (7.12), this can be expressed as:

$$\dot{\alpha_c} = -\gamma \left(\frac{\partial E}{\partial y_{post_c}} - \frac{1}{\gamma} \sum_{s \in O_{post}} \alpha_s \dot{\alpha}_s \frac{\frac{dE}{dy_{post_s}} \circ F'_{post_s}[x_{post_s}]}{\frac{dE}{dy_{post_s}} \circ F'_{post_s}[x_{post_s}] \circ y_{prec_s}} \right) \circ F'_{post_c}[x_{post_c}] \circ y_{prec_c} \tag{7.13}$$

Simplifying this leads to:

$$\dot{\alpha_c} = \left(\sum_{s \in O_{post_c}} \alpha_s \dot{\alpha}_s \frac{\frac{dE}{dy_{post_s}} \circ F'_{post_s}[x_{post_s}]}{\frac{dE}{dy_{post_s}} \circ F'_{post_s}[x_{post_s}] \circ y_{prec_s}} - \gamma \frac{\partial E}{\partial y_{post_c}} \right) \circ F'_{post_c}[x_{post_c}] \circ y_{prec_c}, \quad c \in C \tag{7.14}$$

Due to the equality $y_{post_c} = y_{prec_s}$ Equation (7.14) becomes:

$$\dot{\alpha_c} = \left(\sum_{s \in O_{post_c}} \alpha_s \dot{\alpha}_s \frac{\frac{dE}{dy_{post_s}} \circ F'_{post_s}[x_{post_s}]}{\frac{dE}{dy_{post_s}} \circ F'_{post_s}[x_{post_s}] \circ y_{post_c}} - \gamma \frac{\partial E}{\partial y_{post_c}} \right) \circ F'_{post_c}[x_{post_c}] \circ y_{prec_c}, \quad c \in C \tag{7.15}$$

Based on Equation (7.15) it can be stated that Equation (7.7) is the unique solution of Equation (7.6). The adaptive theory can be applied to any type of system that can be decomposed into devices and where a relationship between the input and output of each device can be formulated [147].

7.2 Problem statement

The goal of this chapter is to obtain a control system for an autonomous underwater vehicle that is robust to changes in the system configuration and to underwater disturbances. It is desired that a simple control structure can be used that does not have high computational requirements. The use of adaptive interaction theory is a valid solution to this problem.

In this section an adaptive tuning for the PILIM (Proportional Integral Limited) controller is proposed. The controller can be implemented on any type of underwater vehicle. The adaption rule is applied for a cascaded controller including a control loop for the position compensation and another control loop for the velocity compensation. It is shown that the proposed structure with adaptive tuning is advantageous due to its simple configuration, energy efficiency and fast convergence. In the following section the dynamic structure of the underwater vehicle is presented and a detailed description of the adaption rule is presented.

7.2.1 System description

The mathematical model used to describe an autonomous underwater vehicle is presented in Equation (7.16). The model represents the closed-loop representation of the system. To

develop this model the Newton-Euler formulation can be used as presented in [21].

$$\begin{aligned} M(\nu)\dot{\nu} + C(\nu)\nu + D(\nu)\nu + g(\eta) &= \tau_F \\ \dot{\eta} &= J(\eta)\nu \end{aligned} \tag{7.16}$$

where $\nu \in \mathbb{R}^6$ is the body-fixed velocity, $J(\eta) \in \mathbb{R}^{6\times6}$ is the Jacobian transformation matrix relating the AUV coordinate system to the earth-fixed coordinate system. $M \in \mathbb{R}^{6\times6}$ is a symmetric positive definite inertia matrix containing the rigid body terms as well as the added mass terms, $C \in \mathbb{R}^{6\times6}$ is the matrix of Coriolis and centripetal terms, $D \in \mathbb{R}^{6\times6}$ is the matrix of hydrodynamic damping terms, $g(\eta) \in \mathbb{R}^6$ represents the vector of restoring forces and moments and $\tau_F \in \mathbb{R}^6$ are the requested forces.

7.2.2 Adaptive tuning for the PILIM controller

The controller used in this chapter for the underwater vehicle is the PILIM compensator which has been used previously in Chapter 4. The PILIM formulation represents a decoupled control structure for an underwater vehicle. For each degree-of-freedom, a separate PILIM controller is used, assuming that each degree-of-freedom is independent. In practice the underwater vehicle represents a coupled system and the coupling forces influence the tuning of the controllers. The adaptive interaction theory aims to solve this tuning problem.

The tuning of the PILIM control law uses an online approach that changes the parameters of the controller based on the changes in the system. The tuning of the gains uses the adaptive interaction theory where the first step is to decompose a complex system into its constituent components.

The underwater vehicle model together with the control structure, presented in Figure 7.1 can be decomposed into four subsystems. Each of these subsystems $i \in \overline{1,4}$ is marked in the structure of the PILIM controller.

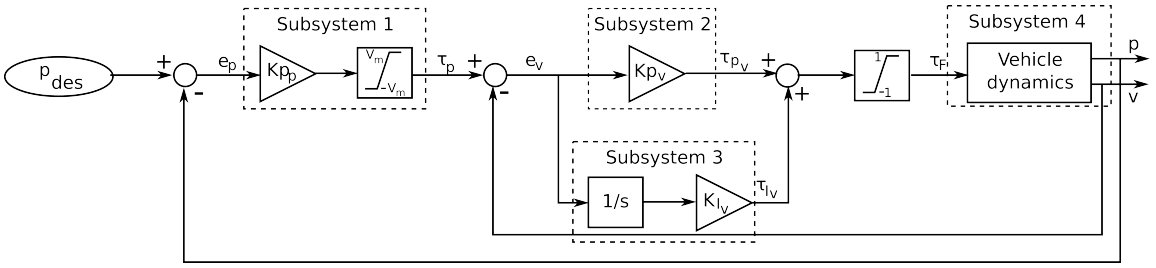

Figure 7.1. Closed-loop structure showing PILIM structure and subsystems representation

The next step for using the adaptive theory is to represent the inputs and outputs of each subsystem. According to the system configuration, Figure 7.1, the following notations can be made: the input for Subsystem 1 (the position controller) is the error in position e_p and the output is the quasi-velocity generated by the position controller τ_p. For the velocity controller, the output for the proportional component (Subsystem 2) is τ_{P_v} describing the force generated by this component and the input is e_v representing the velocity error. For

the integral part of the velocity controller (Subsystem 3) the output is the corresponding force τ_{I_v} and the input is e_v, the velocity error. The output of the fourth subsystem (the model of the vehicle) is the measured acceleration a of the vehicle and the input τ_F is the total output of the PILIM controller. The gains of the controller represent the connections between subsystems and are marked as $\alpha_c = \{K_{P_p}, K_{P_v}, K_{I_v}\}$.

For each of the four subsystems the predecessors are marked with $prec_c$ where c is the connection and the posteriors are marked with $post_c$. The set of input connections for subsystem i is marked with I_i and the set of output connections is represented by O_i. All the connections represent the relation between the predecessors/posteriors of the subsystem and the subsystem itself without any other influences.

Further notations have to be made to represent the adaptive theory for a PILIM controller:

1. Position controller:

   - $post_c = \{\texttt{Subsystem 2}, \texttt{Subsystem3}\}$ consists of the proportional part of the velocity controller and the integral part of the velocity controller. This is because the output of the position controller is input in the two components of the velocity controllers.
   - $O_{post_c} = \emptyset$ is empty. This is because the elements in $post_c$ are not direct inputs to the next subsystem, the dynamic model, but a relationship between them represents the input to the next system.

2. Velocity controller:

   - $post_c = \{\texttt{Subsystem 4}\}$ consists of the dynamic model of the system. This is because the output of the velocity controller is input in the dynamic model.
   - $O_{post_c} = \emptyset$ is empty. This is because the output of $post_c$ is the acceleration and is not a direct input to the position and velocity controllers, but the relationship between this and the desired behaviour of the system represents the input.

Starting with the assumption that the four subsystems connected together replicate a functional AUV, the goal is to compute the connection weights α_c that leads to achieving the desired tasks with the best behaviour possible. As α_c is the set of the gains of the system, the goal can be reformulated as the computation of the best controller gains at each moment in time for the period of the task. According to adaption theory this is a minimization problem where the performance index E is defined according to Equation (7.17). In this case two performance indices are defined to evaluate the cascade structure of the PILIM. The goal is to optimize both the position tracking performance and the velocity tracking performance.

$$\begin{aligned} E_p &= (p_{des} - p)^2 = e_p^2 \\ E_v &= (\tau_p - v)^2 = e_v^2 \end{aligned} \tag{7.17}$$

where E_p is the performance index for the position controller and E_v is the one for the velocity controller.

For the PILIM structure the sets of output connections are empty and this leads to Equation (7.6) in **Theorem 1** to be reformulated as:

$$\dot{\alpha}_c = -\gamma \frac{\partial E}{\partial y_{post_c}} \circ F'_{post_c}[x_{post_c}] \circ y_{prec_c} \tag{7.18}$$

Based on the notations used to define the output and input connection sets, Equation (7.18) used in the computation of PILIM controller gains is defined by Equation (7.19).

$$\begin{aligned} \dot{K}_{P_p} &= -\gamma \frac{\partial (p_{des} - p)^2}{\partial p} \circ F'_p[\tau_F] \circ \tau_p \\ \dot{K}_{P_v} &= -\gamma \frac{\partial (\tau_p - v)^2}{\partial v} \circ F'_v[\tau_F] \circ \tau_{P_v} \\ \dot{K}_{I_v} &= -\gamma \frac{\partial (\tau_p - v)^2}{\partial v} \circ F'_v[\tau_F] \circ \tau_{I_v} \end{aligned} \tag{7.19}$$

where $F'_p[\tau_F]$ and $F'_v[\tau_F]$ represent the Jacobians of the relationships between the position and total control effort generated by the controllers ($F_p[\tau_F]$) and the velocity and total control effort generated by the controllers ($F_v[\tau_F]$) defined as:

$$\begin{aligned} F_v[\tau_F] = \int_0^t \left(M(v)^{-1} \left(\tau_F - C(v)v - D(v)v - g(\eta) \right) \right) d\tau \\ F_p[\tau_F] = \int_0^t F_v[\tau_F] d\tau \end{aligned} \tag{7.20}$$

It can be seen that E_p, E_v, $F_v[\tau_F]$ and $F_p[\tau_F]$ are the instantaneous values and due to this the composition $\circ$ can be replaced by the multiplications as presented in Equation (7.21).

$$\begin{aligned} \dot{K}_{P_p} &= -\gamma \frac{\partial (p_{des} - p)^2}{\partial p} F'_p[\tau_F] \tau_p \\ \dot{K}_{P_v} &= -\gamma \frac{\partial (\tau_p - v)^2}{\partial v} F'_v[\tau_F] \tau_{P_v} \\ \dot{K}_{I_v} &= -\gamma \frac{\partial (\tau_p - v)^2}{\partial v} F'_v[\tau_F] \tau_{I_v} \end{aligned} \tag{7.21}$$

The on-line tuning gains of the PILIM controller are computed at every time step according to Equation (7.22).

$$\begin{aligned} K_{P_p} &= 2\gamma \int_0^t (e_p F'_p[\tau_F] \tau_p) d\tau \\ K_{P_v} &= 2\gamma \int_0^t (e_v F'_v[\tau_F] \tau_{P_v}) d\tau \\ K_{I_v} &= 2\gamma \int_0^t (e_v F'_v[\tau_F] \tau_{I_v}) d\tau \end{aligned} \tag{7.22}$$

7.3 Experimental results

In this section the proposed control strategy using the PILIM controller is experimentally evaluated using the Nessie VII AUV, Figure 7.2. It is a hover-capable autonomous underwater vehicle developed in the Ocean Systems Laboratory. Nessie VII has a cylindrical aluminium pressure hull surrounded by a polymer frame that creates its skeleton. On this skeleton the sensors, actuators and the PVC shell are mounted. The sensors of the vehicle are a Doppler Velocity Log (DVL), a forward looking sonar, four video cameras, a temperature sensor, a pressure sensor, a GPS, a compass and a fibre optic gyroscope. The vehicle state and essential information for the control architecture are provided by these sensors.

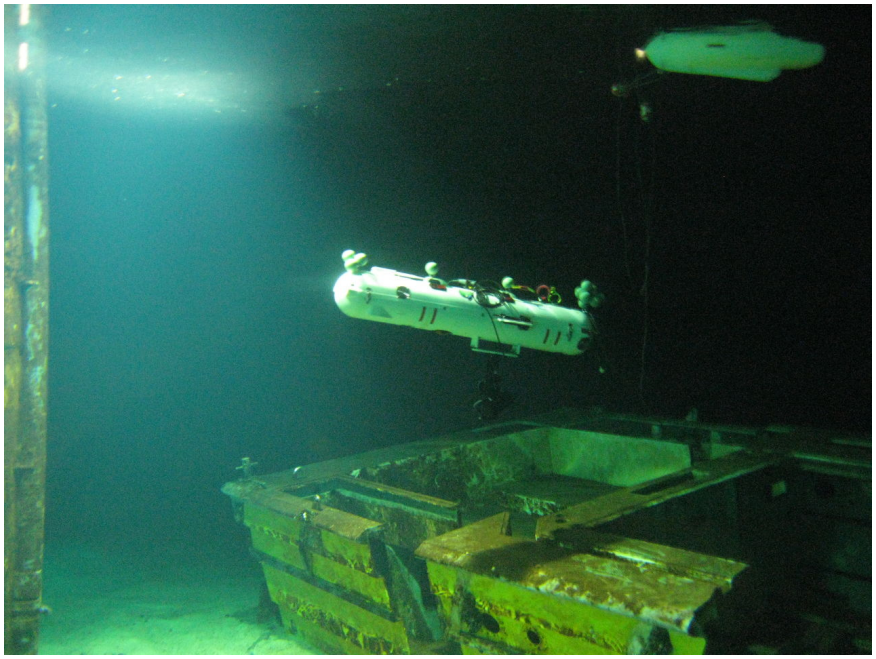

Figure 7.2. Nessie VII AUV during an inspection task

The vehicle has four Li-Ion batteries generating 2.2 kWh of energy and six brushless DC thrusters, mounted as presented in Figure 7.3, each of them producing 250 W of power. The positioning of the thrusters creates a highly coupled system and does not allow rotation around x-axis to be controlled.

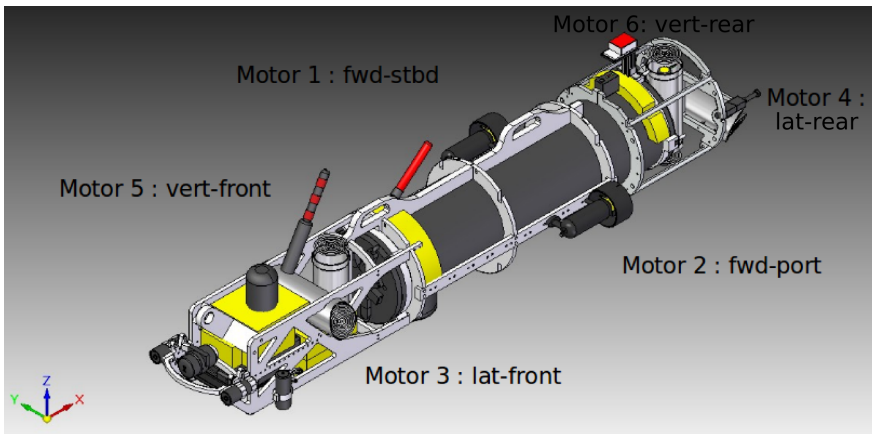

Figure 7.3. Nessie VII AUV thruster placement

The evaluation of the system is presented in comparison with the manually tuned PILIM control structure presented in Chapter 5. The system is tested in an indoor tank with the dimensions of $12 \times 10 \times 4$ m representing a controlled environment, that can be found in the William Arrol Building from the Edinburgh Campus of the Heriot-Watt University. To evaluate the performance of the two methods, different navigation modes are defined.

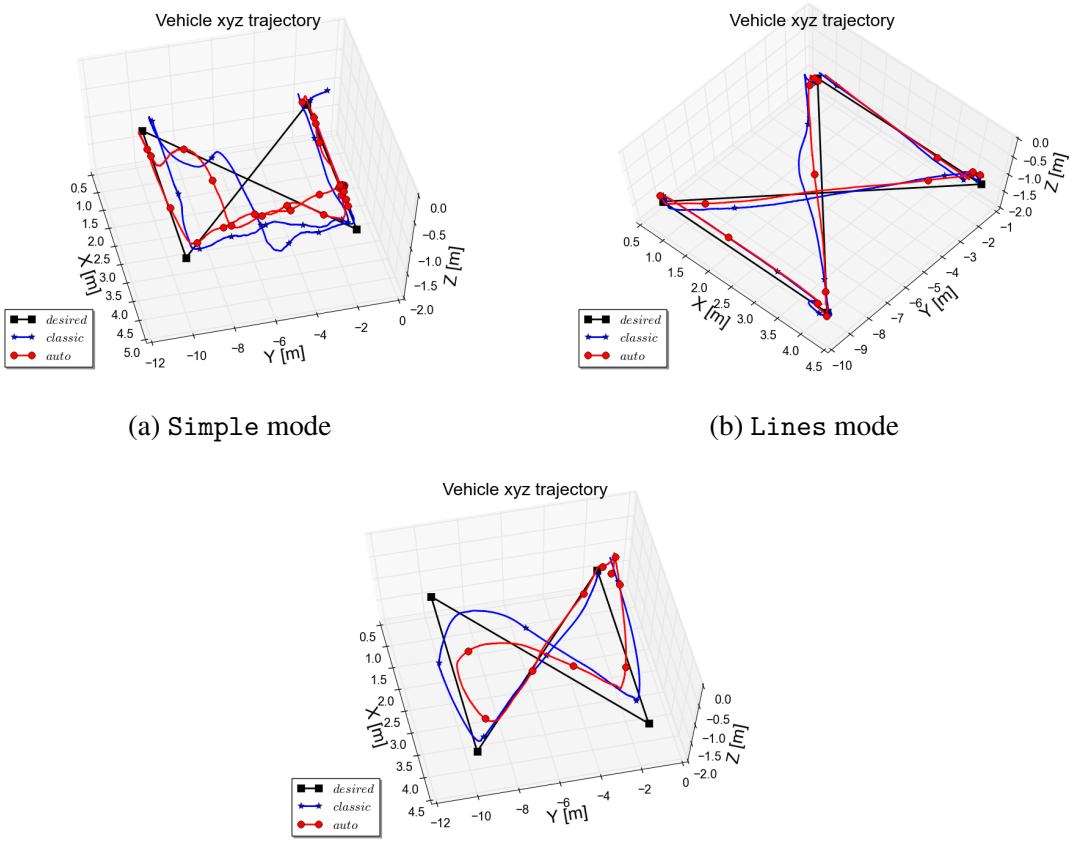

(a) `Simple` mode

(b) `Lines` mode

(c) `Fast` mode

Figure 7.4. Nessie VII AUV trajectory tracking using the three navigation modes

Using these navigation modes helps in evaluating how the control law is performing in cases when exact positioning of the system is expected or when long term navigation is desired. Different navigation strategy is expected for example in inspection scenarios and a different strategy is used when the system has to perform long missions such as long-range navigation. The navigation modes are simple methods that generate a set of waypoints for the system to follow. The modes do not consider any obstacles in the environment and do not include any collision avoidance component. The three navigation modes are referred as `simple`, `lines`, and `fast` modes. The `simple` strategy requires the vehicle to move only using its translational axes without using any of the rotational degrees-of-freedom. The second navigation mode is the `lines` strategy described by a line-of-sight approach. The vehicle is requested to visit all the waypoints, travelling using only forward navigation. This enforces an adjustment of the yaw of the vehicle to reach the next waypoint. The last mode used is the `fast` mode. In this case an intermediate waypoint is defined. This waypoint is moving at a constant velocity according to a given path. The vehicle is requested to reach

this moving waypoint. For each configuration the vehicle is required to complete a figure of eight shape trajectory shown in Figure 7.4. In this figure the results of the experimental testing are presented for all the three navigation modes. It can be observed that when using the `simple` strategy the figure of eight shape is not possible to be executed exactly, as the rotational axes are not used. Nonetheless, the corners of the trajectory are reached in the desired order. In Figure 7.4a both the adaptive PILIM controller (the red plots) and the manually tuned PILIM law (blue plot) reach the four corners in a similar fashion. When the vehicle moves using the lateral DOF the vehicle drifts slightly from moving in a straight line. This is caused due to the coupling effects of the surge, sway and yaw degrees-of-freedom. In Figure 7.4a the behaviour of the two controllers is presented for the case when the `lines` strategy is used. In this case, the figure of eight shape is perfectly replicated as the mode enforces the vehicle to exactly reach the four corners and the orientation of the vehicle is actively used in this case. The adaptive PILIM law performance is similar to the manually tuned approach. In Figure 7.4c the last strategy is used to enforce the behaviour of the system. In this case the exact trajectory is not expected to be matched as the intermediate waypoint is moved with a constant velocity in front of the vehicle. This method does not produce precise navigation, but it reduces the energy consumption due to the small amount of time required to complete a trajectory.

To evaluate the methods discussed in Section 7.1 multiple experiments are performed for all the different strategies. In all these cases a consistent behaviour of the system is observed using the manually tuned and adaptive PILIM architecture. The first set of experiments are carried out in still water, while the second group of experiments consider the effect of waves.

7.3.1 Still water results

The behaviour of the system in a controlled environment is studied in this part. The system is tested using the adaptive PILIM architecture and the manually tuned PILIM controller when the `lines` mode navigation is imposed. This mode is used to analyse the results as it restricts the behaviour of the system and produces a clear representation of the performances of the vehicle. In `lines` mode the most used DOFs are surge and yaw. The vehicle is required to adjust its orientation before navigating between consecutive waypoints.

In Figure 7.5 the position error for each degree-of-freedom of the vehicle is presented for both the adaptive PILIM and the manually tuned control. The latter scheme is the same PILIM structure presented in Figure 7.1 but in this case the control gains are fixed and tuned to give the best performance of the system. In Figure 7.5a peaks can be seen representing an error of 3.5 m in the North direction, while in Figure 7.5b an error of 8 m is visible in the East direction. This behaviour is specific for the case after the vehicle has reached the current goal. At this point the vehicle is hovering and the next navigation waypoint is requested. The error decreases from this peak error value as the vehicle moves towards the next waypoint. The characteristics of an inspection task in the `lines` mode is

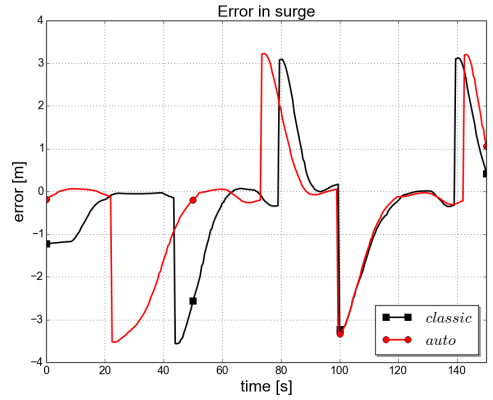

(a) Error in surge

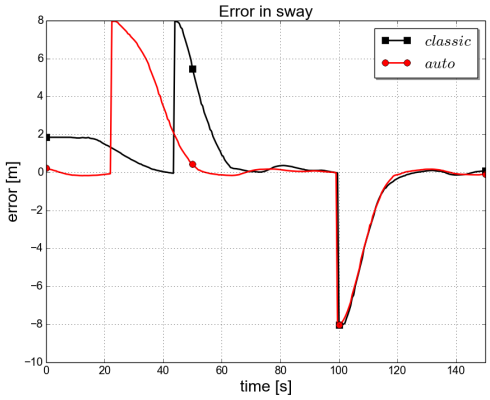

(b) Error in sway

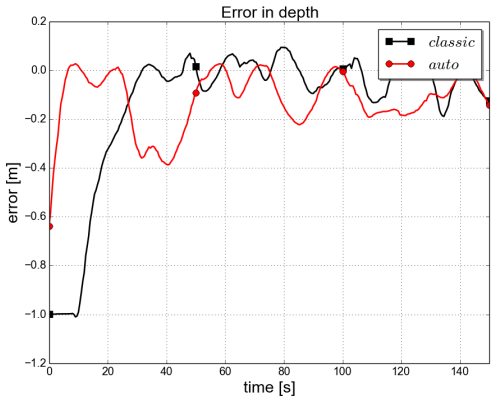

(c) Error in depth

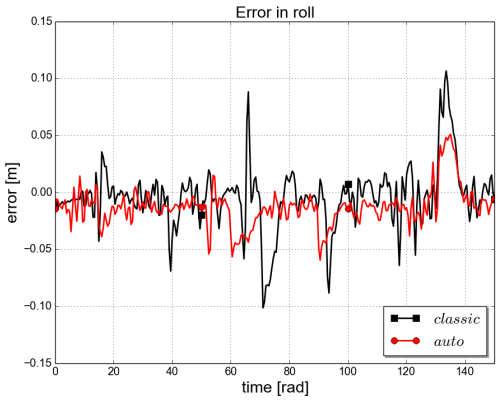

(d) Error in roll

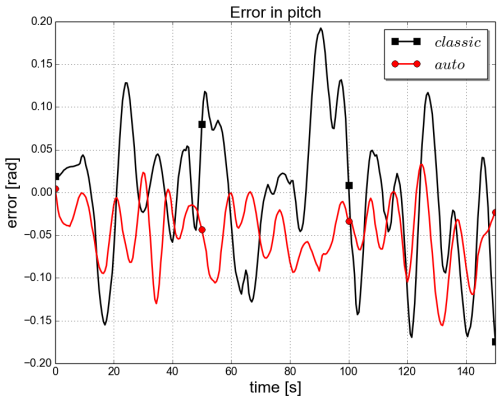

(e) Error in pitch

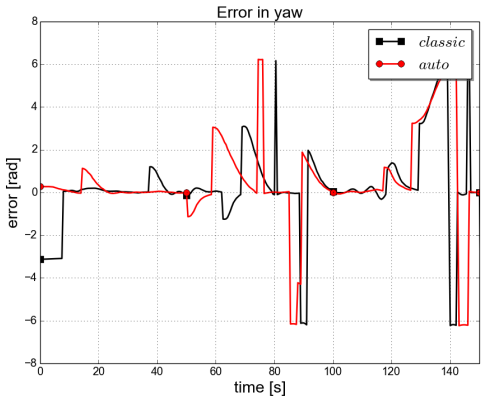

(f) Error in yaw

Figure 7.5. Position errors for vehicle DOFs in reference coordinates for lines mode

seen, especially in the yaw performance. The behaviour of this DOF is characterised by the following practice: as soon as the vehicle has reached its current goal, the system is requested to orientate towards the walls of the tank. This is visible through the yaw error ± 3.14 rad (± 180 deg) in Figure 7.5f. As the vehicle orientates itself towards the walls, the error in yaw decreases. As soon as the desired configuration has been achieved, the navigation is resumed and the following goal is requested. At this point, the vehicle has to orientate itself towards the goal that is at ± 4.72 rad (± 270 deg), represented by the error peaks. As the vehicle changes its orientation, the error decreases. From one set-

point to another the yaw error decreases in less than 10 sec. These results demonstrate

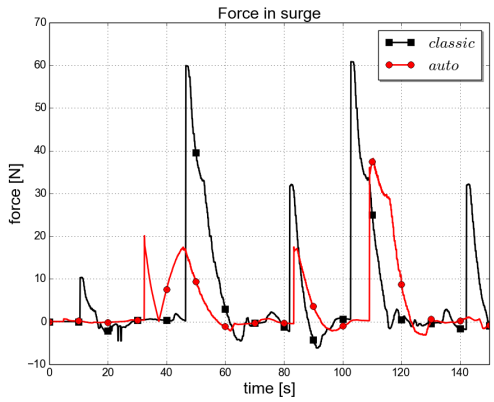

(a) Effort in surge

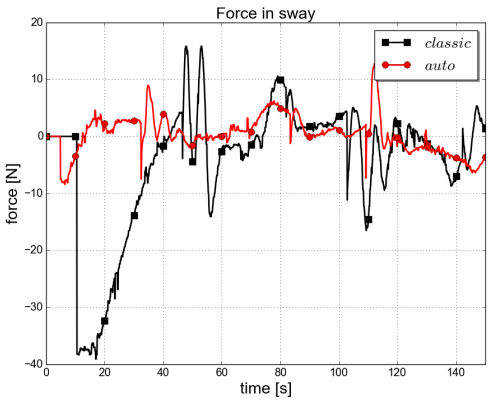

(b) Effort in sway

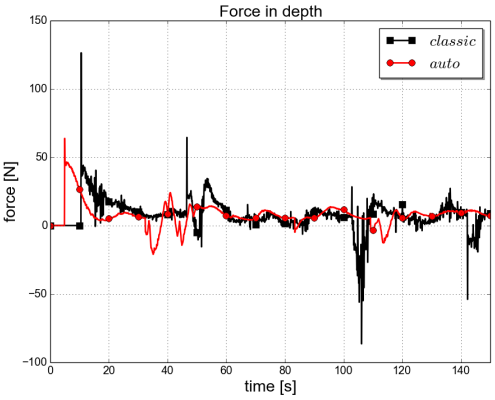

(c) Effort in depth

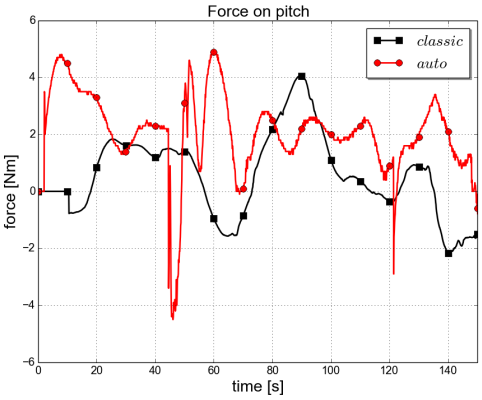

(d) Effort in pitch

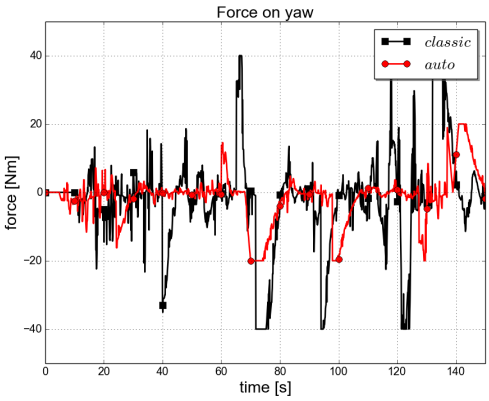

(e) Effort in yaw

Figure 7.6. Control efforts, manual vs. adaptive tuning

that the adaptive tuning method is a valid strategy that produces satisfactory results for the trajectory tracking performance of the vehicle. The method produces results that are comparable with the classical PILIM controller. Small improvements can also be observed using the adaptive tuning algorithm by reducing the coupling effects between DOFs. This aspect is highlighted in Figure 7.5d for the uncontrolled degree-of-freedom. Disturbances are still present using the adaptive tuning for roll but with a lower amplitude. For the pitch, Figure 7.5e, the amplitude is also decreased compared with the case when the classical

PILIM controller is used. The pitch represents the most challenging axis to be controlled as it is coupled to the depth axis and the surge degree-of-freedom. The reduction of the coupling effects is caused by the lower velocity of the vehicle generated when the adaptive controller is used.

The control effort that produces these results is presented in Figure 7.6. The plots show the control effort only for the controlled axes, the control effort for roll being zero in both adaptive and classical tuning. It can be observed that the forces on each degree-of-freedom is related to the type of the trajectory and the degree-of-freedom that is needed. As the surge and yaw DOFs are the most used for the `line` strategy, the applied force on those axes is significant. To compensate for the coupling effects between the DOFs the control effort on the pitch degree-of-freedom is also notable. In Figure 7.6a a new trajectory leg in the navigation corresponds to the peaks in the force request. It can be observed that the force requested in this axis is lower in the case when the adaptive tuning is used. This leads to a lower velocity of the vehicle but nonetheless the desired goals are achieved with the same accuracy as in the case when the manual tuning component is used. Similar comments can be made for most of the degrees-of-freedom of the vehicle. The only difference is represented by the pitch DOF. In this case the control effort is higher when the adaptive tuning is included in the system. This leads to a better behaviour of this DOF and the reduction of the effects of the other DOFs on it, shown in Figure 7.5e. This behaviour is generally observed for all the controlled DOFs along all the navigation trajectories.

7.3.2 The effect of wave disturbances

The wave disturbances represents one of the challenges in developing robust and stable control systems. The adaptive tuning method has the ability to provide a reliable system behaviour even in the presence of these wave disturbances. To evaluate the performance of the system, experiments are performed in the indoor tank where waves are generated. The characteristics of the waves are: height of 0.5 m and a frequency of 0.5 Hz, having a North orientation with respect to the world coordinates and facing the vehicle in surge direction. To test the station keeping capabilities, the vehicle is placed on the surface of the water and requested to maintain its current location.

The adaptive scheme modifies the parameters of the controller and it is able to react to the changes in the environment. This can be seen from the behaviour of the control effort in Figure 7.7. In Figure 7.8 the control effort for the manual tuning is presented.

Similar behaviour in the two control strategies can be seen. The most affected degrees-of-freedom of the vehicle, in the presence of waves, are the z-axis and the yaw DOF. This is caused by the pattern of the waves and due to the positioning of the vehicle with respect to the waves. Nevertheless, for the z-axis, the amplitude and the variation of the oscillations are different in the two cases. While for the manual tuning the oscillations have a clear pattern, the amplitude of the control effort is lower than the case when the auto tuning it is used. In the case of the manual tuning, the average amplitude is of 7 N for the z-axis

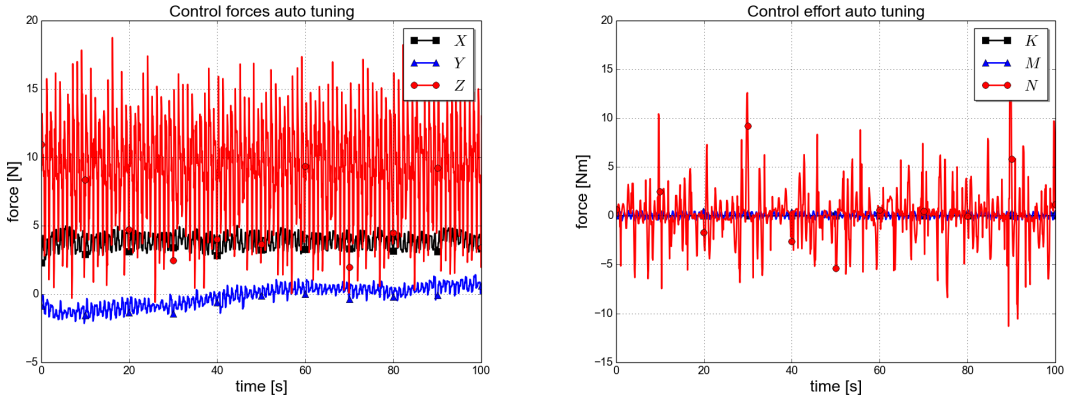

(a) Control forces (b) Control moments

Figure 7.7. Control efforts for station keeping using auto tuning in the presence of wave disturbances

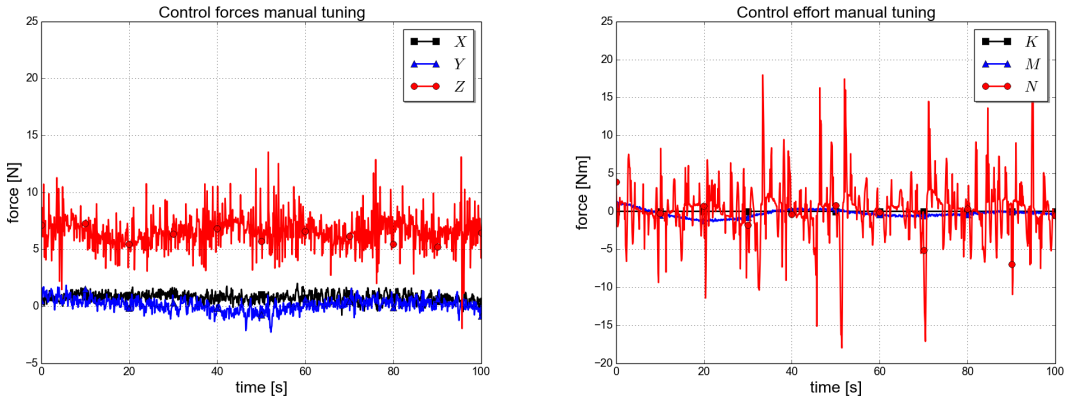

(a) Control forces (b) Control moments

Figure 7.8. Control efforts for station keeping using manual tuning in the presence of wave disturbances

and for the auto tuning the average amplitude is of 10 N. This is caused by the adaptive algorithm that takes into account the error in the system and it is trying to compensate for these disturbances. In the case of the control effort on the yaw axis, Figure 7.7b and Figure 7.8b the control effort has significant oscillations due to the noise in the system. The sensor reading representing the orientation on the z-axis is very noisy and this leads to generating additional control effort.

The behaviour of the vehicle when the system is affected by the waves is presented in Figure 7.9. The noisy yaw orientation can be seen in Figure 7.9e. In Figure 7.9c it can be seen that the auto tuning method maintains a constant position on this axis while the manual tuning produces small oscillations. The adaptive tuning is advantageous as the gains are changing as soon as the wave disturbance is sensed by the system. This leads to larger and more oscillatory control effort but better position keeping of the system. In the case of the manual tuning, as the gains are fixed the system is not able to react immediately to the waves and this leads to changes in depth. For the other DOFs of the system, similar behaviour with the two strategies can be seen. Overall, it can be seen that the station keeping

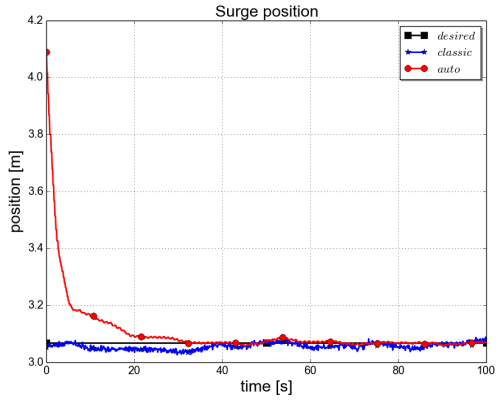

(a) Surge position

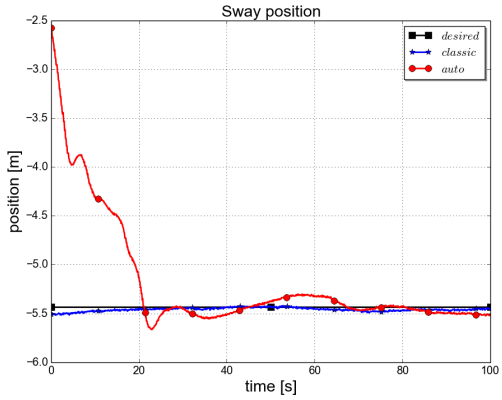

(b) Sway position

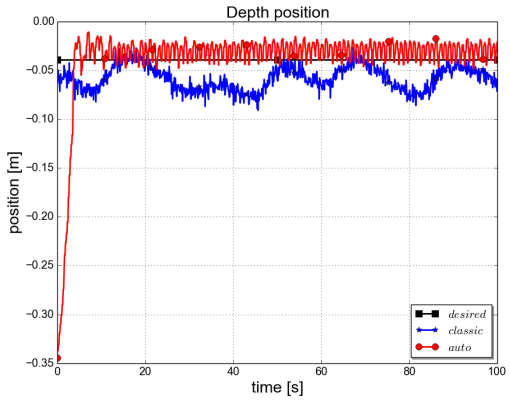

(c) Depth position

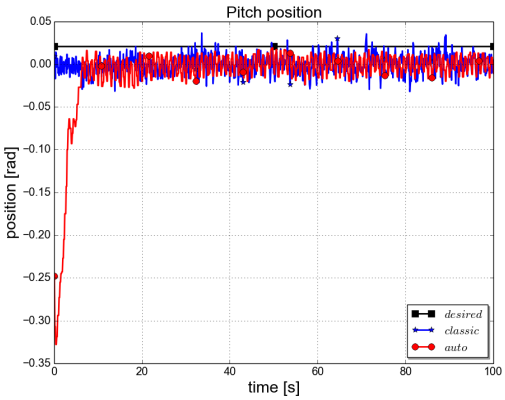

(d) Pitch position

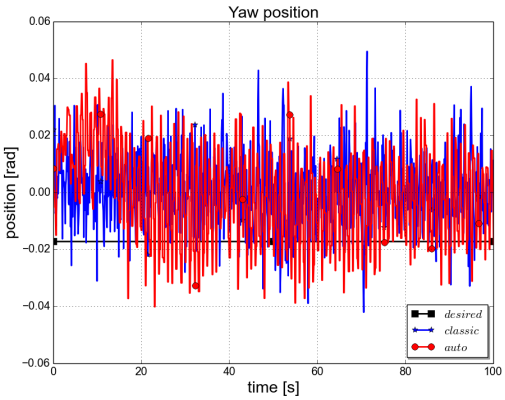

(e) Yaw position

Figure 7.9. Vehicle station keeping in the presence of wave disturbances

of the vehicle is accurately maintained during the time when disturbances are applied to the system. In Figure 7.9 at the beginning of the experiment a different behaviour is observed for the auto tuning case. This is due to the fact that the initial location of the vehicle had an offset to the actual location where the station keeping is required. Due to this, for the auto tuning, the first action of the vehicle is to reach the exact location. Based to the design and location of the thrusters, it is assumed that the y-axis is characterised by a slow system. The validation of this behaviour comes from these results, as the y-axis presents a considerable lag in the response. In Figure 7.9b it is observed that the position is maintained but the time

to reach this desired position is high.

7.3.3 Discussion

The preceding results have shown that the adaptive tuning using interaction theory is a good alternative for the manual tuning. In the case when the vehicle has to navigate using different goals the performance of the adaptive PILIM structure are similar with the manually tuned controller. In this part it is shown that for all navigation modes the two control structures perform in a similar way. Furthermore, it is intended to clearly state the cases when the adaptive tuning is a better choice for the system.

To compare the performances of the control structures the Generalized Root Mean Squared error (GRMS) evaluation metric is used. The metric expressed by Equation (7.23) is computed based on a set of 6 different trajectories for each navigation strategy.

$$GRMS = \sqrt{\frac{1}{N}\sum_{k=1}^{N} e_k^2} \tag{7.23}$$

where N is the number of total measurements and e is the generalized error. The error has been computed separately for the translational (e_x, e_y, e_z) and rotational (e_ϕ, e_θ, e_ψ) DOFs of the system, Equation (7.24), and independently for each navigation mode.

$$\begin{aligned} e_{pos} &= \sqrt{e_x^2 + e_y^2 + e_z^2} \\ e_{or} &= \sqrt{e_\phi^2 + e_\theta^2 + e_\psi^2} \end{aligned} \tag{7.24}$$

Mode	Adaptive		Classic	
	Translation (m)	Rotation (rad)	Translation (m)	Rotation (rad)
`simple`	0.72	0.23	0.84	0.27
`lines`	0.28	0.32	0.63	0.62
`fast`	0.65	0.06	0.57	0.20

Table 7.1. Tracking errors, manual vs. adaptive tuning

In Table 7.1 the position and orientation errors are presented for both controllers studied in this chapter. It can be observed that using the adaptive tuned structure the performances of the vehicle are slightly improved for all navigation trajectories. The most noticeable difference between the adaptive and manual tuning approaches is when the `lines` mode is used. In this case using the adaptive tuning method decreases the generalized error by approximately 50% compared with the manual tuning case. For the `simple` and `fast` navigation strategies the results are more similar. In the `lines` mode the navigation trajectory is restrictive, imposing a strict behaviour on each degree-of-freedom of the vehicle. Based on this it can be said that adaptive tuning of the PILIM controller considerably improves the

results for restrictive tasks where exact positioning of the system is needed. The method is a valid option for inspection tasks. In Figure 7.10 one inspection scenario is presented, where the vehicle has to perform a lawn mode trajectory. The behaviour of the vehicle when the adaptive tuning is used shows the capabilities of the system to accurately solve this challenge. Nevertheless, the method can be used for any type of vehicle mission producing comparable results with the case when manual tuning is used.

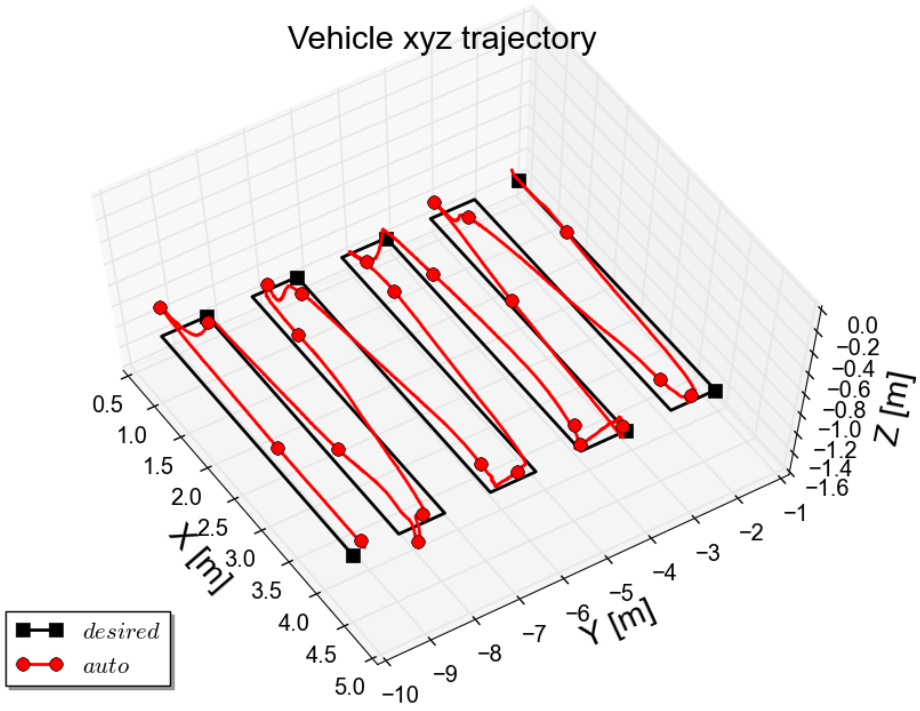

Figure 7.10. Vehicle lawn trajectory tracking

In Figure 7.6 it is shown that the control effort using the adaptive tuning has the same profile as the manual tuning but with lower amplitude. This leads to a better energy consumption during the missions, increasing the time the vehicle can be operated before total discharge of the batteries. In Figure 7.11 the total energy usage is presented for the behaviour of the system presented in Figure 7.5. The adaptive scheme improves the resource consumption of the system. Over a distance of 30 m the system uses 2 Wh using the adaptive tuning while when the manual tuning is in place, the system uses more than 4 Wh. The difference is caused by the characteristic of the adaptive tuning where the gains of the controller are tuned dependent on the error of the system. As the vehicle gets closer to the current goal the thrust required from the motors is reduced. The energy consumption is reduced by not having a constant force that has to be produced by the thrusters.

In Table 7.2 the mean navigation time and energy consumption is presented. The same set of experiments are used as in the case when the generalized error is computed using all three navigation strategies. It can be seen that the time to complete a mission is increased

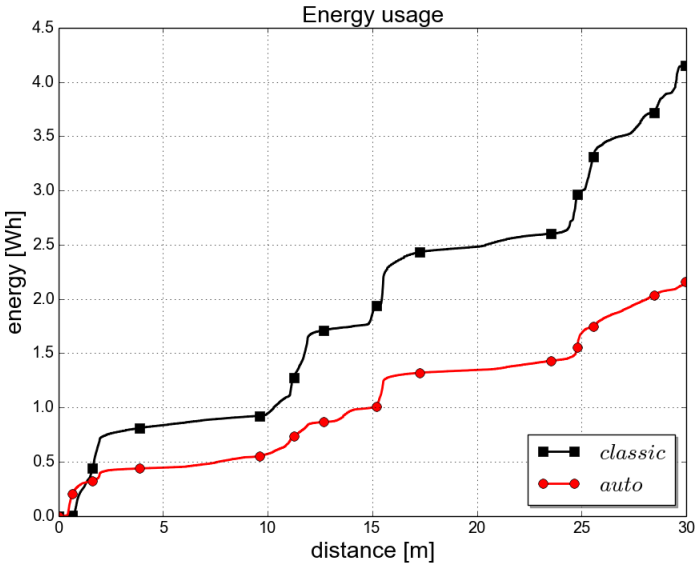

Figure 7.11. Energy usage, manual vs. adaptive tuning

Mode	Adaptive		Classic	
	Time (s)	Energy (Wh)	Time (s)	Energy (Wh)
`simple`	172.74	5.61	150.31	6.12
`lines`	147.12	2.84	113.11	3.81
`fast`	61.85	1.28	60.85	1.66

Table 7.2. Resource usage, manual vs. adaptive tuning

when adaptive tuning is used. This is caused by the reduced velocity generated by the lower amplitude of the control effort. Nevertheless, using the adaptive tuning the energy savings are at least 10% with respect to the classical case. It can be concluded that when the time constrains of a mission are relevant, manual tuning is the preferred option. Nevertheless, in the case when energy savings are a priority and longer missions are required with no time constrains, adaptive tuning represents the appropriate choice.

7.4 Summary

This chapter has presented an adaptive tuning scheme for the Proportional Integral Limited controller used for an underwater vehicle. The method is developed based on the adaptive interaction theory presented at the start of this chapter. The theory of adaptive interaction is applied to a coupled cascade control structure. The method is validated by experimental results obtained with the Nessie VII AUV. The main contribution of this chapter is the usage for the first time of the interaction theory for underwater applications, on a cascaded position-velocity controller. The adaptive tuned PILIM control structure produces a vehicle behaviour comparable to a manually tuned PILIM controller. It is demonstrated that the proposed structure can perform better than the classical method when inspection tasks are

performed. The main advantages of the adaptive strategy are the reduction of the tuning complexity and the improvement in terms of energy consumption. The algorithm is efficient in terms of convergence to appropriate control gain values. The algorithm constantly adapts the gains based on the current state of the vehicle and is able to handle the disturbances and changes in the environment. Moreover, the manually tuned method represents the control structure proposed in Chapter 5 for the vehicle. The work performed here represents a practical validation of that controller. The manually tuned approach represents the appropriate option when strict time constraints are imposed.

Chapter 8

Conclusions

This thesis was focused on the development of the low-level control structures for underwater robotic systems with a special interest in lightweight underwater vehicle-manipulator systems. The proposed control laws aim to reduce the coupling effects between the vehicle and the manipulator in order to produce stable interaction with the environment, reliable motion tracking and accurate behaviour.

Initially, a review of the available methodology for the dynamic and hydrodynamic modelling is presented together with a survey of the most common low-level control strategies. A lightweight underwater vehicle-manipulator system is presented through the kinematic, dynamic and hydrodynamic models. The UVMS is modelled as a single-chain system, the equation of motion being obtained in an iterative way. This allows the coupling effects to be highlighted between the parts of the system and to obtain accurate information about the behaviour of the system. The aim was to obtain a model of the system that would allow a real underwater system to be accurately replicated. Having a reliable simulation environment allows the control structures to be tested in a safe environment and reduces the cost of field operations. Furthermore, obtaining a clear understanding of the coupling effects between the manipulator and the lightweight vehicle offers the advantage of designing control laws that directly deal with this problem. Among the challenges of this work is the representation of the vehicle as an additional manipulator joint and the modelling of the hydrodynamic effects of this complex system. Based on the simulation results it was shown that the manipulator movement mostly affects the rotational degrees-of-freedom of the vehicle. The effects on the vehicle station keeping are proportional to the increase in the vehicle-manipulator mass ratio. Furthermore, it was shown that the hydrodynamic effects reduce the velocity of the manipulator but increase the coupling effects between the vehicle and manipulator.

To reduce these coupling effects a control strategy for station keeping of the lightweight vehicle-manipulator is proposed. The control law is also valid for motion tracking tasks and is part of the model based control structures. The architecture consists of an estimation of the inverse dynamic model, a feedback controller and the coupling effects between subsystems. The simulation results show that the proposed structure is beneficial to reduce the coupling effects between the vehicle and the manipulator and produces a reliable behaviour

from the robot even without having exact information about the system. The control law is evaluated by comparison to a feedback control structure and a feedback linearisation technique.

A control law is proposed for motion and interaction tasks using a lightweight underwater vehicle-manipulator system. The parallel position/force structure is based on sliding mode control theory and incorporates the estimated mathematical model of the system. The method is presented together with two different strategies to incorporate this law on the UVMS. The first strategy, the decoupled method, proposes a separate control structure for the vehicle and the manipulator. The vehicle is controlled through the Proportional Integral Limited Controller and the manipulator using the proposed parallel position/force control law. The second structure, the coupled strategy proposes the use of the parallel position/force control law for the overall system without any additional vehicle control law. Through the simulation results it is shown that both methods are valid choices to control an underwater system that interacts with the environment. Furthermore, both methods are able to handle the coupling effects between the vehicle and the manipulator. Separate manipulator and vehicle experimental evaluations are performed for some of the control laws presented in this thesis.

The low-level parallel position/force control law is evaluated with an underwater manipulator mounted on a fixed base in an underwater tank. The system is requested to move towards a goal and interact with two environments having different stiffnesses. To ensure the goal is placed at a valid location in the workspace a path is generated and the manipulator is requested to follow it. The method is experimentally compared with the impedance control law and the results show the validity of the approach.

The Proportional Integral Limited Controller is tested using a 5 degrees-of-freedom vehicle in an underwater tank. Furthermore, an adaptive tuning method is proposed for this control law based on the adaptive interaction theory. The method is a valid option as it reduces the complexity of the manual tuning and the energy consumption of the vehicle. The experiments show a similar behaviour with the manual tuning in terms of motion tracking.

One of the main contributions of this thesis represents the study of the coupling effects between a vehicle and a manipulator in a lightweight underwater vehicle-manipulator system. Control laws for station keeping of the vehicle, for the motion of the vehicle and the manipulator and for position/force regulation are developed. All these methods incorporate a component that handles the coupling effects and the required task can be reliably fulfilled. To the best of the author's knowledge these control structures are novel developments applied to a lightweight underwater vehicle-manipulator system. Furthermore, the adaptive interaction theory is applied for the first time for a cascaded controller on an underwater vehicle for tuning the gains of the system.

8.1 Suggestions for future work

This thesis can be extended in several areas. Firstly, the hydrodynamic parameters that are modelled in Chapter 3 based on mathematical relationships should be computed based on an experimental set-up. Having access to a real lightweight underwater vehicle-manipulator system and appropriate underwater facilities would lead to obtaining a more accurate simulation model for the system. Moreover, it would be interesting to evaluate the behaviour of the system when the inverse dynamics component in the control structure proposed in Chapter 4 is computed based on the exact system model and not only based on an estimate. A comparative evaluation of the two cases would highlight the effects of the uncertainties of the model in the control structure.

Secondly, it would be good to test the proposed control laws on the lightweight underwater system composed of the Nessie VII AUV and the HDT-MK3-M manipulator. The experimental set-up would be beneficial in evaluating the performances of the control laws in terms of the ability to reduce the coupling effects between the two subsystems. The parallel position/force control structure proposed in Chapter 5 could be extended to obtain the control of the system using all the six axes of the end-effector. In this case, the estimation of the contact force should be extrapolated from the single-point approximation and the control law should be designed using a quaternion representation.

In Chapter 7 an adaptive tuning is proposed for the control of the vehicle. It was shown that the adaptive tuning is beneficial for energy savings while the classical tuning is an appropriate option when the task to be executed is constrained by time. Future work can focus on changing the vehicle pilot by incorporating a decision component to select between the classical tuning and the adaptive tuning dependent on the requirements of the task. Furthermore, it would be interesting to extend this adaptive strategy to be used in the parallel force/position control structure proposed in Chapter 5. In this case the adaptive interaction should take into account that the devices are no longer characterised by the single input-output relationship. This would lead to a different adaptive law to compute the gains of the controllers.

Finally, it would be interesting to investigate the case when the system has two robotic manipulators and the system is requested to interact with the environment. The problems in the coupling effects would increase in this case. One approach to handle the disturbances caused by the movement of one arm would be to request the unused manipulator to balance the system by an opposite movement. In the case of the cooperative mode, the system should be designed in such a way to obtain the requested behaviour while keeping the system stable when performing the task.

Appendix A

Mathematical Preliminaries

This appendix presents the mathematical notations, equations and inequalities used along the thesis. The appendix starts by presenting the basic mathematical concepts and is followed by the definition of the concepts used in the stability analysis, more precisely the Lyapunov stability.

A.1 Mathematical fundamentals

Vector characteristics

For vectors $x,\ y \in \mathbb{R}^n$, the inner product is defined by:

$$x^T y = \sum_{i=1}^{n} x_i y_i \tag{A.1}$$

and has the following properties:

1. $x^T y = y^T x$ for all $x, y \in \mathbb{R}^n$
2. $x^T (y+z) = x^T y + x^T z$ for all $x,\ y,\ z \in \mathbb{R}^n$

Matrix characteristics

The product of matrix $A \in \mathbb{R}^{m\times p}$ and $B \in \mathbb{R}^{p\times n}$ can be defined by $C \in \mathbb{R}^{m\times n}$:

$$C = AB = c_{ij} \in \mathbb{R}^{m\times n}$$

and has the following properties:

1. $(AB)^T = B^T A^T$ for all $A \in \mathbb{R}^{m\times n}$ and $B \in \mathbb{R}^{p\times n}$
2. $A(B+D) = AB + BD$, where $D \in \mathbb{R}^{p\times n}$
3. $x^T A y = \sum_{i=1}^{n} \sum_{j=1}^{m} a_{ij} x_i y_j$, where $x \in \mathbb{R}^n$, $A \in \mathbb{R}^{n\times m}$ and $y \in \mathbb{R}^m$

4. $2 \mid y^T Ax \mid \leq \alpha y^T Ay + \frac{1}{\alpha} x^T Ax$, where $\alpha > 0$

The following concepts for the square matrix $A \in \mathbb{R}^{n \times n}$ are used across the thesis:

- If $A = A^T$ the matrix A is *symmetric*.
- If $A = -A^T$ the matrix A is *skew-symmetric*.
- If the determinant of A is zero, $\mathtt{det}[A] = 0$, the matrix is singular.
- If matrix A is nonsingular, the inverse matrix A^{-1} exists.
- If $x^T Ax > 0$ then A is positive, for all $x \in \mathbb{R}^n$, $x \neq 0$.
- If $x^T Ax \geq 0$ then A is positive semidefinite, for all $x \in \mathbb{R}^n$, $x \neq 0$.

Eigenvalues

For the square matrix $A \in \mathbb{R}^{n \times n}$ the eigenvalues of the matrix are marked with $\lambda_{A1}, \cdots, \lambda_{An}$ and satisfy the following relation:

$$\mathtt{det}\,[\lambda_{Ai} I - A] = 0, \quad i = 1, 2, \cdots, n \tag{A.2}$$

where $I \in \mathbb{R}^{n \times n}$ is the identity matrix.

Rayleigh-Ritz inequality is defined as:

$$\underline{\lambda}_A \parallel x \parallel^2 \leq x^T Ax \leq \overline{\lambda}_A \parallel x \parallel^2 \tag{A.3}$$

where $\underline{\lambda}_A$ is the smallest eigenvalue of A and $\overline{\lambda}_A$ is the largest eigenvalue of A.

Norms

The norm represents a generalization of the distance and length concepts. The norm $\| \cdot \|$ of a vector x is a real-valued function defined on $\mathbb{R}^n$. The most common vector norms are:

1. 1-norm: $\parallel x \parallel_1 = \sum_{i=1}^{n} \mid x_i \mid$
2. 2-norm: $\parallel x \parallel_2 = \sqrt{\sum_{i=1}^{n} \mid x_i^2 \mid}$
3. p-norm: $\parallel x \parallel_p = \left(\sum_{i=1}^{n} \mid x_i^p \mid \right)^{\frac{1}{p}}$
4. 8-norm: $\parallel x \parallel_\infty = \mathtt{max}(\mid x_i \mid)$

Along the thesis the 2-norm (also known as the Euclidean norm) is used, being characterised by the following properties:

1. $\| x \| > 0$ for all $x \in \mathbb{R}^n$, with $\| x \| = 0$ if and only if $x = 0$
2. $\| \alpha x \| = \alpha \| x \|$ for all $x \in \mathbb{R}^n$ and any scalar α
3. $\| x+y \| \leq \| x \| + \| y \|$ for all $x,\ y \in \mathbb{R}^n$
4. $| x^T y | \leq \| x \| \| y \|$ for all $x, y \in \mathbb{R}^n$

The norm of a matrix $A \in \mathbb{R}^{n \times m}$ is represented as the spectral norm and defined as:

$$\| A \| = \sqrt{\overline{\lambda}_{A^T A}} \tag{A.4}$$

where $\overline{\lambda}_{A^T A}$ is the largest eigenvalue of the matrix $A^T A \in \mathbb{R}^{m \times m}$. The following properties have to be considered for the spectral norm:

1. $\| A \| > 0$ if $A \neq 0 \in \mathbb{R}^{n \times m}$
2. $\| A \| = 0$ if and only if $A = 0 \in \mathbb{R}^{n \times m}$
3. $\| A + B \| \leq \| A \| + \| B \|$, where $B \in \mathbb{R}^{n \times m}$
4. $\| \alpha A \| = | \alpha | \| A \|$, where $\alpha \in \mathbb{R}$
5. $\| A^T \| \leq \| A \| \| B \|$, where $B \in \mathbb{R}^{n \times m}$
6. $\| Ax \| \leq \| A \| \| x \|$, where $\| A \|$ is the spectral norm and $\| x \|$ is the Euclidian norm of $x \in \mathbb{R}^m$.

A.2 Lyapunov stability

In this section the basic notions of Lyapunov stability are presented. The goal of the Lyapunov stability is to study the behaviour of the system described by the following relation:

$$\dot{x} = f(t,x), \quad x \in \mathbb{R}^n,\ t > 0 \tag{A.5}$$

where the origin is a constant solution of the differential equation.

If the function f does not depend on time system is said to be autonomous and Equation (A.5) can be expressed by:

$$\dot{x} = f(x), \quad x \in \mathbb{R}^n \tag{A.6}$$

Lyapunov function A continuous and differentiable function $\mathbb{R}^+ \times \mathbb{R}^n \to \mathbb{R}^+$ is said to be a Lyapunov function for the equilibrium $x = 0 \in \mathbb{R}^n$ of the equation $\dot{x} = f(t,x)$ if:

- $V(t,x)$ is locally positive definite
- $\frac{\partial V(t,x)}{\partial t}$ is continuous with respect to t and x

- $\frac{\partial V(t,x)}{\partial x}$ is continuous with respect to t and x
- $\dot{V}(t,x) \leq 0, \quad \forall t \geqslant 0$ and for small $\| x \|$

In the case of autonomous function a function is called a Lyapunov function for the system described by Equation (A.6) if $\dot{V}(x) \leq 0$, for small $\| x \|$.

The following definitions are relevant for the Lyapunov's Direct Method stability study:

Stability The origin of Equation (A.5) is stable in the sense of Lyapunov, if there exists a Lyapunov function candidate $V(t,x)$ such that

- $V(t,x)$ is positive definite with continuous partial derivatives
- The total time derivative satisfies: $\dot{V}(t,x) \leq 0, \ \forall t \geqslant 0$ for small $\| x \|$.

Uniform stability The origin is uniformly stable if in addition to the previous points $V(t,x)$ is descendent for small $\| x \|$

Global asymptotic stability The origin of Equation (A.5) is globally asymptotically stable if there exists a radially unbounded, globally positive definite Lyapunov function candidate $V(t,x)$ such that its time derivative is globally negative definite. If $V(t,x)$ is descendent then the origin is globally asymptotically stable.

Global exponential stability The origin of Equation (A.5) is globally exponentially stable if there exists a Lyapunov function candidate $V(t,x)$ and positive constants $\alpha, \ \beta, \ \gamma, \ p \leq 1$ such that:

- $\alpha \| x \|^p \leq V(t,x) \leq \beta \| x \|^p$
- $\dot{V}(t,x) \leq -\gamma \| x\|^p, \ \forall \geqslant t_0 \geqslant 0, \ \forall x \in \mathbb{R}^n$

A few important theorems and lemas used in Lyapunov stability analysis are further presented according to [40]. A detailed demonstration of these theorems can be found in [152].

Theorem A.2.1: LaSalle's Invariance Principle

Let there be a neighbourhood D of zero and a continuous differentiable (time-invariant) positive definite function $V : D \to \mathbb{R}$ whose orbital derivative $\dot{V}$ is negative semidefinite. Let I be the union of all complete orbits contained in

$$\left\{x \in D \mid \dot{V}(x) = 0\right\}$$

Then there is a neighbourhood U of zero such that for every $x_0 \in U, \ \omega(x_0) \subseteq I$.

Lemma A.2.1: Barbalat

Let $f(t)$ be a differentiable function of t.

- First version: If $\dot{f}(t) = df/dt$ is uniformly continuous and $\lim_{t\to\infty} f(t) = k < \infty$, then $\lim_{t\to\infty} = 0$.
- Second version: If $f(t) \geqslant 0$, $\dot{f}(t) \leqslant 0$ and $\ddot{f}(t)$ bounded, then $\lim_{t\to\infty} \dot{f}(t) = 0$.

Theorem A.2.2

Let $V(x)$ be a Lyapunov function of a continuous-time system that satisfies the following properties:

1. $\lambda_1 \parallel x \parallel^2 \leq V(x) \leq \lambda_2 \parallel x \parallel^2$
2. $\dot{V} \leq 0$, $x_1 < x < x_2$
3. $x(0) = 0$

Then $x(t)$ is uniformly bounded.

Theorem A.2.3

Let $V(x)$ be a Lyapunov function of a continuous-time system that satisfies the following properties:

1. $\lambda_1(\parallel x \parallel) \leq V(x) \leq \gamma_2(\parallel x \parallel)$
2. $\dot{V}(x) \leq -\gamma_3(\parallel x \parallel) + \gamma_3(\eta)$

where η is a positive constant, γ_1 and γ_2 are continuous, strictly increasing functions and γ_3 is a continuous, non-decreasing function. If

$$\dot{V}(x) \leq 0, \quad \text{for } \parallel x(t) \parallel > \eta \tag{A.7}$$

and $x(0) = 0$, $x(t)$ is uniformly bounded.

Summary

In this appendix some basic notions of linear algebra and stability evaluation have beend presented. This notions aim to be a base for the stability analysis study, Appendix B, of some of the controllers presented in this thesis. The detailed explanation of the notions and theorems presented in this part can be found in [153] and [116].

Appendix B

Proof of control laws

This appendix gives the stability analysis for the control laws proposed in Chapter 4 and Chapter 5.

B.1 Proof of Force Coupling - Model Control structure

The dynamic model of the underwater vehicle-manipulator structure is defined with:

$$M(\rho)\dot{\xi} + C(\rho,\xi)\xi + D(\rho,\xi)\xi + g(\rho) + f_f(\rho) = \tau \tag{B.1}$$

The proposed control law is presented by:

$$\begin{aligned}\tau = \tilde{M}(\rho_{des})\dot{\xi}_{des} + \tilde{C}(\rho_{des},\xi_{des})\xi_{des} + \tilde{D}(\rho_{des},\xi_{des})\xi_{des} + \tilde{g}(\rho_{des}) + \tilde{f}_f(\rho_{des}) + \\ + \tilde{M}(\rho)\tau_{v,q} + \mathrm{NE}(\rho,\xi)\dot{\xi}\end{aligned} \tag{B.2}$$

where

$$\tau_{v,q} = \begin{bmatrix} K_{P_v}e_v + K_{I_v}\int_0^t e_v d\tau \\ K_{P_q}e_q + K_{D_q}\dot{e}_q + K_{I_q}\int_0^t e_q d\tau \end{bmatrix}$$

and $\mathrm{NE}(\rho,\xi)\dot{\xi}$ can be reparametrized and described by the following relation:

$$\mathrm{NE}(\rho,\xi)\dot{\xi} = F_c(\rho,\xi)\theta$$

$$\frac{d}{dt}\theta = K_1 F_c(\rho,\xi)e_v, \quad K_1 > 0$$

where $F_c(\rho,\xi)$ represents the function of the known variables and θ is the function dependent of the unknown variables. By making the following notations:

$$e_v = [e_v,\ \dot{e}_q]^T, \quad K = \begin{bmatrix} K_{P_v} & O_{6\times6} \\ O_{6\times6} & K_{D_q} + \frac{a_1}{2}K_{P_q} \end{bmatrix}$$

$$K_P = \begin{bmatrix} K_{P_v} & O_{6\times6} \\ O_{6\times6} & K_{P_q} \end{bmatrix}, \quad K_D = \begin{bmatrix} O_{6\times6} & O_{6\times6} \\ O_{6\times6} & K_{D_q} \end{bmatrix}, \quad K_I = \begin{bmatrix} K_{I_v} & O_{6\times6} \\ O_{6\times6} & K_{I_q} \end{bmatrix}$$

where a_1 is a positive constant. For simplicity, the dynamic model parameters $M(\rho)$, $C(\rho,\xi)$, $D(\rho,\xi)$, $g(\rho)$, $f_f(\rho)$ will be marked as M, C, D, g, f.

The closed-loop system is described by the following relation:

$$\begin{aligned}\Delta\tilde{M}\dot{e}_v = -\Delta\tilde{C}e_v - \Delta\tilde{D}e_v - \Delta\tilde{G} - \Delta\tilde{F}_f - F_c(\rho,\xi)\theta - \\ -\tilde{M}K_P\begin{bmatrix}e_v\\e_q\end{bmatrix} - \tilde{M}K_D\begin{bmatrix}\dot{e}_v\\\dot{e}_q\end{bmatrix} - \tilde{M}K_I\begin{bmatrix}\int_0^t \dot{e}_v d\tau\\\int_0^t \dot{e}_q d\tau\end{bmatrix}\end{aligned} \tag{B.3}$$

where $\Delta\tilde{M}$, $\Delta\tilde{C}$, $\Delta\tilde{D}$, $\Delta\tilde{G}$ and $\Delta\tilde{F}_f$ have been defined in Chapter 4. The following notation is employed:

$$z = \left(\tilde{M}K_I\right)^{-1}\left[\Delta\tilde{G} + \Delta\tilde{f}_f\right] + \begin{bmatrix}\int_0^t \dot{e}_v d\tau\\\int_0^t \dot{e}_q d\tau\end{bmatrix} \tag{B.4}$$

The following Lyapunov function is considered:

$$V = \frac{1}{2}e_v^T\Delta\tilde{M}e_v + \frac{1}{2}\theta^T K_1^{-1}\theta \tag{B.5}$$

Using that $\theta^T K_1^{-1}\theta$ is a positive definite term and the Rayleigh-Ritz inequality V can be expressed as:

$$\underline{\lambda}_{\Delta\tilde{M}} \parallel e_v \parallel^2 \leq e_v^T\Delta\tilde{M}e_v \leq \overline{\lambda}_{\Delta\tilde{M}} \parallel e_v^T \parallel^2 \tag{B.6}$$

Derivative of V with respect to time:

$$\dot{V} = e_v^T\Delta\tilde{M}\dot{e}_v + \frac{1}{2}e_v^T\Delta\dot{\tilde{M}}e_v + \theta^T K_1^{-1}\dot{\theta} \tag{B.7}$$

Using the closed-loop expression in Equation (B.3) to replace $\Delta\tilde{M}\dot{e}_v$ and Equation (B.4)

$$\begin{aligned}\dot{V} = e_v^T\left\{-\Delta\tilde{C}e_v - \Delta\tilde{D}e_v - F_c(\rho,\xi)\theta - \tilde{M}K_P\begin{bmatrix}e_v\\e_q\end{bmatrix} - \tilde{M}K_D\begin{bmatrix}\dot{e}_v\\\dot{e}_q\end{bmatrix} - \tilde{M}K_I\right\} + \\ + \frac{1}{2}e_v^T\Delta\dot{\tilde{M}}e_v + \theta K_1^{-1}K_1F_c(\rho,\xi)e_v\end{aligned} \tag{B.8}$$

By using **Property** 3.4.2 from Chapter 3 and making the appropriate simplifications based on identical terms and based on the notations introduced at the start of this appendix, the following relation stands:

$$\begin{aligned}\dot{V} \leq -e_v^T\Delta\tilde{D}e_v - e_v^T\tilde{M}K_{P_v}e_v - \frac{a_1}{2}\dot{e}_q^T\tilde{M}K_{P_q}\dot{e}_q - \frac{1}{2a_1}e_q^T\tilde{M}K_{P_q}e_q - \dot{e}_q^T\tilde{M}K_{D_q}\dot{e}_q - \\ - \frac{a_2}{2}e_v^T\tilde{M}K_Ie_v - \frac{1}{2a_2}z^T\tilde{M}K_Iz\end{aligned} \tag{B.9}$$

where a_1, a_2 are positive constants.

$$\dot{V} \leq -\overline{\lambda}_{\Delta\tilde{D}} \parallel e_v \parallel^2 -\overline{\lambda}_{\tilde{M}K} \parallel e_v \parallel^2 -\frac{a_2}{2}\overline{\lambda}_{\tilde{M}K_I} \parallel e_v \parallel^2 -\frac{1}{2a_1}\overline{\lambda}_{\tilde{M}K_{P_q}} \parallel e_q \parallel^2 - \\ -\frac{1}{2a_2}\overline{\lambda}_{\tilde{M}K_I} \parallel z \parallel^2 \tag{B.10}$$

This can be further simplified as:

$$\dot{V} \leq -\left[\overline{\lambda}_{\Delta\tilde{D}} + \overline{\lambda}_{\tilde{M}K} + \frac{a_2}{2}\overline{\lambda}_{\tilde{M}K_I}\right] \parallel e_v \parallel^2 \tag{B.11}$$

Based on the Equation (B.6) and Equation (B.11) it can be stated that the origin of Equation (B.1) is exponentially stable and according to **Theorem A.2.2** the solution e_v is bounded.

B.2 Proof of Parallel Variable Sliding Mode Dynamic Controller

The mathematical model of the underwater vehicle-manipulator system in the operational space is described by:

$$M(x)\ddot{x} + C(x)\dot{x} + D(x)\dot{x} + G(x) + F_f(x) = T - F \tag{B.12}$$

The total control law is defined by:

$$T = \tilde{M}(x)\left[\ddot{x}_{eq} + \kappa_1 \mathtt{sign}(\delta) + \kappa_2 \mathtt{sign}(s) + K\sigma\right] + \\ + \tilde{C}(x,\dot{x})\dot{x}_{eq} + \tilde{D}(x,\dot{x})\dot{x}_{eq} + \tilde{G}(x) + \tilde{F}_f(x) + \tilde{F}_{eq} \tag{B.13}$$

The closed-loop system is described by:

$$M(x)\ddot{x} + C(x)\dot{x} + D(x)\dot{x} + G(x) + F_f(x) = \tilde{M}(x)\left[\ddot{x}_{eq} + \kappa_1 \mathtt{sign}(\delta) + \kappa_2 \mathtt{sign}(s) + K\sigma\right] + \\ + \tilde{C}(x,\dot{x})\dot{x}_{eq} + \tilde{D}(x,\dot{x})\dot{x}_{eq} + \tilde{G}(x) + \tilde{F}_f(x) + \tilde{F}_{eq} - F \tag{B.14}$$

For simplicity, the dynamic model parameters $M(x)$, $C(x)\dot{x}$, $D(x)\dot{x}$, $G(x)$, $F_f(x)$ will be marked as M, C, D, G, F_f. Substituting $\ddot{x} = \ddot{x}_{eq} - \ddot{\delta}$ in the closed-loop system:

$$M(x)\ddot{\delta} = -\tilde{M}(x)\ddot{x}_{eq} - \tilde{M}(x)\kappa_1 \mathtt{sign}(\delta) - \tilde{M}(x)\kappa_2 \mathtt{sign}(s) - \tilde{M}(x)K\sigma + \\ + F_{eq} - c_2^{-1}\sigma - \tilde{C}\dot{x}_{eq} - \tilde{D}\dot{x}_{eq} - \tilde{G} - \tilde{F}_f - \tilde{F}_{eq} + \\ + M\ddot{x}_{eq} + C\dot{x}_{eq} + D\dot{x}_{eq} + G + F_f - C\dot{\delta} - D\dot{\delta} \tag{B.15}$$

Using the boundary errors defined in Chapter 5, Equation (B.15) can be expressed as:

$$M(x)\ddot{\delta} = -\tilde{M}(x)\kappa_1 \mathtt{sign}(\delta) - \tilde{M}(x)\kappa_2 \mathtt{sign}(s) - \tilde{M}(x)K\sigma - c_2^{-1}\sigma - C\dot{\delta} - D\dot{\delta} + \\ + \Delta M\ddot{x}_{eq} + \Delta C\dot{x}_{eq} + \Delta D\dot{x}_{eq} + \Delta G + \Delta F_f + \Delta F_{eq} \tag{B.16}$$

Defining the Lyapunov function candidate as:

$$V = \frac{1}{2}\delta^T M \delta \tag{B.17}$$

As $\delta^T M \delta$ is a positive term, the Lyapunov function candidate is positive. Derivative of V is given by:

$$\dot{V} = \frac{1}{2}\delta^T \dot{M} \delta + \delta^T M \dot{\delta} \tag{B.18}$$

Replacing $M\dot{\delta}$ with the expression from Equation (B.16), Equation (B.18) becomes:

$$\begin{aligned}\dot{V} = \delta^T \left[-\tilde{M}(x)\kappa_1 \mathtt{sign}(\delta) - \tilde{M}(x)\kappa_2 \mathtt{sign}(s) - \tilde{M}(x)K\sigma - c_2^{-1}\sigma - C\delta - D\delta\right] + \\ + \delta^T \left[\Delta M\ddot{x}_{eq} + \Delta C\dot{x}_{eq} + \Delta D\dot{x}_{eq} + \Delta G + \Delta F_f + \Delta F_{eq}\right] + \frac{1}{2}\delta^T \dot{M}\delta\end{aligned} \tag{B.19}$$

To simplify the expression of $\dot{V}$ the following notations are made, defining positive matrices:

$$\Lambda_1 = \tilde{M}\kappa_1 \quad \Lambda_2 = \tilde{M}\kappa_2 \quad \Lambda_3 = \tilde{M}K + c_2^{-1}$$

and

$$S = \mathtt{sign}(s)$$

$$\begin{aligned}\dot{V} = -\delta^T \Lambda_1 \mathtt{sign}(\delta) - \delta^T \Lambda_2 S - \delta^T \Lambda_3 \sigma + \delta^T \left[\frac{1}{2}\dot{M}\delta - C\right]\delta - \delta^T D\delta + \\ + \delta^T \left[\Delta M\ddot{x}_{eq} + \Delta C\dot{x}_{eq} + \Delta D\dot{x}_{eq} + \Delta G + \Delta F_f + \Delta F_{eq}\right]\end{aligned} \tag{B.20}$$

Using **Property** 3.4.2, linear algebra properties, the derivative of the Lyapunov function can be expressed as:

$$\begin{aligned}\dot{V} \leq -\delta^T D\delta + \delta^T \left[\Delta M\ddot{x}_{eq} + \Delta C\dot{x}_{eq} + \Delta D\dot{x}_{eq} + \Delta G + \Delta F_f + \Delta F_{eq}\right] - \delta^T \Lambda_1 \mathtt{sign}(\delta) - \\ - \frac{a_1}{2}\delta^T \Lambda_2 \delta - \frac{1}{2a_1} S^T \Lambda S - \frac{a_2}{2}\delta \Lambda_3 \delta - \frac{1}{2a_2}\sigma \Lambda_3 \sigma\end{aligned} \tag{B.21}$$

where a_1, a_2 are positive. By choosing:

$$\lambda_1 \geqslant \mid \left[\Delta M\ddot{x}_{eq} + \Delta C\dot{x}_{eq} + \Delta D\dot{x}_{eq} + \Delta G + \Delta F_f + \Delta F_{eq}\right]_i \mid + \eta_i \tag{B.22}$$

where η_i is positive. Then:

$$\begin{aligned}\dot{V} \leq -\overline{\lambda}_D \parallel \delta \parallel^2 - \sum_{i=1}^{6} \eta_i \mid \lambda \mid - \frac{a_1}{2}\overline{\lambda}_2 \parallel \delta \parallel^2 - \frac{1}{2a_1}\overline{\lambda}_2 \parallel s \parallel^2 - \\ - \frac{a_2}{2}\overline{\lambda}_3 \parallel \delta \parallel^2 - \frac{1}{2a_2}\overline{\lambda}_3 \parallel \sigma \parallel^2\end{aligned} \tag{B.23}$$

As the function V is a positive definite function and $\dot{V}$ is a negative definite function, for the UVMS definite by Equation (B.12) and controlled by Equation (B.13) the sliding mode is guaranteed and the errors converge to zero.

Appendix C

Relevant published/submitted papers

The following conference papers and journal paper have been developed from the work presented in this thesis:

- C. Barbalata, M.W. Dunnigan, and Y. Petillot. "Dynamic coupling and control issues for a lightweight underwater vehicle manipulator system". In: 2014 *IEEE Oceans - St. Johns, Canada*, 2014, pp. $1-6$
- C. Barbalata, M.W. Dunnigan, and Y. Petillot. "Reduction of the dynamic coupling in an underwater vehicle-manipulator system using an inverse dynamic model approach". In: *IFAC Workshop on Navigation, Guidance and Control of Underwater Vehicles*, Apr. 2015
- C. Barbalata, V.D. Carolis, M.W. Dunnigan, Y. Petillot, and D. Lane. "An adaptive controller for autonomous underwater vehicles". In: *IEEE/RSJ International Conference on Intelligent Robots and Systems (IROS)*, 2015, pp. 16581663
- C. Barbalata, M.W. Dunnigan, and Y. Petillot. "Comparison of coupled and decoupled force/motion controllers for an underwater vehicle-manipulator system", submitted to the *Journal of Ocean Engineering, Elsevier*

Dynamic coupling and control issues for a lightweight underwater vehicle manipulator system

Corina Barbălată, Matthew W. Dunnigan, Yvan Pétillot
School of Engineering & Physical Sciences
Heriot-Watt University, EH14 4AS, Edinburgh, UK
Email: cb237@hw.ac.uk

***Abstract*—This paper presents a study of the interaction effects between a lightweight underwater vehicle and the attached manipulator. Based on a tree representation of the system, the dynamic and hydrodynamic model of the UVMS is computed and the coupling effects are analysed. Simulations show that having a manipulator with considerable mass compared with the vehicle significantly influences the stability of the system. Gaining a clear understanding of the coupling effects is important for designing the control laws. Moreover, it is possible that incorporating these disturbances in the control methods can improve the performance of the UVMS.**

I. Introduction

Underwater vehicles are interesting for both research and industry due to their capabilities to inspect the sea floor and provide useful information for military applications, oil industry as well as geological and biological explorations. The need to interact with the underwater environment leads to the development of a more complicated system consisting of an underwater vehicle and a robotic manipulator (UVMS). This system can be used for example in sea mine disposals, pipe maintenance or sampling of geological sites. Understanding and developing simulation models of the UVMS is one of the first requirements to be able to create a robust system, able to achieve the demands of the mission.

The representation of an underwater-vehicle manipulator system is needed to analyse the changes over time in velocity and position of the system based on mathematical equations. The literature presents two different methods for system configuration. The first approach is presented in [11], where the UVMS is considered as two independent subsystems: the vehicle and the manipulator. The equations of motion for each subsystem is developed and the interaction forces between subsystems are added to these equations. The second approach is to consider the UVMS as a single body having a tree representation. This approach can be seen in [1] where the author uses it to decompose the control problem to a set of simple control strategies.

After the system is properly represented, the dynamic model that describes the behaviour of the system, can be developed to design a simulation platform for the UVMS. Newton-Euler and Euler-Lagrange algorithms represent the basis of dynamic modelling. The Newton-Euler algorithm is based on the action and reaction principle and the Euler-Lagrange method is based on the potential and kinetic energies of the system. Fossen [7] proposes to consider the UVMS as a macro-micro manipulator and develops the equations of motion based on the Newton-Euler algorithm. Antonelli *et al.* [1] uses the same dynamic model together with a task-priority inverse kinematics approach for redundancy resolution of a UVMS. The papers [2], [4] develop the dynamic model based on Newton-Euler, further used for the control architecture. A closed-form dynamic model has been obtained based on the Euler-Lagrange algorithm in [9], [17]. The same method is used in [16] for a UVMS to determine the constraint dynamics and apply a passivity-based force/position control scheme. McLain *et al.* [15] analyse the dynamic coupling between a one-link manipulator and a vehicle based on experiments. The goal of the paper is to present the coordinated control of the arm and vehicle. The experiments show that the dynamic coupling forces between the manipulator and the vehicle are the main cause in destabilising the station keeping characteristic of the system. In [5] the authors present the dynamic coupling expression between the two subsystems, analysing the effects on the vehicle and the end-effector, when perfect joint motion is assumed. Korkmaz *et al.* [12] presents a control method for the UVMS based on inverse dynamics. The interaction forces between the vehicle and manipulator are computed and used in the control law that aims to linearise the system.

The stability of motion of the vehicle at low speeds can be influenced by environmental disturbances as well as due to the coupling effects between the manipulator and vehicle. When the UVMS is represented as a highly coupled system, the approach that is chosen by most of the researchers is to decouple the system based on feedback linearisation. After each DOF of the system is represented independently, a basic controller (PD/PI/PID) is applied to each DOF [14]. A more complex controller, that does not need the feedback linearisation is presented in [8] for a 5-DOF vehicle with a 2-link manipulator. Sliding mode control is considered as a robust controller that is not affected by disturbances. The steady-state errors are small and the tracking task is performed accurately. Although the results presented fulfil the requirements, any change in the system will affect the robustness of the controller. The solution to this problem can be the use of an adaptive version of this controller.

The aim in developing a dynamic model of an underwater vehicle-manipulator system is to understand the behaviour of the system. Based on this, an appropriate control architecture can be developed for the UVMS. Understanding the dynamic coupling between the manipulator and the vehicle and how the movement of the manipulator affects the stability of the lightweight vehicle represents the starting point of this research. The answer to these questions rests in the computation of the linear and angular accelerations of the system, described

978-1-4799-4918-2/14/$31.00 ©2014 IEEE

by the forces that act on the vehicle. The Newton-Euler method highlights the interactions between different rigid bodies of the system. As one of the interests in the development of the equations of motion of the overall system is to understand how the movement of the manipulator affects the stability of the vehicle, a Newton-Euler based method is appropriate to compute the equation of motion of the system. To obtain an acceptable representation of the system it is important to model the hydrodynamic effects as accurately as possible. Modelling these effects is an open research topic. The fluid effects that act on the system considered in this work are added mass, drag and restoring forces. The coupling effects present in the system can be further used to develop and tune the controllers for vehicle station keeping and trajectory tracking of manipulator and/or vehicle.

The rest of the paper is structured as follows. In Section II the methodology to develop the simulation platform is presented, together with the control architecture for the vehicle. In Section III the coupling effects between a 3-link manipulator and vehicle are presented and analysed. Section IV presents the conclusions and future work for this research.

II. Methodology

A. System representation

As one of the goals of this work is to represent and analyse the interaction forces between the vehicle and manipulator, a single-chain representation for the UVMS was chosen. This tree representation consists of nodes and arcs. In the UVMS system, the node represents the link while the arc represents the joint of the system. The initial reference system is marked with 0 and the notation is in ascendant order based on the connections between links. The reference frame that describes each individual link is placed at the center of mass. The vehicle is considered as an extension of the manipulator, its representation being described by a 6-DOF joint. In this case, the joint does not represent a real joint, but is a model that incorporates the translational and rotational DOFs of the vehicle, as presented in (1).

$$q = (s_x, s_y, s_z, \phi, \theta, \psi)^T \tag{1}$$

where s_x is translation in x axes (surge), s_y is translation in y axes (sway), s_z is translation in z axes (heave), ϕ represents rotation over the 1st axes (roll), θ represents rotation over the 2nd axes (pitch) and ψ rotation over 3rd axes (yaw). The virtual joint can be represented as six independent joints, connected by zero mass bodies. The node that connects the last degree of freedom of the vehicle with the first joint of the manipulator has all the characteristics of the vehicle. By considering this case, it can be assumed that all degrees-of-freedom of the vehicle together with the manipulator joints act as a fixed base manipulator. This allows conventional algorithms for the serial link manipulator to be applied to the UVMS system. A sketch of the system can be seen in Figure 1.

B. Dynamic modelling

The dynamic model can be divided into two categories, depending on the requirements of the system: (i) forward dynamics and (ii) inverse dynamics. The forward dynamics computes the joint accelerations, velocities and positions based on forces and torques applied to the system. The inverse dynamics computes the forces and torques based on a desired behaviour of the system. The forward dynamics algorithm is used for simulation purposes, while the inverse dynamics is used for feed-forward control [6].

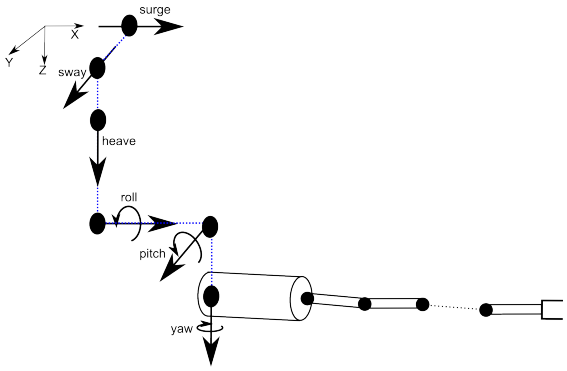

Figure 1. Generic UVMS graph

To compute the acceleration and interaction forces between the vehicle and manipulator, the Composite Rigid Body algorithm is used in this work. A simple dynamic model of the UVMS can be expressed by (2).

$$M(q)\ddot{q} + C(\dot{q}, q)\dot{q} = \tau \tag{2}$$

where C represents the Coriolis and Centripetal forces, M represents the inertia matrix and τ describes the applied forces on the system. The algorithm, as presented in [6], can be divided into three steps. In the first step, the C matrix is computed, followed by the elements of the M matrix in the second step. Having both components, the acceleration of the system is determined.

1) $C(\dot{q}, q)\dot{q}$ can be interpreted as the vector that produces zero acceleration. The Newton-Euler algorithm is a solution for computing these forces. Starting from the base to the last link of the rigid body, the velocity, acceleration and force of each link are computed as presented in (3) to (5).

$$v_i = v_{i-1} + s_i\dot{q}_i \tag{3}$$

$$a_i = a_{i-1} + v_i \times s_i\dot{q}_i + s_i\ddot{q}_i \tag{4}$$

$$f_i^l = I_i \times a_i + v_i \times I_i v_i \tag{5}$$

where s_i represents the allowed movement of the joint, $\ddot{q}_i$, $\dot{q}_i$ and q_i are the acceleration, velocity and position of joint i, v_i and a_i represent the velocity and acceleration of link i and f_i^l is the force of link i. The force on joint i, f_i^j, depends on both the force applied on the current link and the force applied on the following joint, as seen in (6).

$$f_i^j - f_{i+1}^j = f_i^l \tag{6}$$

The $C(\dot{q}, q)\dot{q}$ vector can be represented as (7).

$$C(\dot{q}, q)\dot{q} = [f_1^j \; f_2^j \ldots f_n^j]^T \tag{7}$$

2) Setting $C(\dot{q}, q)\dot{q}$ to zero, $M(q)$ is interpreted as the matrix of forces that distributes an acceleration on a

stationary system. Each column of the M matrix is interpreted as the vector of forces to produce a unit acceleration onto the corresponding link. To compute the values of the column i, it is considered that the links from i to last link are moving, while the previous links are static. Based on this assumption, every joint transmits a force, f_i, onto the subsequent link and the matrix M can be computed according to (8).

$$M_{ji} = h_j^T f_i, \quad \text{for } j \leq i \tag{8}$$

where h_j^T is the unit acceleration on the joint i. The unit force on joint i, f_i is defined based on the inertia of the rigid body I_i^C, (9).

$$f_i = I_i^C h_j \tag{9}$$

The inertia of the i-link is computed based on the sum of inertias of all links that are part of the sub-tree, (10).

$$I_i^C = I_i + \sum_{j=1}^{i-1} I_j^C \tag{10}$$

3) The acceleration of the system, $\ddot{q}$ is obtained by direct inversion of the system.

C. Hydrodynamic modelling

The effects of the underwater environment have to be considered in the dynamic model of the UVMS for developing a realistic simulation platform. Following the work of McLain [15], the added mass, drag and restoring forces can be modelled.

The added mass is the additional weight caused by the volume of the fluid displaced during the movement of the system. The force that appears in this case is opposite in direction to the motion of the system, but is equal in magnitude.

Added mass is dependent on the added mass coefficients. The most common approach to model these coefficients is based on constant parameters dependent on the shape of the rigid body. Following the paper of McLain [15], the added mass coefficients can be related to the distance travelled by the links of the manipulator, as presented in Figure 2. Based on the distance, the vortexes formed around the rigid body will vary in shape and will differently affect the system. The added mass coefficient can be represented as cubic-spline polynomials dependent on the travelled distance. The results of the measurements are fitted to the cubic-spline polynomial based on optimization theory. Taking into account the geometry of the body as well as the distance travelled by the end tip of the manipulator, the added mass coefficients were computed for this work. Based on the desired positions considered in the tested cases, the distance in diameters of the rigid body travelled was always less than 2 diameters of travel. Based on this, the added mass coefficients were set between 0.9 and 1.1.

Drag, in fluid dynamics, is the force dependent on the velocity of the body, opposing the motion of the body with respect to the surrounding fluid. The challenge of studying this effect is high when a complicated geometric representation of the system has to be considered. In order to obtain the drag

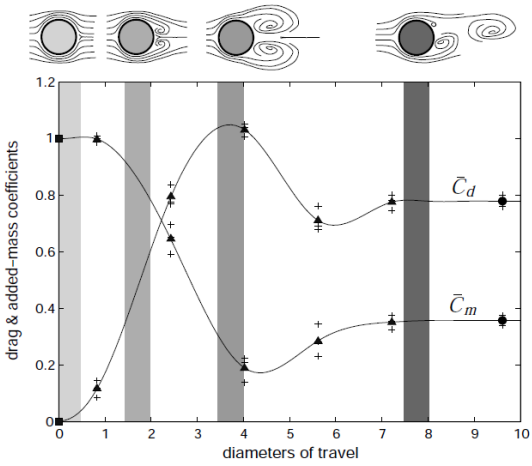

Figure 2. Drag and added mass spline model, [15]

force, the moment integral along the length of the rigid body has to be performed as presented in (11), [15].

$$f_b^D = -\rho C_D r \int_0^l \parallel v(x) \parallel v(x) dx \tag{11}$$

where C_D is the drag coefficient, l is the length of the link, r is the radius of the link and $v(x)$ is the velocity relative to the fluid and normal to the edge of each disk. From (11) the drag component in the direction of the rigid body axes can be computed based on (12), [10].

$$(f_b^D)^x = -0.5\rho C_D \pi r^2 \parallel v(x) \parallel v(x) \tag{12}$$

Although the method of computing the drag effect is straightforward, the challenge remains in the computation of the drag coefficients. One of the methods of computing the drag coefficient, considered in this work, is based on the shape of the rigid body and Reynolds Number.

Based on Figure 2, the drag coefficient can also be described based on the distance travelled by the rigid body. The drag coefficients can be extracted from the spline model, being directly proportional with the distance travelled by the body for small distances, reaching a steady state at larger distances. It was observed that for the configuration tested during this research, the drag coefficient computed based on distance travelled has values lower than 1.2.

The effect of the angle between adjacent links on the computation of the hydrodynamic in-line forces, as presented by Lebourne [13], has been studied. Experiments show that there is a strong connection between the behaviour of the hydrodynamic drag and the manipulator configuration that can be expressed through (13), [13]. In this work the drag coefficients have been computed based on the shape of the body, distance travelled by the body and on the angle between the manipulator links.

Gravitational and buoyancy forces acting on the underwater rigid bodies are grouped together forming the restoring forces. The vehicle weight, buoyancy and relative positions of the centres of gravity and buoyancy are the information needed to compute the restoring forces. To obtain a system that requires minimum effort and to maintain a desired depth, the

underwater systems are designed to be neutral, the center of buoyancy and center of gravity being located at the same place.

$$f(n) = \begin{cases} -0.5\rho C_D \pi r_i^2 - 0.5\rho C_D \pi (r_i^2 + L_i \cos(\theta_{i+1})) & \text{if } i \leq n \\ -0.5\rho C_D \pi r_i^2 & \text{if } i = n \end{cases} \quad (13)$$

The buoyancy force, which is proportional to the mass of the fluid displaced by the moving body, is exerted opposite to the gravitational force as presented by Archimedes principle, (14).

$$f_B = -m_d a_g = \rho V a_g \quad (14)$$

where m_d is the mass of the fluid displaced, V is the volume displaced and a_g is the gravitational acceleration. The restoring force can be described with (15), where m represents the mass of the rigid body.

$$f_R = m a_g + f_B \quad (15)$$

D. PILIM controller

Assuming that the vehicle moves at fairly low speed, the dynamic model can be represented independently for each degree-of-freedom by linear decoupled equations. The decoupling control technique has the advantage of simplifying the design of the model. Proportional-Integral Limited feedback controllers [3] can be applied for each degree-of-freedom x, y, z, ϕ, θ and ψ. The controllers are tuned to provide a fast transient response with no overshoot for a step change in position command.

The Proportional-Integral Limited controller is used for the control of a 6-DOF vehicle in [3]. It is advantageous due to its simple implementation and the fact that compared with the PID controller, the overshoot of the system is decreased. A disadvantage of this type of controller is the tuning difficulty. The PILIM controller uses integrator anti-windup to avoid excessive overshoot when control saturation is present. The design of the controller is based on the thesis [3], where two control loops are present, an outer one that controls the position and an inner one that controls the speed. The diagram of the compensator can be seen in Figure 3. For tuning the controller, the "trial and error" method has been used. The PILIM is

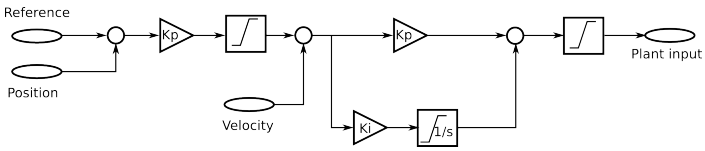

Figure 3. Schematic PILIM compensator, [3]

composed of a proportional controller for position control and a proportional-integral controller for velocity control. The saturation block maintains the velocity for most of the transient response. When the position output of the system is far from the desired value the system is under velocity control. When the desired position is close to be obtained, the system changes to position control.

III. Simulation results

The system used in this research was composed of a cylindrical shape vehicle and a three-link manipulator with revolute joints. The characteristics of the system are presented in Table I.

Parameter	Value
Mass vehicle	125 kg
Length vehicle	2.1 m
Diameter vehicle	0.7 m
Moments of inertia vehicle	
I_x	0.34 $kg \cdot m^2$
I_y	3.71 $kg \cdot m^2$
I_z	3.71 $kg \cdot m^2$
Mass manipulator	
m_1	15.7 kg
m_2	4.65 kg
m_3	4.65 kg
Length manipulator	
l_1	0.6 m
l_2	0.25 m
l_3	0.25 m
Radius manipulator	
r_1	0.15 m
r_2	0.1 m
r_3	0.1 m

Table I. System parameters

The following assumptions were made:

- The vehicle is only included in station keeping tasks.
- The vehicle has three planes of symmetry.
- Actual joint acceleration is well approximated by desired arm-joint acceleration.
- Fluid velocity is considered zero.

A. Coupling interactions between manipulator and vehicle

In the first test no hydrodynamic effects are applied to the system and a 20 Nm torque is applied to actuate the first joint of the manipulator. From the results of the simulation the coupling forces between the arm and the vehicle can be observed. Applying a certain torque on the manipulator joint will produce movement of the arm at a constant speed, proportional to the applied torque. As in this case the speed of the arm is small, the vehicle slightly drifts from its original position. A peak in the pitch velocity can be seen, corresponding to the time needed for the vehicle to change orientation due to the disturbances produced by the manipulator. Simulation results have shown that pitch-DOF is the most affected component of the vehicle. While the roll/yaw rates are affected less than 2 degrees/s, the pitch is affected up to 10 degrees/s, in the case when no hydrodynamics were considered. This behaviour of the system can be explained by the configuration of the UVMS. Tests were performed assuming the manipulator is attached by a revolute joint along the z-axes of the first link.

Based on tests it was observed that increasing the ratio between the manipulator and the vehicle will increase the impact on the vehicle movement, Figure 5. In the case when the manipulator mass is 5% of the mass of the vehicle, the pitch peak velocity is less than $4°/s$. In the case when the mass was considered having 35% of the vehicle mass, the peak velocity is as much as $15°/s$ .The conclusion that can be drawn based on these results is that the vehicle is affected by the movement of the manipulator, a heavier and faster manipulator has a higher impact on the vehicle.

B. Hydrodynamic effect analysis

As mentioned previously, the hydrodynamics will affect the coupling between the two subsystems. Taking into account

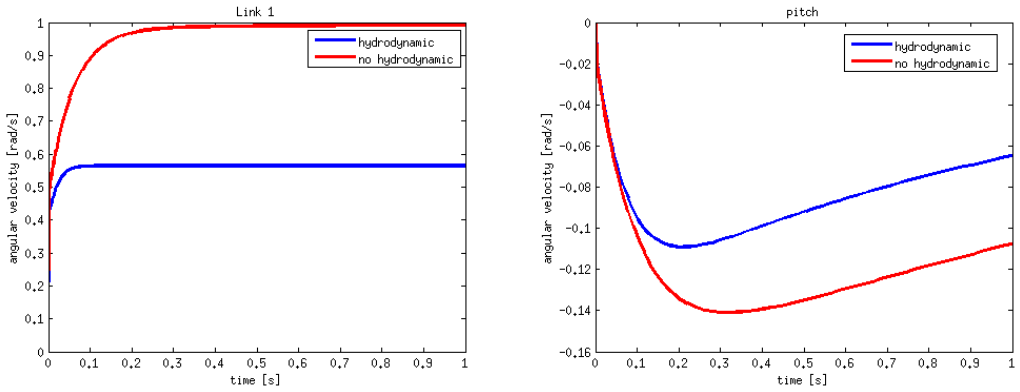

Figure 4. Velocity of first link and pitch velocity (no vehicle control and no manipulator control)

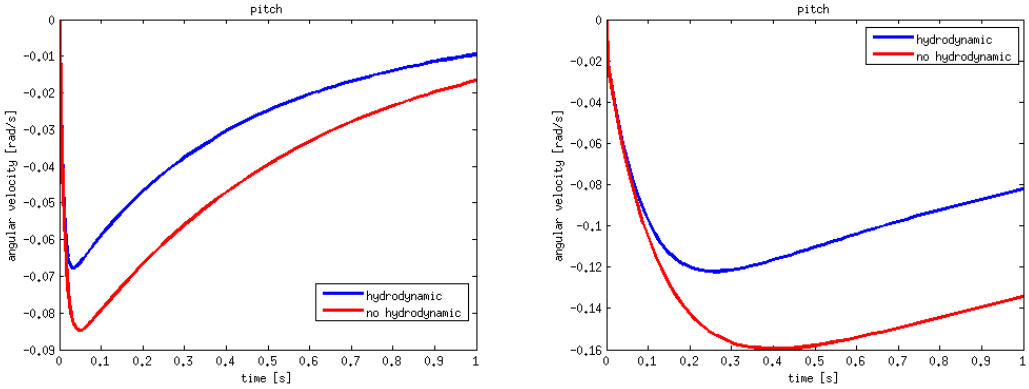

Figure 5. Pitch velocity when manipulator mass is (a) 5% and (b) 35% of vehicle mass

the effects of added mass, drag and restoring forces will help in designing a robust control law that can be used for a real underwater vehicle-manipulator system. Figure 4 shows a comparison between the case when the hydrodynamic effects are incorporated in the model and the case when they are not considered. The hydrodynamic effects will reduce the velocity of the links compared with the case when no hydrodynamic effects are considered. From simulation results, the angular velocity of first joint reaches $5.76°/s$ when a torque of 20 Nm is applied to this link. Including the hydrodynamic effects reduces the coupling between the manipulator and vehicle, due to the decrease in speed of the manipulator. High manipulator velocities affect all degrees-of-freedom of vehicle. When the manipulator velocity is reduced by the effects of the underwater environment, it is normal to observe a decrease in the drift that occurs in yaw, pitch and roll compared with the case when no hydrodynamics are considered. The effects of the added mass will create coupling effects between the degrees-of-freedom of the vehicle.

Taking into account the distance travelled by the rigid-body in order to compute the added mass and drag coefficients has the advantage of creating a realistic approximation of these effects but it has the disadvantage of being time consuming. Computing the distance of the end-tip of each link at every time step can be computationally expensive, slowing the process. Moreover, the added mass and drag coefficients have to be computed for all linear and angular components.

Modelling the hydrodynamic effects is challenging due to the uncertainties in the underwater environment as well as the complicated shape of the system. Approximating the rigid bodies by known geometrical shapes creates uncertainties with respect to the model that can be avoided if identification methods are used for determining the hydrodynamic coefficients. A specialised experimental facility would be needed to practically determine these coefficients. If this is not available, mathematical approaches can be combined to compute them as accurately as possible.

C. *PILIM controller*

Using a PID controller for each link of the manipulator and the PILIM controller for the vehicle, permits reasonable control of the UVMS and will reduce the coupling effects between the two subsystems. As mentioned previously, the pitch-DOF was the most affected by the movement of the manipulator. Using the PILIM controller based on the knowledge of these disturbances will cause a drift in position for pitch of only 3 degrees, while the roll/yaw are less than 0.5 degrees, as seen in Figure 6. With this case it can be concluded that in order to obtain the desired results, control for the vehicle is needed as well as control for the manipulator. Although the controller proposed here is a basic controller, the results show the potential of adding a compensation component for all DOFs of the UVMS system. Further research will aim to develop advanced controllers that will make the system robust.

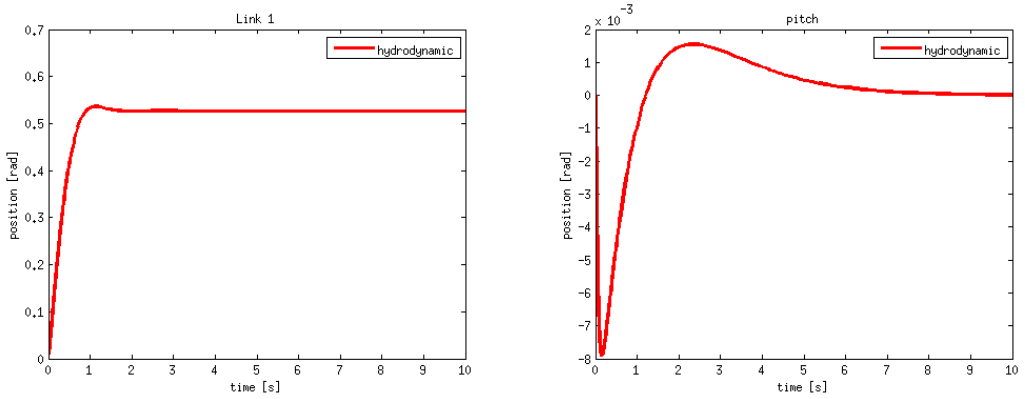

Figure 6. Position of first link and pitch, with PID controller for manipulator and PILIM controller for vehicle

IV. Conclusion

In this work a lighweight vehicle-manipulator system based on the single-chain system representation, dynamic and hydrodynamic effects was analysed. The dynamic model provides an insight into the subsystem coupling effects. Analysing the obtained results it has been shown that the movement of the manipulator will affect the vehicle motion, the pitch angle being the most influenced. Having a clear understanding of the interactions between the vehicle and the manipulator will help deciding the appropriate control architecture for the UVMS. The challenge of this work was to obtain a correct representation of the system, especially in the design of the vehicle as an additional link of the manipulator and the modelling of the hydrodynamic effects. Although the results were satisfactory a more robust control architecture is aimed to be implemented in the future work.

Acknowledgement

The authors would like to thank and acknowledge the financial support provided for this research by the Energy Technology Partnership program Scotland and SeeByte Ltd.

References

[1] G. Antonelli and S. Chiaverini. Task-priority redundancy resolution for underwater vehicle-manipulator systems. In *Robotics and Automation, 1998. Proceedings. 1998 IEEE International Conference on*, volume 1, pages 768–773, May 1998.

[2] G. Antonelli, S. Chiaverini, and N. Sarkar. External force control for underwater vehicle-manipulator systems. *Robotics and Automation, IEEE Transactions on*, 17(6):931–938, Dec 2001.

[3] P. Bellec. *Simulation of the six-degree-of-freedom motion of a remotely-controlled unmanned submersible*. PhD thesis, Electrical and Electronic Engineering, Heriot-Watt University, 1980.

[4] M.W. Dunnigan and G. Russell. Evaluation and reduction of the dynamic coupling between a manipulator and an underwater vehicle. *Oceanic Engineering, IEEE Journal of*, 23(3):260–273, Jul 1998.

[5] M.W. Dunnigan and G.T. Russell. Reduction of the dynamic coupling between a manipulator and rov using variable structure control. In *Control, 1994. Control '94. International Conference on*, volume 2, pages 1578–1583 vol.2, March 1994.

[6] R. Featherstone. *Rigid Body Dynamics Algorithms*. Springer-Verlag New York, Inc., Secaucus, NJ, USA, 2007.

[7] T.I. Fossen. Adaptive macro-micro control of nonlinear underwater robotic systems. In *Advanced Robotics, 1991. 'Robots in Unstructured Environments', 91 ICAR., Fifth International Conference on*, pages 1569–1572, June 1991.

[8] Y. Guo, G. Xu, X. Xiang, and Z. Xiao. A new motion control scheme for underwater vehicle-manipulator systems. In *Proceedings of the 13th IASTED International Conference on Robotics and Applications*, RA '07, pages 52–57, 2007.

[9] J. Han and W.K. Chung. Coordinated motion control of underwater vehicle-manipulator system with minimizing restoring moments. In *Intelligent Robots and Systems, 2008. IROS 2008. IEEE/RSJ International Conference on*, pages 3158–3163, Sept 2008.

[10] M.K Hosseini, A. Omidi, O. Meghdari, and G. Vossoughi. A composite rigid body algorithm for modeling and simulation of an underwater vehicle equipped with manipulator arms. *Journal of Offshore Mechanics and Arctic Engineering*, 128(2):119–132, 2005.

[11] J. Kim, W. Chung, and J. Yuh. Dynamic analysis and two-time scale control for underwater vehicle-manipulator systems. In *Intelligent Robots and Systems, 2003. (IROS 2003). Proceedings. 2003 IEEE/RSJ International Conference on*, volume 1, pages 577–582, Oct 2003.

[12] O. Korkmaz, S.K. Ider, and M.K. Ozgoren. Control of an underactuated underwater vehicle manipulator system in the presence of parametric uncertainty and disturbance. In *American Control Conference (ACC), 2013*, pages 578–584, June 2013.

[13] K.N. Leabourne and S.M. Rock. Model development of an underwater manipulator for coordinated arm-vehicle control. In *OCEANS '98 Conference Proceedings*, volume 2, pages 941–946 vol.2, Sep 1998.

[14] B. Lynch and A. Ellery. Efficient control of an auv-manipulator system: An application for the exploration of europa. volume PP, pages 1–19, 2013.

[15] T. W. McLain, S.M. Rock, and M.J. Lee. Experiments in the coordinated control of an underwater arm/vehicle system. *Autonomous Robots*, 3(2-3):213–232, 1996.

[16] E. Olguin-Diaz, G. Arechavaleta, G. Jarquin, and V. Parra-Vega. A passivity based model free force motion control of underwater vehicle manipulator systems. *Robotics, IEEE Transactions on*, 29(6):1469–1484, Dec 2013.

[17] J.H. Ryu, D.S Kwon, and P.M. Lee. Control of underwater manipulators mounted on an rov using base force information. In *Robotics and Automation, 2001. Proceedings 2001 ICRA. IEEE International Conference on*, volume 4, pages 3238–3243 vol.4, 2001.

Available online at www.sciencedirect.com

ScienceDirect

IFAC Papers Online
CONFERENCE PAPER ARCHIVE

IFAC-PapersOnLine 48-2 (2015) 044–049

Reduction of the dynamic coupling in an underwater vehicle-manipulator system using an inverse dynamic model approach

Corina Barbălată Matthew W. Dunnigan Yvan Pétillot

Ocean Systems Laboratory, School of Engineering & Physical Sciences, Heriot-Watt University, EH14 4AS, Edinburgh, UK (email: cb237@hw.ac.uk).

Abstract: This paper proposes a control strategy for station keeping of an underwater vehicle-manipulator system when the manipulator is asked to perform a certain task. The control structure consists of an inverse dynamic feedforward controller, the interaction forces between subsystems and a PILIM feedback controller for pitch control of the vehicle. The UVMS includes a 6-DOF vehicle and a 3-link manipulator, where the manipulator has a significant mass compared to the vehicle. The equations of motion are based on a tree representation of the UVMS and are described with the Newton-Euler algorithm. Hydrodynamic effects and friction considerations are taken into account in the forward dynamic model, while in the inverse dynamic model they are ignored. Simulation results show the validity of the inverse dynamic model approach without perfect knowledge of the system for station keeping of the vehicle. A key contribution of the study is that it is based on a lightweight underwater system. The main problem addressed in this paper is the station keeping of an underwater vehicle when the attached manipulator is moving. It is demonstrated that an inverse dynamic model used as a feedforward controller is a viable solution in the presence of system uncertainties.

Keywords: underwater vehicles, manipulators, modeling, dynamic coupling, inverse dynamics, PILIM control.

1. INTRODUCTION

The interest in underwater vehicle-manipulator systems has increased over the past years due to the need for interaction in underwater environments. More recently, robots have been deployed to inspect and collect information for the oil and gas industry, military purposes and biological/geological studies. Manipulation in underwater environments is the next step that allows faster and safer development of oil and gas sites, disposal of mines or geological data collection. Technological development has led to lighter and more compact underwater robots. Integrating a manipulator on such a robot may perturb the system if appropriate control methods are not developed. These types of systems are referred to as lightweight underwater-vehicle manipulator systems (UVMS).

To reduce time and cost for analyzing the lightweight UVMS, the system can be defined through the equations of motion. The UVMS can be described through a single chain representation as presented by Antonelli and Chiaverini (1998b) or as two independent systems, Kim et al. (2003). The equations of motion have to represent as closely as possible the real system. Fossen (1991) considered the UVMS as a macro-micro manipulator and developed the equations of motion based on the Newton-Euler algorithm. A similar approach was used by Antonelli and Chiaverini (1998b) to represent the UVMS. The goal of the paper was to develop a control architecture for redundant systems based on the inverse kinematics. The Euler-Lagrange method for system representation has also been used extensively. Olguin-Diaz et al. (2013) used this method to develop a force/position control scheme for a UVMS. A modified version of the Euler-Lagrange algorithm, the Quasi-Lagrange algorithm was used by Sarkar and Podder (2001) to obtain the trajectories of the manipulator and vehicle using a minimum hydrodynamic drag. In the Quasi-Lagrange approach the equations of motion are presented in the body-fixed frame. This representation is considered advantageous due to the fact that it matches the information from the on-board sensors.

Using the model of the system, studies of the interaction of the manipulator on the position keeping of the vehicle was performed by Dunnigan and Russell (1998). The study established the most affected DOF and proposed a control method for this specific DOF. McLain et al. (1996) analyzed the coupling effects based on a real system consisting of the OTTER AUV and a single link manipulator attached to the vehicle. The paper presented a coordinated control scheme for the vehicle-arm system and investigated the hydrodynamic effects of the UVMS. Studies on underwater vehicle-manipulator systems have been conducted previously e.g. Antonelli and Chiaverini (1998a); Antonelli et al. (1999, 2001). However, in all the cases the dry mass of the vehicle is considerably larger than the mass of the manipulator and no conclusions about the interaction between subsystems are stated. The inverse dynamic model is considered as an inverse problem where the model of the robot is known and can be used to

10.1016/j.ifacol.2015.06.008

determine the joint torques and vehicle forces when the desired position, velocity and acceleration are known. The model can be used either as a linearizaion technique for nonlinear systems or as part of the controller for motion control. The model based controller can improve the performances of the classical control strategies by reducing the tracking error. Morales and Carelli (2003) and Piltan et al. (2012) used the inverse dynamic model to linearize a second order system. To control the motion of the manipulator a feedback controller was used. Simulation results with a 3-link manipulator showed reliable results for the motion tracking. Boerlage et al. (2003) presented the inverse dynamic model as a feedforward controller. The authors proposed an analysis technique that relates the inverse dynamic model with a second order filter. Korkmaz et al. (2013) present a control method for the UVMS based on inverse dynamics. The interaction forces between the vehicle and manipulator are computed and used in the control law that aims to linearise the system. Simulation results show an improvement in the behavior of the system when the inverse dynamic model is used. The progress is due to a perfect knowledge of the system. Abdessemed (2012), Pott et al. (2011) stated that the inverse dynamic model is useful for performance improvement only in the case when full knowledge of the system is known.

In this work a method for reducing the coupling effects between the vehicle and manipulator is proposed. Using the Newton-Euler principle for modeling the system, the interactions between the manipulator and vehicle are highlited. A new control methodology is proposed for station keeping of the vehicle. The control incorporates the "inexact" inverse model as a feedforward controller and takes into account the coupling effects. The feedback part is present only for the DOFs that are significantly affected by the interactions.

The rest of the paper is structured as follows. In Section 2 the methodology to develop the simulation platform is presented. In Section 3 the control architecture for the vehicle is presented. In Section 4 results of the proposed controller are analysed. Section 5 presents the conclusions and future work for this research.

2. SYSTEM REPRESENTATION AND EQUATIONS OF MOTION

A simulation model for the UVMS is used to study the effects of the inverse dynamic model incorporated in the control strategy. The simulation model is composed of two parts: the kinematic representation and the equations of motion of the system. A single chain representation of the UVMS has been chosen. This means that the vehicle is considered as an extension of the manipulator. The links of the manipulator have a cylindrical shape, similar to the shape of the vehicle. Choosing a single chain representation of the UVMS is advantageous for producing a general model of the system: if any part of the system is changed, the equations do not have to be rewritten, they are recomputed automatically. Furthermore, the chain representation is useful for highlighting the interaction effects between subsystems. This chain representation, also called a "tree-representation" consists of nodes (the links) and arcs (the joints) of the system. The reference frame for each part of the system is placed at the center of mass. In Fig. 1 a sketch of the system is presented. The

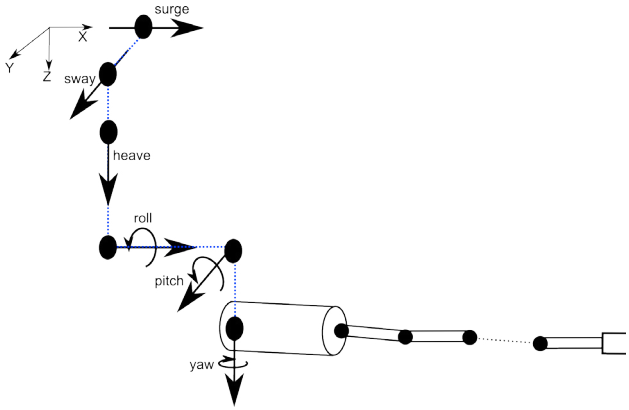

Fig. 1. Generic UVMS graph

vehicle is considered as a virtual 6-DOF joint, having the three translational movements of the real vehicle (surge, sway, heave) and the three rotational movements (roll, pitch, yaw). For simplification of the kinematic problem, the virtual 6-DOF joint can be decomposed into six independent joints with zero mass. The connection between the first joint of the manipulator and last DOF of the vehicle is represented through a node that preserves the characteristics of the vehicle: mass, length, radius. These assumptions lead to the representation of the UVMS as a manipulator.

The dynamic model of the UVMS is described through a matrix representation shown in 1.

$$M(q)\dot{\zeta} + C(\zeta, q)\zeta + D(\zeta, q) + g(\eta) = \tau \qquad (1)$$

where M is the inertia matrix, C is the Coriolis and Centripetal matrix, both consisting of rigid body terms and added mass terms, D is the damping matrix and g represents the restoring forces. τ are the forces applied to the overall system. The hydrodynamic terms are modeled based on the research of McLain et al. (1996) with a few other characteristics taken into account. The added mass terms can be related to the distance travelled by the links of the manipulator and by the shape of the body. By studying these effects a spline model can be used to develop these hydrodynamic effects. The moment integral along the length of the rigid body has to be performed to compute the hydrodynamic drag. For calculating the drag coefficients, the shape of the body, the Reynolds number and the distance traveled by the body are considered. Furthermore, it was observed by Leabourne and Rock (1998) that the position of the consecutive rigid bodies alters the effects of the underwater environment. The effect produced on the system is called the "shadowing-effect" and it was considered in the hydrodynamic model. A detailed description of the dynamic and hydrodynamic model can be found in Barbălată et al. (2014).

3. CONTROL STRATEGY

The movement of the manipulator has a significant effect on the position keeping ability of the lightweight vehicle. Developing a control strategy for reducing the coupling effects is of interest in this paper. The control method

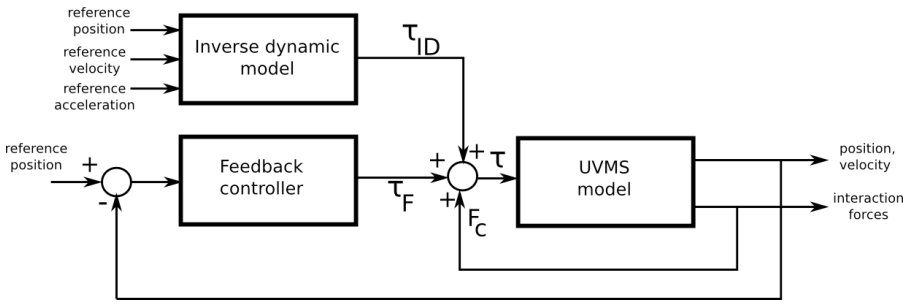

Fig. 2. Controller model

consists of the inverse dynamic model as a feedforward control, a PILIM controller as a pitch feedback control and the coupling effects between subsystems.

3.1 PILIM controller

To develop the feedback control for the UVMS, it is assumed that the vehicle moves at low speed and the system can be controlled independently for each DOF. The Proportional-Integral Limited (PILIM) controller is used for the pitch DOF due to its simplicity and for the capability of providing fast transient response with no overshoot. The controller is characterized by two control loops, one for position control, containing a proportional controller and another control loop for velocity control, defined by a proportional-integral controller. The system includes integrator anti-windup that is responsible for eliminating the overshoot in the case of control saturation. The first usage of this controller was proposed by Bellec (1980) and can be represented as seen in Fig. 3. The equations characterizing the system are presented in 2.

$$\begin{aligned} e_p &= p - p_{des} \\ e_v &= v - \tau_p \\ \tau_p &= K_{p_p} e_p \\ \tau_F &= K_{p_v} e_v + K_{i_v} \int_0^t e_v \end{aligned} \tag{2}$$

where p represents the position of the system, v is the velocity of the robot, p_{des} is the desired position, e_p is the error in position, e_v is the error in velocity, τ_p is the force generated by the position controller, τ_F is the force acting on the system, K_{p_p} is the position proportional gain, K_{p_v} is the velocity proportional gain and K_{i_v} is the velocity integral gain. In the case of the vehicle being close to the goal, the system is under position control, while if the distance from the goal is large then the vehicle is under velocity control.

3.2 Feedforward control

The inverse dynamic (ID) model is used to compute the forces acting on a system when a certain acceleration is given. These forces are taken into account for position keeping of the underwater vehicle. One of the simplest and most efficient methods for computing the forces acting on the system is the recursive Newton-Euler algorithm. It has to be highlighted that for the ID model, hydrodynamic effects and friction forces are not taken into account. The equations used are based only on the rigid bodies characteristics. Due to single-chain representation, the NE algorithm can be used for both the vehicle and manipulator. Starting from the base to the last link of the rigid body, the velocity, acceleration and force of each link are computed. The feedforward torque/force can be computed based on the Newton-Euler equations and rewritten in a matrix form as (3).

$$\tau_{ID} = M(q_d)\ddot{q}_d + C(\dot{q}_d, q_d)q_d \tag{3}$$

where q_d, $\dot{q}_d$, $\ddot{q}_d$ represent the desired positions, velocities and accelerations of the system.

Having a clear knowledge of the interaction forces can be beneficial in order to maintain the station keeping of the vehicle under the effect of disturbances from both the manipulator and underwater environment. In the case of the lightweight vehicle-manipulator system, the force that the manipulator exerts on the vehicle F_C, can be considered in the command applied to the system. Knowing which degree-of-freedom of the vehicle is the most affected by the movement of the manipulator can be beneficial. If the influence of the manipulator on the vehicle is significant, the ID model used as a feedforward controller might not be enough to remove these disturbances. To achieve optimal vehicle position keeping a feedback controller is needed to eliminate error accumulation on these specific DOFs, marked with x. Taking this into account, the control command can be represented by 4.

$$\tau_i = \begin{cases} \tau_{ID_i} + \tau_{F_i} + F_{C_i} & \text{if } i = x \\ \tau_{ID_i} + F_{C_i} & \text{otherwise} \end{cases} \tag{4}$$

where i is the DOF to be controlled, τ_i is the command torque/force, τ_{F_i} is the force/torque from the feedback controller, τ_{ID_i} is the force/torque from the feedforward component and F_{C_i} represents the interaction force acting on the i-th DOF.

4. SIMULATION RESULTS

The system that is simulated for studying the effects of the inverse dynamic model consists of a cylindrical shape vehicle and a three-link manipulator with revolute joints. The following assumptions are made:

- Fluid velocity is considered zero.
- The vehicle is only included in station keeping tasks.
- The vehicle has three planes of symmetry.
- The pitch DOF is the most affected by manipulator movement.
- No hydrodynamic/friction effects are taken into account in the inverse-dynamic model.

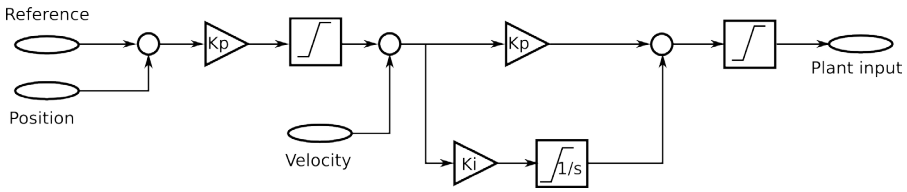

Fig. 3. Schematic PILIM compensator, Bellec (1980)

The first group of tests is performed considering the desired trajectory for the first link of the manipulator as a cycloidal function.

PID feedback controllers for all links of manipulator are used and no feedback controllers are applied for the rest of the degrees-of-freedom of the UVMS. The inverse dynamic (ID) model is present for all DOFs. It is observed from Fig. 4 that the coupling effects between the links of the manipulator are reduced to 0.8° when the ID and the interaction forces are used in the control structure. When only feedback controllers are incorporated the error is 2.3°. These results can be explained by the fact that the ID introduces torques in the forward dynamic model of the links. These will compensate for the movement of the first link. Not only the coupling effects between the links of

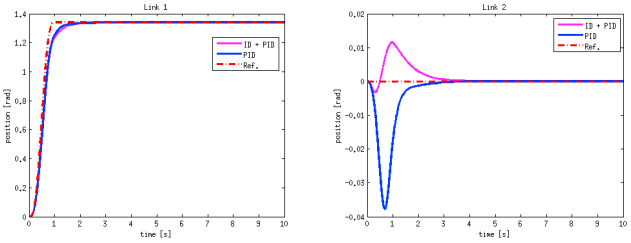

Fig. 4. Position of manipulators links, with PID feedback controller and ID feedforward controller for cycloidal desired trajectory

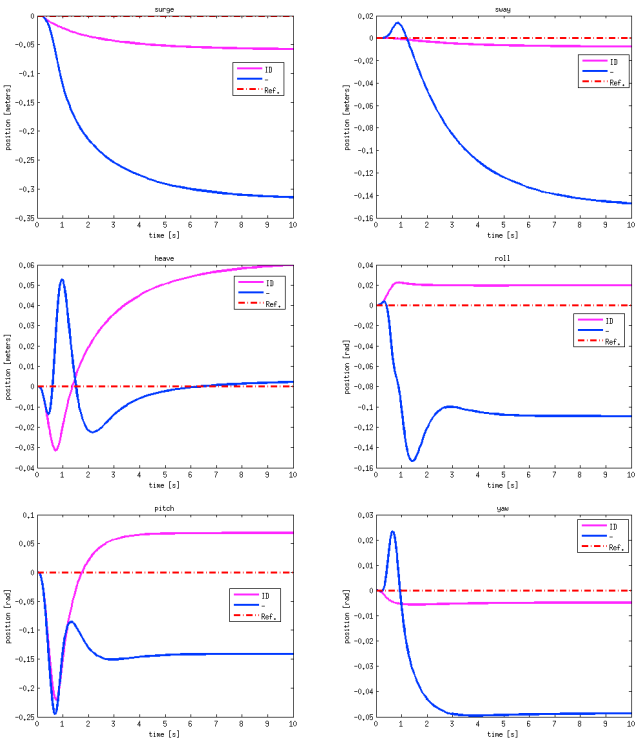

Fig. 5. Coupling effects on the vehicle caused by a cycloid movement of the manipulator when inverse dynamic model and coupling effects are used for the control

manipulator are reduced using the inverse model and the interaction forces, but also the effects of the manipulator movement on the vehicle can be reduced, as seen in Fig. 5. In this case cycloidal movements of all the links of the manipulator are considered. In the simulation results, a comparison between the feedforward controller and no control on all DOFs of the vehicle is presented. The most affected DOF is the pitch of the vehicle. The peak of the pitch displacement is in both cases around 14°. It can be seen that using the ID and the interaction forces computed from the forward dynamic model reduces the coupling to a constant offset value of 2.9°, compared to 8.6° when no control is used. Furthermore, a drift in the x-direction of 0.3 meters in 6 seconds is reduced to less than 0.02 meters displacement. The only DOF for which the feedforward controller cannot compensate is the heave. The center of gravity and center of buoyancy are not aligned and without taking this fact into account in the inverse dynamic model it is not possible to compensate for the error in depth. In Fig. 6 the error in pitch is presented when no control is used, when ID and coupling effects are used and when feedback is added. As mentioned previously the pitch is the most affected DOF of the vehicle. Although the use of the ID model improves the coupling effects, a high peak can be observed when the manipulator reaches the desired position. To reduce these effects, the PILIM controller is a valid solution. A drift in position for pitch of less than 0.6° can be achieved using the feedback and feedforward controller. A second

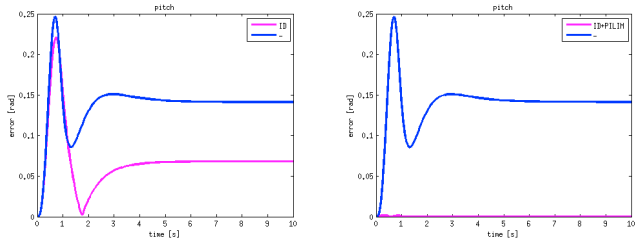

Fig. 6. Error in pitch position when cycloidal movement performed by manipulator

trajectory movement of the manipulator is represented by a sinusoidal function, Fig. 7. In this case, all three links of the manipulator are considered to move. Similar observations can be made as previously mentioned. The effects of the manipulator on the vehicle follow the pattern

of the manipulator movement, that is the pitch has a sinusoidal behavior. In this case the amplitude of the manipulator joints movement is equivalent to 30°. This will create an error of 5.7° on the pitch DOF when no control for station keeping is used. Nevertheless, using the inverse dynamic model for all DOFs and the PILIM control for the pitch of the vehicle, the vehicle is capable of achieving station keeping, the error in pitch being less than 1°. In

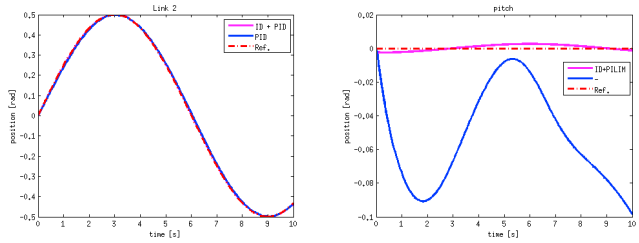

Fig. 7. Sinusoidal trajectory for manipulator and effects on pitch angle

Fig. 8, the error plots for the first link of the manipulator and for the yaw DOF are presented. The effects of the manipulator movement on the yaw are not as significant as the effects on the pitch. In this case, no feeedback control is needed to reduce the coupling effects. The use of the "inexact" inverse dynamic model reduces the coupling effects between subsystems.

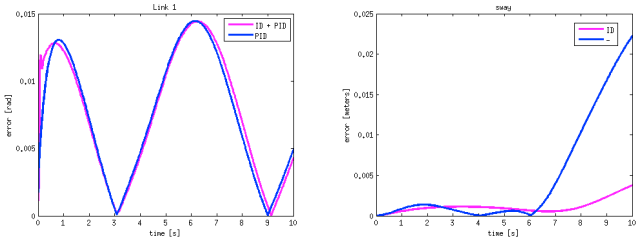

Fig. 8. Error in manipulator and yaw position, when sinusoidal movement of the manipulator

The literature presents the inverse dynamic model as a computed-torque controller in Middletone and Goodwin (1986). An experimental evaluation was performed by An et al. (1986), where the authors state that in the presence of perfect knowledge of the model of the system, there is no significant difference in using the ID as a feedforward or as a computed-torque controller. In this paper experiments with the proposed formulation of the ID as a computed-torque controller are performed. It has to be highlighted that the ID model takes into account only the characteristics of the the rigid body of the UVMS, ignoring the added mass, the hydrodynamic effects and the restoring forces. In this case as can be seen from the simulation results, Fig. 9, the behavior of the system is not improved as the incomplete model of the ID introduces disturbances to the system. Represented by the `magenta` colour the computed torque controller is not able to reduce the coupling between the subsystems. When the first link of the manipulator is moved, effects can be seen on the other links of the manipulator as well as on the station keeping of the vehicle. Moreover, the computed-torque controller increases the computation time, slowing down the system. On the other hand, as was already shown, the ID feedforward control, represented by `blue` colour, improves the behaviour of the system in the case when uncertainties are present.

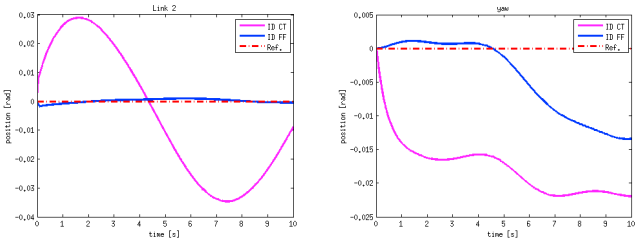

Fig. 9. Comparison between feedforward and computed torque

To analyze the performance of the proposed controller the Generalized Root Mean Squared Error is used. The error has been computed separately for the transnational and rotational DOFs of the system. The error in table 1 represents the mean error over a set of 20 different experiments. For 10 experiments, cycloidal movement of the manipulator was considered, each of the simulations having a different final value. The desired position of the manipulator is in the range 10° to 120°. For the rest of the experiments, sinusoidal functions were used with different amplitudes and frequencies. The overall error of the system is reduced in the case when the inverse dynamic model is used as a feedforward controller. Using the PILIM controller for pitch reduces the rotational error for the UVMS. Furthermore, comparing the results of the inverse dynamic model used as a computed torque controller (ID CT) with the results of the inverse dynamic used as a feedforward controller (ID FF) it can be observed that the system performs better in the second case, reducing both the rotational and translational errors.

Table 1. Generalized Root Mean Square Error

	Translation (m)	Rotation (rad)
No control	0.0639	0.1775
ID FF/Coupling	0.0241	0.1583
ID FF/Coupling/PILIM	0.0241	0.1027
ID CT	0.0421	0.1602

The conclusion that can be drawn from these simulations is that the influence between subsystems can be reduced taking into account the coupling effects from the forward-dynamic model and a feedforward controller based on the inverse dynamic model. The inverse dynamic model, takes into account only the characteristics of the rigid-body system, without the hydrodynamic effects. In the literature, it is presented that the inverse dynamic model is useful only if there are no uncertainties in the model and the system is perfectly known. Based on the simulations presented in this paper, it can be stated that an inverse dynamic model with uncertainties can be beneficial, if the goal is to improve coupling effects without using a feedback controller.

5. CONCLUSIONS

In this work a control strategy for station keeping of a lightweight vehicle-manipulator systems is proposed. Having an insight into the coupling effects between the subsystems, it is shown that the movement of the manipulator affects the vehicle position, especially the pitch angle. To reduce these influences for vehicle station keeping, an inverse dynamic feedforward controller is proposed in this work. Without having an exact knowledge of the system a feedforward controller is beneficial for reducing the interaction between subsystems. Moreover, the knowledge of the forces acting on each subsystem is incorporated into the control strategy. In the case when the influence of the manipulator movement highly affects the position keeping of the robot, a feedback PILIM controller is proposed for reducing the coupling effects. The simulation results have shown positive results and have demonstrated that even without having perfect knowledge of the system, the inverse dynamic model can be useful for control purposes. The next step for this research is to present an "inexact" inverse dynamic model that can be beneficial for both station keeping and trajectory tracking of the underwater-vehicle manipulator systems.

ACKNOWLEDGEMENTS

The authors would like to thank and acknowledge the financial support provided for this research by the Energy Technology Partnership program Scotland and SeeByte Ltd.

REFERENCES

Abdessemed, F. (2012). Svm-based control system for a robot manipulator. *International Journal of Advance Robotic Systems*, 9(247).

An, C., Atkeson, C., and Hollerbach, J. (1986). Experimental determination of the effect of feedforward control on trajectory tracking errors. In *Robotics and Automation. Proceedings. 1986 IEEE International Conference on*, volume 3, 55–60.

Antonelli, G., Caccavale, F., and Chiaverini, S. (1999). A modular scheme for adaptive control of underwater vehicle-manipulator systems. In *American Control Conference, 1999. Proceedings of the 1999*, volume 5, 3008–3012.

Antonelli, G. and Chiaverini, S. (1998a). Singularity-free regulation of underwater vehicle-manipulator systems. In *American Control Conference, 1998. Proceedings of the 1998*, volume 1, 399–403 vol.1.

Antonelli, G. and Chiaverini, S. (1998b). Task-priority redundancy resolution for underwater vehicle-manipulator systems. In *Robotics and Automation, 1998. Proceedings. 1998 IEEE International Conference on*, volume 1, 768–773.

Antonelli, G., Chiaverini, S., and Sarkar, N. (2001). External force control for underwater vehicle-manipulator systems. *Robotics and Automation, IEEE Transactions on*, 17(6), 931–938.

Barbălată, C., Dunnigan, M., and Pétillot, Y. (2014). Dynamic coupling and control issues for a lightweight underwater vehicle manipulator system. In *Proceedings of IEEE Oceans - St. John's Canada*.

Bellec, P. (1980). *Simulation of the six-degree-of-freedom motion of a remotely-controlled unmanned submersible*. Ph.D. thesis, Electrical and Electronic Engineering, Heriot-Watt University.

Boerlage, M., Steinbuch, M., Lambrechts, P., and van de Wal, M. (2003). Model-based feedforward for motion systems. In *Control Applications, 2003. CCA 2003. Proceedings of 2003 IEEE Conference on*, volume 2, 1158–1163 vol.2.

Dunnigan, M. and Russell, G. (1998). Evaluation and reduction of the dynamic coupling between a manipulator and an underwater vehicle. *Oceanic Engineering, IEEE Journal of*, 23(3), 260–273.

Fossen, T. (1991). Adaptive macro-micro control of nonlinear underwater robotic systems. In *Advanced Robotics, 1991. 'Robots in Unstructured Environments', 91 ICAR., Fifth International Conference on*, 1569–1572.

Kim, J., Chung, W., and Yuh, J. (2003). Dynamic analysis and two-time scale control for underwater vehicle-manipulator systems. In *Intelligent Robots and Systems, 2003. (IROS 2003). Proceedings. 2003 IEEE/RSJ International Conference on*, volume 1, 577–582.

Korkmaz, O., Ider, S., and Ozgoren, M. (2013). Control of an underactuated underwater vehicle manipulator system in the presence of parametric uncertainty and disturbance. In *American Control Conference (ACC), 2013*, 578–584.

Leabourne, K. and Rock, S. (1998). Model development of an underwater manipulator for coordinated arm-vehicle control. In *OCEANS '98 Conference Proceedings*, volume 2, 941–946 vol.2.

McLain, T.W., Rock, S., and Lee, M. (1996). Experiments in the coordinated control of an underwater arm/vehicle system. *Autonomous Robots*, 3(2-3), 213–232.

Middletone, R. and Goodwin, G. (1986). Adaptive computed torque control for rigid link manipulators. In *Decision and Control, 1986 25th IEEE Conference on*, 68–73.

Morales, B. and Carelli, R. (2003). Robot control with dynamics and non-linear gains. *Latin American Applied Research*, 3(11), 393–397.

Olguin-Diaz, E., Arechavaleta, G., Jarquin, G., and Parra-Vega, V. (2013). A passivity based model free force motion control of underwater vehicle manipulator systems. *Robotics, IEEE Transactions on*, 29(6), 1469–1484.

Piltan, F., Keshavarz, M., Badri, A., and Zarzari, A. (2012). Design novel nonlineat controller applied to robot manipulator: Design new feedback linearization fuzzy controller with minimum rule base tuninng method. *International Journal of Robotics and Automation*, 3, 1–12.

Pott, P.P., Wagner, A., Badreddin, E., Weiser, H.P., and Schwarz, M. (2011). Inverse dynamic model and a control application of a novel 6-dof hybrid kinematics manipulator. *Journal of Intelligent and Robotics Systems*, 63(1), 3–23.

Sarkar, N. and Podder, T. (2001). Coordinated motion planning and control of autonomous underwater vehicle-manipulator systems subject to drag optimization. *Oceanic Engineering, IEEE Journal of*, 26(2), 228–239.

2015 IEEE/RSJ International Conference on Intelligent Robots and Systems (IROS)
Congress Center Hamburg
Sept 28 - Oct 2, 2015. Hamburg, Germany

An Adaptive Controller for Autonomous Underwater Vehicles

Corina Barbălată, Valerio De Carolis, Matthew W. Dunnigan, Yvan Pétillot, David Lane

Abstract— **This paper introduces an adaptive tuning method for the controllers of a 4 degrees-of-freedom autonomous underwater vehicle. The proposed scheme consists of two control loops, one for position control and an inner one for velocity control. The gains of the controller are determined on-line, according to the position/velocity errors. Using the proposed adaptive architecture, the uncertainties in the parameters of the system are addressed and the system is able to operate when hydrodynamic disturbances are present. The complexity of the fixed gain tuning procedure is also greatly decreased for underwater vehicles when the algorithm suggested here is used. Experimental results with the Nessie VII AUV show that the adaptive controller is beneficial for underwater vehicles. Finally it is shown that the current approach reduces the energy consumption of the system.**

I. Introduction

The use of underwater vehicles is increasing constantly as they are needed for a wide variety of missions, such as the study of maritime environments, the inspection of oil and gas sites or for military applications. The control architecture is an important element in obtaining the desired behavior of the underwater vehicle. A stable system produces accurate navigation and improves the quality of the data gathering. The control schemes are based on the specific vehicle configuration and in most cases do not take into account the uncertainties present in the vehicle, such as changes in payload configuration or disturbances produced by the underwater environments. Manually tuned controllers are used regularly for underwater vehicles. The tuning is done considering the worst case scenario, leading to sub-optimal control and inefficient power consumption. Furthermore, in most cases the vehicle design tries to minimise the number of thrusters, producing highly coupled systems that are challenging to tune. Fixed gain controllers for underwater vehicles are difficult to tune and require knowledge of the vehicle coupling and underlying control. In operational experiments, often expert knowledge is not available and if the controller parameters cannot handle the changes in the environment or vehicle payload, it may lead to sub-optimal behavior or even vehicle failure.

In this paper, we propose the use of an auto-tuning scheme for underwater vehicles that constantly adapts the control parameters to the changes in the vehicle and environmental conditions, does not require an accurate model of the vehicle and is robust to unforeseen conditions. The proposed scheme converges rapidly at the start of the mission to stable parameters and adapts these during the mission.

C. Barbălată, V. De Carolis, M. W. Dunnigan, Y. Pétillot and D.M. Lane are with the Ocean Systems Laboratory at Heriot-Watt University, Edinburgh, Scotland, UK. {cb237, m.w.dunnigan, y.r.petillot, d.m.lane}@hw.ac.uk {valerio.decarolis}@ieee.org

II. Related Work

The advantage of adaptive control is that the model of the system does not need to be perfectly known and may change over time. Adaptive schemes might be applied either in the case when the model is given with some uncertainties [1] or in the case when the overall system model has to be approximated [2]. The latter case is complex and difficult to implement. In underwater environments, adaptive control has been used by Fossen [3]. The authors present an adaptive sliding mode controller for a 6-DOF underwater vehicle where uncertainties are present in the thruster allocation matrix. This controller is based on an on-line parameter estimation algorithm and a switch term to compensate for the uncertainties in the model. An adaptive sliding controller is presented in [4]. The paper presents the experimental setup and the method for adapting the controller parameters based on the dynamic model of the system. An adaptive model based controller is presented in [5]. In this paper, the authors propose a proportional-derivative controller with an adaptive compensation of the dynamics. Aguiar *et. al* [6] demonstrate how the adaptive switching supervisory control together with a Lyapunov-based control law solves unmodeled dynamics. In [7] the authors introduce the notion of sub-regions in order to control the vehicle. The control architecture is designed in the task space and two sub-regions are assigned. Adaptive learning is presented on a real vehicle in [8]. The learning of the dynamic model is used together with PID controllers. Wang *et al.* [9] propose an adaptive controller. The control scheme is composed of a PD feedback controller coupled with a neuro-fuzzy system trained to model the inverse dynamics of the AUV. The inverse dynamics is then used as a feedforward controller to compute the nominal torque of the AUV along a desired trajectory. The theory of adaptive interaction [10] introduces a method to describe a complex system as a composition of N subsystems, called devices, that are interconnected to each-other. Each device is described by its inputs x_n, outputs y_n and the relation with the neighbouring subsystems, that depends on an interaction weight α_c. The main problem is to determine the interaction weights based on the subsystems characteristics. The adaptive interaction theory can be applied to a closed-loop system for control purposes as presented in [11].

In this paper we propose the use of the subsystems interactions for the control of underwater vehicles. An adaptive PILIM (Proportional Integral Limited) controller is implemented for the first time in the pilot of an underwater vehicle and experiments in an indoor tank are presented. The adaption rule is applied for a coupled two-loop controller that

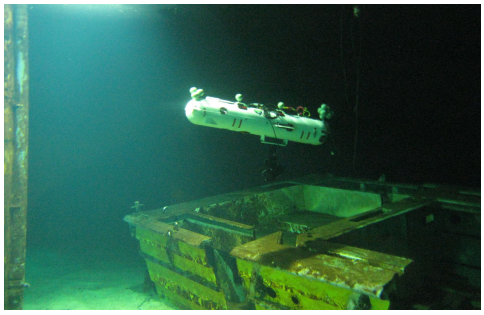

Fig. 1: Nessie VII AUV during an inspection task with sunken barge and human-made structures

regulates both position and velocity requests. The control strategy is powerful due to its simplicity, small convergence time and energy savings. The rest of the paper is structured as follows. In Section III the system used in this work is introduced. In Section IV the control architecture for the vehicle is presented. In Section V results of the proposed architecture are analysed. Section VI presents the conclusions and future work.

III. System description

The experimental setup is based on the Nessie VII, Figure 1, a hover-capable AUV developed in the Ocean Systems Laboratory. The vehicle is a torpedo-shape AUV with six brushless DC thrusters, each of them capable of producing up to 250 W of power. Nessie VII can be controlled in five degrees-of-freedom: surge, sway, heave, pitch and yaw. The natural frequency in roll/pitch for Nessie VII is approximately 0.3 Hz. During this work the pitch is uncontrolled as it is not required for the trajectories used in the experiments. The platform sensors used for navigation are a fiber optic gyroscope, a compass, a DVL and a pressure sensor. The dynamic model that describes the generic 6-DOF AUV is described by the equation of motion (1) as presented by Fossen [12]:

$$\begin{aligned} M(\nu)\dot{\nu} + C(\nu)\nu + D(\nu)\nu + g(\eta) &= \tau_F \\ \dot{\eta} &= J(\eta)\nu \end{aligned} \tag{1}$$

where ν is the body-fixed velocity, $J(\eta)$ is the 6×6 Jacobian transformation matrix relating the AUV coordinate system to the earth-fixed coordinate system. M is a 6×6 symmetric positive definite inertia matrix containing the rigid body terms as well as the added mass terms, C is a 6×6 matrix of Coriolis and centripetal terms, D is a 6×6 matrix of hydrodynamic damping terms, $g(\eta)$ represents the vector of restoring forces and moments and τ_F are the requested forces.

IV. Adaptive tuning controller

Based on the adaptive interaction theory, an on-line tuning algorithm for the gains of the PILIM controller is proposed in this paper. A decoupled off-line PILIM controller is presented in [13] and is described by:

$$\begin{aligned} e_p &= p_{des} - p \\ e_v &= \tau_p - v \\ \tau_p &= K_{P_p} e_p \\ \tau_F &= K_{P_v} e_v + K_{I_v} \int_0^t e_v \end{aligned} \tag{2}$$

where p and v represent the position and velocity of the system, p_{des} is the desired position, e_p is the error in position, e_v is the error in velocity, τ_p is the quasi-velocity generated by the position controller, τ_F is the force acting on the system, K_{p_p} is the position proportional gain, K_{p_v} is the velocity proportional gain and K_{I_v} is the velocity integral gain. The proposed architecture uses an independent PILIM controller for each degree-of-freedom. In the case when large errors occur, the limiter before the velocity controller requests the velocity to be regulated between $\pm V_{max}$, representing the maximum velocity that the vehicle can reach. Integrator anti-windup is used to eliminate the overshoot when saturation is present. This type of controller when arranged as a cascaded subsystem is advantageous over classical PID controller due to its ability to switch between operational modes.When the vehicle is close to the goal the system is under position control, while if the distance from the goal is large then the vehicle is under velocity control.

To apply the adaptive interaction theory for tuning the gains of the PILIM controller implemented on Nessie VII, the closed-loop system is divided into four independent subsystems. The proportional part of the position controller is considered as the first subsystem, the proportional part of the velocity controller is the second subsystem, the integral part of the velocity controller is the third subsystem and the dynamic model of the AUV is the fourth subsystem. For each subsystem, the inputs and outputs of each device are defined. As can be seen from Figure 2, the input for the position controller e_p represents the error in position and the output τ_p represents the quasi-velocity generated by the position controller. For the velocity controller, the output for the proportional component is τ_{P_v} describing the force generated by this component. For the integral part of the velocity controller the output τ_{I_v} represents the corresponding force. For both the proportional and integral parts of the velocity controller the input e_v describes the velocity error. The output of the fourth subsystem is the measured position p and velocity v of the vehicle. The input τ_F represents the total force of the PILIM controller. The gains of the controller represent the connections between subsystems and are marked as $\alpha_c = \{K_{P_p}, K_{P_v}, K_{I_v}\}$.

For each subsystem i, a predecessor $i - 1_c$ is defined as the subsystem whose output is transmitted through the connections c to the subsystem i. Similarly, the posterior $i + 1_c$ can be defined as the subsystem whose input is coming from subsystem i based on a connection c. Furthermore, the set of input connections $\mathcal{I}_i$ and the set of output connections $\mathcal{O}_i$ for a subsystem i are defined as all the connections that directly relate the predecessors/posteriors to the the

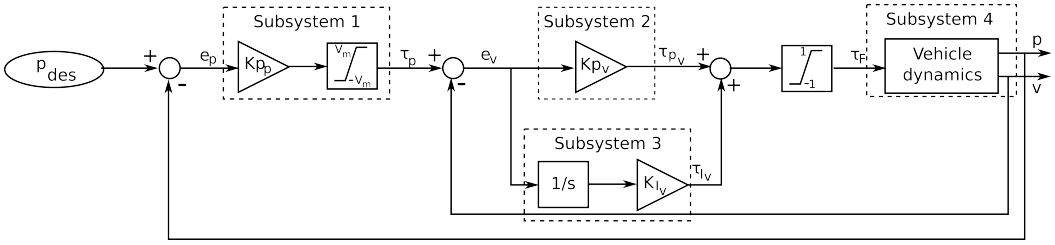

Fig. 2: Closed-loop system showing PILIM structure

subsystem i without any other influences. For the position controller, the posteriors $i+1_c$ are the proportional part of the velocity controller and the integral part of the velocity controller. The set of output connections for the posteriors $\mathcal{O}_{i+1_c}$ for the position controller is empty. This is because the output of the proportional part of the velocity controller and the integral part of the velocity controller are not direct inputs to the next subsystem, the dynamic model, but a relationship between them represents the input to the next system. For the velocity control the posterior $i+1_c$ is the dynamic model. Similar to the previous case, the set of output connections for the posteriors $\mathcal{O}_{i+1_c}$ of the velocity controller is empty. This is because the outputs of the dynamic model, the position and velocity, are not direct inputs to the other systems, but relationships between them and desired position/velocity represent the inputs.

Assuming that the interconnected subsystems can perfectly replicate the expected AUV behaviour, the goal that has to be achieved is to find the best connection weights for this assumption to be valid at any time. The problem of finding the gains of the system is reduced to a minimization problem, where a performance index E has to be defined. As the PILIM is a cascade controller two different performance indexes have to be defined:

$$\begin{aligned} E_p &= (p_{des} - p)^2 = e_p^2 \\ E_v &= (\tau_p - v)^2 = e_v^2 \end{aligned} \tag{3}$$

where E_p is the performance index for the position controller and E_v is the one for the velocity controller. According to [10], in a system where the input x_n is dependent on the output of other subystems y_{i-1_c} and an external signal u_n, the connection weights α_c are adapted based on the following theorem:

Theorem 1 *For the system with dynamics given by*

$$y_n = \mathcal{F}_n\left[x_n\right] = \mathcal{F}_n\left[u_n + \sum_{c \in I_n} \alpha_c y_{i-1_c}\right], \quad n \in \mathcal{N}$$

if connections weights α_c are adapted according to

$$\dot{\alpha_c} = \left(\sum_{s \in O_{i+1_c}} \frac{\frac{dE}{dy_{i+1_s}} \circ \mathcal{F}'_{i+1_s}[x_{i+1_s}]}{\frac{dE}{dy_{i+1_s}} \circ \mathcal{F}'_{i+1_s}[x_{i+1_s}] \circ y_{i+1_s}} \alpha_s \dot{\alpha}_s - \gamma \frac{\partial E}{\partial y_{i+1_c}} \right) \circ \mathcal{F}'_{i+1_c}[x_{i+1_c}] \circ y_{i-1_c}, \quad c \in C$$

and the above equation has a unique solution, then the performance index E will decrease monotonically with time.

In fact, the following is always satisfied

$$\dot{\alpha_c} = -\gamma \frac{\partial E}{\partial \alpha_c}, \quad c \in C$$

where $\gamma > 0$ is the adaption coefficient, $\mathcal{F}$ is the Fréchet derivative, x and y are the input and output of the subsystem and $\circ$ represents the mathematical composition function.

Based on the schematic representation and the fact that the sets of output connections are empty, the formulation of **Theorem 1** for the PILIM controller can be simplified as:

$$\dot{\alpha_c} = -\gamma \frac{\partial E}{\partial y_{i+1_c}} \circ \mathcal{F}'_{i+1_c}[x_{i+1_c}] \circ y_{i-1_c} \tag{4}$$

The PILIM gains are computed based on the corresponding performance function and taking into account the inputs and outputs of each component:

$$\begin{aligned} \dot{K}_{P_p} &= -\gamma \frac{\partial (p_{des} - p)^2}{\partial p} \circ \mathcal{F}'_p[\tau_F] \circ \tau_p \\ \dot{K}_{P_v} &= -\gamma \frac{\partial (\tau_p - v)^2}{\partial v} \circ \mathcal{F}'_v[\tau_F] \circ \tau_{P_v} \\ \dot{K}_{I_v} &= -\gamma \frac{\partial (\tau_p - v)^2}{\partial v} \circ \mathcal{F}'_v[\tau_F] \circ \tau_{I_v} \end{aligned} \tag{5}$$

After simplifications, the on-line tuning of the PILIM controller can be written as:

$$\begin{aligned} K_{P_p} &= 2\gamma \int (e_p \circ \mathcal{F}'_p[\tau_F] \circ \tau_p) dt \\ K_{P_v} &= 2\gamma \int (e_v \circ \mathcal{F}'_v[\tau_F] \circ \tau_{P_v}) dt \\ K_{I_v} &= 2\gamma \int (e_v \circ \mathcal{F}'_v[\tau_F] \circ \tau_{I_v}) dt \end{aligned} \tag{6}$$

where $\mathcal{F}'_p[\tau_F]$ and $\mathcal{F}'_v[\tau_F]$ represent the Jacobians of the relationships between the position and total force generated by the controllers ($\mathcal{F}_p[\tau_F]$) and the velocity and total force generated by the controllers ($\mathcal{F}_v[\tau_F]$) defined as:

$$\begin{aligned} \mathcal{F}_p[\tau_F] &= \int \int M(\nu)^{-1} \left(\tau_F - C(\nu)\nu - D(\nu)\nu - g(\eta)\right) \\ \mathcal{F}_v[\tau_F] &= \int M(\nu)^{-1} \left(\tau_F - C(\nu)\nu - D(\nu)\nu - g(\eta)\right) \end{aligned} \tag{7}$$

The adaption coefficient γ has the same value for all the components of the controller. The initial values set for the controller gains are zero.

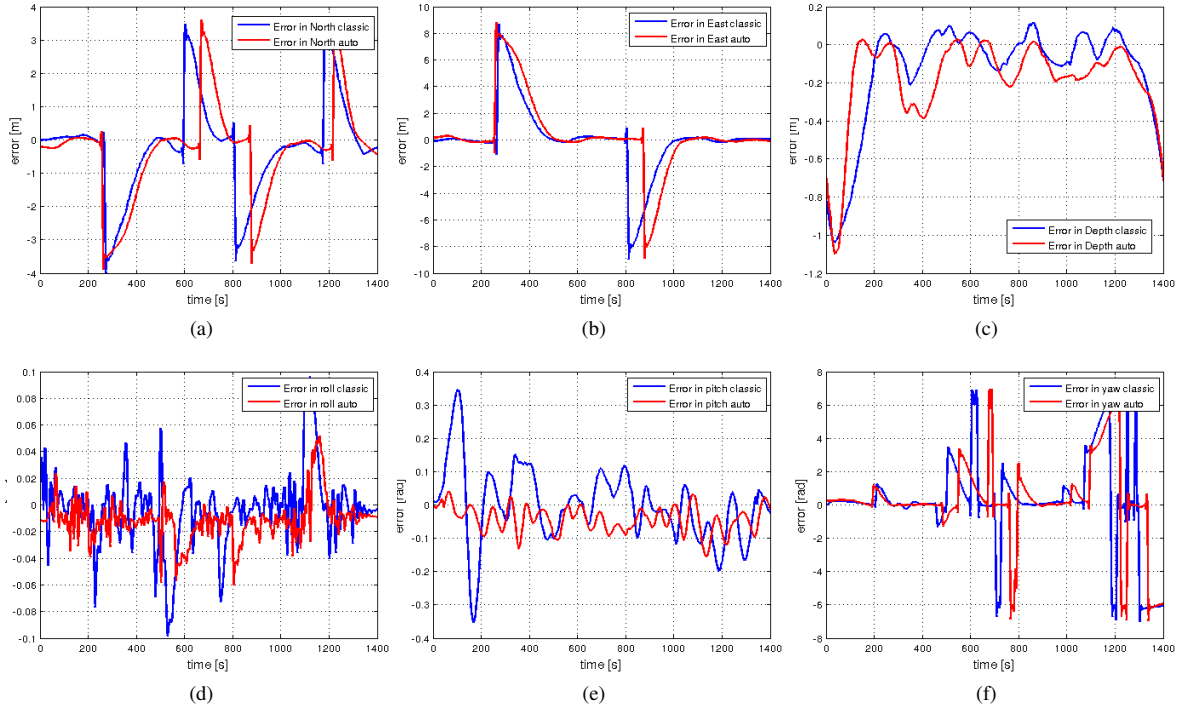

Fig. 4: Mean Error for the DOFs in reference coordinates for `lines` mode

V. Experimental results

The proposed architecture is evaluated in an indoor tank of $12 \times 10 \times 4$ meters under controlled conditions. The adaptive tuning method has been tested based on three navigation modes (`simple`, `lines`, `fast`) to evaluate the performances of the vehicle in different mission scenarios such as inspection and long-range navigation. The `simple` mode is a basic strategy that requires the vehicle to adjust its attitude as soon as the following waypoint is requested. The `lines` strategy is a line-of-sight navigation mode. The vehicle is requested to visit all the waypoints, travelling using only forward navigation that will force a rotation movement in order to face the next waypoint. The `fast` computes the next waypoint based on the requested target velocity and the time needed to reach this waypoints. This method does not produce precise navigation, but it reduces the energy consumption due to the small amount of time required to complete a trajectory. For each configuration the vehicle is requested to follow the trajectory shown in Figure 3, controlling only the surge, sway, heave and yaw degrees-of-freedom. Multiple tests are conducted and their results averaged for each navigation mode. In all these cases a consistent behaviour is observed. The proposed algorithm is advantageous over other methods that utilise adaptive tuning of PID controllers, presented in [14], [15], due to the fact that it does not require the knowledge of the approximate model of the system. Moreover, the simplicity of the tuning procedure is an important factor, requiring only a single parameter to be tuned. The first set of experiments are carried out in still water, while the second group of

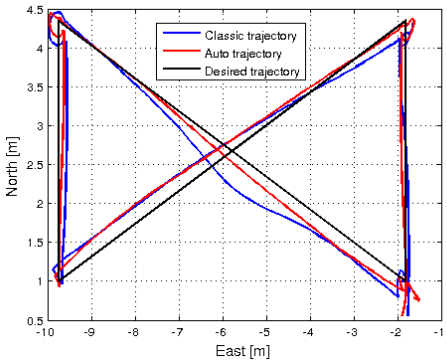

Fig. 3: Comparison of real trajectories using classical and adaptive PILIM architectures

experiments are under the effect of waves. In Figure 4, the mean error plots for each degree-of-freedom in reference coordinates for the `lines` mode are presented together with the performance of the classical control. This scheme makes use of the same PILIM architecture presented in Figure 2 with fixed gains. These off-line gains represent the best values that can be selected using a manual tuning procedure. These plots show that the adaptive tuning approach provides satisfactory results for the trajectory tracking performance of the vehicle and reduces the coupling effects between DOFs. This aspect is highlighted in Figure 4(d) and Figure 4(e) for the uncontrolled degrees-of-freedom. Disturbances are still present using the adaptive tuning for both pitch and roll but with a lower amplitude. Using the classical PILIM

controller, the vehicle has small displacements from the set point. This effect is reduced with the introduction of the adaptive PILIM controller. While operating in `lines` mode the most used DOFs are surge and yaw. The vehicle is required to adjust its orientation before navigating between consecutive waypoints. In Figure 4(a) four peaks can be seen representing an error of 3.5 m in the North direction, while in Figure 4(b) an error of 8 m can be seen in the East direction. This is when the vehicle is hovering at the current waypoint and the next navigation goal is requested. The error decreases until the vehicle reaches the next waypoint. For the yaw DOF, errors of about 180 degrees are observed during the moment the vehicle is requested to change its orientation and resume the navigation in the opposite direction. In this case the yaw error decreases in less than 10 seconds. During these tests no overshoot is observed. Analysing the overall navigation trajectory, as shown in Figure 3, it can be seen that both controllers perform in a similar way with the adaptive tuning offering a smoother trajectory. These aspects are observed for all the navigation modes used for these experiments.

$$GRMSE = \sqrt{\frac{1}{N}\sum_{k=1}^{N} e_k^2} \tag{8}$$

Results are supported also by the evaluation metric Generalized Root Mean Squared Error (GRMSE) in (8), as shown in Table I. N is the number of total measurements and e is the generalized error. The error has been computed separately for the translational (e_x, e_y, e_z) and rotational (e_ϕ, e_θ, e_ψ) DOFs of the system, (9) and independently for each navigation mode.

$$\begin{aligned} e_{pos} &= \sqrt{e_x^2 + e_y^2 + e_z^2} \\ e_{or} &= \sqrt{e_\phi^2 + e_\theta^2 + e_\psi^2} \end{aligned} \tag{9}$$

As can be seen from Table I the performances for both

TABLE I: Generalized Root Mean Square Error

Mode	Adaptive		Classic	
	Translation (m)	Rotation (rad)	Translation (m)	Rotation (rad)
`simple`	0.72	0.23	0.84	0.27
`lines`	0.28	0.32	0.63	0.62
`fast`	0.65	0.06	0.57	0.20

position and orientation are improved for all navigation trajectories. Noticeable changes in the behaviour of the system can be seen in the case of `lines` mode, the performances of the system being improved compared with the classical control. A lower improvement can be observed for the other two navigation trajectories. It can be said that having a more restrictive navigation trajectory that imposes a certain behaviour for each degree-of-freedom of the vehicle improves the performances of the system using the adaptive tuning. Analysing the control effort for the DOFs it can be observed that the forces required by the vehicle are dependent on the

TABLE II: Resource usage

Mode	Adaptive		Classic	
	Time (s)	Energy (Wh)	Time (s)	Energy (Wh)
`simple`	172.74	5.61	150.31	6.12
`lines`	147.12	2.84	113.11	3.81
`fast`	61.85	1.28	60.85	1.66

trajectory and the active DOF. As can be seen in Figure 6(a), the peaks in the force request correspond to the start of the navigation on a new trajectory leg. In the graphs the maximum requests using the adaptive tuning algorithm are considerably smaller, around 40 N, compared to the classical tuning, around 60 N. This characteristic influences the energy

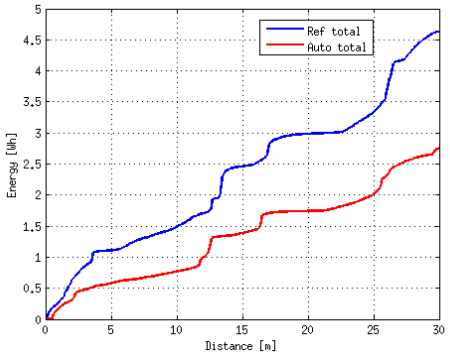

Fig. 5: Energy usage

consumption during the execution of the navigation task, as can be observed from Figure 5 where the total energy usage is presented. The resource consumption improves using the adaptive tuning algorithm due to the fact that the force required by the controller is dependent only on position errors. Not having a constant force that has to be produced by the thrusters also reduces the energy consumption. The results shown in Table II present the mean navigation time and energy consumption, over the group of experiments executed with the same mode. Despite an increase in the execution time the adaptive tuning has energy savings of at least 10% with respect to the classic case. Furthermore, the adaptive system is always operational and therefore is able to adapt to the environmental changes. Experiments are performed in the indoor tank where waves are produced, with a height of 0.5 meters and a frequency of 0.5 Hz, having a North orientation with respect to the world coordinates and facing the vehicle in surge direction. The vehicle is placed on the surface of the water and its task is to maintain the location. From Figure 7(a) a clear difference is observed between the cases when the waves are turned on and off. Due to the pattern of the waves the most affected degree-of-freedom for station keeping, in the presence of waves, is the z-axis. At the beginning of the experiment the waves are turned on establishing different controller efforts due to the adaptive scheme which alters the parameters of the controller to take into account the disturbances. In the second part of

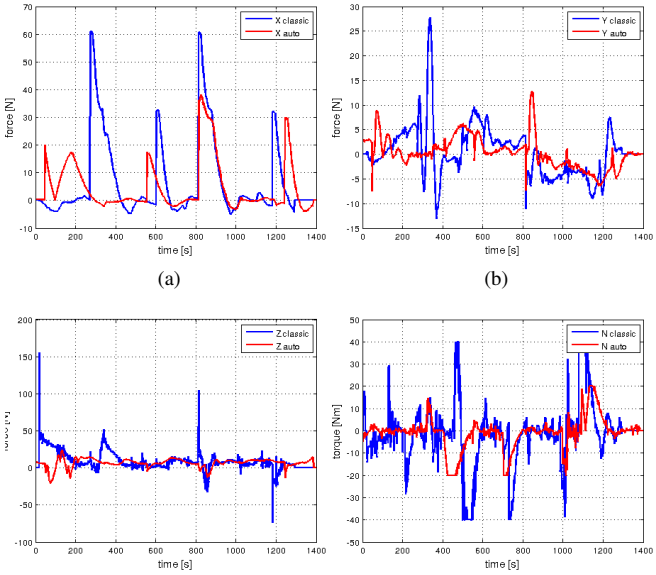

Fig. 6: Control effort

the experiment the waves are turned off and smaller changes can be seen in the controller effort as the disturbance is no longer present.

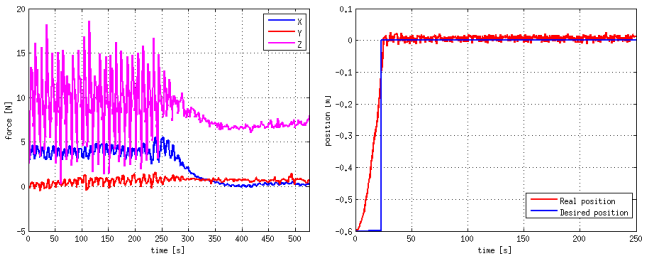

(a) Controller forces (b) Z-axis position

Fig. 7: System behavior in the presence of waves

VI. Conclusions

In this work an adaptive tuning scheme for the PILIM controller is presented. The main contributions of the work are applying the theory of adaptive interactions for the PILIM controller and using the adaptive tuning scheme in a real underwater system. It was demonstrated that the proposed controller performs better than the manually tuned controller. It avoids the use of an empirical tuning procedure, significantly reducing the time and complexity of the manual tuning and improves the performance of the system in terms of energy consumption. From the experiments it was seen that the time needed for the algorithm to converge to appropriate values for the gains is not significant and the vehicle is able to execute the missions without delays. Moreover, the adaptive algorithm is always running, able to adapt to the changing conditions of the underwater environment or changes in payload of the vehicle. Future work will focus on improving the vehicle pilot module by adding a decision component to select one of the two control schemes (classical controller or adaptive tuned controller) according to the needs of the current tasks.

VII. Acknowledgement

The authors would like to acknowledge the financial support provided by the ETP program Scotland, SeeByte Ltd. and European Union Seventh Framework Programme FP7/2007-2013 - Challenge 2 - Cognitive Systems, Interaction, Robotics - under grant agreement No 288273 - PANDORA.

References

[1] T. Fossen and S. I. Sagatun, "Adaptive control of nonlinear underwater robotic systems," in *Robotics and Automation, 1991. Proceedings., 1991 IEEE International Conference on*, Apr 1991, pp. 1687–1694 vol.2.

[2] S. Zhao, J. Yuh, and H. T. Choi, "Adaptive dob control of underwater robotic vehicles," in *OCEANS, 2001. MTS/IEEE Conference and Exhibition*, vol. 1, 2001, pp. 397–402 vol.1.

[3] T. Fossen and S. I. Sagatun, "Adaptive control of nonlinear underwater robotic systems," in *Robotics and Automation, 1991. Proceedings., 1991 IEEE International Conference on*, Apr 1991, pp. 1687–1694 vol.2.

[4] D. Yoerger and J.-J. Slotine, "Adaptive sliding control of an experimental underwater vehicle," in *Robotics and Automation, 1991. Proceedings., 1991 IEEE International Conference on*, Apr 1991, pp. 2746–2751 vol.3.

[5] G. Antonelli, S. Chiaverini, N. Sarkar, and M. West, "Adaptive control of an autonomous underwater vehicle: experimental results on odin," *Control Systems Technology, IEEE Transactions on*, vol. 9, no. 5, pp. 756–765, Sep 2001.

[6] A. P. Aguiar and J. Hespanha, "Logic-based switching control for trajectory-tracking and path-following of underactuated autonomous vehicles with parametric modeling uncertainty," in *American Control Conference, 2004. Proceedings of the 2004*, vol. 4, June 2004, pp. 3004–3010 vol.4.

[7] Z. Ismail and M. Dunnigan, "Tracking control scheme for an underwater vehicle-manipulator system with single and multiple sub-regions and sub-task objectives," *Control Theory Applications, IET*, vol. 5, no. 5, pp. 721–735, March 2011.

[8] S. Choi and J. Yuh, "Experimental study on a learning control system with bound estimation for underwater robots," in *Robotics and Automation, 1996. Proceedings., 1996 IEEE International Conference on*, vol. 3, Apr 1996, pp. 2160–2165 vol.3.

[9] J.-S. Wang and C. Lee, "Self-adaptive recurrent neuro-fuzzy control for an autonomous underwater vehicle," in *Robotics and Automation, 2002. Proceedings. ICRA '02. IEEE International Conference on*, vol. 2, 2002, pp. 1095–1100.

[10] R. D. Brandt and F. Lin, "Adaptive interaction and its application to neural networks," *Information Sciences*, vol. 121, no. 3, pp. 201–215, 1999.

[11] F. Lin, R. Brandt, and G. Saikalis, "Self-tuning of pid controllers by adaptive interaction," in *American Control Conference, 2000. Proceedings of the 2000*, vol. 5, 2000, pp. 3676–3681 vol.5.

[12] T. I. Fossen, *Guidance and control of ocean vehicles*. Wiley, 1994.

[13] C. Barbalata, M. Dunnigan, and Y. Petillot, "Dynamic coupling and control issues for a lightweight underwater vehicle manipulator system," in *Oceans - St. John's, 2014*, Sept 2014, pp. 1–6.

[14] M. Santhakumar and T. Asokan, "A self-tuning proportional-integral-derivative controller for an autonomous underwater vehicle, based on taguchi method," *Journal of Computer Science*, vol. 6, no. 8, p. 862, 2010.

[15] D. Maalouf, V. Creuze, A. Chemori, I. T. Tamanaja, E. C. Mercado, J. T. Munoz, R. Lozano, and O. Tempier, "Real-time experimental comparison of two depth control schemes for underwater vehicles regular paper," *International Journal of Advanced Robotic Systems*, pp. 1–15, 2014.

Comparison of coupled and decoupled force/motion controllers for an underwater vehicle-manipulator system

Corina Barbalata[a,*], Matthew W. Dunnigan[a], Yvan Petillot[a]

[a] *Ocean Systems Laboratory, Heriot-Watt University, Edinburgh, Scotland, UK*

Abstract

Autonomous interaction with the underwater environment has increased the interest of scientists in the study and development of force/motion controllers for lightweight underwater vehicle-manipulator systems. The paper presents a parallel position/force control law based on the sliding mode theory together with a comparison evaluation of two different strategies of the control law for an underwater vehicle-manipulator system. The first strategy aims to separately control the vehicle and the manipulator and hereafter is referred to as the decoupled approach. The second method, the coupled approach, proposes to control the system at the operational space level, treating the underwater vehicle-manipulator system as a single system. It is demonstrated that both methods are able to handle a highly non-linear system and compensate for the coupling effects between the vehicle and the manipulator. The simulation results demonstrate the validity of the two different control strategies when the goal is located in various positions, as well as the reliable behaviour of the system when different environment stiffnesses are considered.

Keywords:
underwater vehicle-manipulator system, low level control, coupling effects, interaction force

1. Introduction

In a world where only 5 % of the oceans has been explored, the challenges of underwater exploration is driving the development of new technologies. The barrier of deep-water exploration, not reachable by humans, is removed by the emergence of underwater robotics. Remotely operated vehicles (ROV) were one of the first robotics systems used to survey underwater environments. Using artificial intelligence, autonomous-underwater vehicles (AUV)s are one of the main systems being developed and constantly improved on to explore and survey deep-waters. The real challenge is to interact with the environment. To solve this a robotic manipulator is added to the underwater vehicle, the complete system being referred to as an underwater vehicle-manipulator system (UVMS).

Underwater vehicle-manipulator systems are highly complex systems, characterized by a high number of degrees-of-freedom, coupled and non-linear dynamics (Schempf and Yoerger, 1992). The dynamics of the system are highly affected by the dry mass ratio between the two subsystems that form the UVMS. In the case when the vehicle has a considerable mass with respect to the manipulator, e.g. SAUVIM UVMS (Yuh et al., 1998), the effects of the manipulator motion are not significant. This is not true if the manipulator is attached to a light vehicle. This type of structure is known as a lightweight underwater vehicle-manipulator system (Sanz et al., 2010). Using this type of system presents challenges regarding the stability of the robot and simple control laws are not sufficient to perform the required tasks.

Interaction tasks in the underwater environment using a lightweight vehicle-manipulator system are highly challenging and research in this area is slowly developing. Most of the available literature is based on classic force control approaches: impedance, hybrid or parallel control. Impedance control is based on the dynamic relation between the position and the force variable, controlling one of them through the other (Hogan, 1985). Hybrid control is based on the assumption that ideal conditions are available in the robot space and the task that has to be performed by the robot can be defined in two separate orthogonal and complementary directions covering the 6D space (Khatib, 1987). The parallel control ap-

*Corresponding author
Email addresses: cb237@hw.ac.uk (Corina Barbalata), m.w.dunnigan@hw.ac.uk (Matthew W. Dunnigan), y.r.petillot@hw.ac.uk (Yvan Petillot)

proach combines a motion controller and a force controller. It is claimed to increase the robustness of the force/position control as it incorporates the advantages of both the impedance and hybrid control. It is as simple and robust as the impedance control and enables the control of the position and separately force (Siciliano, 1996).

The difficulties encountered in the interaction between the UVMS and the environment include uncertainties in the UVMS model knowledge, the hydrodynamic effects, redundancy of the system, the coupling effects between the manipulator and the vehicle and the effects on the vehicle stability when interacting with the environment. Most of these challenges have been analyzed in the available literature. In (Cui et al., 1999) the authors present the impedance controller considering the UVMS as a single dynamic system. The authors argue that this type of control is appropriate as the motion of the end-effector is slow. Simulation results have been made with a 6DOF vehicle and a 3DOF manipulator in contact with the environment while sliding down a surface. Good results are obtained using an appropriate tuning for the impedance control. The contact force does not have significant effect on the vehicle as the contact forces are small and the mass of the vehicle is large (1073 kg in air). The same vehicle equipped with two manipulators, each having a weight of 53 kg in air, is used in the work presented by (Farivarnejad and Moosavian, 2014). The goal is to move a heavy cylinder and put it in an underwater structure using two manipulators mounted on a moving base. The multiple impedance controller proposed by the authors is based on enforcing the same impedance behaviour on all the parts that contribute to the manipulation. The authors consider uncertainties in the UVMS dynamic model that are treated as disturbing forces/moments. In the simulation results the authors present good trajectory tracking and robust contact with the environment but the method is not suited for cases when an exact force to interact with the environment is needed.

An adaptive impedance controller is used together with a hybrid controller in (Cui and Yuh, 2003). The system switches between the two controllers by using a fuzzy logic approach. The authors argue that using both types of controllers is beneficial for systems where uncertainties are present in the system. Moreover, for underwater tasks it is difficult to have environment information and the proposed controller is able to track the trajectory for the force. The simulation system consists of a heavy vehicle and a light manipulator. In (Dunnigan et al., 1996) a hybrid position/force control strategy is presented for a hydraulic manipulator. Simulation and practical results are presented and good results are obtained. Hybrid control is used in (Lapierre et al., 1998). The goal of the paper is to present a method to improve the behaviour of the ROV when the manipulator is in contact with the environment. The authors state that the main challenge in controlling the effects of the arm on the vehicle is to estimate the torque produced by the manipulator on the platform. The authors propose the use of a sensor placed between the two subsystems, which produces the information used to design an internal force control. This force control is needed to correct the command for the vehicle thrusters. The simulation results presented in the paper display a stable response for the vehicle. A free-floating base with a manipulator is presented in (Kosuge et al., 1996). The restoring forces produced by the thrusters are used to compensate for the interaction forces between the manipulator and environment. The goal of the proposed method is to use the reaction forces so as to not lose contact with the environment. A 2DOF manipulator on a floating base is presented in the simulation section. Good performance plots are shown but no interpretation of the results are provided.

An external force control approach is presented by (Antonelli et al., 2001). The control structure contains an internal loop for position control and an external PID controller for force regulation. One of the challenges of this type of system that has to be taken into account is the difference between the control bandwidth of the vehicle and the manipulator. The simulation results show that the control law is advantageous in the case when loss of contact appears. In (Olguin-Diaz et al., 2013) the authors use the notion of closed-loop passive mapping to simultaneously track the pose, control the contact force and maintain a redundant pose. The authors assume no knowledge of the system dynamics and use a model-free nominal continuous control law. The simulations show an example for welding on the nose of a submarine with a free floating body and a 7DOF manipulator. The results show how the UVMS preserves passivity during the contact task when the end-effector is moving on a rigid surface.

Underwater vehicle-manipulator systems can be controlled at a low level either in the operational space or in the vehicle/joints space. Two main categories of control strategies for complex systems can be identified. One approach investigates a separate type of controller for the vehicle and another type of controller for the manipulator. The paper of (McLain et al., 1996) presents a coordinated-control approach for a UVMS having a single link manipulator. A separate feedback controller for the vehicle and a different controller for the manipulator are designed and

the hydrodynamic model of the manipulator is used to coordinate and reduce the effects of the manipulator on the vehicle. The paper of (Canudas de Wit et al., 1998) approaches the issue of different bandwidth properties for the vehicle and manipulator. A Proportional-Derivative Controller is implemented for the manipulator, whose gains are limited according to the bandwidth of the manipulator. The authors propose the use of a non-linear controller for the vehicle (the slow-subsystem) that compensates the effects from the arm on the vehicle. Comparative results between this controller, based on singular perturbation theory and a simple PD controller are presented. A similar problem is solved in the paper of (Kim et al., 2003) where the UVMS is presented as a decentralized system. A proportional vehicle controller is designed in operational space and a feedback linearised controller is used for the manipulator. The manipulator control law takes into account the slow dynamic behaviour of the vehicle in order to compensate for the effects of the manipulator motion. The results presented in the paper show the tracking errors are considerably reduced by taking into account the slow vehicle system in the control of the manipulator. A different group of control strategies for a UVMS includes a single type of controller designed for the overall system. In most cases, the control law is designed in the operational space. (Antonelli and Chiaverini, 1998) propose the use of a sliding-mode controller (SMC) to track a desired trajectory with the UVMS. The method is advantageous for the system as there is no need to have an exact dynamic model as the method handles uncertainties and disturbances. In (Santhakumar et al., 2015) the authors present a comparison between an operational-space sliding mode controller and a classical Proportional-Derivative Operational Space Controller. The advantages of the SMC can be observed through the simulation results.

In this paper we propose a new method of controlling the position and force of lightweight underwater vehicle-manipulator system with 11 degrees-of-freedom. The architecture combines the theory of sliding mode control for force regulation and the integrative sliding mode control for position regulation in a parallel implementation. The method is robust to disturbances by incorporating the dynamic model of the underwater vehicle-manipulator system in the control architecture. Furthermore a new comparative analysis is presented in this paper. The evaluation aims to study the differences between the case when the proposed controller is applied in a centralized (coupled) strategy with the case when a descentalized (decoupled) strategy is used. Details of both strategies are discussed in this paper. The system model is described in Section 2, followed by the control architecture in Section 3. The two strategies are described in Section 4. A comparative evaluation of the two methods is presented in Section 5 and a discussion based on the comparative simulation results is made in Section 6.

2. System model

In this section the underwater vehicle-manipulator system is presented, including the characteristics of the system, the kinematic relationship between different coordinate frames and the dynamic model used to describe the UVMS.

2.1. Kinematic model

Multiple coordinate systems are available to represent the UVMS: vehicle (body) coordinates, joint coordinates, end-effector (operational/task space) coordinates and earth-fixed inertial coordinates. The system position is defined based on the manipulator joint position vector $q = [q_1 \cdots q_n]^T$, vehicle position $\eta_1 = [x,\ y,\ z,]^T$ and orientation $\eta_2 = [\phi,\ \theta,\ \psi,]^T$. The end-effector velocities, $\dot{\eta}_{ee}$ can be expressed with respect to the system velocities by Eq. (1) (Antonelli, 2006).

$$\dot{\eta}_{ee} = J(R_I^B, q)\zeta \tag{1}$$

where $\eta_{ee} \in \mathbb{R}^6$ represents the position and orientation of the end-effector, $\zeta = [\nu_1,\ \nu_2,\ \dot{q}]^T$ is the system velocity vector composed of the vehicle linear $\nu_1 \in \mathbb{R}^3$ and rotational $\nu_2 \in \mathbb{R}^3$ components and the manipulator joint velocities $\dot{q} \in \mathbb{R}^n$ and $J(R_I^B, q) \in \mathbb{R}^{6\times(6+n)}$ is the Jacobian of the overall system expressed using Euler angles, hereafter being mentioned as J.

2.2. Dynamic model

A single chain-representation is used to describe the dynamic model of the underwater-vehicle manipulator based on the work presented in (Featherstone, 2008). This representation starts by considering the vehicle to be a part of the manipulator, an extra link with 6 DOFs: 3 prismatic joints and 3 revolute joints. The Composite Rigid Body Algorithm and the classical principle of Newton-Euler that transmits the velocities and forces between subsystems are used to describe the robot's behaviour in time and to present the interactions between subsystems. The dynamics of the UVMS can be further described in a matrix form by the following equation:

$$M(q)\dot{\zeta} + C(\zeta, q)\zeta + D(\zeta, q)\zeta + g(\eta, R_B^I) = \tau - J^T\tilde{F} \tag{2}$$

where $M(q) \in \mathbb{R}^{(6+n)\times(6+n)}$ is the inertia matrix, $C(\zeta, q)\zeta \in \mathbb{R}^{(6+n)}$ is the Coriolis and Centripetal vector, both consisting of rigid body terms and added mass terms, $D(\zeta, q)\zeta \in \mathbb{R}^{(6+n)}$ is the damping and lift forces vector, $g(\eta, R_B^I) \in \mathbb{R}^{(6+n)}$ represents the restoring forces, $\tau = [\tau_v \ \tau_m] \in \mathbb{R}^{(6+n)}$ is the vector of total forces and moments applied to the vehicle $\tau_v \in \mathbb{R}^6$ and the torques applied to the manipulator $\tau_p \in \mathbb{R}^6$ and $\tilde{F} \in \mathbb{R}^6$ is the external disturbance vector produced by the interaction with the environment, modelled by Eq. (3).

$$\tilde{F}(t) = K_e(p_{ee} - p_0) \tag{3}$$

where p_0 is the point of a plane at rest, p_{ee} is the end-effector position and $K_e \in \mathbb{R}^{6\times6}$ is the stiffness matrix of the environment (Siciliano and Villani, 1999).

In mobile manipulation the tasks to be solved are naturally expressed in task space coordinates. The dynamic description of the system in operational space can be described by Eq. (4) (Khatib, 1987), where $x \in \mathbb{R}^6$ represents the independent parameters vector described in the operational space.

$$M(x)\ddot{x} + C(x)\dot{x} + D(x)\dot{x} + G(x) = T - \tilde{F}(t) \tag{4}$$

where $M(x) \in \mathbb{R}^{6\times6}$ is a positive operational space inertia matrix, $C(x)\dot{x} \in \mathbb{R}^6$ is the vector of Coriolis and Centripetal forces, $D(x)\dot{x} \in \mathbb{R}^6$ is the damping vector, $G(x) \in \mathbb{R}^m$ is the vector of restoring forces, all defined in operational space coordinates and $T \in \mathbb{R}^6$ is the vector of generalized forces at the end-effector. The dynamic components in the operational space are defined with respect to the system coordinates by the following equations:

$$\begin{aligned} M(x) &= J^{-T}M(q)J^{-1} \\ C(x) &= J^{-T}C(\zeta, q)J^{-1} - J^{-T}M(q)J^{-1}\dot{J}J^{-1} \\ D(x) &= J^{-T}D(\zeta, q)J^{-1} - J^{-T}M(q)J^{-1}\dot{J}J^{-1} \\ G(x) &= J^{-T}g(\eta, R_B^I) \\ T &= J^T\tau \end{aligned} \tag{5}$$

3. Parallel sliding mode dynamic controller

The task that the system has to solve is a motion/force task where the system has to interact with the environment. In this section a parallel force/position control law (Chiaverini and Sciavicco, 1993) is developed based on the sliding mode control (SMC) theory (Edwards and Spurgeon, 1998), defined in the operational space coordinates.

The parallel force/position control is composed of a position controller acting in parallel with a force control law, as expressed by Eq. (6).

$$T = u_p + u_f \tag{6}$$

where u_p is the position control law and u_f defines the force control law:

- For the position control law: $u_p = u(e_p, t)$ is a SMC control law that makes the position asymptotically follow a reference profile.
- For the force control law: $u_f = u(e_f, t)$ is a SMC control law that keeps the contact force between the end-effector and environment to a desired known value.

3.1. Position control law

For the position component of the parallel controller (Chiaverini and Sciavicco, 1993) an Integral Sliding Mode Controller (Utkin and Shi, 1996) is used. The control law is a type of sliding mode controller that maintains the order of the compensated systems dynamics in the sliding mode. The method is advantageous for a complex system such as the underwater vehicle-manipulator system, handling non-linearities, uncertainties, coupling effects and parameter variations.

The control function is divided into two parts:

$$u_p = u_1 + u_2 \tag{7}$$

where the auxiliary sliding mode, u_1, compensates for the bounded disturbances and u_2 drives the sliding variable to zero as time increases, taking into account that the sliding variable dynamics are no longer perturbed.

The primary sliding variable is designed based on the following equation:

$$\sigma = \dot{e}_p + c_1 e_p + c_2 \int_0^t e_p dt, \quad c_1, c_2 > 0 \tag{8}$$

where e_p is the error in the end-effector position, $e_p = p_{des} - x$, defined based on the difference between the desired position $p_{des} \in \mathbb{R}^6$ and the current end-effector position $x \in \mathbb{R}^6$. The sliding variable dynamics for this variable is given by:

$$\dot{\sigma} = \ddot{e}_p + c_1\dot{e}_p + c_2 e_p \tag{9}$$

where $c_1, \ c_2 \ \in \mathbb{R}^{6\times6}$ are positive constant diagonal matrices defined to model the sliding mode dynamics.

The auxiliary sliding variable is designed by:

$$\begin{cases} s = \sigma - z \\ \dot{z} = M^{-1}(x)u_2 \end{cases} \tag{10}$$

where $M^{-1}(x)$ is the inverse of the inertia matrix in end-effector coordinates, as defined previously in Eq. (4).

The dynamic compensator for the auxiliary sliding variable is given by:

$$\begin{aligned} \dot{s} &= \dot{\sigma} - \dot{z} = \ddot{e}_p + c_1\dot{e}_p + c_2 e_p - M^{-1}(x)u_2 \\ &= \ddot{x} - \ddot{p}_{des} + c_1\dot{e}_p + c_2 e_p - M^{-1}(x)u_2 \end{aligned} \tag{11}$$

Using Eq. (4) to define $\ddot{x}$, Eq. (6) and Eq. (7) for the control input, the dynamics of the auxiliary variable can be re-written as:

$$\begin{aligned} \dot{s} = M^{-1}(x)u_1 + M^{-1}(x)u_2 + \varphi(e_p, \dot{e}_p, \tilde{F}) - M^{-1}(x)u_2 \\ = M^{-1}(x)u_1 + \varphi(e_p, \dot{e}_p, \tilde{F}) \end{aligned} \tag{12}$$

where

$$\begin{aligned} \varphi(e_p, \dot{e}_p, \tilde{F}) &= M^{-1}(x)\mu - \ddot{p}_{des} + c_1\dot{e}_p + c_2 e_p \\ \mu &= u_f - C(x,\dot{x})\dot{x} - D(x,\dot{x})\dot{x} - G(x) - \tilde{F}(t) \end{aligned} \tag{13}$$

The term $\varphi(e_p, \dot{e}_p, \tilde{F})$ is considered as the disturbance term and is assumed bounded, i.e $\mid \varphi(e_p, \dot{e}_p, \tilde{F}) \mid \leq \Omega$.

In order for the sliding variable to be driven to zero in finite time the sliding mode control u_1 can be defined as:

$$u_1 = \rho_1 \mathtt{sign}(s) \tag{14}$$

The primary and auxiliary sliding mode variable dynamics compensated by u_1 can be expressed by:

$$\begin{cases} \dot{\sigma} = M^{-1}(x)u_1 + M^{-1}(x)u_2 + \varphi(e_p, \dot{e}_p, \tilde{F}) \\ \dot{s} = M^{-1}(x)u_1 + \varphi(e_p, \dot{e}_p, \tilde{F}), \quad u_1 = \rho_1 \mathtt{sign}(s) \end{cases} \tag{15}$$

To prove that the primary sliding mode dynamics does not depend on the disturbances, the σ dynamics can be described in the auxiliary sliding mode ($s = 0$). In order to satisfy the condition $\dot{s} = 0$, the equivalent control u_{1eq} is computed:

$$\begin{aligned} \dot{s} = 0 \Leftrightarrow M^{-1}(x)u_{1eq} + \varphi(e_p, \dot{e}_p, \tilde{F}) = 0 \\ \Rightarrow u_{1eq} = M(x)\varphi(e_p, \dot{e}_p, \tilde{F}) \end{aligned} \tag{16}$$

Substituting this into Eq. (15) the primary sliding mode variable dynamics is defined by the following equation:

$$\dot{\sigma} = M^{-1}(x)u_2 \tag{17}$$

It can be observed that the primary sliding mode dynamics does not depend on the disturbance term, $\varphi(e_p, \dot{e}_p, \tilde{F})$. The control function for the primary sliding variable is given by:

$$u_2 = kM^{-1}(x)\sigma, \quad k > 0 \tag{18}$$

where $k \in \mathbb{R}^{6\times6}$ is a positive matrix.

3.2. Force control law

A sliding mode controller is used to drive the system so that the force tracking error asymptotically converges to zero:

$$\lim_{t\to\infty} e_f = 0 \tag{19}$$

where e_f is the force error defined as $e_f = F_{des} - \tilde{F}$.

The sliding variable is expressed by Eq. (20). A sliding mode control u_f has to be designed that drives $\delta \to 0$ in finite time.

$$\delta = c_3 e_f + \int_0^t e_f dt, \quad c_3 > 0 \tag{20}$$

where $c_3 \in \mathbb{R}^{6\times6}$ is a positive matrix.

Eq. (21) drives the output force error e_f ensuring zero convergence.

$$\delta = c_3 e_f + \int_0^t e_f dt = 0, \quad c_3 > 0 \tag{21}$$

The dynamics of the sliding variable are described by:

$$\dot{\delta} = c_3\dot{e}_f + e_f, \quad c_3 > 0 \tag{22}$$

Using the dynamic model of the UVMS as presented in Eq. (4) the dynamics of the sliding variable can be described by:

$$\dot{\delta} = c_3\dot{e}_f + F_{des} - \tilde{F} = \theta(x,\dot{x}) - u_f \tag{23}$$

where

$$\begin{aligned} \theta(x,\dot{x}) &= c_3\dot{e}_f + F_{des} + \nu(x,\dot{x}) - u_p \\ \nu &= M(x)\ddot{x} + C(x,\dot{x})\dot{x} + D(x,\dot{x})\dot{x} + G(x) \end{aligned} \tag{24}$$

assuming that $\theta(x,\dot{x})$ is the cumulative disturbance and is bounded by $\mid \theta(x,\dot{x}) \mid \leq \Omega_f$, the control force u_f can be defined by the sliding mode existence condition (Shtessel et al., 2014):

$$\delta\dot{\delta} \leq -\bar{\alpha} \mid \delta \mid, \quad \bar{\alpha} = \frac{\alpha}{\sqrt{2}}, \quad \alpha > 0 \tag{25}$$

$$\delta\dot{\delta} = \delta\left[\alpha(x,\dot{x}) - u_f\right] \leq \mid \delta \mid \Omega_f - \delta u_f \tag{26}$$

$$u_f = \rho_2 \mathtt{sign}(\delta) \tag{27}$$

Choosing the control law as presented by Eq. (27) then

Eq. (26) becomes:

$$\delta\dot{\delta} \leq \mid \delta \mid (\Omega_f - \rho_2) = -\bar{\alpha} \mid \delta \mid \tag{28}$$

This leads to computing the control gain based on:

$$\rho_2 = \Omega_f + \bar{\alpha} \tag{29}$$

3.3. Singularity avoidance

One issue that has to be addressed when handling complex systems is the singular configuration. Whenever the robot is close to a singularity the joint forces can have high values and the robot can become uncontrollable. The problem can be avoided by establishing which of the dimensions is the issue and setting the correspondent force to zero. The inertia matrix, $M(x)$ in the task coordinates is used to set the forces to zero. To detect singularities in the workspace the determinant of the Jacobian is computed. If the system is close to a singular configuration the Singular Value Decomposition of $M_x^{-1} = VSU^T$ is computed. The algorithm used to describe the singularity avoidance is presented in Algorithm 1.

Algorithm 1 Singularity avoidance

```
M_x^{-1} = J^{-T} M^{-1} J^{-1}
if | JJ^T | ≥ th then
    M_x = inv(M_x^{-1})
else
    u, s, v = svd(M_x^{-1})
    if s < th then
        s = 0
    else
        s = 1/s
    end if
    M_x = v diag(s) u^T
end if
```

3.4. Total control law

A feedback linearization technique is used to obtain the input-output dynamics and reduce the disturbances between the subsystems.

$$T = \tilde{M}(x)\left[\ddot{p}_{des} + u_p + u_f\right] + \alpha \tag{30}$$

where

$$\begin{aligned}
u_p &= u_1 + u_2 \\
u_1 &= \rho_1 \mathtt{sign}(s) \quad \rho_1 > 0 \\
u_2 &= kM^{-1}(x)\sigma \quad k > 0 \\
u_f &= \rho_2 \mathtt{sign}(\delta), \quad \rho_2 > 0 \\
\sigma &= \dot{e}_p + c_1 e_p + c_2 \int_0^t e_p dt, \quad c_1, c_2 > 0 \\
s &= \sigma - z \\
\dot{z} &= M^{-1}(x) u_2 \\
\delta &= c_3 e_f + \int_0^t e_f dt, \quad c_3 > 0 \\
\alpha &= \tilde{C}(x, \dot{x})\dot{x} + \tilde{D}(x, \dot{x})\dot{x} + \tilde{G}(x)
\end{aligned} \tag{31}$$

$\tilde{M}(x)$ is an estimate of the inertia term, $\tilde{C}(x, \dot{x})$, $\tilde{D}(x, \dot{x})$, $\tilde{G}(x)$ are estimates of the real values of the system defined in operational space coordinates according to the boundary errors, $\delta M(x)$, $\delta C(x, \dot{x})$, $\delta D(x, \dot{x})$, $\delta G(x)$ by Eq. (32):

$$\begin{aligned}
\mid \Delta M(x) \mid &\leq \delta M(x) \quad \Delta M(x) = M(x) - \tilde{M}(x) \\
\mid \Delta C(x, \dot{x}) \mid &\leq \delta C(x, \dot{x}) \quad \Delta C(x, \dot{x}) = C(x, \dot{x}) - \tilde{C}(x, \dot{x}) \\
\mid \delta D(x, \dot{x}) \mid &\leq \delta D(x, \dot{x}) \quad \Delta D(x, \dot{x}) = D(x, \dot{x}) - \tilde{D}(x, \dot{x}) \\
\mid \Delta G(x) \mid &\leq \delta G(x) \quad \Delta G(x) = G(x) - \tilde{G}(x)
\end{aligned} \tag{32}$$

To remove the chattering effect, a continuous/smooth control function should be designed. This leads to approximate the discontinuous function by a smooth function, that is by replacing the `sign` function with the sigmoid function:

$$\mathtt{sign}(a) \simeq \frac{a}{\mid a \mid + \epsilon} \tag{33}$$

where ϵ is a small positive scalar.

4. Control strategy

This section describes two different strategies of applying the control law proposed in Section 3. The first strategy proposes the use of the parallel controller for the manipulator and a separate vehicle controller. The second strategy involves the use of the parallel control approach for the entire system, with no additional vehicle control for the vehicle.

4.1. Decoupled strategy

The decoupled controller is defined as a vehicle controller and a manipulator controller joint together by an interaction strategy. In this section both controllers are described and the interaction strategy is presented.

Interaction strategy The tasks the UVMS system has to perform are to move close to an object placed in the underwater environment, interact with the object by applying a certain force and keep the system stable while performing these operations. The object is defined based on its 3D position with respect to the fixed inertial frame. In order for the manipulator to interact with the environment the object has to be in the working space of the manipulator. If the object is too far from the manipulator, the vehicle has to move until the object can be reached by the manipulator. The current approach is based on the Euclidian distance between the center of mass of the vehicle and the object the system is supposed to interact with. This distance is computed at every time step and if it is larger than the total length of the manipulator, the vehicle is required to move and the manipulator is in station keeping mode. At the moment when the vehicle is close enough to the object the vehicle is in station keeping and the manipulator is commanded to move and interact with the object with the desired force. The approach is summarized in Algorithm 2, where p_{des} is the desired (object) position, p_v is the vehicle position, v_{des} is the vehicle desired position and m_{des} is the manipulator desired position.

Algorithm 2 Interaction strategy

$d(p_{des}, p_v) = \sqrt{\sum_{i=1}^{n} (p_{des_i} - p_{v_i})^2}$
if $d(p_{des}, p_v) \geq L$ **then**
    $v_{des} = p_{des}$
    $m_{des} = p_m$
else
    $v_{des} = p_v$
    $m_{des} = p_{des}$
end if

Vehicle controller The vehicle controller proposed in this strategy is based on the work presented in (Barbalata et al., 2015). In the underwater environment the operational speed of the AUV is relatively small when undertaking an interaction task and each degree-of-freedom of the vehicle can be independently controlled. In the case when a manipulator is added to a lightweight AUV the effects of the manipulator motion are noticeable on the DOFs of the vehicle. Nevertheless, the approach presented in this work is robust to these effects. The vehicle controller, a PILIM (Proportiona-Integrative LIMited) scheme is designed using two control loops one for position and one for velocity. The position controller is based on the error in position of the vehicle $e_{p_v} \in \mathbb{R}^6$ and the positive matrix of proportional gain $K_{p_p} \in \mathbb{R}^{6\times6}$. The velocity loop takes into account the error in vehicle velocity $e_{v_v} \in \mathbb{R}^6$ and has two components, one proportional and another integral with positive gain matrices $K_{p_v},\ K_{i_v} \in \mathbb{R}^{6\times6}$. The system is characterized by the following equations:

$$\begin{aligned} e_{p_v} &= v_{des} - p_v \\ u_{p_v} &= K_{p_p} e_{p_v} \\ e_{v_v} &= v_v - u_{p_v} \\ \tau_v &= K_{p_v} e_{v_v} + K_{i_v} \int_0^t e_{v_v} dt \\ \tau_v &= \mathtt{sat}(\tau_v, -l, l) \end{aligned} \tag{34}$$

where $p_v \in \mathbb{R}^6$ represents the position of the vehicle, $v_v \in \mathbb{R}^6$ is the velocity of the vehicle, $p_{des} \in \mathbb{R}^6$ is the desired position in vehicle coordinates, $u_{p_V} \in \mathbb{R}^6$ is the output forces and moments of the position loop and τ_v are the control output for the vehicle, taking into account the saturation limits $\pm\, l$.

Manipulator controller The control law for the manipulator is based on Eq. (6), as described in Section 3. The parallel controller is designed in the operational space. The position of the end-effector is computed using the following kinematic transformation:

$$v_m = J_m(q)\dot{q} \tag{35}$$

where $v_m \in \mathbb{R}^6$ is the manipulator end-effector velocity and $J_m(q) \in \mathbb{R}^{n\times n}$ is the manipulator task Jacobian matrix. The control law at the joint level is further described by Eq. (36).

$$\tau_m = J_m^T(q)T \tag{36}$$

where T is defined as in Eq. (30) with the dynamic components defined only for the manipulator system. The overall control for the UVMS is computed based on Eq. (37)

$$\tau = [\tau_v\ \tau_m]^T \tag{37}$$

4.2. Coupled strategy

The coupled controller considers the UVMS as a single system and the same controller is used for all degrees-of-freedom of the system. The task that the system has to solve is a motion/force task where the system has to interact with the environment. In this case, similar to the decoupled controller the parallel force/position law with sliding mode dynamics is implemented, the difference being that in the coupled system, the control law is applied to the full UVMS and not only to the manipulator. In this case, the final

control law in joint space is defined by Eq. (38).

$$\tau = J^T T \tag{38}$$

where T is defined as in Eq. (30) with the dynamic model defined based on the overall vehicle-manipulator system. In this case the coupling effects between the vehicle and manipulator are incorporated in the dynamic model and have an active role in the control strategy.

5. Results

In this section the simulation results demonstrate the proposed control methods based on a underwater vehicle-manipulator system with 11 degrees-of-freedom. The work presented in this paper is developed based on two real robotic systems available in Ocean Systems Laboratory: Nessie VII an autonomous underwater vehicle developed as a research platform in the laboratory and a commercially available underwater manipulator, HDT-MK3-M developed by HDT Global. Nessie VII AUV is a torpedo shaped 5 degrees-of-freedom (DOFs) vehicle with a mass of 50 `kg`, a length of 1.1 `m` and 0.7 `m` in diameter. The vehicle *roll* degree-of-freedom is not controlled. The manipulator has 6 revolute joints and a total weight of 10 `kg`. The system is shown in Fig. 1 and describes a lightweight UVMS characterized by significant interactions between the manipulator and vehicle that affects the overall stability of the UVMS.

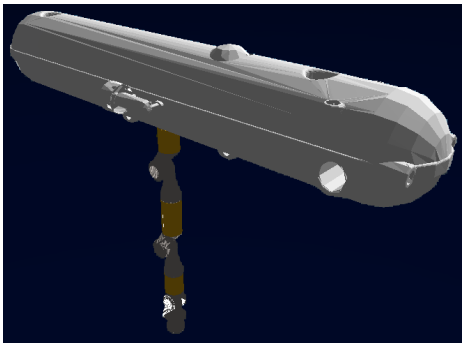

Fig. 1: UVMS model

The results of the decoupled strategy are compared with the results of the coupled approach. The simulation environment is built in Python according to a real underwater environment consisting of all the hydrodynamic effects. The main objective of the simulation is to command the end-effector of the UVMS to interact with the environment at a specified force.

The interaction with the environment is considered as a point-contact acting on the x-axis of the end-effector. The manipulator interacts with the environment only at the moment when the location of the goal has been reached. Different environments are used, having stiffnesses between $K_e = 10^3$ N/m and $K_e = 5 \cdot 10^4$ N/m. The desired interaction force is $F_{des} = 100$ N. In this work, the orientation of the end-effector is not of interest and only the x, y, z axes of the end-effector are controlled. Throughout this section the initial and desired positions of the end-effector are expressed in meters. The end-effector initial position with respect to the world coordinates is $p_{init} = (0.0,\ 0.0,\ 0.97)$ meters. Different goals for the end-effector are defined in world coordinates, coinciding with the location of the object with which the manipulator is expected to maintain contact. The cycloid function, Eq. (39), is used to define the end-effector desired position. The function is an interpolation for the position $p_{des}(t)$ starting with an initial value $p_{init}(0)$ and a desired final value $p_{des}(t_f)$.

$$p_{des}(t) = p_{init}(0) + \Delta/2\pi[\omega t - \sin(\omega t)] \tag{39}$$

where

$$\omega = 2\pi/t_f, \quad \Delta = p_{des}(t_f) - p_{init}(0), \quad 0 \le t \le t_f$$

Fig. 3 presents the behaviour of the end-effector of the UVMS for the case when the goal is located at $p_{des} = (4.0,\ 2.0,\ -3.0)$ meters and has the desired interaction force $F_{des} = 100$ N and the stiffness of the environment $K_e = 10^3$ N/m. The results are presented in the world coordinate system and the end-effector is able to reach the goal due to the movement of the vehicle. The results show the expected behaviour of the end-effector as well as the actual performance using both the decoupled and the coupled methods. Both proposed strategies perform well in following the desired trajectories on the three axes. Small overshoot is present in the results of the decoupled approach that can be related to the characteristics of the interaction strategy. A clearer understanding of the effects of the interaction strategy is given in Fig. 2 which represents the 3D behaviour of the end-effector. The start point is (0.0, 0.0, 0.0) meters in world coordinates which corresponds to the center of mass of the vehicle. At the beginning of the simulation the end-effector is placed at $(0.0,\ 0.0,\ -0.97)$ meters in world coordinates. From this initial position the end-effector is commanded to move towards the goal.

In the decoupled approach when the vehicle is in station keeping and the manipulator is commanded to move to reach the object, the manipulator has to

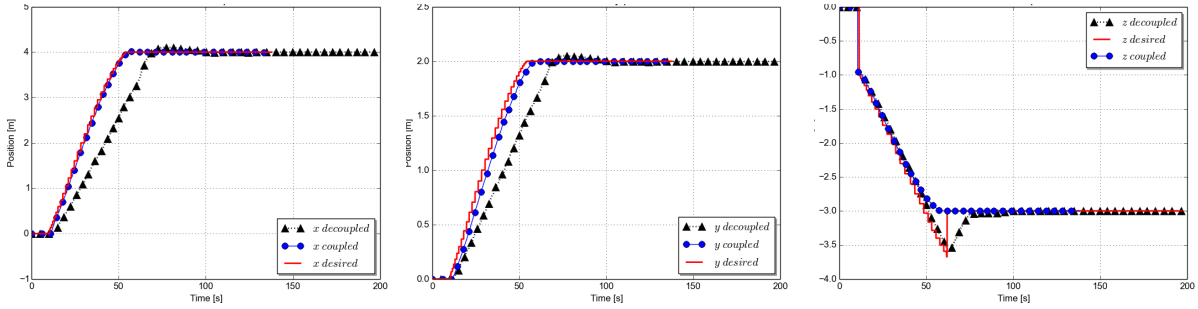

(a) (b) (c)

Fig. 3: Position tracking for end-effector, goal at $(x, y, z) = (4.0, 2.0, -3.0)$

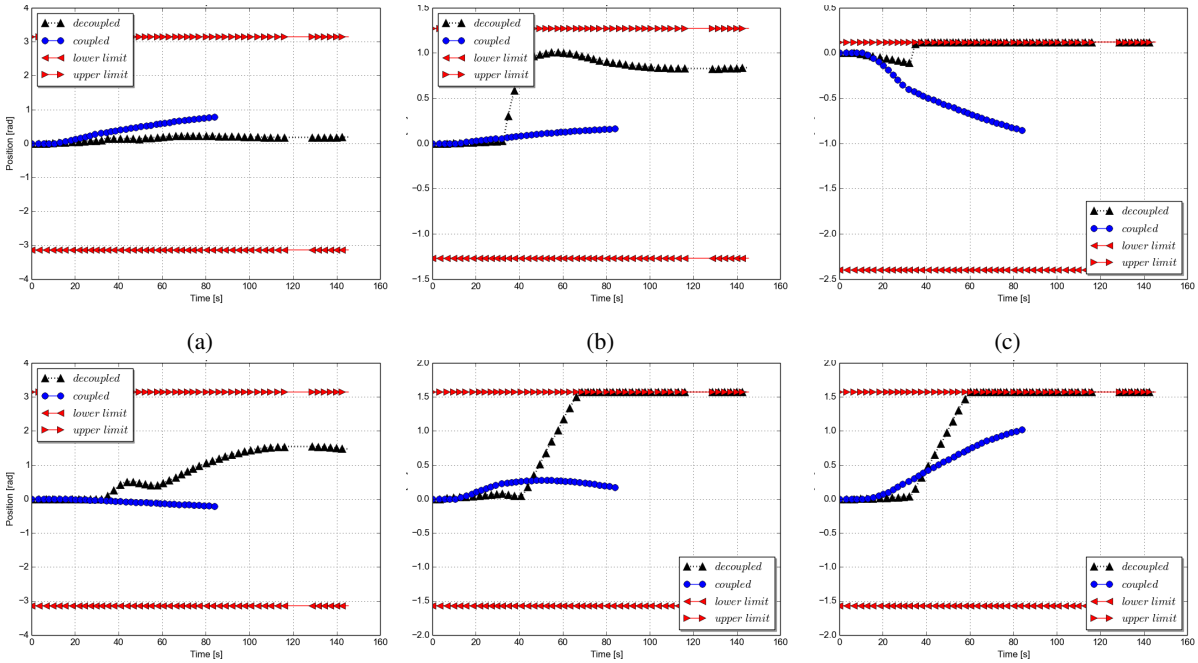

(a) (b) (c)

(d) (e) (f)

Fig. 4: Joint positions when goal at $(x, y, z) = (2.0, 0.0, -2.0)$

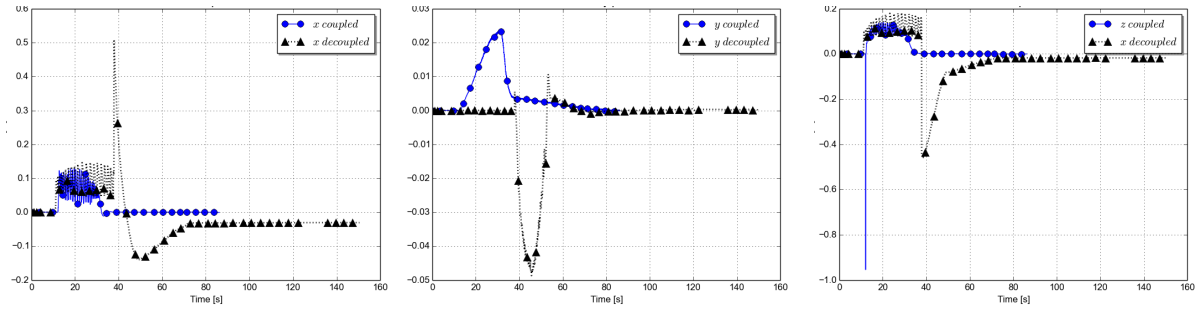

(a) (b) (c)

Fig. 5: Error in end-effector position for goal at $(x, y, z) = (2.0, 0.0, -2.0)$

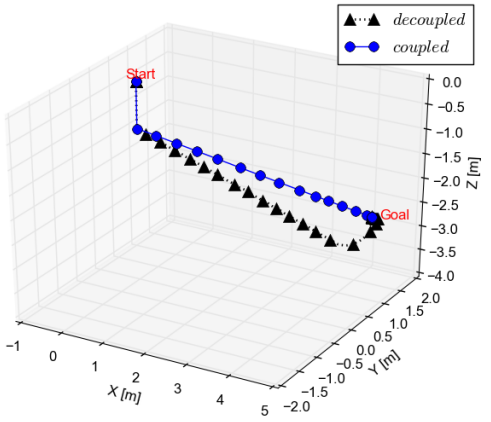

Fig. 2: End-effector 3D position, goal at $(x, y, z) = (4.0, 2.0, -3.0)$

perform an extensive movement. In the coupled approach, the behaviour of the manipulator is more restricted based on the fact that the end-effector has a straightforward behaviour. In this case the UVMS is treated as a single system and the error in position takes into account both the behaviour of the vehicle and manipulator. This will limit the movement of the manipulator, as can be seen in Fig. 4. In this case the joint positions in the coupled and decoupled cases are shown together with the physical limits of the respective joints. The movement of the arm for the case when the desired location of the end-effector is $p_{des} = (2.0,\ 0.0,\ 2.0)$ meters is presented in Fig. 4. It can be seen from Fig. 4c, Fig. 4e, Fig. 4f that in the decoupled method three of the joints are at the upper joint limit, locking the manipulator. This will prevent the end-effector from reaching the goal, as can be seen from Fig. 5 where a constant error in the x axis of the end-effector is maintained. A poor choice of the threshold in the interaction strategy is responsible for this behaviour. Using the proposed controller in the decoupled strategy creates a system where the correct threshold is directly dependent on the location of the goal. Once the goal has been reached the contact with the object takes place, maintaining the desired interaction force of $F_{des} = 100$ N, Fig. 6. Different environment stiffnesses are considered. For Fig. 6a the goal is located at $p_{des} = (4.0,\ 2.0, 3.0)$ meters and the stiffness is $K_e = 10^3$ N/m while for Fig. 6b the goal is located at $p_{des} = (2.0,\ 0.0,\ -2.0)$ meters and the stiffness is $K_e = 10^5$ N/m. Using both methods, an overshoot is present in the force response. At the moment when contact with the environment is taking place, the manipulator compensates for the force and is trying not to lose position while maintaining contact. This will drive the manipulator to apply a larger force that results in an overshoot. The stiffer the environment the larger the force that is applied on the manipulator and an increase in the overshoot of the force contact is seen. The contact with the environment takes

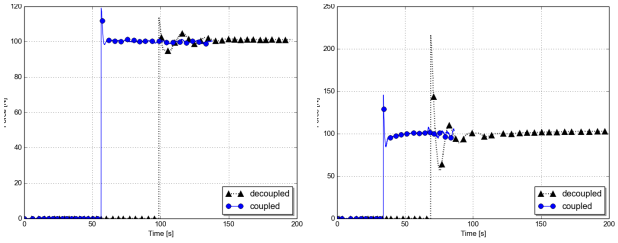

(a) $K_e = 10^3$ N/m (b) $K_e = 10^5$ N/m

Fig. 6: Interaction forces

place at a different time for the coupled and decoupled strategies. Treating the system as a single case and due to the straightforward behaviour of the approach the contact with the environment happens faster when the coupled method is used. At the beginning of the contact it can be seen that the decoupled strategy produces an oscillatory response to the interaction force which is reduced after the system stabilizes. The coupled method does not present these large oscillations at the beginning but during all the interaction period very small oscillatory behaviour is observed.

It can be seen from Fig. 7 and Fig. 8 that in the coupled approach, the vehicle, especially the yaw DOF, is trying to compensate for the interaction force, reducing the oscillations at the beginning of contact. Using the decoupled strategy the effects of the interaction are almost fully compensated for by the manipulator controller, with small control effort from the vehicle controller.

6. Discussion

Some comments are now made on the work presented in this paper. The control method used in this paper combines the Integrative Sliding Mode Control for position tracking with the classical Sliding Mode Control for force tracking by means of the operational space parallel force/position implementation. The parallel controller combines the advantages of both hybrid and impedance control while the Sliding Mode Controllers solve the high coupling effects between the subsystems and the uncertainties in the model. The control law is applied to the underwater vehicle-manipulator system using two different strategies.

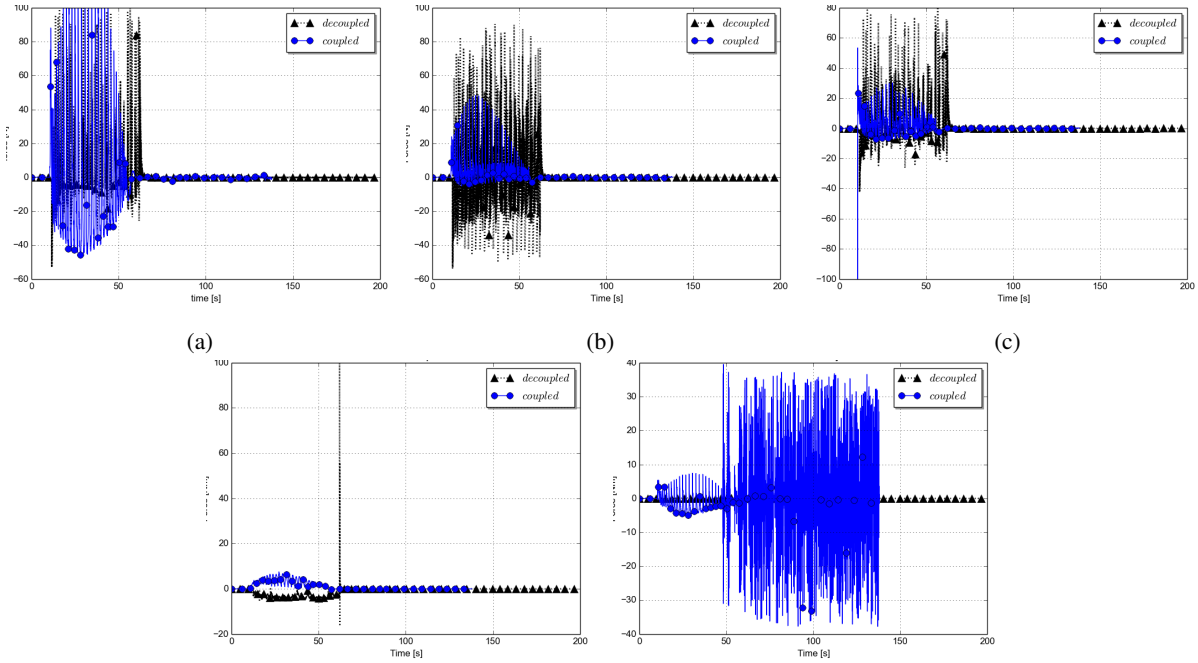

Fig. 7: Control effort for vehicle

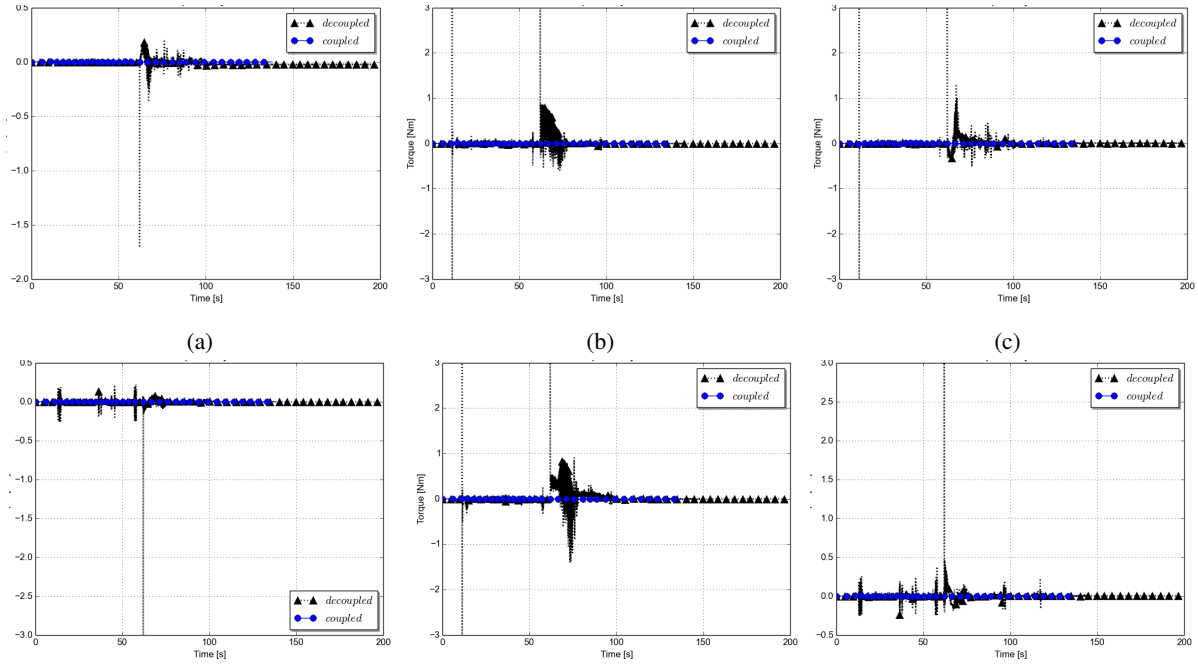

Fig. 8: Control effort for manipulator

Table 1: Generalized Root Mean Square Error

	Decoupled				Coupled			
K_e (N/m)	$1 \cdot 10^3$	$5 \cdot 10^3$	$1 \cdot 10^4$	$5 \cdot 10^4$	$1 \cdot 10^3$	$5 \cdot 10^3$	$1 \cdot 10^4$	$5 \cdot 10^4$
Position error (m)	0.13	0.13	0.13	0.13	0.10	0.10	0.10	0.10
Force error (N)	1.98	10.25	13.48	47.74	2.80	4.07	8.89	39.97

The decoupled approach proposed represents a classical method to control real underwater-vehicle systems (McLain et al., 1996) where different type of controllers are used for the vehicle and manipulator. The system is straightforward, easy to implement, having low computational load making it an ideal option for coupled systems such as the lightweight UVMS. It was demonstrated that with appropriate control for the manipulator the coupling effects between the two subsystems can be overcome even at the moment of interaction with the environment. In the decoupled method the interaction with the environment is handled by the manipulator controller, little effect being sensed by the vehicle. Moreover, during contact with the environment the vehicle maintains position. Compared with the coupled approach the decoupled strategy presents lag in following the desired end-effector trajectory, as seen in Fig. 3. It was shown in Section 5 that the interaction strategy can play an essential role in this approach. Choosing a large threshold for the interaction strategy can lead to not achieving interaction with the environment. Choosing a very small threshold could put all the system in collision with the environment.

The coupled control law is designed in the end-effector coordinates and both the manipulator and vehicle are controlled through the inverse kinematics. This method takes into account the effects of the manipulator movement on the vehicle by integrating the dynamic model of the full underwater vehicle-manipulator system. In this case both the vehicle and manipulator are compensating for the interaction with the environment. The coupled strategy is advantageous due to the fact that it reduces the complexity of the problem, by not having to design an interaction strategy and deciding the corresponding threshold based on the location of the goal. Due to this the coupled strategy is less prone to failures compared with the decoupled approach, the position and force steady states always being achieved. Moreover the method has a faster response and the time of execution is reduced.

It has to be noted that both strategies are very sensitive to proper tuning, especially regarding the force contact. A poorly tuned controller may result in not achieving steady-state or high oscillations.

The proposed controller together with the two strategies have been extensively tested with a range of goals, at different environment stiffnesses from $K_e = 10^3$ N/m and $K_e = 5 \cdot 10^5$ N/m. The generalized root mean square error, Eq. (40), is used to compare the behaviour of the two strategies. N is the number of total measurements and e is the generalized error. The evaluation metric has been computed separately for the position and force and the results can be seen in Table 1. The results presented are based on 10 different goals.

$$GRMSE = \sqrt{\frac{1}{N}\sum_{k=1}^{N} e_k^2} \tag{40}$$

In Table 1 it can be seen that the stiffness of the environment does not affect the performance of the end-effector position tracking. The coupled method produces more accurate results for this case, although the difference with respect to the decoupled strategy is not highly significant. It can be seen that the coupled approach, on average, has a smaller error in force and position. Overall the coupled approach performs better as a result of the fact that the disturbances that appear in the system caused by the interaction with the environment are handled by the overall dynamic model of the UVMS that it is taken into account in the control strategy. Whenever contact with the environment is taking place, in the coupled strategy, the vehicle reacts to these forces, allowing the end-effector to maintain the required position. In the decoupled method, the vehicle has to both handle the interaction force and maintain the location of the end-effector, while the vehicle has to maintain position.

7. Conclusions

This paper presents a parallel position/force control based on sliding mode control theory together with two different strategies to control a lightweight underwater vehicle-manipulator system that interacts with an object in the underwater environment. The model of the system is developed using the Newton-Euler algorithm together with the Composite Rigid-Body Algorithm. The decoupled method describes an

approach where the vehicle and manipulator are controlled separately, taking into account the interaction forces between the subsystems. The coupled method treats the underwater-vehicle manipulator system as a single system and the control method is designed in the operational space coordinates. The simulation results show that both methods can be used for control of lightweight systems where interaction with the environment is required. The desired interaction force is achieved both in compliant and stiff environments and the steady state is maintained. The control methods demonstrate that they can compensate for the coupling effects between subsystems removing the unwanted disturbances.

8. Acknowledgement

The authors would like to acknowledge the financial support provided by the ETP program Scotland and SeeByte Ltd.

References

H. Schempf, D. Yoerger, Coordinated Vehicle/Manipulator Design and Control Issues For Underwater Telemanipulation, in: International Federation of Automatic Control, CAMS92, 1992.

J. Yuh, S. Choi, C. Ikehara, G. Kim, G. McMurty, M. Ghasemi-Nejhad, N. Sarkar, K. Sugihara, Design of a semi-autonomous underwater vehicle for intervention missions (SAUVIM), in: Underwater Technology, 1998. Proceedings of the 1998 International Symposium on, 63–68, 1998.

P. J. Sanz, P. Ridao, G. Oliver, C. Melchiorri, G. Casalino, C. Silvestre, Y. Petillot, A. Turetta, TRIDENT: A framework for autonomous underwater intervention missions with dexterous manipulation capabilities, in: Proceedings of the 7th Symposium on Intelligent Autonomous Vehicles IAV-2010. IFAC, 2010.

N. Hogan, Impedance control: An approach to manipulation: Part II Implementation, Journal of dynamic systems, measurement, and control 107 (1) (1985) 8–16.

O. Khatib, A unified approach for motion and force control of robot manipulators: The operational space formulation, IEEE Journal on Robotics and Automation 3 (1) (1987) 43–53.

B. Siciliano, Parallel force/position control of robot manipulators, in: Robotics Research, Springer, 78–89, 1996.

Y. Cui, T. K. Podder, N. Sarkar, Impedance control of underwater vehicle-manipulator systems (UVMS), in: Intelligent Robots and Systems. Proceedings. 1999 IEEE/RSJ International Conference on, vol. 1, IEEE, 148–153, 1999.

H. Farivarnejad, S. A. A. Moosavian, Multiple Impedance Control for object manipulation by a dual arm underwater vehicle–manipulator system, Ocean Engineering 89 (2014) 82–98.

Y. Cui, J. Yuh, A unified adaptive force control of underwater vehicle-manipulator systems (UVMS), in: Intelligent Robots and Systems, Proceedings. 2003 IEEE/RSJ International Conference on, vol. 1, IEEE, 553–558, 2003.

M. Dunnigan, D. Lane, A. Clegg, I. Edwards, Hybrid position/force control of a hydraulic underwater manipulator, in: Control Theory and Applications, IEE Proceedings-, vol. 143, IET, 145–151, 1996.

L. Lapierre, P. Fraisse, N. K. M'Sirdi, Hybrid position/force control of a ROV with a manipulator, in: OCEANS'98 Conference Proceedings, vol. 2, IEEE, 931–935, 1998.

K. Kosuge, H. Kajita, T. Fukuda, Force control of manipulator/vehicle system floating on the water utilizing vehicle restoring force, in: Advanced Motion Control, 1996. AMC'96-MIE. Proceedings., 1996 4th International Workshop on, vol. 2, IEEE, 506–511, 1996.

G. Antonelli, S. Chiaverini, N. Sarkar, External force control for underwater vehicle-manipulator systems, Robotics and Automation, IEEE Transactions on 17 (6) (2001) 931–938.

E. Olguin-Diaz, G. Arechavaleta, G. Jarquin, V. Parra-Vega, A Passivity-Based Model-Free Force–Motion Control of Underwater Vehicle-Manipulator Systems, Robotics, IEEE Transactions on 29 (6) (2013) 1469–1484.

T. W. McLain, S. M. Rock, M. J. Lee, Experiments in the coordinated control of an underwater arm/vehicle system, in: Underwater Robots, Springer, 139–158, 1996.

C. Canudas de Wit, E. Olguin Diaz, M. Perrier, Robust nonlinear control of an underwater vehicle/manipulator system with composite dynamics, in: Robotics and Automation, 1998. Proceedings. 1998 IEEE International Conference on, vol. 1, 452–457 vol.1, 1998.

J. Kim, W. K. Chung, J. Yuh, Dynamic analysis and two-time scale control for underwater vehicle-manipulator systems, in: Intelligent Robots and Systems, 2003. (IROS 2003). Proceedings. 2003 IEEE/RSJ International Conference on, vol. 1, 577–582 vol.1, 2003.

G. Antonelli, S. Chiaverini, Singularity-free regulation of underwater vehicle-manipulator systems, in: American Control Conference, 1998. Proceedings of the 1998, vol. 1, ISSN 0743-1619, 399–403 vol.1, 1998.

M. Santhakumar, J. K., S. Yogesh, A robust task space position tracking control of an underwater vehicle manipulator system, in: Proceedings of the 2015 Conference on Advances In Robotics, ACM, 2, 2015.

G. Antonelli, Underwater Robots Motion and Force Control of VehicleManipulator Systems, vol. 2 of *Springer Tracts in Advanced Robotics*, Springer-Verlag Berlin Heidelberg, Berlin, 2 edn., 2006.

R. Featherstone, Rigid Body Dynamics Algorithms, Springer US, 1 edn., 2008.

B. Siciliano, L. Villani, Robot Force Control, vol. 540 of *The Springer International Series in Engineering and Computer Science*, Springer US, 1999.

S. Chiaverini, L. Sciavicco, The parallel approach to force/position control of robotic manipulators, Robotics and Automation, IEEE Transactions on 9 (4) (1993) 361–373.

C. Edwards, S. Spurgeon, Sliding Mode Control: Theory And Applications, Series in Systems and Control, Taylor & Francis, 1998.

V. Utkin, J. Shi, Integral sliding mode in systems operating under certain conditions, in: Decision and Control, Proceedings of the 35th IEEE Conference on, vol. 4, 4591–4596, 1996.

Y. Shtessel, C. Edwards, L. Fridman, A. Levant, Sliding Mode Control and Observation, Birkhuser Basel, 2014.

C. Barbalata, V. De Carolis, M. W. Dunnigan, Y. Ptillot, D. Lane, An adaptive controller for autonomous underwater vehicles, in: Intelligent Robots and Systems (IROS), 2015 IEEE/RSJ International Conference on, 1658–1663, 2015.

Bibliography

[1] J. Yuh, J. Nie, and C. S. G. Lee, "Experimental study on adaptive control of underwater robots," in *Proceedings of IEEE International Conference on Robotics and Automation*, vol. 1, pp. 393–398, 1999.

[2] RoboticOperatingSystem. `http://www.ros.org/`, 2016.

[3] M. Prats, J. Pérez, J. J. Fernández, and P. J. Sanz, "An open source tool for simulation and supervision of underwater intervention missions," in *IEEE/RSJ International Conference on Intelligent Robots and Systems*, pp. 2577–2582, IEEE, 2012.

[4] R. Featherstone, *Robot Dynamics Algorithms*. PhD thesis, Edinburgh University, 1984.

[5] I. Schjlberg and T. I. Fossen, "Modelling and control of underwater vehicle-manipulator systems," in *Proceedings of Marine Craft Maneuvering and Control Conference*, pp. 45–57, 1994.

[6] G. Antonelli and S. Chiaverini, "Task-priority redundancy resolution for underwater vehicle-manipulator systems," in *Proceedings of IEEE International Conference on Robotics and Automation*, vol. 1, pp. 768–773, 1998.

[7] M. Dunnigan and G. Russell, "Evaluation and reduction of the dynamic coupling between a manipulator and an underwater vehicle," *IEEE Journal of Oceanic Engineering*, vol. 23, no. 3, pp. 260–273, 1998.

[8] N. Sarkar and T. Podder, "Coordinated motion planning and control of autonomous underwater vehicle-manipulator systems subject to drag optimization," *IEEE Journal of Oceanic Engineering*, vol. 26, no. 2, pp. 228–239, 2001.

[9] E. Olguin-Diaz, G. Arechavaleta, G. Jarquin, and V. Parra-Vega, "A passivity based model free force motion control of underwater vehicle manipulator systems," *IEEE Transactions on Robotics*, vol. 29, no. 6, pp. 1469–1484, 2013.

[10] S. Soylu, B. J. Buckham, and R. Podhorodeski, "Exploiting redundancy in underwater vehicle-manipulator systems," in *Proceedings of the Eighteenth International Offshore and Polar Engineering Conference*, pp. 443–451, 2008.

[11] G. Xu, Y. Guo, X. Xiang, and Z. Xiao, "Motion control and computer simulation for underwater vehicle-manipulator systems," in *International Conference on Mechatronics and Automation*, pp. 1368–1373, 2007.

[12] T. Tarn, G. Shoults, and S. Yang, "A dynamic model of an underwater vehicle with a robotic manipulator using kanes method," in *Underwater Robots*, pp. 195–209, 1996.

[13] T. Tarn and S. P. Yang, "Modeling and control for underwater robotic manipulators - an example," in *Proceedings IEEE International Conference on Robotics and Automation*, vol. 3, pp. 2166–2171, 1997.

[14] P. From, V. Duindam, K. Pettersen, J. Gravdahl, and S. Sastry, "Singularity-free dynamic equations of vehicle-manipulator systems," *Simulation Modelling Practice and Theory*, vol. 18, no. 6, pp. 712–731, 2010.

[15] R. Featherstone, *Rigid Body Dynamics Algorithms*. Secaucus, NJ, USA: Springer-Verlag New York, Inc., 2007.

[16] M. Hosseini, A. Omidi, O. Meghdari, and G. Vossoughi, "A composite rigid body algorithm for modeling and simulation of an underwater vehicle equipped with manipulator arms," *Journal of Offshore Mechanics and Arctic Engineering*, vol. 128, no. 2, pp. 119–132, 2005.

[17] S. McMillan, D. Orin, and R. Mcghee, "Efficient dynamic simulation of an underwater vehicle with a robotic manipulator," *IEEE Transactions on Systems, Man and Cybernetics*, vol. 25, pp. 1194–1206, Aug 1995.

[18] J. Han, J. Park, and W. K. Chung, "Robust coordinated motion control of underwater vehicle-manipulator system with minimizing restoring moments," *Ocean Engineering*, vol. 38, no. 10, pp. 1197–1206, 2011.

[19] J. Park, "Principle of dynamical balance for multibody systems," *Multibody System Dynamics*, vol. 14, no. 3, pp. 269–299, 2005.

[20] T. Periasamy, T. Asokan, and M. Singaperumal, "Controller design for manipulator trajectory control of an auv - manipulator system," in *IEEE Region 10 and the Third international Conference on Industrial and Information Systems (ICIIS)*, pp. 1–6, Dec 2008.

[21] T. I. Fossen, *Guidance and control of ocean vehicles*. Wiley, 1994.

[22] T. W. McLain, S. Rock, and M. Lee, "Experiments in the coordinated control of an underwater arm/vehicle system," *Autonomous Robots*, vol. 3, no. 2-3, pp. 213–232, 1996.

[23] A. Ross, T. Fossen, and T. Johansen, "Identification of underwater vehicle hydrodynamic coefficients using free decay tests," in *IFAC Conference on Control Applications in Marine Systems*, 2004.

[24] E. Yh, L. Ws, E. Low, and S. Ggl, "Identification of the hydrodynamics coefficients of an underwater vehicle using free decay pendulum motion," in *International MultiConference of Engineers and Computer Scientists*, pp. 423–430, 2008.

[25] K. Leabourne and S. Rock, "Model development of an underwater manipulator for coordinated arm-vehicle control," in *OCEANS '98 Conference Proceedings*, vol. 2, pp. 941–946, 1998.

[26] R. Li, A. P. Anvar, A. M. Anvar, and T.-F. Lu, "Dynamic modeling of underwater manipulator and its simulation," in *World Academy of Science, Engineering and Technology*, pp. 27–36, 2012.

[27] W. Kolodziejczyk, "Some considerations on an underwater robotic manipulator subjected to the environmental disturbances caused by water current," *Acta Mechanica et Automatica*, vol. 10, no. 1, pp. 43–49, 2016.

[28] J. Morison, J. Johnson, and S. Schaaf, "The force exerted by surface waves on piles," *Journal of Petroleum Technology*, vol. 2, no. 05, pp. 149–154, 1950.

[29] B. Lvesque and M. J. Richard, "Dynamic analysis of a manipulator in a fluid environment.," *International Journal of Robotic Research*, vol. 13, no. 3, pp. 221–231, 1994.

[30] O. Korkmaz, S. Ider, and M. Ozgoren, "Control of an underactuated underwater vehicle manipulator system in the presence of parametric uncertainty and disturbance," in *American Control Conference (ACC), 2013*, pp. 578–584, 2013.

[31] C. M. Wronka, *Modelling and control of a robotic manipulator subject to base disturbances*. PhD thesis, School of Engineering and Pysical Sciences, Heriot-Watt University, 2010.

[32] Y. Kim, S. Mohan, and J. Kim, "Task space-based control of an underwater robotic system for position keeping in ocean currents," *Advanced Robotics*, vol. 28, no. 16, pp. 1109–1119, 2014.

[33] F. Lizarralde, J. T. Wen, and L. Hsu, "Quaternion-based coordinated control of a subsea mobile manipulator with only position measurements," in *Proceedings of the 34th IEEE Conference on Decision and Control*, vol. 4, pp. 3996–4001, 1995.

[34] O. Fjellstad and T. Fossen, "Position and attitude tracking of auvs: a quaternion feedback approach," *IEEE Journal of Oceanic Engineering*, vol. 19, no. 14, pp. 512–518, 1994.

[35] R. Kelly, "A tuning procedure for stable pid control of robot manipulators," *Robotica*, vol. 13, pp. 141–148, 3 1995.

[36] Z. Qu and J. Dorsey, "Robust pid control of robots.," *International Journal of Robotics & Automation*, vol. 6, no. 4, pp. 228–235, 1991.

[37] E. Sariyildiz, H. Yu, and K. Ohnishi, "A practical tuning method for the robust pid controller with velocity feedback," *Machines*, vol. 3, no. 3, pp. 208–222, 2015.

[38] O. Kermorgant, "A dynamic simulator for underwater vehicle-manipulators," in *International Conference on Simulation, Modeling, and Programming for Autonomous Robots*, pp. 25–36, 2014.

[39] S. Mohan and J. Kim, "Robust pid control for position tracking of an underwater manipulator," in *2015 IEEE International Conference on Advanced Intelligent Mechatronics (AIM)*, pp. 1707 – 1712, 2015.

[40] Z. Ismail, *Task-space dynamic control of underwater robots*. PhD thesis, Engineering and Physical Sciences, Heriot-Watt University, 2011.

[41] B. Morales and R. Carelli, "Robot control with inverse dynamics and non-linear gains," in *Latin American Applied Research*, vol. 4, pp. 293–397, 2003.

[42] J. S. Thorp and B. R. Barmish, "On guaranteed stability of uncertain linear systems via linear control," *Journal of Optimization Theory and Applications*, vol. 35, no. 4, pp. 559–579, 1981.

[43] M. W. Spong, "On the robust control of robot manipulators," *IEEE Transactions on Automatic Control*, vol. 37, no. 11, pp. 1782–1786, 1992.

[44] C. Kim and K. Lee, "Robust control of robot manipulators using dynamic compensators under parametric uncertainty," *International Journal of Innovative Computing, Information and Control*, vol. 7, no. 7, 2011.

[45] G. Antonelli and S. Chiaverini, "Singularity-free regulation of underwater vehicle-manipulator systems," in *Proceedings of the American Control Conference, 1998*, vol. 1, pp. 399–403, 1998.

[46] G. Bartolini, M. Coccoli, and E. Punta, "Sliding mode control of an underwater robotic manipulator," in *Proceedings of the 39th IEEE Conference on Decision and Control*, vol. 3, pp. 2983–2988, 2000.

[47] B. Xu, S. R. Pandian, M. Inoue, N. Sakagami, S. Kawamura, *et al.*, "Model-based sliding mode control of underwater robot manipulators," *International Journal of Offshore and Polar Engineering*, vol. 16, no. 03, 2006.

[48] D. Kim, H.-S. Choi, J.-Y. Kim, J.-H. Park, and N.-H. Tran, "Trajectory generation and sliding-mode controller design of an underwater vehicle-manipulator system with redundancy," *International Journal of Precision Engineering and Manufacturing*, vol. 16, no. 7, pp. 1561–1570, 2015.

[49] H. Wang, "Adaptive control of robot manipulators with uncertain kinematics and dynamics," *arXiv preprint arXiv:1403.5204*, 2014.

[50] T. Fossen and S. I. Sagatun, "Adaptive control of nonlinear underwater robotic systems," in *Proceedings of IEEE International Conference on Robotics and Automation*, pp. 1687–1694, 1991.

[51] S. Zhao, J. Yuh, and H. T. Choi, "Adaptive dob control of underwater robotic vehicles," in *MTS/IEEE Conference and Exhibition OCEANS*, vol. 1, pp. 397–402, 2001.

[52] G. Antonelli, S. Chiaverini, N. Sarkar, and M. West, "Adaptive control of autonomus underwater vehicle: experimental results on odin," *IEEE Transactions on Control System Technology*, vol. 9, no. 5, 2001.

[53] N. Sarkar, J. Yuh, and T. Podder, "Adaptive control of underwater vehicle-manipulator systems subject to joint limits," in *IEEE/RSJ International Conference on Inteligent Robots and Systems*, pp. 142–147, 1999.

[54] B. Xu, S. R. Pandian, N. Sakagami, and F. Petry, "Nuro-fuzzy control of underwater vehicle-manipulator systems," *Journal of the Franklin Institute*, vol. 349, no. 3, pp. 1125–1138, 2012.

[55] M. Lee and H.-S. Choi, "A robust neural network controller for underwater robot manipulators," *IEEE Transactions on Neural Networks*, vol. 11, no. 6, pp. 1456–1470, 2000.

[56] K. Ishii, T. Fujii, and T. Ura, "An on-line adaptation method in a neural network based control system for auvs," *IEEE Journal of Oceanic Engineering*, vol. 20, no. 3, pp. 221–228, 1995.

[57] W. Lee and G. Kang, "A fuzzy model-based controller of an underwater robotic vehicle under the influence of thruster dynamics," in *Proceedings of IEEE international Conference on Robotics and Automation*, pp. 750–755, 1998.

[58] S. M. Suboh, I. A. Rahman, M. R. Arshad, and M. N. Mahyuddin, "Modeling and control of 2-dof underwater planar manipulator," *Indian Journal of Marine Sciences*, vol. 38, no. 3, pp. 365–371, 2009.

[59] J. Wang and C. S. G. Lee, "Self-adaptive recurrent neuro-fuzzy control of an autonomous underwater vehicle," *IEEE Transactions on Robotics and Automation*, vol. 19, pp. 283–295, Apr 2003.

[60] D. Wettergreen, C. Gaskett, and A. Zelinsky, "Autonomous guidance and control for an underwater robotic vehicle," in *Proceedings of the International Conference on Field and Service Robotics (FSR99), Pittsburgh, USA*, 1999.

[61] A. El-Fakdi, M. Carreras, N. Palomeras, and P. Ridao, "Autonomous underwater vehicle control using reinforcement learning policy search methods," in *Europe Oceans 2005*, vol. 2, pp. 793–798, IEEE, 2005.

[62] N. Sakagami and S. Kawamura, "Time optimal control for underwater robot manipulators based on iterative learning control and time-scale transformation," in *OCEANS 2003. Proceedings*, vol. 3, pp. 1180–1186, IEEE, 2003.

[63] S. Chiaverini and L. Sciavicco, "The parallel approach to force/position control of robotic manipulators," *IEEE Transactions on Robotics and Automation*, vol. 9, no. 4, pp. 361–373, 1993.

[64] D. E. Whitney, "Force feedback control of manipulator fine motions," *Journal of Dynamic Systems, Measurement and Control*, vol. 99, no. 2, pp. 91–97, 1977.

[65] J. L. Nevins and D. E. Whitney, *The force vector assembler concept*. 1972.

[66] K. P. Tee, R. Yan, and H. Li, "Adaptive admittance control of a robot manipulator under task space constraint," in *IEEE International Conference on Robotics and Automation (ICRA)*, pp. 5181–5186, IEEE, 2010.

[67] H. Seraji, "Adaptive admittance control: an approach to explicit force control in compliant motion," in *Proceedings of IEEE International Conference on Robotics and Automation*, pp. 2705–2712, 1994.

[68] N. Hogan, "Impedance control: an approach to manipulation: Part ii - implementation," *Journal of Dynamic Systems, Measurement and Control*, vol. 107, no. 1, pp. 8–16, 1985.

[69] S. Chan, B. Yao, W. Gao, and M. Cheng, "Robust impedance control of robot manipulators.," *International Journal of Robotics & Automation*, vol. 6, no. 4, pp. 220–227, 1991.

[70] Z. Lu and A. Goldenberg, "Robust impedance control and force regulation: theory and experiments," *The International Journal of Robotics Research*, vol. 16, no. 3, pp. 225–254, 1995.

[71] R. Kelly, R. Carelli, M. Amestegui, and R. Ortega, "On adaptive impedance control of robot manipulators," in *Proceedings of IEEE International Conference on Robotics and Automation*, pp. 572–577, 1989.

[72] H. Park and J. Lee, "Adaptive impedance control of a haptic interface," *Mechatronics*, vol. 14, no. 3, pp. 237–253, 2004.

[73] S. A. Fatemi, V. J. Majd, and M. R. Ebrahimpour, "Parallel force and position control with the aid of variable impedance model in robot manipulators," in *20th Iranian Conference on Electrical Engineering (ICEE)*, pp. 952–956, IEEE, 2012.

[74] M. Perez Plius, M. Yilmaz, U. Seven, and K. Erbatur, "Fuzzy controller scheduling for robotic manipulator force control," in *12th IEEE International Workshop on Advanced Motion Control (AMC)*, pp. 1–8, IEEE, 2012.

[75] Y. Cui, T. K. Podder, and N. Sarkar, "Impedance control of underwater vehicle-manipulator systems (uvms)," in *Intelligent Robots and Systems, 1999. IROS'99. Proceedings. 1999 IEEE/RSJ International Conference on*, vol. 1, pp. 148–153, 1999.

[76] H. Farivarnejad and S. A. A. Moosavian, "Multiple impedance control for object manipulation by a dual arm underwater vehicle–manipulator system," *Ocean Engineering*, vol. 89, pp. 82–98, 2014.

[77] M. H. Raibert and J. J. Craig, "Hybrid position/force control of manipulators," *Journal of Dynamic Systems, Measurement and Control*, vol. 103, no. 2, pp. 126–133, 1981.

[78] A. De Luca, C. Manes, and F. Nicolo, "A task space decoupling approach to hybrid control of manipulators," in *Robot Control 1988 (SYROCO'88): Selected Papers from the 2nd IFAC Symposium*, 1998.

[79] O. Khatib, "A unified approach for motion and force control of robot manipulators: The operational space formulation," *IEEE Journal of Robotics and Automation*, vol. 3, no. 1, pp. 43–53, 1987.

[80] A. Jafari, M. Rezaei, A. Talebi, S. S. Ghidary, and R. Monfaredi, "An adaptive hybrid force/motion control design for robot manipulators interacting in constrained motion with unknown non-rigid environments," in *ASME 2012 International Mechanical Engineering Congress and Exposition*, pp. 1063–1069, 2012.

[81] C. Bechlioulis, Z. Doulgeri, and G. Rovithakis, "Robot force/position tracking with guaranteed prescribed performance," in *IEEE International Conference on Robotics and Automation, ICRA'09.*, pp. 3688–3693, IEEE, 2009.

[82] M. Dunnigan, D. Lane, A. Clegg, and I. Edwards, "Hybrid position/force control of a hydraulic underwater manipulator," in *IEE Proceedings of Control Theory and Applications*, vol. 143, pp. 145–151, 1996.

[83] L. Lapierre, P. Fraisse, and N. K. M'Sirdi, "Hybrid position/force control of a rov with a manipulator," in *OCEANS'98 Conference Proceedings*, vol. 2, pp. 931–935, 1998.

[84] K. Kosuge, H. Kajita, and T. Fukuda, "Force control of manipulator/vehicle system floating on the water utilizing vehicle restoring force," in *Proceedings of the 4th International Workshop on Advanced Motion Control, AMC'96-MIE.*, vol. 2, pp. 506–511, 1996.

[85] Y. Cui and J. Yuh, "A unified adaptive force control of underwater vehicle-manipulator systems (uvms)," in *Proceedings of IEEE/RSJ International Conference on Intelligent Robots and Systems (IROS)*, vol. 1, pp. 553–558, 2003.

[86] B. Siciliano, "Parallel force/position control of robot manipulators," in *Robotics Research*, pp. 78–89, Springer, 1996.

[87] J. De Schutter, "Improved force control laws for advanced tracking applications," in *Proceedings of IEEE International Conference on Robotics and Automation*, pp. 1497–1502, IEEE, 1988.

[88] Y. Karayiannidis, G. Rovithakis, and Z. Doulgeri, "Force/position tracking for a robotic manipulator in compliant contact with a surface using neuro-adaptive control," *Automatica*, vol. 43, no. 7, pp. 1281–1288, 2007.

[89] R. Osypiuk, T. Kroger, B. Finkemeyer, and F. M. Wahl, "A two-loop implicit force/position control structure, based on a simple linear model: Theory and experiment," in *Proceedings of IEEE International Conference on Robotics and Automation ICRA*, pp. 2232–2237, IEEE, 2006.

[90] F. Passold and M. R. Stemmer, "Force control of a scara robot using neural networks," in *Proceedings of the Fourth International Workshop on Robot Motion and Control, RoMoCo'04.*, pp. 247–252, IEEE, 2004.

[91] S. Heshmati-Alamdari, A. Nikou, A. Eqtami, and K. J. Kyriakopoulos, "A novel control approach for underwater vehicle manipulator systems in interaction with compliant environments," in *IEEE International Conference on Robotics and Automation (ICRA)*, 2016.

[92] G. Antonelli, S. Chiaverini, and N. Sarkar, "External force control for underwater vehicle-manipulator systems," *IEEE Transactions on Robotics and Automation*, vol. 17, no. 6, pp. 931–938, 2001.

[93] E. Olguin-Diaz, G. Arechavaleta, G. Jarquin, and V. Parra-Vega, "A passivity-based model-free force-motion control of underwater vehicle-manipulator systems," *IEEE Transactions on Robotics and Automation*, 2013.

[94] R. M. Murray, Z. Li, and S. S. Satry, *A mathematical introduction to robotic manipulation*. CRC press, 1994.

[95] K. S. Fu, R. Gonzalez, and C. G. Lee, *Robotics: Control, sensing, vision and intelligence*. Tata McGraw-Hill Education, 1987.

[96] J. Denavit and R. Hartenberg, "A kinematic notation for lower-pair mechanisms based on matrices," *Journal of Applied Mechanics*, vol. 2, pp. 215–221, 1955.

[97] M. Abderrahim, *Modelling of robotic manipulators*. PhD thesis, University of Glasgow, 1996.

[98] W. A. Wolovich and H. Elliott, "A computational technique for inverse kinematics," in *The 23rd IEEE Conference on Decision and Control*, pp. 1359–1363, 1984.

[99] S. R. Buss, "Introduction to inverse kinematics with jacobian transpose, pseudoinverse and damped least squares methods," *IEEE Journal of Robotics and Automation*, vol. 17, pp. 1–19, 2004.

[100] Y. Nakamura and H. Hanafusa, "Inverse kinematics solutions with singularity robustness for robot manipulator control," *Journal of Dynamic Systems, Measurements and Control*, vol. 108, pp. 163–171, 1986.

[101] G. E. Owen, *Fundamentals of scientific mathematics*. Courier Corporation, 2003.

[102] M. W. Walker and D. E. Orin, "Efficient dynamic computer simulation of robotic mechanisms," *Journal of Dynamic Systems, Measurement, and Control*, vol. 104, no. 3, pp. 205–211, 1982.

[103] T. W. McLain and S. M. Rock, "Development and experimental validation of an underwater manipulator hydrodynamic model," *The International Journal of Robotics Research*, vol. 17, no. 7, pp. 748–759, 1998.

[104] J. Newman, *Marine hydrodynamics*. MIT Press, Cambridge, MA, 1989.

[105] G. K. Batchelor, *An introduction to fluid dynamics*. Cambridge university press, 2000.

[106] I. A. Rahman, S. M. Suboh, and M. R. Arshad, "Theory and design issues of underwater manipulator," in *Proceedings of International Conference on Control, Instrumentation and Mechatronics Engineering*, pp. 725–731, 2007.

[107] B. Armstrong-Hélouvry, P. Dupont, and C. C. De Wit, "A survey of models, analysis tools and compensation methods for the control of machines with friction," *Automatica*, vol. 30, no. 7, pp. 1083–1138, 1994.

[108] A. Harnoy, B. Friedland, and S. Cohn, "Modeling and measuring friction effects," *IEEE Control Systems*, vol. 28, no. 6, pp. 82–91, 2008.

[109] C. C. de Wit, H. Olsson, K. Astrom, and P. Lischinsky, "Dynamic friction models and control design," in *American Control Conference*, vol. 30, pp. 1920–1926, 1993.

[110] P. R. Dahl, "Solid friction damping of mechanical vibrations," *AIAA Journal*, vol. 14, no. 12, pp. 1675–1682, 1976.

[111] N. Hogan, "Impedance control of industrial robots," *Robotics and Computer-Integrated Manufacturing*, vol. 1, no. 1, pp. 97–113, 1984.

[112] Y. Xu, R. P. Paul, and P. I. Corke, "Hybrid position force control of robot manipulator with an instrumented compliant wrist," in *Experimental Robotics I*, pp. 244–270, Springer, 1990.

[113] R. Volpe and P. Khosla, "A theoretical and experimental investigation of impact control for manipulators," *The International Journal of Robotics Research*, vol. 12, no. 4, pp. 351–365, 1993.

[114] K. Johanastrom and C. Canudas-De-Wit, "Revisiting the lugre friction model," *IEEE Control Systems*, vol. 28, no. 6, pp. 101–114, 2008.

[115] HDTGlobal. `http://www.hdtglobal.com/`, 2016.

[116] F. L. Lewis, D. M. Dawson, and C. T. Abdallah, *Robot manipulator control:theory and practice*. CRC Press, 2003.

[117] L. Hunt, R. Su, and G. Meyer, "Global transformations of nonlinear systems," *IEEE Trans. Autom. Control*, vol. 28, no. 1, pp. 24–31, 1983.

[118] M. Honegger and P. Corke, "Model-based control of hydraulically actuated manipulators," in *Proceedings IEEE International Conference on Robotics and Automation*, vol. 3, pp. 2553–2559, IEEE, 2001.

[119] F. Piltan, M. H. Yarmahmoudi, M. Shamsodini, E. Mazlomian, and A. Hosainpour, "Puma-560 robot manipulator position computed torque control methods using matlab/simulink and their integration into graduate nonlinear control and matlab courses," *International Journal of Robotics and Automation*, vol. 3, no. 3, pp. 167–191, 2012.

[120] F. Reyes and R. Kelly, "Experimental evaluation of model-based controllers on a direct-drive robot arm," *Mechatronics*, vol. 11, no. 3, pp. 267–282, 2001.

[121] G. Feng, "A survey on analysis and design of model-based fuzzy control systems," *IEEE Transactions on Fuzzy systems*, vol. 14, no. 5, pp. 676–697, 2006.

[122] M. W. Spong and M. Vidyasagar, *Robot dynamics and control*. John Wiley & Sons, 2008.

[123] N. T. Duy, M. Seegar, and J. Peters, "Computed torque control with nonparametric regression models," in *IEEE Conference Proceedings of American Control*, pp. 212–217, 2008.

[124] R. Kelly, V. Davila, V. Santibanez, and A. Loria, *Feedforward control and PD control plus feedforward"*, pp. 263–285. Springer London, 2005.

[125] P. K. Khosla and T. Kanade, "Experimental evaluation of nonlinear feedback and feedforward control schemes for manipulators," *The International Journal of Robotics Research*, vol. 7, no. 1, pp. 18–28, 1988.

[126] V. Santibanez and R. Kelly, "Pd control with feedforward compensation for robot manipulators:analysis and experimentation," *Robotica*, vol. 19, no. 01, pp. 11–19, 2001.

[127] P. Bellec, *Simulation of the six-degree-of-freedom motion of a remotely-controlled unmanned submersible*. PhD thesis, Electrical and Electronic Engineering, Heriot-Watt University, 1980.

[128] J. W. Harris and H. Stocker, *Handbook of mathematics and computational science*. Springer Science & Business Media, 1998.

[129] S. Chiaverini and L. Sciavicco, "Force/position control of manipulators in task space with dominance in force," *Proceedings IFAC Robotic Control*, pp. 137–143, 1989.

[130] R. J. Anderson and M. W. Spong, "Hybrid impedance control of robotic manipulators," *IEEE Journal on Robotics and Automation*, vol. 4, no. 5, pp. 549–556, 1988.

[131] J. T. Wen and S. Murphy, "Stability analysis of position and force control for robot arms," *IEEE Transactions on Automatic Control*, vol. 36, no. 3, pp. 365–371, 1991.

[132] Y. Shtessel, C. Edwards, L. Fridman, and A. Levant, *Sliding mode control and observation*. Springer, 2014.

[133] V. I. Utkin, "Sliding mode control design principles and applications to electric drives," *IEEE Transactions on Industrial Electronics*, vol. 40, no. 1, pp. 23–36, 1993.

[134] M.-L. Tseng and M.-S. Chen, "Chattering reduction of sliding mode control by low-pass filtering the control signal," *Asian Journal of Control*, vol. 12, no. 3, pp. 392–398, 2010.

[135] B. Siciliano and L. Villani, *Robot Force Control*, vol. 540 of *The Springer International Series in Engineering and Computer Science*. Springer US, 1999.

[136] V. Utkin and J. Shi, "Integral sliding mode in systems operating under uncertainty conditions," in *Proceedings of the 35th IEEE Conference on Decision and Control*, vol. 4, pp. 4591–4596, IEEE, 1996.

[137] P. Donelan, *Kinematic singularities of robot manipulators*. INTECH Open Access Publisher, 2010.

[138] W. S. Lu and Q. H. Meng, "Impedance control with adaption for robotic manipulators," *IEEE Transactions on Robotics and Automation*, pp. 408–415, 1991.

[139] S. Jung and T. Hsia, "Force tracking impedance control of robot manipulators for environment with damping," in *33rd Anual Conference of the IEEE Industrial Electrocics Society*, pp. 2742–2747, 2007.

[140] D. A. Lawrence, "Impedance control stability properties in common implementations," in *IEEE International Conference on Robotics and Automation*, pp. 1185–1190, 1998.

[141] A. Stolt, M. Linderoth, A. Robertsson, and R. Johansson, "Force controlled robotic assembly without a force sensor," in *IEEE International Conference on Robotics and Automation (ICRA)*, pp. 1538–1543, IEEE, 2012.

[142] M. Van Damme, P. Beyl, B. Vanderborght, V. Grosu, R. Van Ham, I. Vanderniepen, A. Matthys, and D. Lefeber, "Estimating robot end-effector force from noisy actuator torque measurements," in *IEEE International Conference on Robotics and Automation (ICRA)*, pp. 1108–1113, IEEE, 2011.

[143] J. Jung, J. Lee, and K. Huh, "Robust contact force estimation for robot manipulators in three-dimensional space," *Proceedings of the Institution of Mechanical Engineers, Part C: Journal of Mechanical Engineering Science*, vol. 220, no. 9, pp. 1317–1327, 2006.

[144] K. S. Eom, I. H. Suh, W. K. Chung, and S.-R. Oh, "Disturbance observer based force control of robot manipulator without force sensor," in *Proceedings of IEEE International Conference on Robotics and Automation*, vol. 4, pp. 3012–3017, IEEE, 1998.

[145] E. R. Parker, *Materials Data Book for Engineers and Scientists*. 1967.

[146] MoveIT. `http://moveit.ros.org/`, 2016.

[147] R. D. Brandt and F. Lin, "Theory of adaptive interaction," 1998.

[148] F. Lin, R. D. Brandt, and G. Saikalis, "Self-tuning of pid controllers by adaptive interaction," in *Proceedings of the American Control Conference*, vol. 5, pp. 3676–3681, IEEE, 2000.

[149] R. D. Brandt and F. Lin, "Adaptive interaction and its application to neural networks," *Information Sciences*, vol. 121, no. 3, pp. 201–215, 1999.

[150] G. Saikalis and F. Lin, "A neural network controller by adaptive interaction," in *Proceedings of the American Control Conference*, vol. 2, pp. 1247–1252, IEEE, 2001.

[151] D. G. Luenberger, *Optimization by vector space methods*. John Wiley & Sons, 1969.

[152] N. P. Bhatia and G. P. Szegö, *Stability theory of dynamical systems*. Springer Science & Business Media, 2002.

[153] S. S. Sastry, *Nonlinear systems: analysis, stability, and control*, vol. 10. Springer Science & Business Media, 2013.